Cis-chelating cavity-shaped ligands for selective metal-catalyzed oligomerization of ethylene

Yang Li

UNIVERSITÉ DE STRASBOURG

ÉCOLE DOCTORALE DES SCIENCES CHIMIQUES

Equipe Confinement Moléculaire et Catalyse (ECMC) - UMR 7177 CNRS

THÈSE présentée par :

Yang LI

soutenue le : **28 septembre 2022**

pour obtenir le grade de : **Docteur de l'université de Strasbourg**

Discipline/ Spécialité : Chimie

Ligands cavitaires *cis*-chélatants pour l'oligomérisation métallo-catalysée sélective de l'éthylène

THÈSE dirigée par :

M. ARMSPACH Dominique	Professeur, Université de Strasbourg
M. BRAUNSTEIN Pierre	Directeur de recherche émérite CNRS, Université de Strasbourg, Membre de l'Académie des sciences

RAPPORTEURS :

M. TILLOY Sébastien	Professeur, Université d'Artois
M. PERUCH Frédéric	Directeur de recherche CNRS, Université de Bordeaux

---

AUTRES MEMBRES DU JURY :

M. LIU Shaofeng	Professeur, Qingdao University of Scicence & Technology (Chine)
M. DJUKIC Jean-Pierre	Directeur de recherche CNRS, Université de Strasbourg

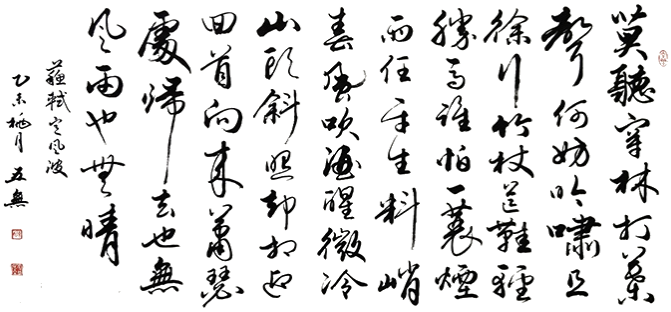

莫听穿林打叶声，何妨吟啸且徐行。

–[宋]苏轼《定风波》

Listen not to the rain beating against the trees.

Why don’t you slowly walk and chant at ease ?

– [Song dynasty] SU Shi <Calming the waves>

Acknowlegement

This doctoral work was carried out in the “Equipe Confinement Moléculaire et Catalyse” (UMR 7177 CNRS) at the Université de Strasbourg, supervised by Prof. Dominique ARMSPACH and Prof. Pierre BRAUNSTEIN. I would like to express my gratitude to all those people who helped me during my PhD and the writing up of this manuscript.

First of all, I would like to thank my two supervisors for giving me the opportunity to join their team. I would like to thank Dominique for his listening, his constant encouragement and guidance. He is a very nice and patient supervisor. He taught a lot of experimental skills and provided me with many valuable suggestions during the course of my PhD. I would like to thank Pierre. He is a very respected supervisor and his scientific rigor, vast knowledge have been a great asset throughout my thesis work.

I would like to thank Prof. Sébastien TILLOY, Prof. Frédéric PERUCH, Prof. Shaofeng LIU and Prof. Jean-Pierre DJUKIC for agreeing to be on my thesis committee and for the time they spent on assessing my work.

I would also like to thank all the present and former members of our lab in no particular order): Marcel WESOLEK, Geordie CRESTE, Katrin PELZER, Sébastian JUNG, Tuan-Anh PHAN, Fengkai HE, Giovanni PREDA, Mingyang HAN…

This work would never have been possible without the contribution of the partners and the scientific services of the University of Strasbourg. I would like to thank Marc Mermillon-Fournier for his help with oligomerization catalytic experiments. I would like to thank the entire team of the NMR department, in particular Bruno VINCENT and Maurice COPPE. I am also grateful to Lydia KARMAZIN, Corinne BAILLY, Nathalie GRUBER for their help of X-ray characterization. My gratitude also goes to the staff of the Mass Spectrometry and Microanalysis departments for their contribution and assistance.

I would also like to thank all my Chinese friends in Strasbourg for their support. Without them, my life abroad would not be so interesting.

I would like to thank the China Scholarship Council (CSC) for the financial support.

Finally, I want to express my thanks to my beloved parents and close family for their unconditional support and encouragements.

Table of Contents

List of Abbreviations

c. d.	Circular dichroism
CD	Cyclodextrin
COD	Cycloocta-1,5-diene
COSY	COrrelation SpectroscopY
CTV	Cyclotriveratrilene
δ	Chemical shift (ppm)
DCM	Dichloromethane
DEPT	Distortionless Enhancement by Polarization Transfer
DMAP	4-dimethylaminopyridine
DME	1,2-dimethoxyethane
DMF	*N*,*N*-dimethylformamide
DPPE	1,2-bis(diphenylphosphino)ethane
DSC	Differential scanning calorimetry
ESI	Electro-spray ionization
equiv.	(mole) equivalent
FE-SEM	Field Emission Scanning Electron Microscopes
FT-IR	Fourier-transform infrared spectroscopy
GC	Gas chromatography
HMBC	Heteronuclear Multiple Bond Correlation
HMQC	Heteronuclear Multiple Quantum Correlation
HSQC	Heteronuclear Single Quantum Correlation
$^{n}J_{A,B}$	Coupling constant (Hz) between nuclei A and B through n bonds
LDA	Lithium diisopropylamide
MMAO	Modified Methylaluminoxane
MS	Mass Spectrometry
nbd	norbornadiene
n-BuLi	*n*-butyllithium
NMR	Nuclear Magnetic Resonance
NOESY	Nuclear Overhauser Effect SpectroscopY
Ph	Phenyl
ppm	Parts per million
ROESY	Rotation frame Overhauser Effect SpectroscopY
r.t.	room temperature
THF	Tetrahydrofuran

tht	Tetrahydrothiophene
TOCSY	TOtal Correlation SpectroscopY
TOF	TurnOver Frequency
^{s}Tr	supertrityl, tris(*p*-*tert*-butylphenyl)methyl
UV-vis	Ultraviolet-visible spectroscopy

RÉSUMÉ

1. Introduction

Avec une production annuelle de plus de 150 millions de tonnes, les polyoléfines sont les polymères de synthèse les plus répandus au monde et sont présents dans tous les aspects de la vie courante.[1,2] Leurs analogues de plus petite taille que sont les α-oléfines linéaires (LAO) sont également produits en grande quantité car ils constituent non seulement des intermédiaires clés pour la production de détergents et lubrifiants mais sont également des co-monomères entrant dans la composition de polyoléfines de structures variées et notamment du polyéthylène haute densité et du polyéthylène linéaire de basse densité.[3-7] Parallèlement au développement de catalyseurs dérivés de métaux de transition de la gauche du Tableau Périodique, tels que le titane ou le zirconium à la suite des travaux précurseurs de Ziegler et Natta, et des catalyseurs au chrome faisant intervenir des intermédiaires métallacycliques,[8-17] les catalyseurs à base de métaux de transition de la droite du Tableau Périodique, en particulier le nickel, ont fait l'objet d'un intérêt croissant en raison de leur plus grande robustesse et de leur réactivité spécifique.[15,18-28] En effet, les complexes de nickel favorisent les réactions de terminaison, ce qui conduit à des oléfines à chaîne courte, en particulier des butènes et notamment des butènes internes. Cependant, en 1995, Brookhart a mis au point des catalyseurs dérivés de nickel(II) et de palladium(II) complexés par des ligands bidentes de type diimine stériquement encombrés.[29] Ces derniers se sont montrés très efficaces en polymérisation de l'éthylène, d'α-oléfines et d'oléfines disubstituées. Il a notamment montré que les réactions de terminaison pouvaient être inhibées dans une certaine mesure, ce qui favorise la propagation de la chaîne macromoléculaire.[30] De nombreux complexes de nickel(II) and palladium(II) comportant des ligands bidentes stériquement encombrés de différentes nature ont depuis lors été synthétisés et testés en catalyse d'oligomérisation et de polymérisation de l'éthylène.[31-35]

Mon travail de thèse s'inscrit également dans cette démarche et, reprenant en partie les concepts énoncés par Brookhart, les applique à des ligands possédant une cavité moléculaire spécifique. Mon premier objectif a été de synthétiser et de caractériser des précatalyseurs d'oligomérisation de l'éthylène comportant des métaux à configuration électronique d^8 (nickel et palladium) encapsulés dans une cavité α-cyclodextrine équipée de différents atomes donneurs (P,N et P,P). La présence d'un environnement capsulaire autour du métal permet d'encombrer les positions axiales des complexes plan carré comme dans les systèmes non macrocycliques. Cependant, la présence d'une cavité moléculaire de dimension bien définie

For references, see page 10.

devrait être à même de mieux contrôler la première sphère de coordination du métal et par là même limiter la croissance de la chaîne carbonée et donc favoriser la formation d'oléfines à chaîne courte présentant une distribution de masses étroite et de structure bien définie (α-oléfines ou oléfines internes, oléfines linéaires ou branchées). Le deuxième objectif de ma thèse a donc été de tester les différents précatalyseurs synthétisés en oligomérisation de l'éthylène après activation à l'aide d'un co-catalyseur adéquat et d'identifier leurs conditions optimales d'utilisation.

2. Résultats et discussions

Divisé en deux parties, le premier chapitre du manuscrit de thèse est consacré à l'analyse de l'état de l'art sur les ligands bidentes cavitaires et leurs applications, notamment en catalyse homogène. La première partie porte sur les cavités moléculaires équipées d'un seul bras coordinant conduisant à des complexes chélates relativement flexibles. La deuxième partie a trait à des ligands cavitaires comportant deux fragments coordinants directement liés à la plateforme macrocyclique qui par chélation fournissent des complexes beaucoup plus rigides. L'impact de la cavité et de la nature du ligand chélatant sur les propriétés coordinantes et catalytiques est discuté de manière systématique. Faisant suite à cette revue de la littérature sur les molécules d'intérêt, les deuxième et troisième chapitre sont consacrés à la synthèse d'une série de ligands cavitaires *cis*-chélatants et de leurs complexes de palladium et de nickel ainsi que de leurs analogues non cavitaires, ce qui permet des comparaisons très révélatrices. Le dernier chapitre décrit les propriétés catalytiques des différents complexes obtenus en oligomérisation de l'éthylène.

2.1 Synthèse et caractérisation de ligands P,N *cis*-chélatants et de leurs complexes de palladium et de nickel[36]

Le premier ligand P,N cavitaire *cis*-chélatant capable de confiner un centre métallique (**L1**) a été synthétisé selon le schéma réactionnel ci-dessus (Schéma 1) avec un rendement de 63% à partir du dimésylate **1b**[37] et du phosphure résultant de la déprotonation de la phosphine primaire fonctionnalisée en position ortho **2**.[38,39] Une synthèse améliorée de **2** a été développée en partant de la 2-bromoaniline par couplage palladocatalysé avec le phosphonate **3** suivi d'une double méthylation de l'amine primaire. A des fins de comparaison, l'analogue non cavitaire **L2** a également été synthétisé avec un rendement de 40% à partir de la 2-bromo-*N*,*N*-diméthylaniline par ortho-lithiation suivie de la substitution nucléophile de la

For references, see page 10.

chlorodiéthylphosphine par l'organolithien. Les ligands **L1** et **L2** ont ensuite été utilisés pour la synthèse des complexes de palladium **4**, **5**, **8**-**11** ainsi que des complexes du nickel **6** et **12**. En présence de [$PdCl_2$(COD)] (COD = cycloocta-1,5-diène) ou de [PdMeCl(COD)] dans le dichloromethane, le ligand cavitaire **L1** ne fournit que les complexes chélates **4** et **5**, respectivement, même en présence d'un excès de ligand. Au contraire, le ligand non cavitaire **L2** fournit dans les mêmes conditions avec [$PdCl_2$(COD)] ou [PdMeCl(COD)] un mélange de complexes neutres (**8** et **10**) et cationiques (**9**, **11**, respectivement) dont la composition dépend de l'excès de ligand utilisé. Par contre, seul le complexe neutre **12** se forme en présence de [$NiBr_2$(DME)] (DME = éthylène glycol diméthyl éther) comme dans le cas du ligand cavitaire **L1** (complexe **6**).

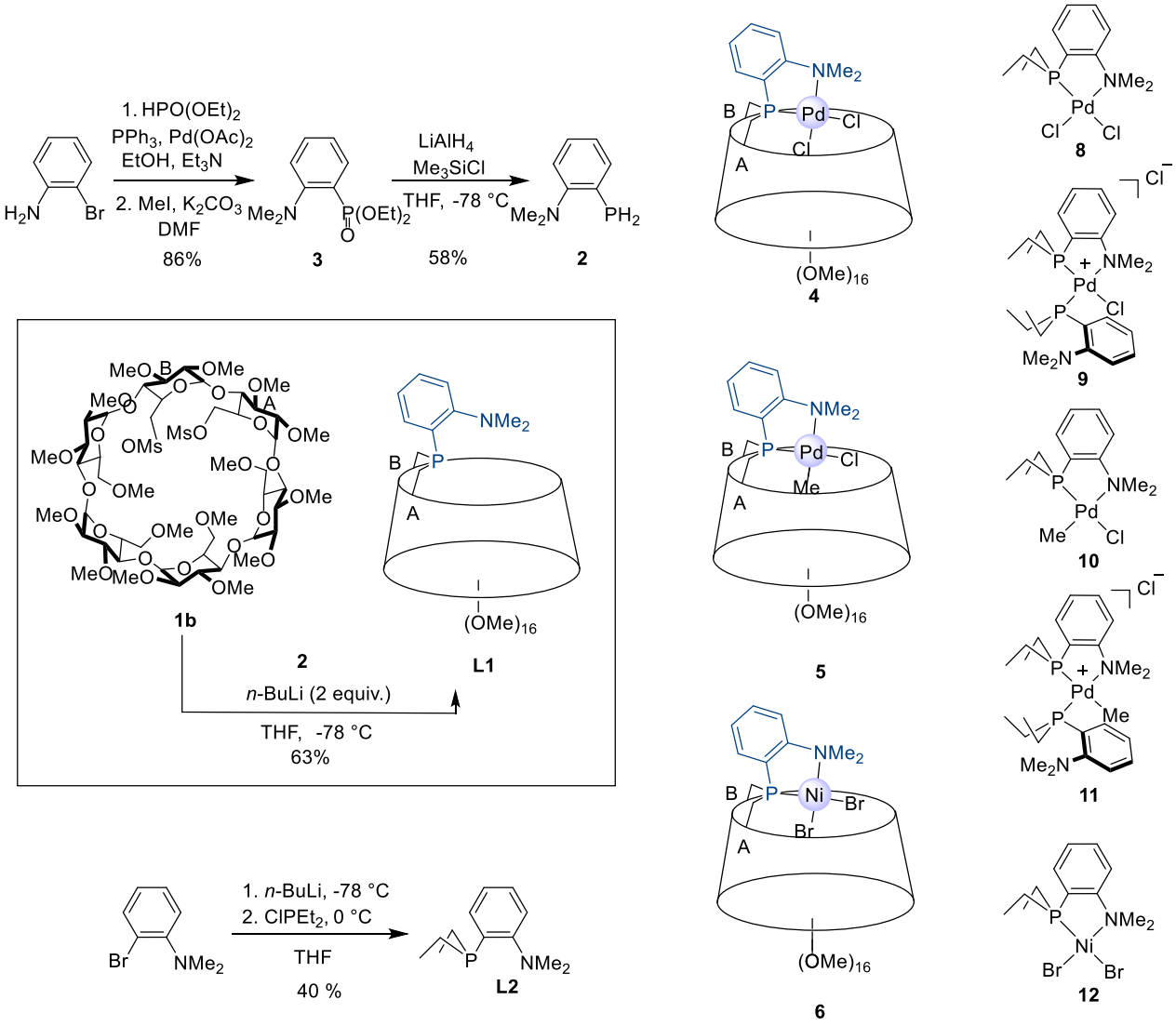

Schéma 1. Synthèse des ligands P,N et structures de leurs complexes métalliques

For references, see page 10.

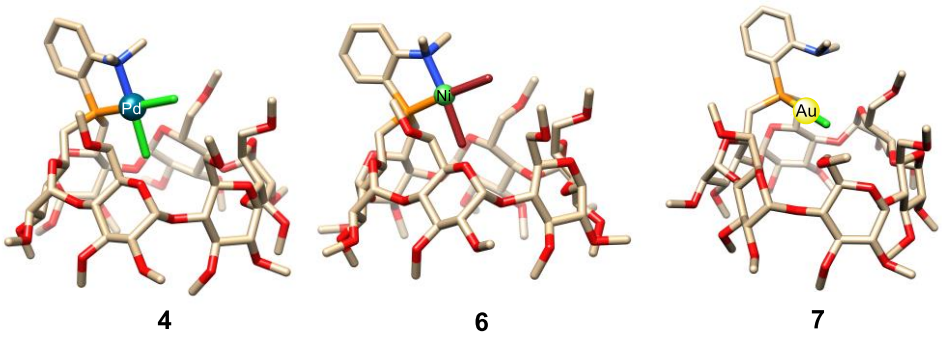

Figure 1. Structures moléculaires des complexes cavitaires **4**, **6** et **7**

La présence d'une cavité cyclodextrine empêche clairement la formation d'un complexe bis(phosphine) et permet de ce fait un contrôle efficace de la sphère de coordination du métal. La structure moléculaire du complexe cavitaire **6** a été déterminée par diffraction des rayons X et montre que les deux ligands halido se trouvent dans des environnements stériques radicalement différents, l'un des halogénures étant encapsulé et l'autre pointant vers l'extérieur. Dans le cas du complexe **5**, le groupe méthyle lié au palladium est encapsulé tandis que l'halogénure, en position *trans* du phosphore en raison de son influence *trans*, pointe vers l'extérieur de la cavité. Le complexe d'or(I) (**7**) dans lequel **L1** se comporte comme un ligand monodente a également été synthétisé. Sa structure moléculaire indique clairement que c'est bien l'atome de phosphore qui est responsable du confinement du métal et non l'azote car dans ce complexe, l'unité NMe_2 n'est pas coordinée.

2.2 Synthèse et caractérisation de diphosphines *cis*-chélatantes et de leurs complexes de palladium et de nickel

Une méthode de pontage similaire à celle utilisée dans la synthèse du ligand P,N **L1** a été utilisée pour préparer le ligand **L3** à partir de la diphosphine **13** (Schéma 2).[40] Ce ligand **L3** présente une structure très proche de **L1** avec cependant un encombrement stérique plus important.

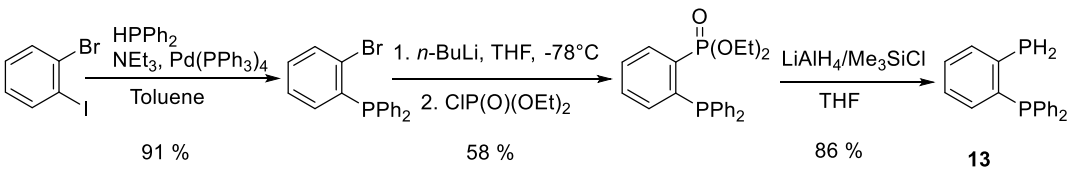

Schéma 2. Synthèse de la diphosphine **13**

For references, see page 10.

Une deuxième diphosphine métalloconfinante (**L4**) a également été synthétisée à partir de la même diphosphine **13** grâce à un réarrangement de Smiles[41,42] qui a lieu en présence d'un excès de *n*-BuLi (Schéma 3).

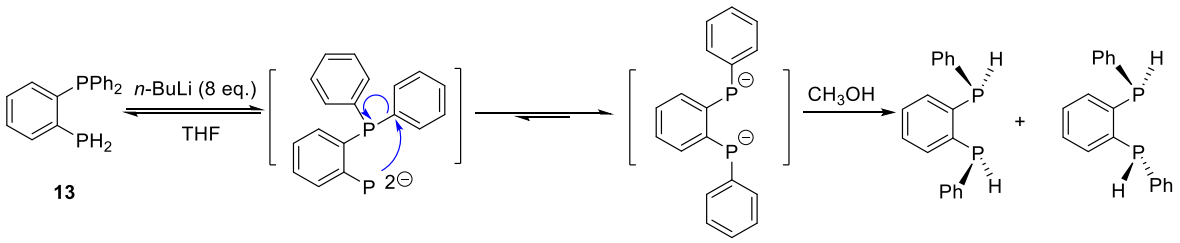

Schéma 3. Réarrangement de type Smiles de la diphosphine **13** en présence d'un excès de *n*-BuLi

Comme pour le ligand P,N **L1**, les diphosphines **L3** et **L4** (Schéma 4) forment exclusivement des complexes chélates neutres (**17-22**), aussi bien en chimie du palladium, avec les précurseurs [$PdCl_2$(COD)] ou [PdMeCl (COD)] que du nickel, avec [$NiBr_2$(DME)].

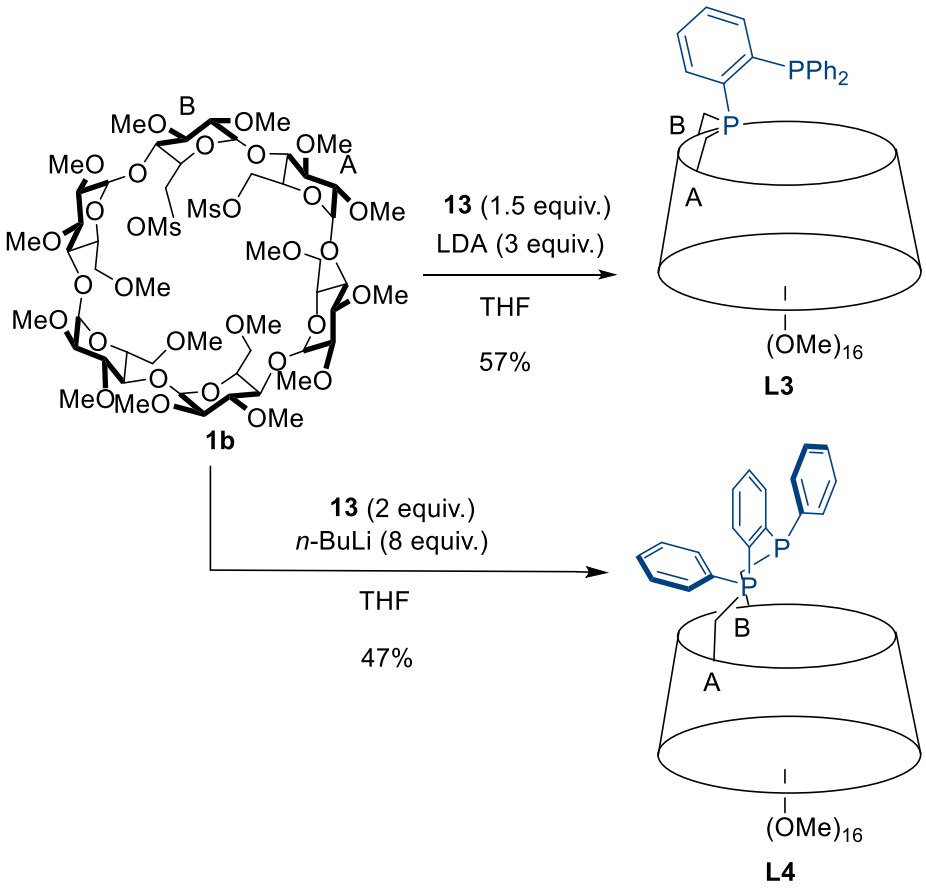

Schéma 4. Synthèse de deux diphosphines métalloconfinantes à partir du dimésylate **1b**.

For references, see page 10.

Bien que les diphosphines **L3** et **L4** soient toutes les deux capables d'encapsuler un centre métallique, l'environnement stérique autour du métal dans les complexes **17-19** est très différent de celui présent dans les complexes **20-22**. En effet, dans les complexes **17-19**, comme le montre la structure moléculaire de **17**, le plan formé par l'unité chélate P_2MX_2 est parallèle à l'axe passant par le milieu de la cavité, comme dans les complexes formés à partir du ligand P,N **L1**, alors que cette unité est quasiment perpendiculaire au même axe dans les complexes **20-22**. Comme pour les complexes P,N, les sites axiaux sont protégés par la paroi interne de la cavité cyclodextrine dans **17-19** ce qui n'est pas le cas des complexes **20-22**. Par ailleurs, l'encombrement stérique autour des deux ligands exogènes (méthyle ou chlorido) est fortement différencié comme dans les complexes chélates du ligand **L1** et contrairement aux complexes **20-22**. La réaction des diphosphines **L3** et **L4** avec [PdMeCl(COD)], au contraire du ligand P,N, fournit des proportions variables des deux isomères possibles (**18a,b** pour **L3** et **21a,b** pour **L4**) et nous avons étudié l'influence de la température et la nature du solvant sur la composition du mélange.

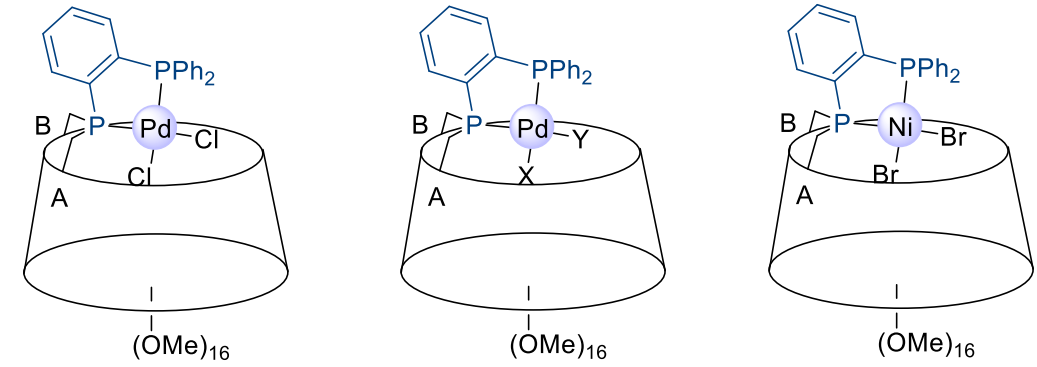

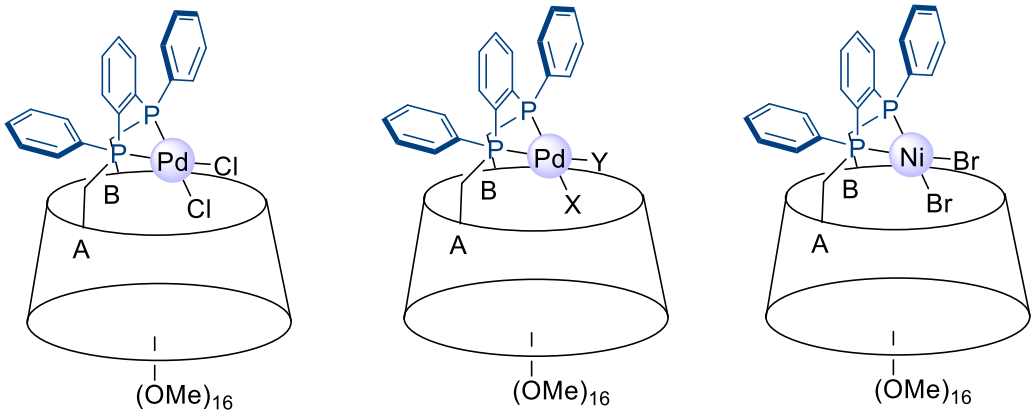

Figure 2. Complexes de Ni(II) et de Pd(II) des diphosphines **L3** et **L4**.

For references, see page 10.

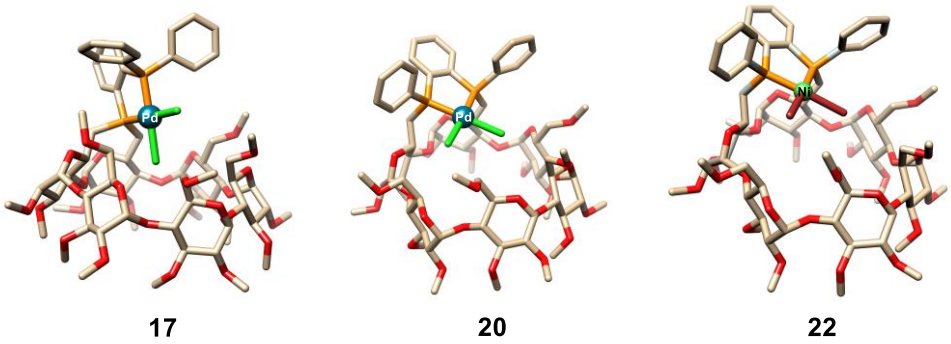

Figure 3. Structures radiocristallographiques des complexes **17**, **20** et **22**.

2.3 Evaluation des propriétés catalytiques des complexes de nickel en oligomérisation de l'éthylène

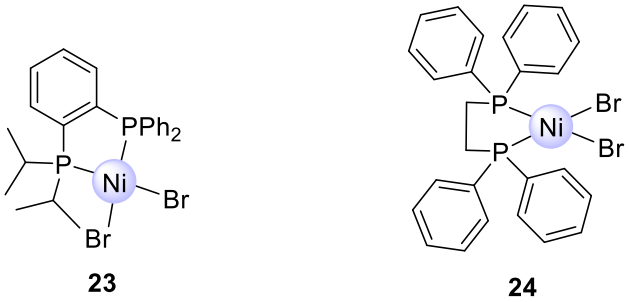

Figure 4. Structures des complexes non cavitaires **23** et **24**.

Tous les complexes du nickel, qu'ils soient cavitaires ou non, ont été testés en catalyse d'oligomérisation de l'éthylène. A des fins de comparaison, [$NiBr_2$(DPPE)] (**24**) (DPPE = 1,2-bis(diphenylphosphino)ethane) et l'analogue non cavitaire de **19** (**23**) ont également été inclus dans l'étude. Nous avons observé que le co-cotalyseur MMAO-12 (méthylaluminoxane modifié) donne les meilleurs résultats avec l'ensemble des précatalyseurs étudiés. Une étude préliminaire a montré que les conditions standard pouvaient être utilisées (quantité de catalyseur : 1×10^{-5} mol, MMAO-12 (400 equiv), toluène, éthylène (10 bar), volume total = 20 mL) pour ce type de complexes. Contrairement aux précatalyseurs non cavitaires, les complexes équipés d'une unité cyclodextrine fournissent presque exclusivement des oléfines C_4, en particulier les complexes présentant un encombrement stérique important au niveau des sites axiaux tels que **19** (jusqu'à 98% d'oléfines C_4). Par ailleurs, tous les catalyseurs cavitaires conduisent à une forte proportion d'α-oléfines, en particulier **6** et **19** (jusqu'à 91% de 1-butène pour **6**), ce qui n'est pas le cas de leurs homologues dépourvus de cavité. Par ailleurs, ces

For references, see page 10.

mêmes précatalyseurs (**6** et **19**) après activation par le MMAO sont également les moins actifs sur une durée de réaction courte (35 min) mais ne se désactivent que très peu après 24 h de réaction, ce qui témoigne de leur robustesse contrairement aux catalyseurs non cavitaires et au complexe **11** dans lequel les sites axiaux ne sont pas protégés.

3. Conclusion générale

La synthèse d'un nouveau ligand *cis*-chélatant de type P,N comportant une unité α-cyclodextrine perméthylée a été mise au point. En plus de ce ligand P,N, deux autres ligands cavitaires de type diphosphine ont été utilisés pour *cis*-chélater des métaux d^8 d'intérêt catalytique à l'intérieur d'une cavité α-cyclodextrine. La présence du métal à l'intérieur de la cavité cyclodextrine a pu être mise en évidence grâce à une caractérisation poussée des complexes par RMN 2D et de nombreuses études radiocristallographiques. Une étude portant sur l'oligomérisation de l'éthylène a permis de comparer les propriétés catalytiques des complexes de nickel métalloconfinés à leurs homologues non cavitaires. Il s'avère que le confinement du métal améliore significativement la sélectivité de la réaction, tant en termes de longueur de chaîne (C_4) que de regiosélectivité (formation d'α-oléfines), ainsi que la robustesse des catalyseurs.

4. Références

1. Sauter, D. W.; Taoufik, M.; Boisson, C., Polyolefins, a Success Story. *Polymers* **2017,** *9*, 185.

2. Hutley, T. J.; Ouederni, M., Polyolefins – The History and Economic Impact. In *Polyolefin Compounds and Materials*, Switzerland: Springer. Cham., **2016**; pp 13-50.

3. Breuil, P.-A. R.; Magna, L.; Olivier-Bourbigou, H., Role of Homogeneous Catalysis in Oligomerization of Olefins: Focus on Selected Examples Based on Group 4 to Group 10 Transition Metal Complexes. *Catal. Lett.* **2015,** *145*, 173-192.

4. Forestière, A.; Olivier-Bourbigou, H.; Saussine, L., Oligomerization of Monoolefins by Homogeneous Catalysts. *Oil Gas Sci. Technol. - Revue de l'IFP* **2009,** *64*, 649-667.

5. Belov, G. P.; Matkovsky, P. E., Processes for the production of higher linear α-olefins. *Pet. Chem.* **2010,** *50*, 283-289.

6. Skupinska, J., Oligomerization of .alpha.-olefins to higher oligomers. *Chem. Rev.* **1991,** *91*, 613-648.

7. Nicholas, C. P., Applications of light olefin oligomerization to the production of fuels and

For references, see page 10.

chemicals. *Appl. Catal. A-Gen.* **2017,** *543*, 82-97.

8. Makio, H.; Terao, H.; Iwashita, A.; Fujita, T., FI Catalysts for Olefin Polymerization—A Comprehensive Treatment. *Chem. Rev.* **2011,** *111*, 2363-2449.

9. Fischer, K.; Jonas, K.; Misbach, P.; Stabba, R.; Wilke, G. N., The "Nickel Effect" *Angew. Chem. Int. Ed. Engl.* **1973,** *12*, 943-953.

10. Galli, P., Forty years of industrial developments in the field of isotactic polyolefins. *Macromol Symp.* **1995,** *89*, 13-26.

11. Galli, P.; Vecellio, G., Technology: driving force behind innovation and growth of polyolefins. *Prog. Polym. Sci.* **2001,** *26*, 1287-1336.

12. Kaiser, J. M.; Long, B. K., Recent developments in redox-active olefin polymerization catalysts. *Coord. Chem. Rev.* **2018,** *372*, 141-152.

13. Sinn, H.; Kaminsky, W.; Vollmer, H.-J.; Woldt, R., "Living Polymers" on Polymerization with Extremely Productive Ziegler Catalysts. *Angew. Chem. Int. Ed. Engl.* **1980,** *19*, 390-392.

14. Keim, W., Oligomerization of Ethylene to α-Olefins: Discovery and Development of the Shell Higher Olefin Process (SHOP). *Angew. Chem. Int. Ed.* **2013,** *52*, 12492-12496.

15. Luk, Y.-Y. G.; Foucher, D. A.; Gossage, R. A., Recent advances in the homogeneous polymerisation of olefins mediated by nickel complexes. *Cr. Chim.* **2013,** *16*, 573-579.

16. Nifant'Ev, I.; Ivchenko, P., Fair Look at Coordination Oligomerization of Higher α-Olefins. *Polymers* **2020,** *12*, 1082.

17. McGuinness, D. S., Olefin oligomerization via metallacycles: dimerization, trimerization, tetramerization, and beyond. *Chem. Rev.* **2011,** *111*, 2321-41.

18. Olivier-Bourbigou, H.; Breuil, P. A. R.; Magna, L.; Michel, T.; Espada Pastor, M. F.; Delcroix, D., Nickel Catalyzed Olefin Oligomerization and Dimerization. *Chem. Rev.* **2020,** *120*, 7919-7983.

19. Bekmukhamedov, G. E.; Sukhov, A. V.; Kuchkaev, A. M.; Yakhvarov, D. G., Ni-Based Complexes in Selective Ethylene Oligomerization Processes. *Catalysts* **2020,** *10*, 498.

20. Dwadnia, N.; Roger, J.; Pirio, N.; Cattey, H.; Hierso, J.-C., Input of P, N-(phosphanyl, amino)-ferrocene hybrid derivatives in late transition metals catalysis. *Coord. Chem. Rev.* **2018,** *355*, 74-100.

21. Chen, Z.; Brookhart, M., Exploring Ethylene/Polar Vinyl Monomer Copolymerizations Using Ni and Pd α-Diimine Catalysts. *Acc. Chem. Res.* **2018,** *51*, 1831-1839.

22. Wang, Z.; Liu, Q.; Solan, G. A.; Sun, W.-H., Recent advances in Ni-mediated ethylene chain growth: Nimine-donor ligand effects on catalytic activity, thermal stability and oligo-/polymer structure. *Coord. Chem. Rev.* **2017,** *350*, 68-83.

For references, see page 10.

23. Guo, L.; Dai, S.; Sui, X.; Chen, C., Palladium and Nickel Catalyzed Chain Walking Olefin Polymerization and Copolymerization. *ACS Catal.* **2016,** *6*, 428-441.

24. Mu, H.; Pan, L.; Song, D.; Li, Y., Neutral Nickel Catalysts for Olefin Homo- and Copolymerization: Relationships between Catalyst Structures and Catalytic Properties. *Chem. Rev.* **2015,** *115*, 12091-137.

25. Wang, S.; Sun, W.-H.; Redshaw, C., Recent progress on nickel-based systems for ethylene oligo-/polymerization catalysis. *J. Organomet. Chem.* **2014,** *751*, 717-741.

26. Ye, Z.; Xu, L.; Dong, Z.; Xiang, P., Designing polyethylenes of complex chain architectures via Pd–diimine-catalyzed "living" ethylene polymerization. *Chem. Commun.* **2013,** *49*, 6235.

27. Sun, W.-H., Novel Polyethylenes via Late Transition Metal Complex Pre-catalysts. In *Polyolefins: 50 years after Ziegler and Natta II*, Berlin Heidelberg: Springer, **2013**; pp 163-178.

28. Ravasio, A.; Boggioni, L.; Tritto, I., Late-Transition Metal Complexes with Mixed NO, NS, NP Chelating Ligands for Olefin Polymerization Catalysis. In *Olefin Upgrading Catalysis by Nitrogen-based Metal Complexes I*, Dordrecht: Springer, **2011**; pp 27-118.

29. Johnson, L. K.; Killian, C. M.; Brookhart, M., New Pd(II)- and Ni(II)-Based Catalysts for Polymerization of Ethylene and .alpha.-Olefins. *J. Am. Chem. Soc.* **1995,** *117*, 6414-6415.

30. Bézier, D.; Daugulis, O.; Brookhart, M., Oligomerization of Ethylene Using a Diphosphine Palladium Catalyst. *Organometallics* **2017,** *36*, 443-447.

31. Lu, Z.; Chang, G.; Wang, H.; Jing, K.; Dai, S., A Dual Steric Enhancement Strategy in α-Diimine Nickel and Palladium Catalysts for Ethylene Polymerization and Copolymerization. *Organometallics* **2021**, *41*, 124-132.

32. Guan, Z., *Metal Catalysts in Olefin Polymerization*. Berlin Heidelberg: Springer, **2009**.

33. Guan, Z., Recent Progress of Catalytic Polymerization for Controlling Polymer Topology. *Chem.: Asian J.* **2010,** *5*, 1058-1070.

34. Camacho, D. H.; Guan, Z., Designing late-transition metal catalysts for olefin insertion polymerization and copolymerization. *Chem. Commun.* **2010,** *46*, 7879.

35. Guo, L.; Gao, H.; Guan, Q.; Hu, H.; Deng, J.; Liu, J.; Liu, F.; Wu, Q., Substituent Effects of the Backbone in α-Diimine Palladium Catalysts on Homo- and Copolymerization of Ethylene with Methyl Acrylate. *Organometallics* **2012,** *31*, 6054-6062.

36. Li, Y.; Pelzer, K.; Sechet, D.; Creste, G.; Matt, D.; Braunstein, P.; Armspach, D., A cavity-shaped *cis*-chelating P,N ligand for highly selective nickel-catalysed ethylene dimerisation. *Dalton Trans.* **2022**, 51, 11226-11230.

For references, see page 10.

37. Armspach, D.; Poorters, L.; Matt, D.; Benmerad, B.; Balegroune, F.; Toupet, L., A new approach to A,B-difunctionalisation of cyclodextrins using bulky 1,3-bis[bis(aryl)chloromethyl]benzenes as capping reagents. *Org. Biomol. Chem.* **2005,** *3*, 2588-92.

38. Engeldinger, E.; Poorters, L.; Armspach, D.; Matt, D.; Toupet, L., Diastereospecific synthesis of phosphinidene-capped cyclodextrins leading to "introverted" ligands. *Chem. Commun.* **2004,** 634-635.

39. Jouffroy, M.; Armspach, D.; Matt, D., Cyclodextrin and phosphorus(III): a versatile combination for coordination chemistry and catalysis. *Dalton Trans.* **2015,** *44*, 12942-69.

40. Phan, T.-A., PhD Thesis, *Université de Strasbourg* **2019**.

41. Henderson, A. R. P.; Kosowan, J. R.; Wood, T. E., The Truce–Smiles rearrangement and related reactions: a review. *Can. J. Chem.* **2017,** *95*, 483-504.

42. Snape, T. J., A truce on the Smiles rearrangement: revisiting an old reaction – the Truce-Smiles rearrangement. *Chem. Soc. Rev.* **2008,** *37*, 2452.

For references, see page 10.

Chapter I

General Introduction

I. 1. Cavity-shaped molecules within the context of catalysis

With the continuous development of science and technology, synthetic chemistry is playing an increasingly important role in our daily life as it allows the production of structurally very diverse molecular objects that are capable of performing a given function. Amongst those, synthetic catalysts occupy a place of choice as the development of compounds capable of speeding up a given reaction with high selectivity and low catalyst/substrate ratio is a key research area within the general context of green chemistry.[1] Nature's own catalysts that are enzymes are often a source of inspiration for the design of novel artificial catalysts.[2] Enzymes are proteins that act as biocatalysts with high catalytic efficiency, high substrate specificity compared to man-made catalysts as well as high selectivity (chemo-, regio- and stereoselectivity). In addition, natural enzymes work best under physiological conditions, namely in aqueous solution, at room temperature or slightly above and neutral pH.[3] However, the limited number of reactions that they are capable of catalyzing, their lack of robustness, their structural complexity and high molecular weight, the difficulty of geting hold of large quantities in a pure form and their limited reaction condition range make their use often uneconomical. In spite of these drawbacks, the exceptional catalytic properties of enzymes have prompted generations of chemists to develop simplified versions of the biocatalysts, in particular metal containing ones – the so-called metalloenzymes – since metals, in particular transition metals, considerably extent the reactivity and scope of the catalysts.[4] As early as the 1950s, small molecule polyamine copper complexes were used to catalyze the hydrolysis of fluorophosphates[5]. However, the first metal complex mimicking enzymes was not developed until 1970 by Breslow who was the first to use the term "artificial enzyme".[6] In order to reach the high selectivity displayed by enzymes, control of the steric environment all around the active site is needed in these so-called enzyme mimics. This is the reason why chemists working in this field focused from an early stage on macrocyclic and later on more sophisticated cage-like compounds. As early as 1967, C. J. Pedersen reported the first metal complex involving crown ether macrocycles,[7] which aroused great interest among chemists, and marked the emergence of macrocyclic chemistry within the more general context of supramolecular chemistry, the "chemistry beyond molecules" as adequately defined by J.-M. Lehn.[8] Not long after Pedersen's discovery, Lehn and Sauvage went a step further by creating a three-dimensional macrobicyclic structure, capable of fully encapsulating a metal ion to give what they called a cryptate.[9] In 1978, inspired by research on the noncovalent complexation of

For references, see page 59.

not only metal ions but also organic molecules by macrocyclic ligands, Cram proposed the concept of host-guest chemistry that is also key to enzyme mimicry.[10] Because of their brilliant contributions to supramolecular chemistry and its use in molecular machinery, Pedersen, Lehn and Cram were awarded the Nobel Prize in Chemistry in 1987[8,10-11], and later on Sauvage in 2016.[12]

In order to achieve full steric control of the active site, chemists soon turned their attention to macrocyclic compounds with thicker walls than the early macrocycles. Many of these cavity-shaped molecules can also act a supramolecular host towards organic guests which make them particularly attractive for enzyme mimicry since enzymes behave as supramolecular catalysts.[13] The four most common classes of cavity-shaped compounds are the cyclotriveratrilenes (CTVs), calix[n]arenes, and cucurbit[n]urils which are all synthetic molecular receptors together with cyclodextrins (CDs) which are naturally occurring. More recent representatives are the pillar[n]arenes, etc. although their use for catalytic purposes is far less developed.

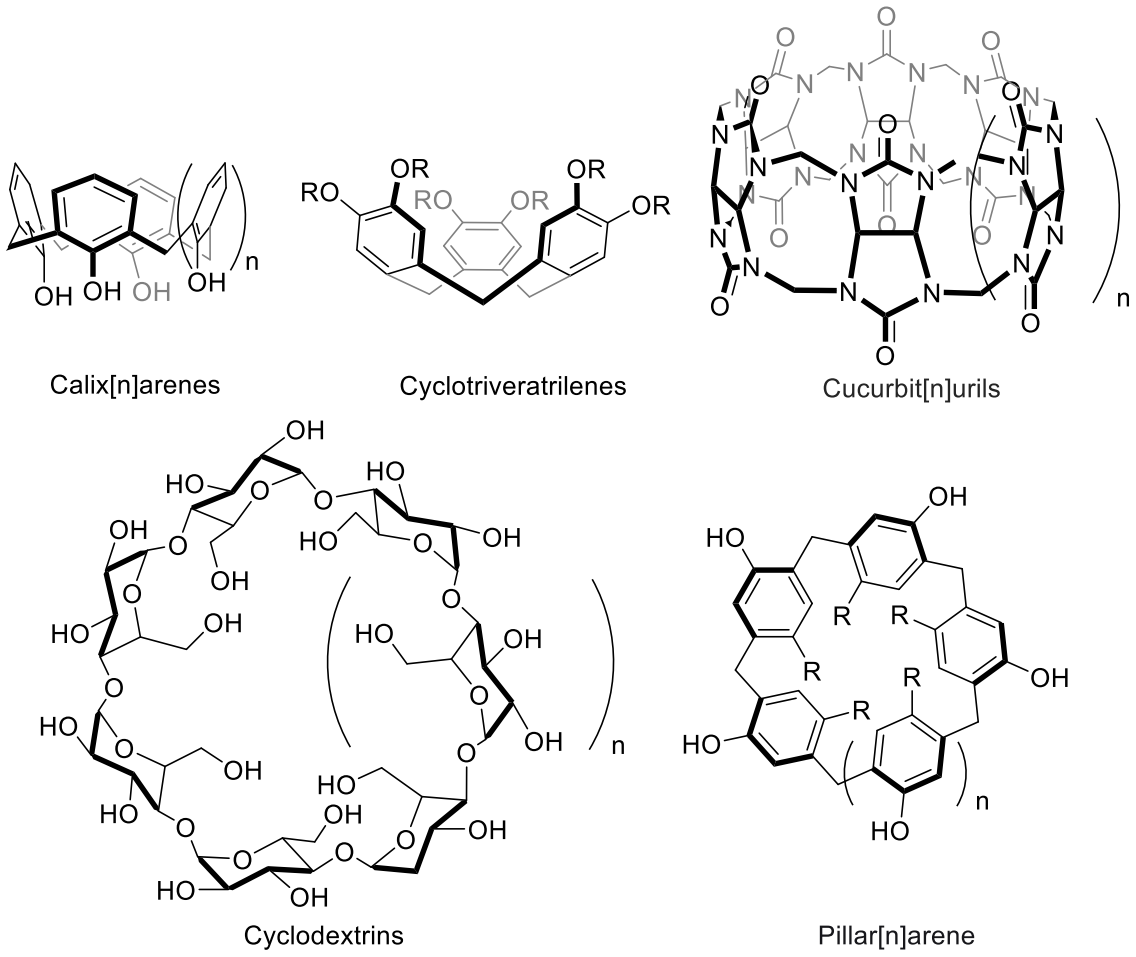

Fig 1. Cavity-shaped molecules that can act as supramolecular hosts.

For references, see page 59.

Cyclotriveratrilenes (CTVs) and calix[n]arenes belong to the cyclophane family. They are very hydrophobic macrocycles composed of benzene rings linked together by methylene bridges. CTVs were first synthesized independently by Ewins and Robinson in 1909 and 1915 respectively.[14] Chemically unmodified CTV is a macrocyclic trimer of veratrole with phenolic functions that can be used for introducing different substituents and functional groups. The bowl-shaped conformation of CTV and its derivatives allows them to complex guest molecules through a variety of non-covalent interactions. Owing to their electron-rich molecular concavity and the possibility of functionalizing its wide rim with diverse chemical groups, CTV derivatives have raised increasing interest in supramolecular chemistry. [15]

Calix[n]arenes are condensation products between phenol and formaldehyde, and represent the third generation of macrocycles after crown ethers and cyclodextrins in the field of supramolecular chemistry.[16] First reported in 1942, calix[n]arenes are characterized by their unique bowl-shaped structure of electron-rich cavities, the presence of two rims of different nature, one hydrophobic and one hydrophilic, and the possiblity to control the size of the cavity by adjusting the number of repeat units within the macrocycle.[17]

Cucurbit[n]urils, commonly made up of 5 to 8 glycoluril monomers linked by methylene bridges, are the fourth generation supramolecule obtained by the acid-catalyzed condensation reaction between glycoluril and formaldehyde.[18] Their shape is reminiscent of a pumpkin (a vegetable belonging to the Cucurbitaceae family), hence the name "cucurbituril" that was given to them. The cucurbit[n]uril has a rigid structure and hydrophobic cavity, and along the upper and lower edges are carbonyl functional groups with strong dipoles, which can efficiently complex cations. In addition, cucurbit[n]uril molecules equipped with large cavities can even complex two guest molecules to form ternary host-guest complexes, providing the opportunity to prepare multidimensional nanomaterials.[19] Despite their relatively late discovery, cucurbit[n]uril macrocycles have developed very rapidly and are now successfully used in *i.a.* molecular recognition, self-assembly, catalysis, drug delivery, biosensors, and luminescent materials.[20]

Chronologically, cyclodextrins (CDs) are the second generation of macrocyclic molecules after crown ethers, and consist of cyclic oligosaccharides produced from starch by enzymatic degradation.[21] They contain between 6 to 12 D-glucopyranose units but only the first three representatives, which are even commercially available, display a well-defined cavity. These are the α-, β- and γ-CDs, made up of 6, 7 or 8 glucopyranose units, respectively.[22] The main feature of CDs is their unique hydrophobic cavity capable of hosting a wide range of lipophilic guests in water and a hydrophilic outer surface that ensures water solubility.[23] Since CDs are

For references, see page 59.

made of glucose repeat units, they are water-soluble, non-toxic, relatively easy to modify thanks to their numerous hydroxyl groups, inexpensive and optically active. They display two rims, also called faces. The wider one displays secondary hydroxyl groups hence the name secondary face, while the narrow one is endowed with primary hydroxyl groups, hence the name primary face. The presence of all these features allows them to serve as ideal macrocyclic platforms for the construction of supramolecular assemblies involving diverse organic and inorganic molecules in water. [24] Because of their exceptional host-guest properties in this medium and their lack of toxicity, they have been widely used in fields as diverse as catalysis, including e.g. asymmetric catalysis, polymerization, materials science, drug delivery, and nanotechnology.[25]

Pillar[n]arenes, which were first reported by Ogoshi's group in 2008, are a new class of supramolecular hosts with a "pillar" type symmetrical structure, formed by hydroquinone units bridged in *p*-position by methylene bridges[26]. It has been proven that pillar[n]arenes combine many of the interesting features of conventional macrocyclic compounds. Furthermore, pillar[n]arenes also possess several other properties, such as excellent host-guest capabilities, planar chirality, and the ability to engage in self-assembling processes with a highly symmetrical structure due to their shape, which make them promising for applications in life sciences, nanoscience, molecular machines, molecular devices, self-assembly, biomaterials and fluorescence detection.[26-27]

In recent years, additional approaches involving supramolecular or coordination-assembled cages have been developed, notably those pioneered by Reek, to create a cavity-like environment around the metal center.[28] An extension to theese purely molecular systems are metal-organic frameworks (MOFs), which represent an important class of novel materials consisting of metal centers and organic multifunctional ligands. Over 15000 MOFs have been synthesized so far.[29] They combine the disciplines of organic and inorganic chemistry as well as material science, and display many interesting properties, of which the most important are their crystalline nature, permanent porosity, high specific surface area and low density.[30] All of these are relevant to their potential applications in e.g. gas storage, drug delivery, catalysis, and photoluminescence.[29,31]

I. 2. Metalloreceptors for catalytic applications

Metalloreceptors have recently attracted a great deal of attention because they can bind substrates through their primary ligand layer (i.e., metal-substrate binding), secondary ligand

For references, see page 59.

layer (i.e., ligand-substrate binding), or a combination of both to form a stable supramolecular system that provides robust and selective recognition as well as high catalytic efficiency.[32] Amongst all the catalytic systems, metal catalysts, especially those based on transition metals, occupy a place of choice including in nature with the so-called metalloenzymes, because of the diversity of reactions they can perform.[4a,33] Transition metal catalysts can easily give or accept electrons from other molecules, and therefore play an important role in electron transfer processes that occur in many catalytic reactions. In both natural and artificial systems, control of the active site which is the metal center itself is vital for achieving a high degree of selectivity in catalytic reactions. Only cavity-shaped ligands, whether supramolecularly assembled or purely covalent, decorated with specific donor atoms at given positions within the ligand's framework are capable of fully controlling the metal first coordination sphere.[34] To this end, several strategies have been devised to design macrocyclic ligands equipped with several and different donor atoms. Amongst those, chelating, bidentate systems are the most common as they are relatively easy to access and provide increased rigidity and control.[35]

I. 3. Cavity-shaped chelating hybrid ligands with differentiated donor groups

Hybrid ligands are bidentate or multidentate ligands containing at least two different types of chemical functions that are capable of binding a metal center (Fig 1).[36] Hybrid ligands include ligands that differ in the nature of the donor atoms such as hard and soft, ass well as those possessing similar donor atoms in chemically different moieties.[37] Combining different and contrasting metal binding functions in the same molecule is a highly desirable goal as hybrid ligands often display unique coordination and catalytic properties that cannot be reached with homofunctional ligands.[36]

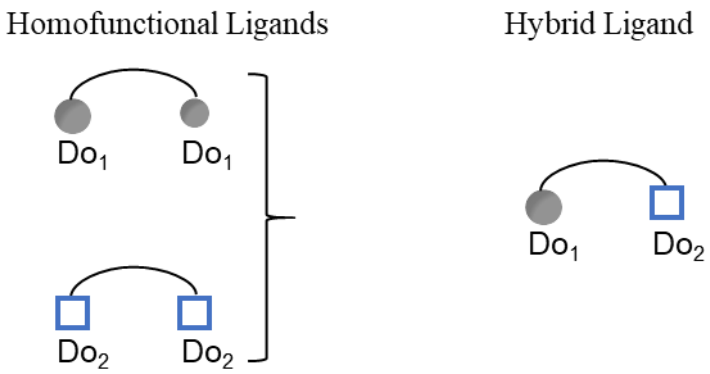

Fig 1. Homofunctional and hybrid ligands.[36]

For references, see page 59.

In recent years, there has been a proliferation of research work on the synthesis and applications of hybrid ligands and their transition metal complexes. The field has become very broad and diverse and we will concentrate here on the design and preparation of covalently constructed, cavity-shaped bidentate ligands (excluding supramolecularly assembled systems[25d,25g,28,29b,31h,38]), with different coordinating units are differentiated since the new molecules that have been synthesized during the course of this thesis all belong to that class of compounds. In the following, the cavity-shaped systems will be compared when possible to their cavity-free analogs. Particular attention will be put on the capacity of the cavity-shaped ligands to force metal encapsulation.

This particular class of ligands can be divided into two different types according to the electronic properties of the donor groups and the way they are connected to the macrocyclic structure (Fig 2). Bidentate podands in which a single dangling coordinating arm contains the two coordinating units with different or identical donor groups constitute the first type. In the second type, two chemically different or identical but nonequivalent coordinating units are grafted on two separate locations of the macrocyclic structure.

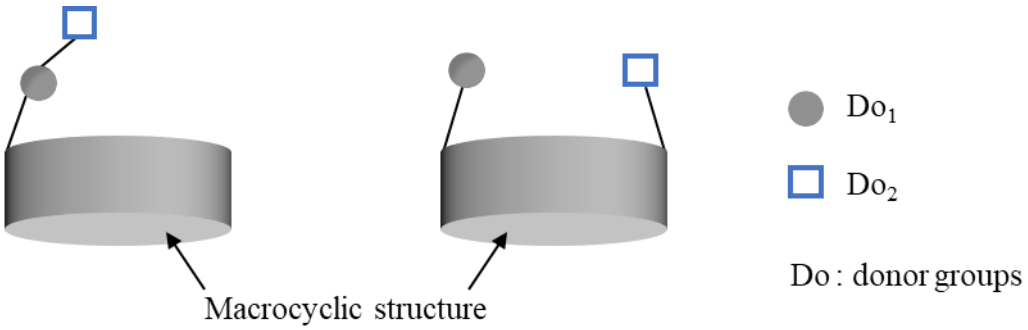

Fig 2. Schematic representation of the two different types of cavity-shaped bidentate ligands with nonequivalent coordinating units.

I. 3. 1. Cavity-shaped bidentate ligands equipped with a single coordinating arm

The first chelating ligand containing a molecular cavity was synthesized as early as the 1970s. In 1970, Breslow and Overman[6] synthesized a metalloenzyme mimic (**R1**)* called for the first

* The numbering of the compounds described in this chapter is preceded by an "**R**" (**R** = review).

For references, see page 59.

time “artificial enzyme” by esterification of a secondary alcohol group belonging to the wider rim of an α-CD with the 5-*m*-nitrophenyl ester of pyridine-2,5-dicarboxylic acid (Fig 3). Its nickel complex **R2** was found to be efficient at catalyzing the hydrolysis of *p*-nitrophenyl acetate in water. The effective catalytic cleavage of the ester function (10^3 times the uncatalyzed rate) was believed to result from the presence of the substrate within the CD host in water and its binding to the chelated nickel cation. As already postulated by the authors at that time, a greater rigidity which cannot be achieved with a dangling coordinating bidentate unit should improve the catalytic performance.

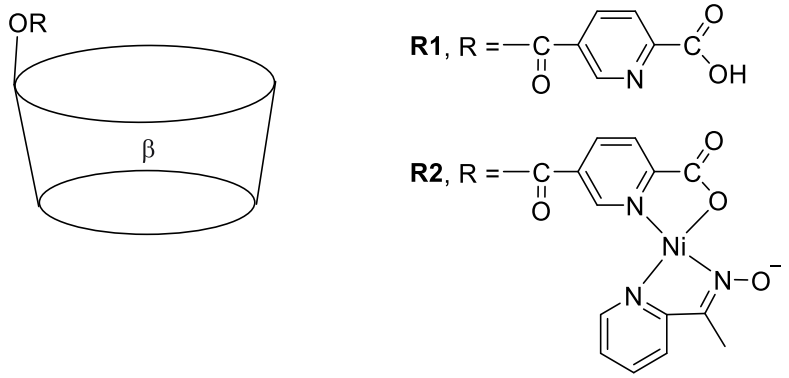

Fig 3. The first example of a cavity-containing bidentate ligand and its Ni(II) complex.

CDs are an important class of host molecules, and their ability to include guest molecules of suitable size, shape and chirality makes them potential chiral discriminating agents.[2,24,25g,39] In the early 1990s, Rizzarelli and Vecchio reported the synthesis of a series of histamine-modified β-CD ligands (**R3**, **R4**, **R5**, **R6**) (Fig 4) and the copper (II) complexes of the first three ones. The chiral discrimination towards the same enantiomeric pairs of amino acids was studied[40]. The authors showed that the unprotonated heterocyclic ring of ligand **R3** was located outside the cavity. However, the interaction of the imidazole ring with the β-CD cavity becomes stronger with an increasing degree of protonation suggesting partial inclusion of the protonated imidazole ring in water. In a similar way, the histamine fragment in **R3** when coordinated to copper(II) appears to interact with the cavity causing a “stiffening” of the whole structure. As the copper ion is dragged close to the cavity, the metal-coordinated L- or D-tryptophan guests are efficiently discriminated by the chiral CD since the two enantiomers lead to heteroleptic metal complexes with **R3**. These have very different stability constants in aqueous solution. While D-tryptophan may be included in the CD hollow, its L counterpart is likely to be located outside. The high enantiodiscrimination ability of **R4** when bound to copper(II) towards L- and

For references, see page 59.

D-tryptophan and the opposite order of elution for the two enantiomers in LEC experiments in which tryptophan-free copper CD complexes are present in the mobile phase were suggested to result from the "*cis*-effect". In such a case, similar donor groups belonging to the CD ligand and to the aminoacid guest are *cis* to each other in the CD/Cu/aminoacid ternary complex (here adjacent primary or secondary amino groups). However, because the α value which corresponds to the ratio of the stability constants between the L- and D-tryptophan complexes is highly dependent on the nature of the CD-based chelating *N,N* ligand (Table 1), a *cis*-*trans* equilibrium was postulated although this was not substantiated with an experimental study (Scheme 1).

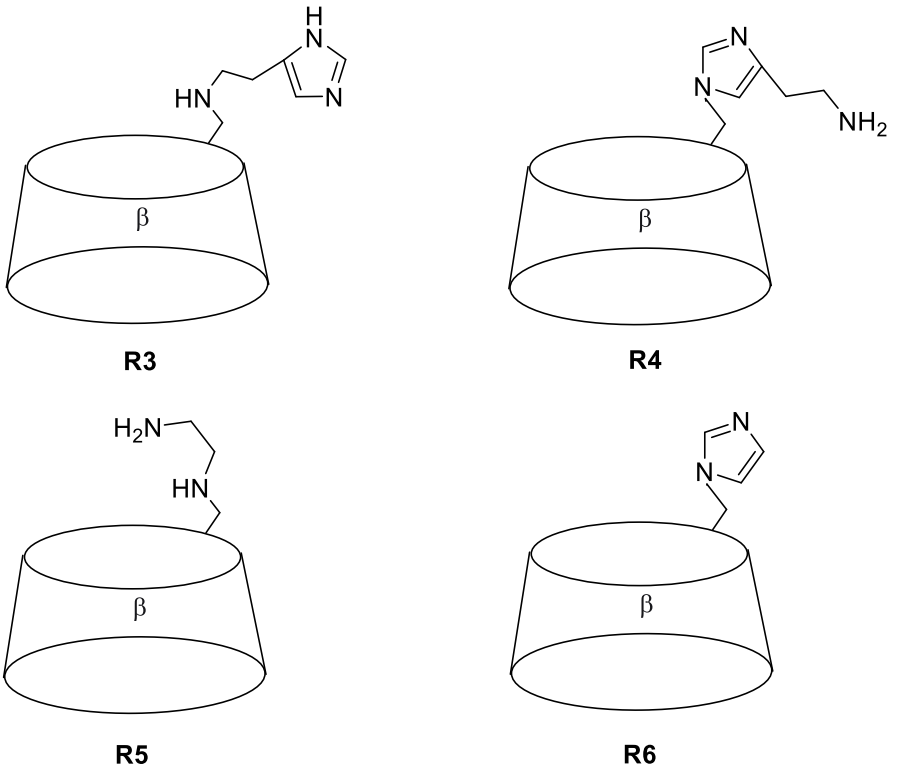

Fig 4. A series of histamine-modified β-CD ligands.

Table 1. Enantioselectivity factors α for tryptophan enantiomers in LEC using Cu(II)-L as chiral eluent

L	α (K'_L / K'_D)
R3	1.41
R4	2.4
R5	0.8

For references, see page 59.

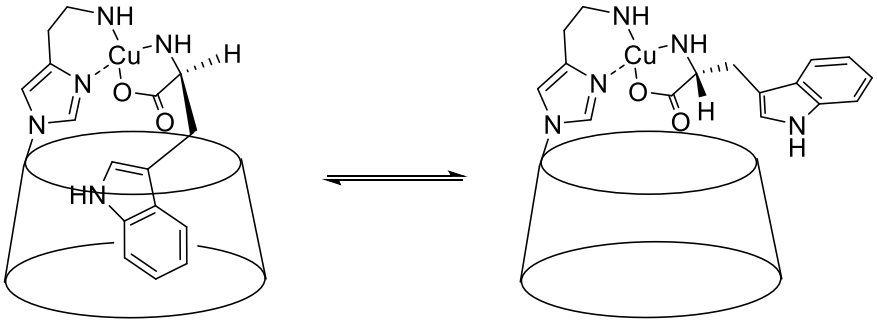

Scheme 1. Postulated *cis-trans* equilibrium for the CD/Cu/aminoacid ternary complex.

In 1995, a series of CD-based chelating ligands was reported by Carofiglio.[41] Diamines **R5**, **R7**, diaminophenol **R8** and iminoaminophenol **R9** were used as chiral ligands for Mo(VI)-catalyzed asymmetric oxidation of thioanisoles with hydrogen peroxide in three different media containing HEPES (4-(2-hydroxyethyl)piperazine-1-ethanesulfonic acid) buffer solution at pH 7 – heterogeneous (pure HEPES acid buffer solution), biphasic (HEPES buffer solution and 1,2-dichloroethane) and homogeneous (HEPES buffer solution/methanol) (Scheme 2). 6-Diamino-β-CD **R5** produced *ee* values above 50% whereas low *ee* values were observed with all the other ligands. Upon changing the reaction medium, only small variations of *ee* values (between 53% and 60% *ee*) were observed, which points to a scenario where the host-guest properties of the CD are not involved in enantiodiscrimination, although the inclusion of the substrate in the β-CD cavity even in the presence of methanol (homogeneous case) cannot be totally ruled out.

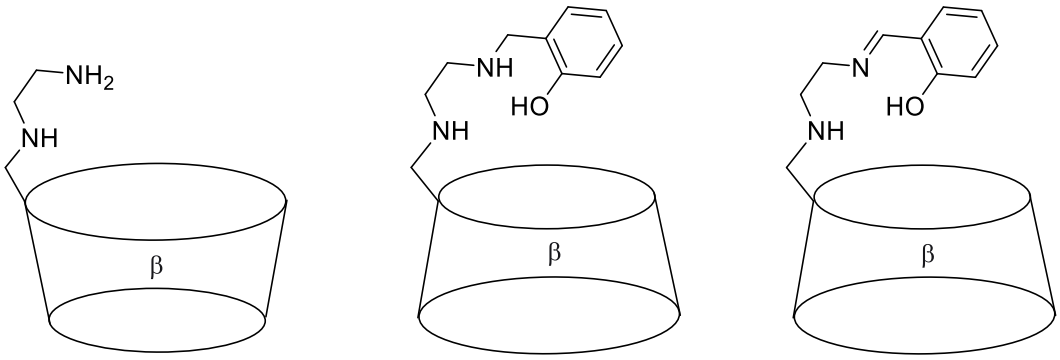

R7 **R8** **R9**

For references, see page 59.

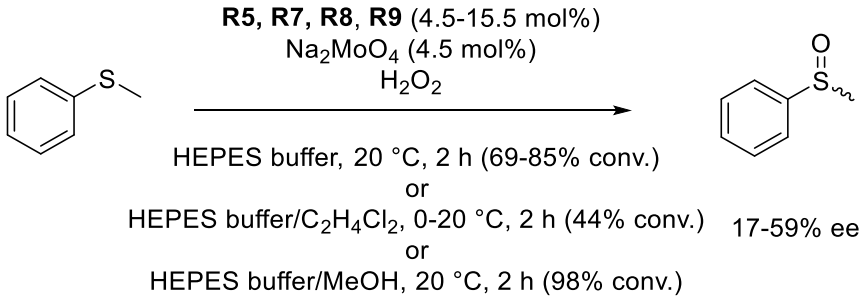

Scheme 2. Asymmetric oxidation of thionanisole in the presence of β-CD-based ligands.[41]

It has been noted that the amino derivatives of cyclodextrins can act as first coordination sphere ligands for a number of metal ions. Lincoln et al.[42] prepared a 6^A-(3-aminopropylamino)-6^A-deoxy-β-CD (**R10**) (Fig 5) as well as the nickel(II) complex obtained by reacting ligand **R10** with $Ni(ClO_4)_2$. Although the structure of the complex is unclear, it was shown from a pH titration study that in the presence of the Ni salt, **R10** binds the two enantiomers of the tryptophan anion with unequal strength and exhibits a tenfold enantioselectivity between (*R*)-trp$^-$ and (*S*)-trp$^-$ enantiomers in aqueous solution, possibly as a result of the inclusion of the indole moiety in the stronger (*R*)-trp$^-$ complex, although this feature was not fully established. This study also indicated that the presence of the metal is important for chiral discrimination and the cavity has a significant role to play in promoting the formation of heteroleptic complexes at the expense of homoleptic ones involving two CD ligands. The influence of the metal ion on this enantiodiscrimination process was also examined with M = Co(II), Cu(II) or Zn(II)) in the CDligand/M/trp$^-$ combination using again pH titration. However, compared to Ni(II), the enantiodiscrimination with these metal ions ranged from modest to none in the case of Zn(II). This observation was believed to be related to the flexibility of [Zn(**R10**)(*R*)-trp]$^+$ and [Zn(**R10**)(*S*)-trp]$^+$ caused by the absence of ligand-field-generated geometric constraints on d^{10} Zn^{2+}.

For references, see page 59.

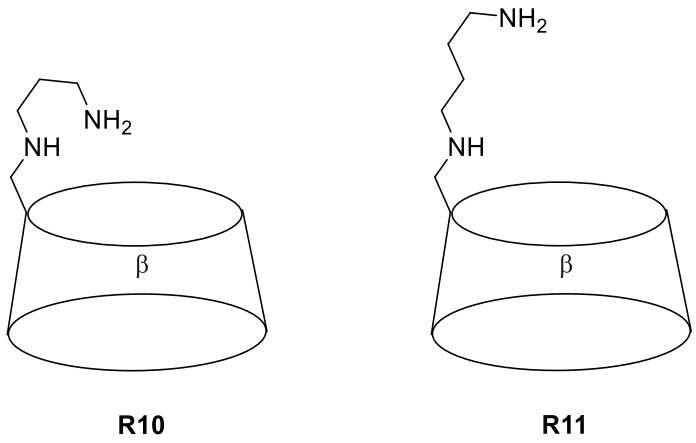

Fig 5. Bidentate N,N ligands **R10** and **R11** derived from β-CD.

On the basis of previous studies, three diaminoalkane-type derivatives, including 6-deoxy-6-[1-(2-amino)ethylamino]-β-CD (**R5**), 6-deoxy-6-[1-(3-amino)propylamino]-β-CD (**R10**) and 6-deoxy-6-[1-(4-amino)butylamino]-β-CD (**R11**) (Fig 5), were used in 2006, by McNamara et al. to investigate the influence of an increasing chain length in the diaminoalkane moiety on enantioselectivity.[43] Circular dichroism was used to study the inclusion of the enantiomers of phenylalanine, tyrosine and DOPA (dihydroxyphenylalanine) in the CD cavity for Cu(II) heteroleptic complexes involving the CD ligands and the various aminoacids. Comparison between the circular dichroic molar extinction coefficients (Δε) of two diastereomeric complexes involving enantiomeric aminoacids allowed to assess the degree of guest inclusion in each case. The studies point to a scenario in which the D-enantiomer is always more encapsulated than the L-enantiomer (scheme 3), knowing that the presence of the known competitive guest 1-adamantanol produces most changes in the CD spectra of complexes involving D-enantiomers, in particular in the case of D-DOPA. The results also suggest that [Cu(**R5**)] is the most enantioselective host for all of three guests. The order of enantioselectivity towards the different guests in the series is as follows: [Cu(**R5**)] > [Cu(**R10**)] > [Cu(**R11**)] for phenylalanine and DOPA while for tyrosine the order is: [Cu(**R5**)] > [Cu(**R11**)] > [Cu(**R10**)]. Furthermore, due to its d^9 configuration, Cu(II) displays a tetragonally distorted octahedral coordination sphere and thus should inhibit the inclusion of the L-enantiomer because of severe steric constraints caused by the coordination of this stereoisomer. For [Cu(**R10**)], the enantioselection process is not possible due to the structure of the 1,3-diaminopropane moiety, which is too flexible to allow each enantiomer to interact with the cavity in a distinc manner. In the case of CuCDBn the length of the alkane chain may prevent

For references, see page 59.

the diaminoalkane moiety from acting as a bidentate ligand, thus again facilitating the inclusion of both enantiomers in the cavity.

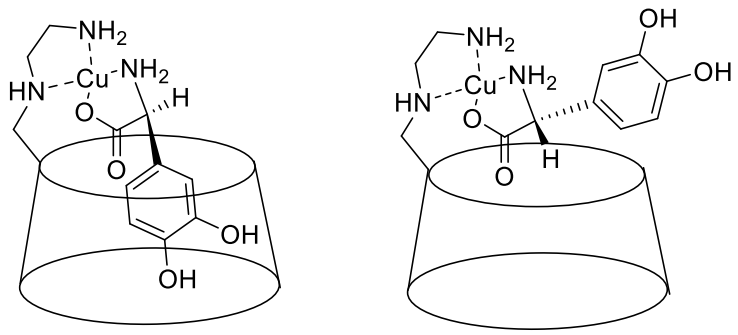

Scheme 3. Proposed structures of the diastereomers [Cu(**R5**)(D-DOPA)]$^+$ (left) and [Cu(**R5**)(L-DOPA)]$^+$ (right).

Woggon reported water-soluble Ru(II) complexes of the β-CD modified amino alcohols **R12** and **R13**.[44] These Ru(II) catalysts were able to reduce both aromatic and aliphatic ketones with high enantioselectivities (*ee* value up to 97% for **R13**) in a mixture of H_2O/DMF (3:1) (Scheme 4). Conversely, the CD-free analogous Ru complex only produced 50% *ee* in favor of the same isomer, which points to the fact that β-CD plays an important role in enantiodiscrimination, probably via substrate encapsulation. The significance of the N-H group in the coordinating arm was also proven since its replacement with a tertiary amine led to an inactive system that was unable to activate the carbonyl group through hydrogen transfer.

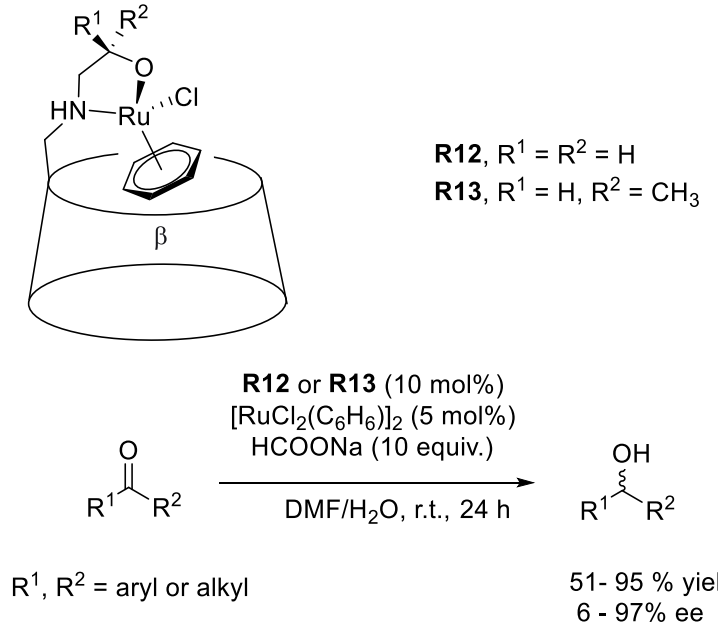

Scheme 4. Ru(II)-catalyzed asymmetric reduction of ketones using monosubstituted CDs **R12**, **R13** as ligands.[44]

For references, see page 59.

In 2012, Ji et al.[45] reported similar podands based on amino alcohol-modified β-CDs in part previously described by Woggon (Fig 6). These ligands were reacted with sodium molybdate and the resulting complexes were used for the asymmetric oxidation of thioanisole. A moderate *ee* value (56%) was achieved in aqueous buffer solution for the best performing ligand **R14a**. The enantioselectivity was highly dependent on pH and the structure of the coordinating unit. Surprisingly, the presence of an additional stereogenic (*S*) center in the coordinating arm did not improve the enantioselectivity. This moderate result was ascribed to two competing catalytic processes taking place within the CD cavity. One of them involved a thioether group located near the metal unit at the primary face is intramolecular and highly enantioselective whereas the second is intermolecular and poorly selective because the thiophenol function is upside down in the inclusion complex, away from the primary face-grafted metal unit.

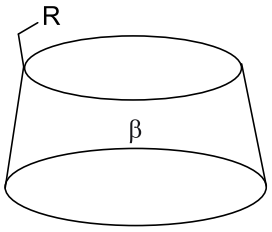

R14a: R = $NHCH_2CH_2OH$
R14b: R = $N(CH_2CH_2OH)_2$
R14c: R = $NHCH_2CH_2CH_2OH$
R14d: R = $NHCH_2CH(CH_3)OH$
R14e: R = (S)-$NHCH_2CH(CH_3)OH$
R14f: R = $N[CH_2CH(CH_3)OH]_2$
R14g: R = $N(CH_3)CH_2CH_2OH$

Fig 6. A series of ligands based on amino alcohol-modified β-CDs.

One year later, the same ligands together with **R5** were employed by the same group to form Ru(II) artificial metalloenzymes, which were then applied to the asymmetric hydrogenation of aromatic ketones in DMF/water mixture (Scheme 5).[46] Only *ee* values up to 80% could be obtained with the combination of **R5** and $[RuCl_2(Mesitylene)]_2$ and only with bulky ketones such as 2-acetylnaphtalene. As in Woggon's study[44], tertiary amine-based systems proved to be nonselective and poorly active. Catalysts with bulky aromatic ligands, such as with a mesitylene bound to the metal tend to perform better in terms of enantioselectivity than less sterically crowded benzene analogs albeit with reduced activity.

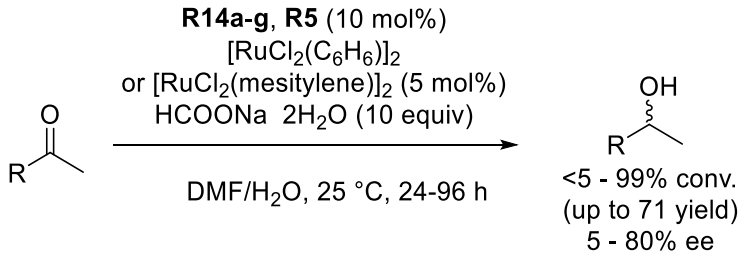

Scheme 5. Ru(II)-catalyzed asymmetric reduction of aromatic methyl ketones using monosubstituted CDs **R14a-g**, **R5** as ligands.[46]

For references, see page 59.

Moving away from traditional enzyme mimics which solely deal with biological relevant reactions such as hydrolysis, Reetz et al. sought to combine in the same system host-guest effects with transition-metal and phase-transfer catalysis in 1993.[47] He prepared a water-soluble phosphine equipped with a β-CD unit (**R15**) and its corresponding rhodium complex **R16** (Fig 7). Their intention was to test the catalytic activity of such a potential supramolecular catalyst in a two phase (org-H_2O) system. However, this Rh-complex was found not to be an effective catalyst, but later in 2001[48], his group conducted a further study on this ligand. The crystal structure analysis of **R15** revealed selective intramolecular complexation of one of the two diastereotopic phenyl groups, which induced chirality at phosphorus. Despite the fact that no unequivocal explanation for the observed *S*-configuration in the crystal was given, this phenomenon of diastereotopic group recognition, which occurs when selective recognition of heterotopic groups takes place within the same chiral molecule (Scheme 6), was believed to be the first such example. As an extension of the ongoing work, a gold (I) complex (**R17**) derived from the same ligand was also prepared[49]. Further investigations are needed since this complex may act as an antiarthritic drug.

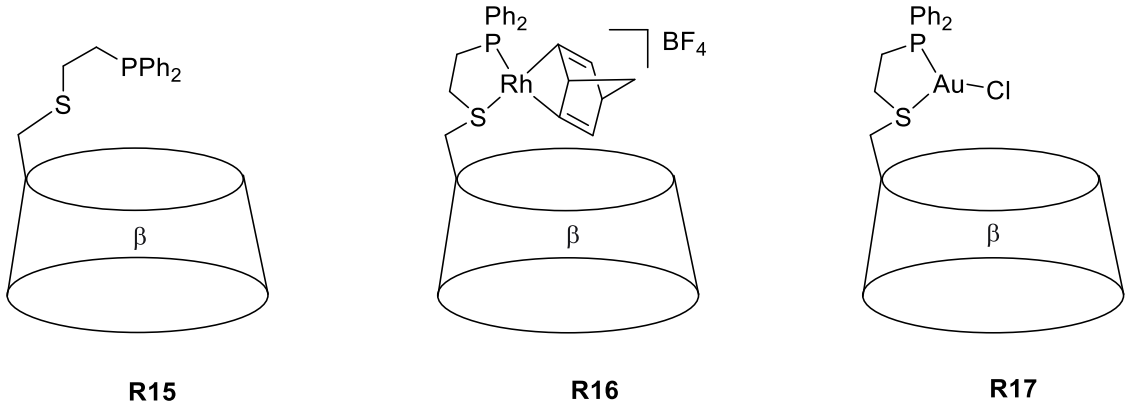

Fig 7. β-CD-based ligand **R15** and its metal complexes **R16** and **R17**.

For references, see page 59.

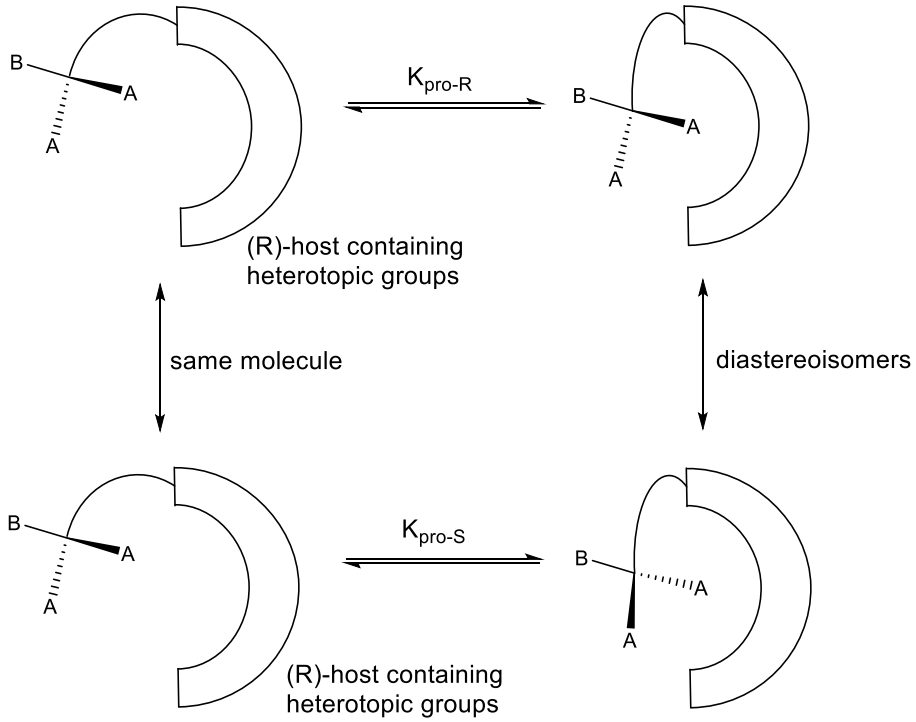

Scheme 6. Diastereotopic group recognition by a chiral host.[48]

In the same vein, Krepinsky and Jia[50] grafted a β-CD unit to a PPM ligand [PPM = (2S, 4S)-(−)-4-(diphenylphosphino)-2-(diphenylphosphinomethyl)pyrrolidine] (**R18**), which displays good catalytic properties.[51] In order to keep the active metal center further away from the β-CD cavity, another ligand CD-containing PPM ligand (**R19**) was prepared for comparative purposes.[52] Rhodium and platinum complexes of these two ligands were then synthesized (Fig 8). NMR studies revealed that [Rh(COD)(**R18**)]$^+$ and [$PtCl_2$(**R18**)] adopt a square-planar four-coordinate geometry, with two coordinated phosphorus atoms of the CD ligand. As for the complexes derived from **R19**, the coordination sphere of the $PtCl_2$ complex was the same as that of **R18**, but in the case of rhodium, a five-coordinated complex was formed in which the nitrogen atom is also coordinated to the metal as in cavity-free PPM[53]. Significant steric hindrance caused by the proximity of the CD unit to the coordinating PPM unit in **R18** was invoked to explain the difference in coordination behavior between the two ligands. Unfortunately, no catalytic study was conducted to compare the performances of these ligands.

For references, see page 59.

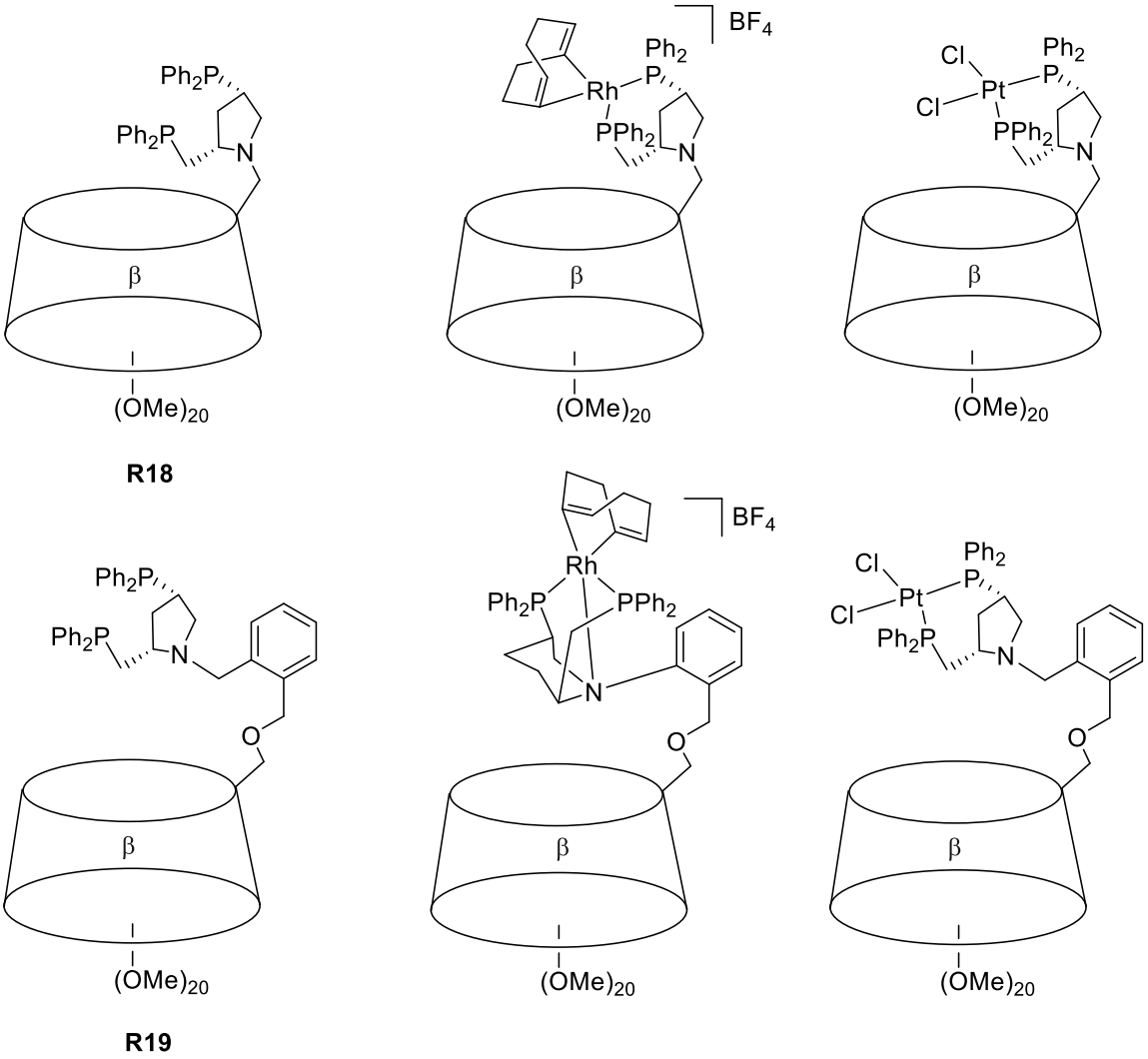

Fig 8. β-CD-based ligand **R18**, **R19** and their metal complexes.

In 2004, a Pd(II) chelate complex (**R20**) of a β-CD-derived disulfide was synthesized by Kostic et al.[54] Although the exact structure of the complex is not known, chelation of Pd(II) was confirmed by NMR studies. The aqua complex $[Pd(H_2O)_4]^{2+}$ was shown to promote the challenging hydrolysis of the X-proline amide bonds in peptides such as bradykinin in neutral aqueous solutions albeit in an unselective manner. When the Pd(II) catalytic center was grafted on a CD unit as in **R20**, only one out of the three X-proline bonds of bradykinin was cleaved as a result of the inclusion of the aromatic residue of a phenylanaline unit neighboring the proline unit undergoing hydrolysis as suggested by ROESY experiments (Fig 9). This work exemplifies the fact that when associated with metals, the CD cavity can act as an efficient recognition unit and bring selectivity to an otherwise unselective metal-mediated reaction.

For references, see page 59.

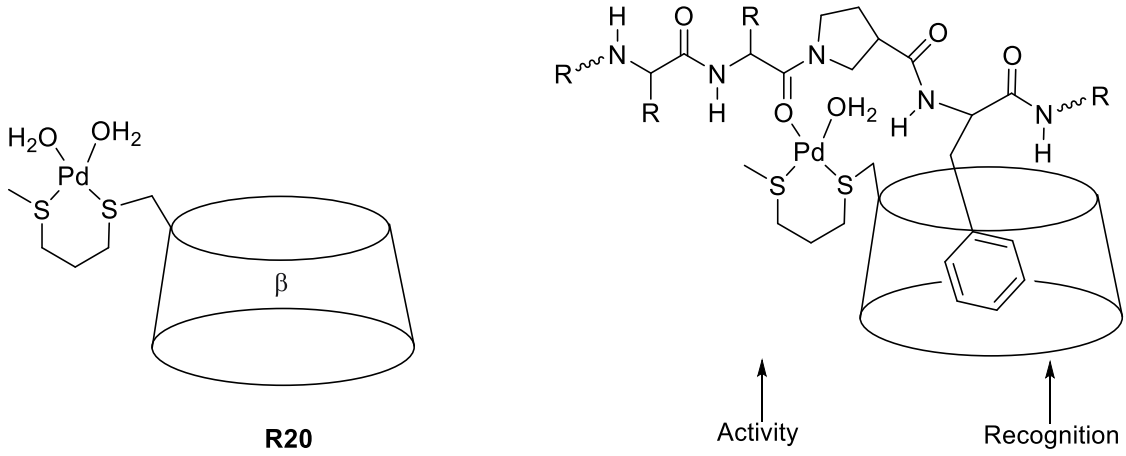

Fig 9. Pd(II) chelate complex (**R20**) and prompted sequence-specific, hydrolytic cleavage of the X-Pro bond.

Ding et al. prepared a water-soluble triazolyl β-CD supported palladium complex **R21a**, which was then applied in Suzuki-Miyaura cross-coupling reactions in neat water (Scheme 7).[55] The reaction conditions were optimized using *p*-bromobenzaldehyde and phenylboronic acid as model substrates. The reaction of boronic acids with halobenzenes in the presence of Na_2CO_3 as a base and **R21a** (10^{-7} mol%) as a catalyst resulted in very high yields of the corresponding biaryl products, with turnover numbers (TONs) and turnover frequencies (TOFs) reaching 9.9 $\times 10^8$ and 4.9×10^8 h^{-1}, respectively. Both the cavity-free complex **R21b**[56] and $Pd(OAc)_2$ performed much more poorly compared to CD containing **R21a**, in particular with hydrophobic substrates, with yields not exceeding 40% vs up to 98% for **R21a**. This clearly points to an active role played by the CD cavity. Obviously, the strongly hydrophilic β-CD fragment of the complex improves the water solubility of the catalyst, which is likely to act as a phase-transfer-catalyst capable of accelerating transformations in biphasic media. Moreover, the 2D ROESY NMR spectrum of **R21a** in the presence of the *p*-bromobenzaldehyde in D_2O shows correlations between aromatic protons of the substrate and CD inner-cavity protons, indicating that the cavity is able to accommodate the substrate and capable of acting as a recognition unit.

For references, see page 59.

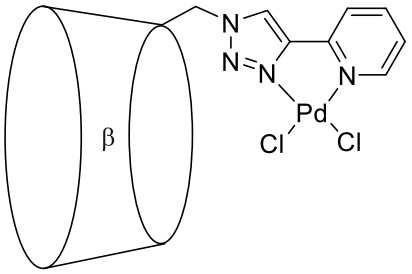

R21a

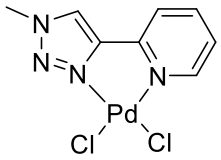

R21b

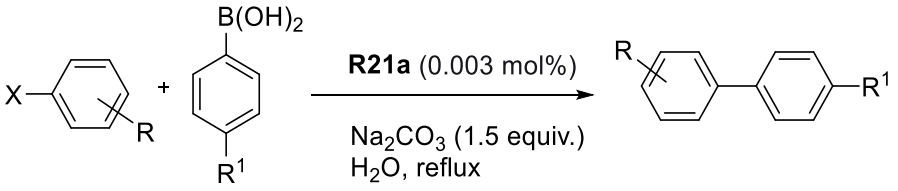

R^1 = H; X = Br; R = H, CHO, COOH, 3-NO_2, CH_3; yield = 98%, 98%, 93%, 18%;
R^1 = OCH_3; X = I; R = H, F, $COCH_3$, 3-NO_2; yield = 95%, 93%, 90%, 93%.

Scheme 7. Suzuki coupling reaction catalyzed by **R21a**.

Very recently, Jung synthesized a similar nitrogen ligand, by grafting an aminoethylamino arm onto a native β-CD platform.[57] Again a water-soluble Pd(II) complex (**R22**) was formed upon reaction of the free ligand with $Pd(OAc)_2$. Coordination of the N,N ligand to palladium was confirmed by NMR, FT-IR, FE-SEM, DSC and MS studies. This catalyst **R22** was used in Suzuki-Miyaura cross-coupling reactions between arylboronic acid/arylboronic ester and aryl halides in water under mild conditions (Scheme 8). Good catalytic activity (up to 94% yield) over a short period of time (1 h) was noted with both aryl bromides and iodides, but as expected less so with aryl chlorides (54%). Only traces of cross-coupling products were detected when a β-CD and $Pd(OAc)_2$ mixture was used as catalyst. It is difficult to assess the importance of the cavity in the catalytic reaction since a cavity-free N,N analogous ligand was not tested under the same reaction conditions. However, clear evidence for the ability of catalyst **R22** to form an inclusion complex with the substrate molecule 1-bromo-4-nitrobenzene came from ROESY experiments pointing to a reaction taking place, at least in part within the CD cavity. The yield of the reaction dropped from 94% to 89% after performing seven recycling runs involving the extraction of the organic product from the catalyst-containing aqueous phase with ethyl acetate. This indicates a low degree of catalyst leaching from the water phase to the organic one.

For references, see page 59.

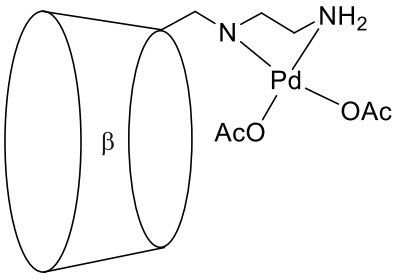

R22

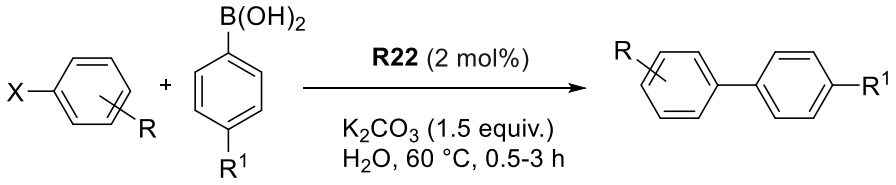

X = I; R = H, R^1 = H, 2-/3-/4-Me, 2-pyridyl, yield = 92-95%
X = Br; R = 3-/4-/MeO, 2,4-diF, 2,4- diCF_3, 2-CHO
R^1 = 4-MeO, 4-NO_2, 4-HO, yield = 90-98%
X = Cl; R = H, R^1 = 4-NO_2, yield = 54%

Scheme 8. Suzuki cross-coupling reaction catalyzed by **R22**.

In the same vein, three novel water-soluble picolinamide-modified β-CDs were also synthesized and reacted with $Pd(OAc)_2$ by Yang et al.[58] The resulting Pd(II) complexes act as supramolecular catalysts for Suzuki-Miyaura cross-coupling of aryl, benzyl and allyl halides with arylboronic acids in aqueous solution (Scheme 9). The catalytic results showed that the length of the spacer linking the picolinamide unit to the CD affects the catalytic activity, with the efficiency sharply decreasing with increasing linker length. This might be the result of the metal moving away from the cyclodextrin cavity. The complex **R23** gave rise to very high TONs and TOFs (TON 1.5-2.0 × 10^7, TOF 2.6 × 10^6-2.0 × 10^8 h^{-1}) with low catalyst loadings (5 × 10^{-6} mol%). Moreover, as in the previous study, the aqueous phase containing the catalyst can be reused for at least eight runs after extraction of the organic products with ethyl acetate without a significant loss of activity (97% to 90%). A putative mechanism involving Pd(II)/Pd(IV) centers was proposed (Scheme 10) based on experimental observations and DFT calculations.

For references, see page 59.

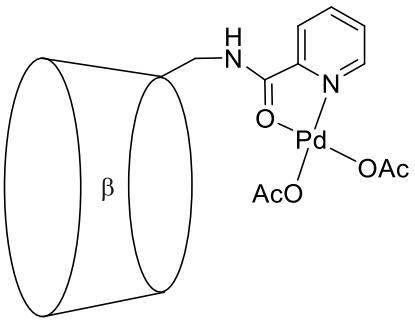

R23

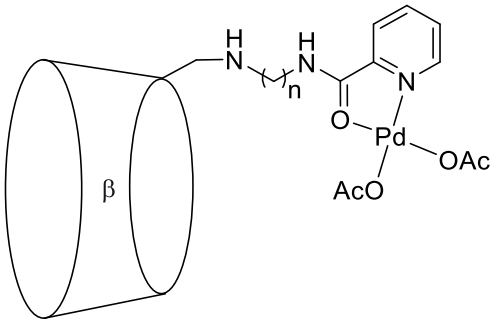

R24, n=2
R25, n=3

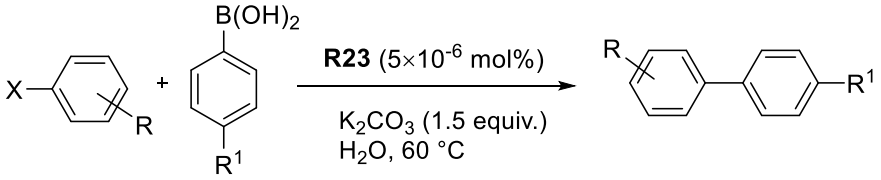

X = I; R = 2-/3-/4-Ac,4-NO_2, R^1 = 4-Me, 4-MeO, (30min), yield = 92-99%
X = Br; R = 2-/3-/4-/MeO, 2-/3-/4-Ac, 2-CN, 2-/3-/4-NO_2
R^1 = 3-/4-Me, 3-/4-F, (0.5-1.5 h), yield = 74-98%
X = Cl; R = 3-/4-Me, 2-/3-/4-Ac, 3-/4-CN, 4-NO_2, R^1 = 4-MeO, 4-Ac, (3-6 h), yield = 92-99%

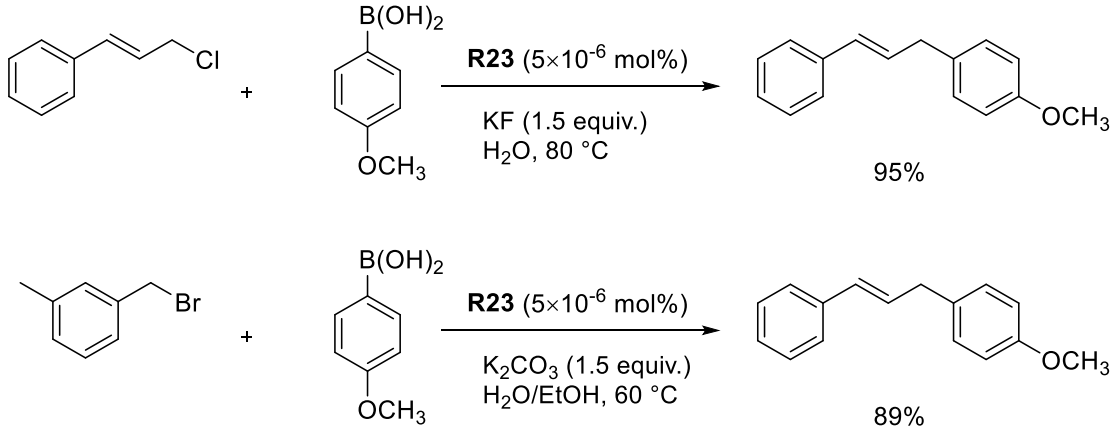

Scheme 9. Suzuki-Miyaura cross-couplings with **R23** as catalyst.[58]

For references, see page 59.

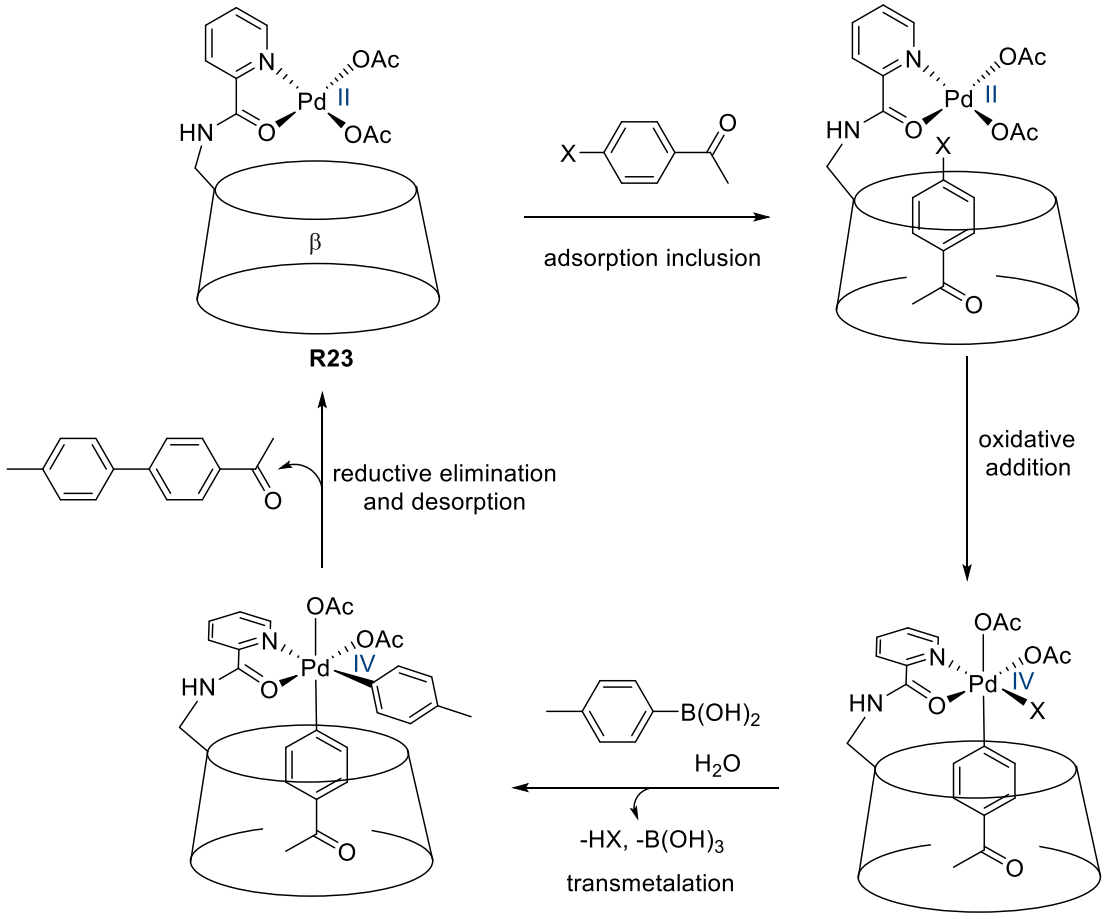

Scheme 10. Possible mechanism for the Suzuki coupling catalyzed by **R23**.[58]

Capitalizing on the fact that randomly-methylated β-CDs (RAME-β-CDs) are efficient mass transfer agents[39] in aqueous biphasic media, Hapiot et al.[35b] synthesized Pd(II) complexes from β-CD-based N,N-bidentate ligands (Fig 10). The water-soluble Na_2PdCl_4/N,N ligand catalytic systems are efficient catalysts for the Heck coupling of aryl iodides with functional olefins such as styrene and methyl acrylate in aqueous medium at 100 °C (Scheme 11). Fast equilibrium between free ligand **R26** and the Pd-species was detected by NMR measurements, whereas the observation of three sets of resonances in the ^{1}H spectra revealed a slow equilibrium between free ligand **R27** and the Pd(II) complexes **R28** and **R29** on the NMR time scale. This difference in coordination behavior was believed to result from the hemilability of the amino group of **R26** towards the Pd center, which incidentally also makes it a more effective catalyst. As in the aforementioned analogous complexes, inclusion of an aryl halide substrate such as *p*-methoxyphenyl iodide in the CD cavity was clearly established by means of a 2D T-ROESY NMR experiment in D_2O and recyclability of the system was demonstrated even if its activity tends to decrease after recycling not because of catalyst desactivation but increase of salt concentration (NaI) in the catalyst-containing aqueous phase. The latter three

For references, see page 59.

examples prove that CD-based catalysts when sufficiently water-soluble act as true supramolecular catalysts for industrially relevant carbon-carbon couplings with the reaction likely to take place just above the primary face. Indeed, the efficacy of the catalytic systems is greatly reduced if the substrate is too large to fit in the CD cavity.

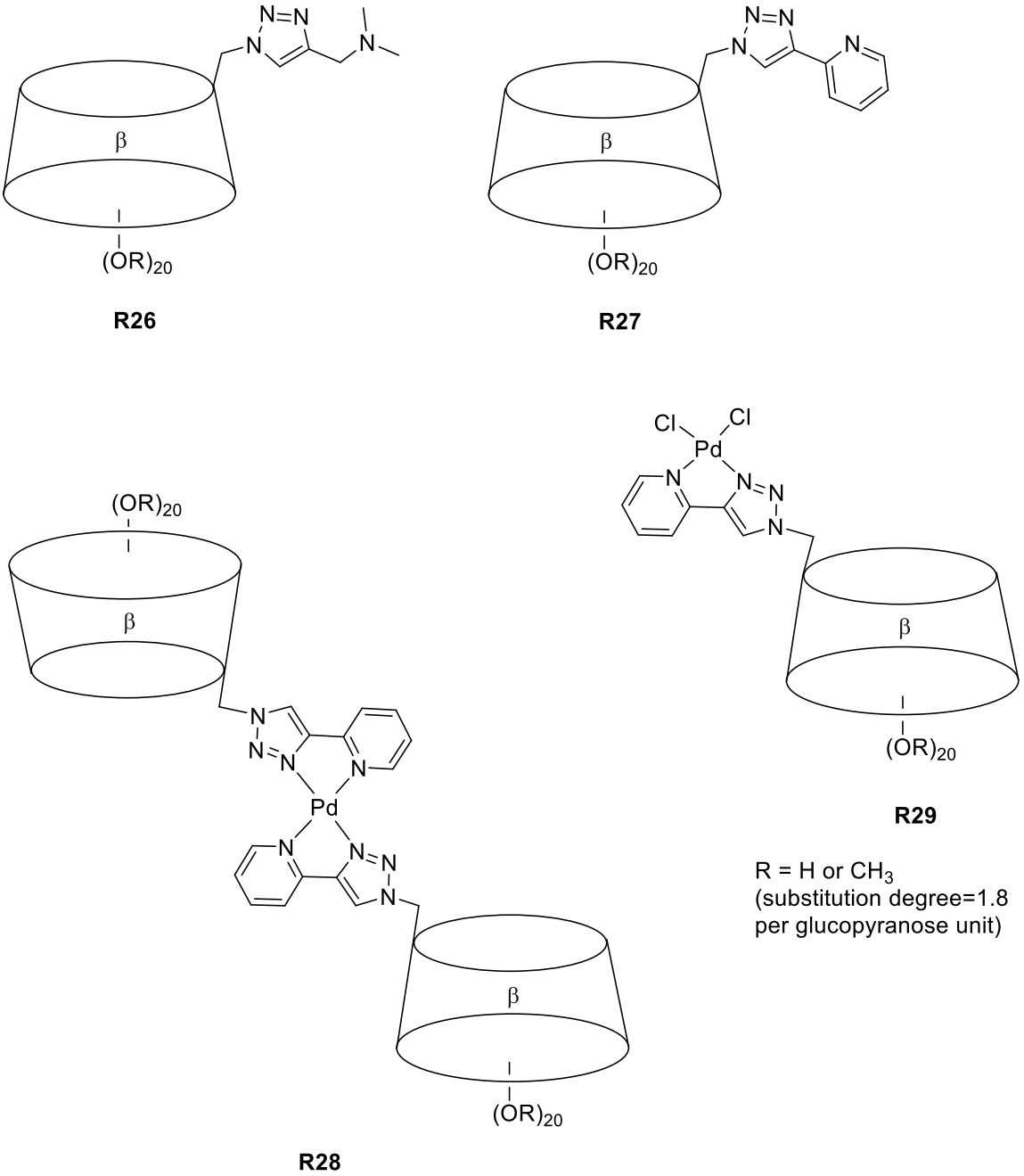

Fig 10. β-CD-based N,N-bidentate ligands **R26**, **R27** and Pd(II) complexes derived from **R27**.

For references, see page 59.

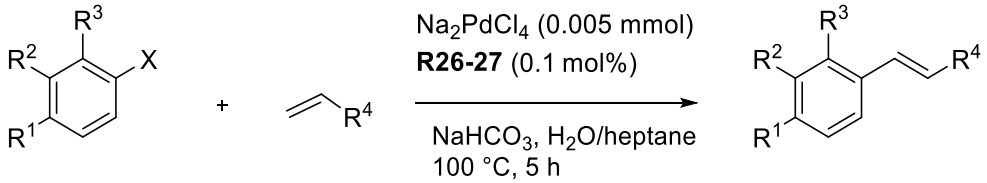

X = I, Br, Cl;
R^1, R^2, R^3 = H, Me, OMe, NH_2, CN, OH, NO_2 etc.; R^4 = COOMe, Ph;
conversion up to 99%; TON up to 198; TOF up to 39.6 h^{-1}

Scheme 11. Heck reaction using **R26** or **R27** as a water-soluble ligand.

Another palladium complex involving a CD monosubstituted with a N,N chelating ligand (**R30**), namely cyclohexanediamine was designed by Yang and coworkers (Scheme 12)[59]. Although it is not clear whether the catalyst is purely molecular or contains nanoparticule formed by reaction with $NaBH_4$, it was used for the reduction of various nitroarenes in the presence of $NaBH_4$ in water at room temperature. The catalytic results revealed good yields of the desired aromatic amines (up to 99%) without the formation of other reduction products and without palladium leaching into the organic solution during the extraction of the organics products with ethyl acetate after each run. Moreover, the recycled water-soluble catalyst still retains high catalytic activity after five cycles (93%) which makes it environmentally-friendly, efficient and recyclable.

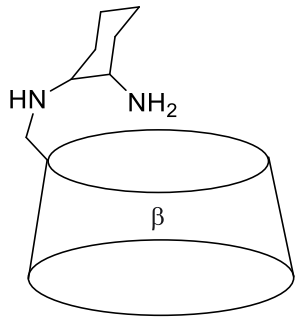

R30

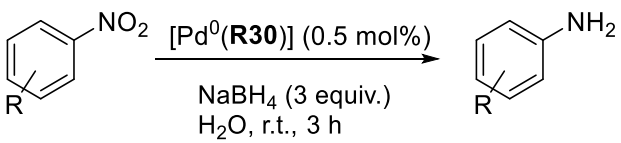

R = H, 2-/3-/4-Me, 4-CH_2OH, 4-CHO, 2-F, 4-Cl, 3-Cl-4-F, 3-Br, 2,4-diBr, 2-I, 2-/3-/4-NH_2, 4-NO_2, 4-OH, yield = 88-98%

Scheme 12. Pd-catalyzed reduction of nitrobenzenes using **R30** as ligand.

For references, see page 59.

Finally, another N,N ligand consisting of a β-CD monosubstituted with a *N*'-(pyridine-2-yl)propane-1,3-diamine unit (**R31**) was reported by Pichumani and Khan (Scheme 13).[60] As for the previous systems, the Pd(II) complex is highly soluble in water. It was characterized by FI-IR, NMR, mass, UV-vis spectroscopic methods and molecular modeling studies. This complex proved to be an efficient catalyst for the transfer hydrogenation of various aromatic carbonyl compounds with isopropyl alcohol as a hydrogen source. Up to 96% yield was reached with fresh catalyst. Only a slight drop in yield was observed (84% yield after 5 runs) using the same catalyst recycling procedure as above. The presence of KOH as a base was found to be crucial for product formation as the yield dropped significantly in its absence or with other bases. Unlike previous studies on analogous complexes, the authors were not able to experimentally prove the formation of inclusion complexes between the Pd(II) complex and substrate molecules even if molecular modeling studies point to this possibility. The authors mention a significant chiral induction by the chiral cavity during the reduction of prochiral ketones without giving further details.

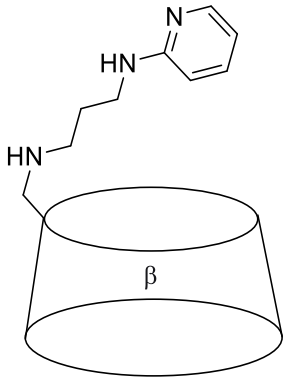

R31

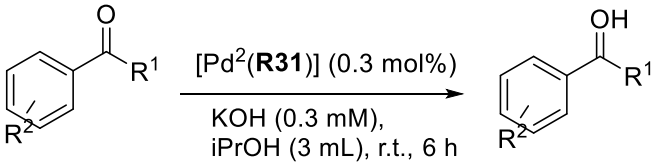

R^1 = H; R^2 = H, 3-MeO, 3,4-diMeO, yield = 80-93%
R^1 = Me; R^2 = H, Ph, 2-/3-/4-MeO, 3,4-diMeO, 2-/3-/4-Cl, 3,4-diCl, yield = 80-96%
R^1 = Ph; R^2 = 4-Cl, yield = 85%; R^1 = 4-$MeOC_6H_4$, R^2 = H, yield = 83%

Scheme 13. Pd-catalyzed transfer hydrogenation of ketones using **R31** as ligand.

Cyclodextrins can also be used in supramolecular water-soluble photocatalysis. In 2015, Li, Sun et al.[61] developed highly active supramolecular assemblies (**R34**) comprising a β-CD-

For references, see page 59.

modified ruthenium complex (**R32**) as the photosensitizer, and a phenyl-modified ruthenium complex (**R33a**/**b**) as the catalyst together with sodium persulfate which acts as the sacrificial electron acceptor (Fig 11). The catalysts and photosensitizers were self-assembled by host-guest interaction in neutral aqueous buffer solution (H_2O/MeCN 9:1), giving a TON and quantum yield of up to 267 and 84%, respectively. The corresponding values found with a photosensitizer lacking the β-CD cavity were only 28 and 10%, indicating that the host-guest interaction is key in facilitating the electron transfer from the catalyst to the photosensitizer, as also confirmed by stopped-flow measurements.

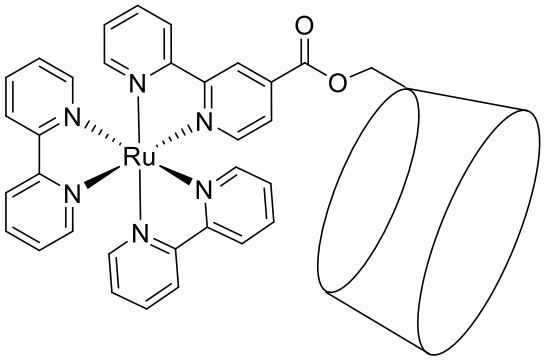

R32

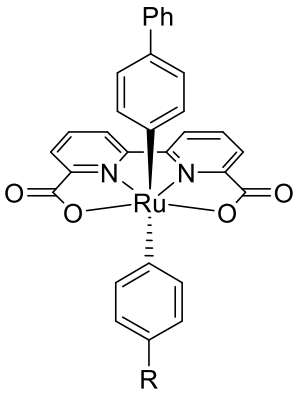

R33a, R = Ph
R33b, R = Me

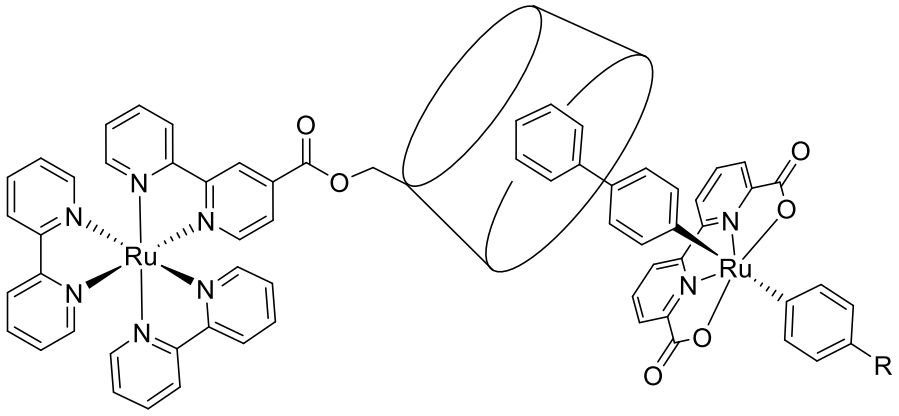

R34

Fig 11. Photosensitizers and catalyst used for highly active supramolecular assemblies.

Armspach, Matt et al. described the preparation of a range of aza-capped CDs by using the nitrogen nucleophile 2-nitrobenzensulfonamide (2-$NsNH_2$) as a capping agent (Scheme 14).[62] Two adjacent glucose units in both methylated α- and β-CD derivatives can be connected through the very short NH spacer. In methylated CDs equipped with a tertiary amine cap,

For references, see page 59.

nitrogen inversion can be blocked at room temperature provided the aglycone N-substituent is bulky enough and the cyclo-oligosaccharide core is sufficiently rigid as in the small α-CD-based complex, the crystal lattice of which displayed a discrete left-handed, four-folded helix. In the case of the larger and more flexible β-CD ligand **R37a**, nitrogen invension cannot be blocked and the complex with an encapsulated metal **R39a** no longer forms helical assemblies in the solid state, but columnar arrays instead, as direct connection between the CD units via hydrogen bonding does not occur in this case. The endo orientation of the nitrogen lone pair in the α-CD-derived ligands makes the confinement of metal within the CD cavity possible, thus opening the way for nitrogen-based metal catalysts operating in a restricted chiral space.

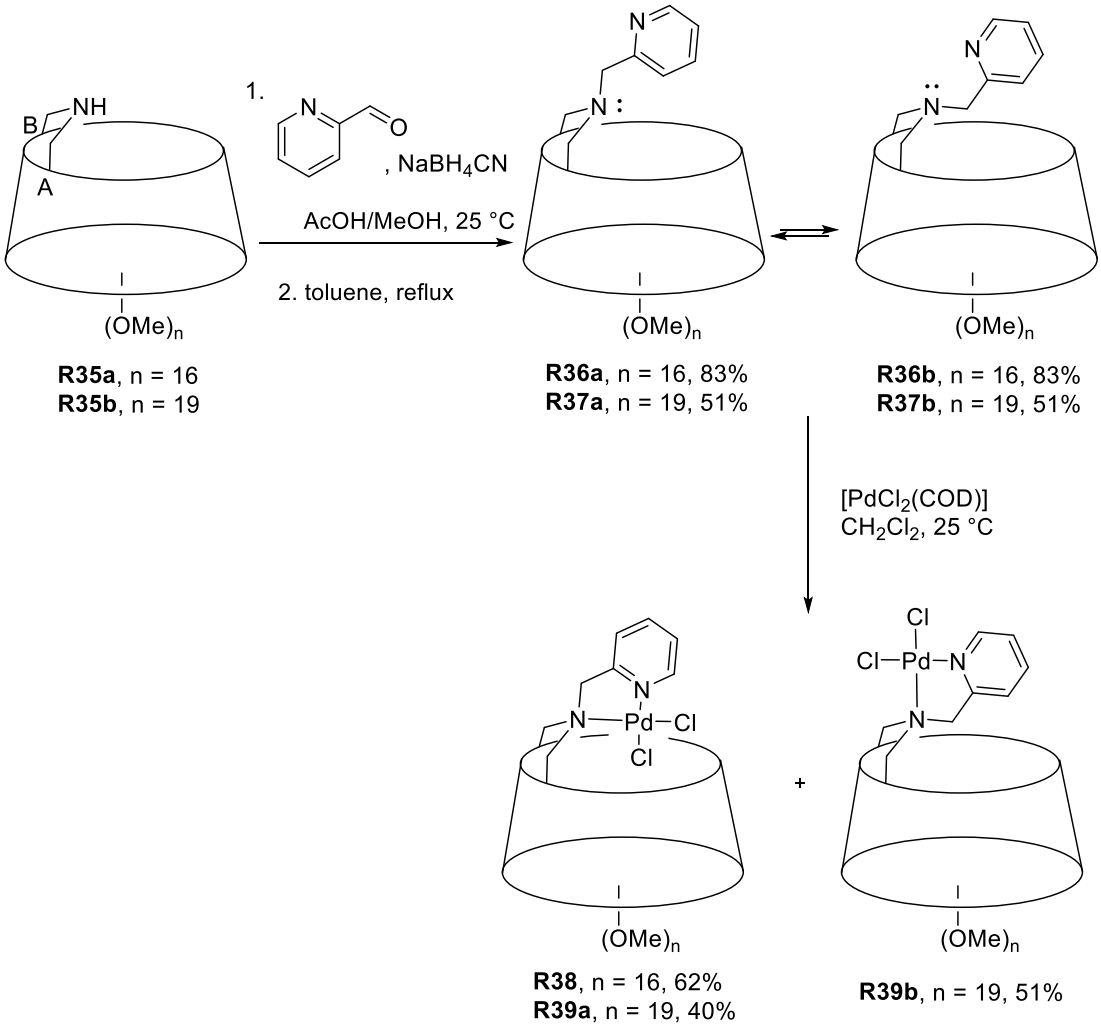

Scheme 14. Synthesis of N,N bidentate ligands and metal complexes.[62]

Apart from the highly hydrophilic CDs, much more hydrophobic, polyaromatic host molecules such as the calixarenes and the resorcinarenes have also been modified to access well-defined

For references, see page 59.

cavity-shaped ligands. Among all calix[n]arenes species, the calix[4]arene is one of the most popular cavity-shaped platforms in the field of catalysis and supramolecular chemistry even if its inner-space is often too small to carry out intra-cavity reactions.[63] Furthermore, resorcin[4]arenes, which can be obtained by acid-catalyzed condensation of resorcinol with aldehyde, display a larger hollow than calix[4]arenes and therefore make them more attractive for inner-cavity reactions. In 2001, Rudkevich and Rebek[64] reported the synthesis and host-guest properties of a novel metallocavitand **R40** derived from a resorcin[4]arene platform, the cavity of which is extended thanks to aromatic walls held together by a cyclic array of cooperative hydrogen bonds involving amide substituents (Scheme 15). One of the aromatic walls could be equipped with a rigid coordinating phenanthroline unit resulting in a rigid cavity-shaped ligand with self-folding capability, relatively large inner space (8 × 10 Å) and metal-confining properties as the metal binding site is directed toward the cavity. Whether metalated with zinc(II) or not, the cavitand is capable of binding quinuclidine and 1,4-diazabicyclo[2,2,2]octane within its hollow, though the binding is stronger when the metal is present (1 kcal mol^{-1} additional stability). The inclusion and expulsion of these tertiary amines from the cavity, whether metalated or not, was shown to be a slow process on the ^{1}H NMR time scale since both complexed and uncomplexed amines are present in the reaction mixture at room temperature. The exact coordination geometry of the Zn atom is not known, but this zinc-containing cavity was regarded as a promising metalloenzyme mimic for catalyzing hydrolysis and esterification reactions in a selective manner.

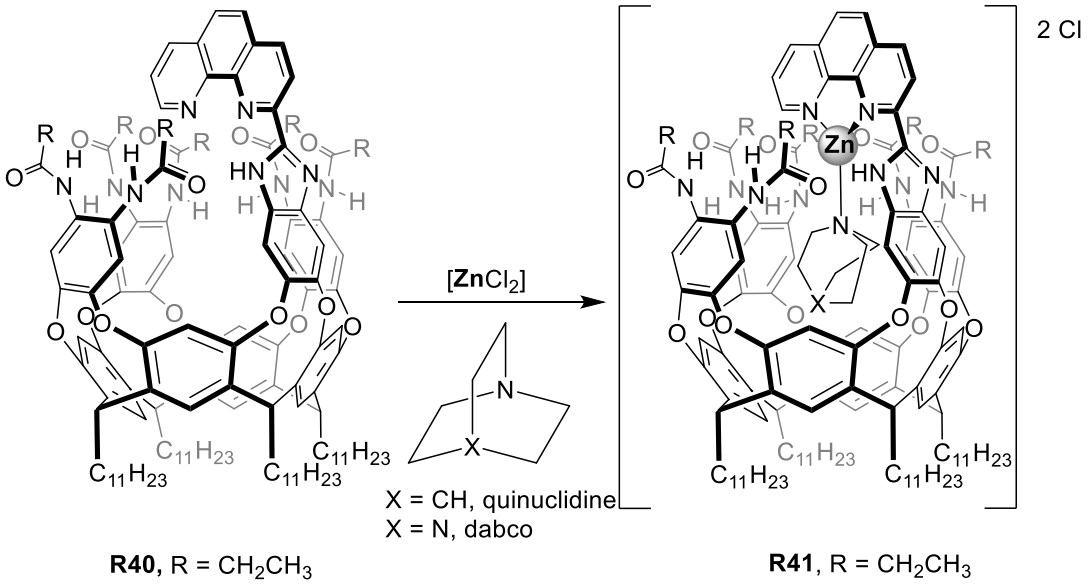

Scheme 15. Reaction of the metallocavitand **R40** with $ZnCl_2$.[64]

For references, see page 59.

One year later, the same group reported a resorcin[4]arene platform, phosphite-oxazoline chelator (**R42**).[65] This ligand produced a η^3-complex when treated with palladium and various allyl acetates. There are two possible ways of coordinating the allyl part (H_2C–CH=CHR'), one of which involves the allyl terminus *cis* or *trans* to the Pd-P bond (**R43a**, **R43b** respectively) (Scheme 16). The steric hindrance caused by the geminal phenyl groups of the oxazoline unit favors a reaction pathway involving a η^3-complex (**R43a**), that eventually results in the formation of the linear product. Substrate selectivity was shown to take place thanks to competition experiments. It appears that the rate of oxidative addition depends on the connectivity of the homoallylic carbon atoms, and it decreased with increasing substrate bulkiness in the order R' = ^{i}Bu (S1) > ^{i}Pr (S2) > ^{t}Bu (S3). The ability of this catalyst to stabilize the transition state of the oxidative addition decrease in the order S4 > S2 > S5. Clearly, both the substrate and regioselectivity of the allylic substitution is a direct result of the presence of a cavity which acts as a molecular recognition unit, making substrate and metal encapsulation a promising strategy for the development of regio- and enantioselective catalysts.

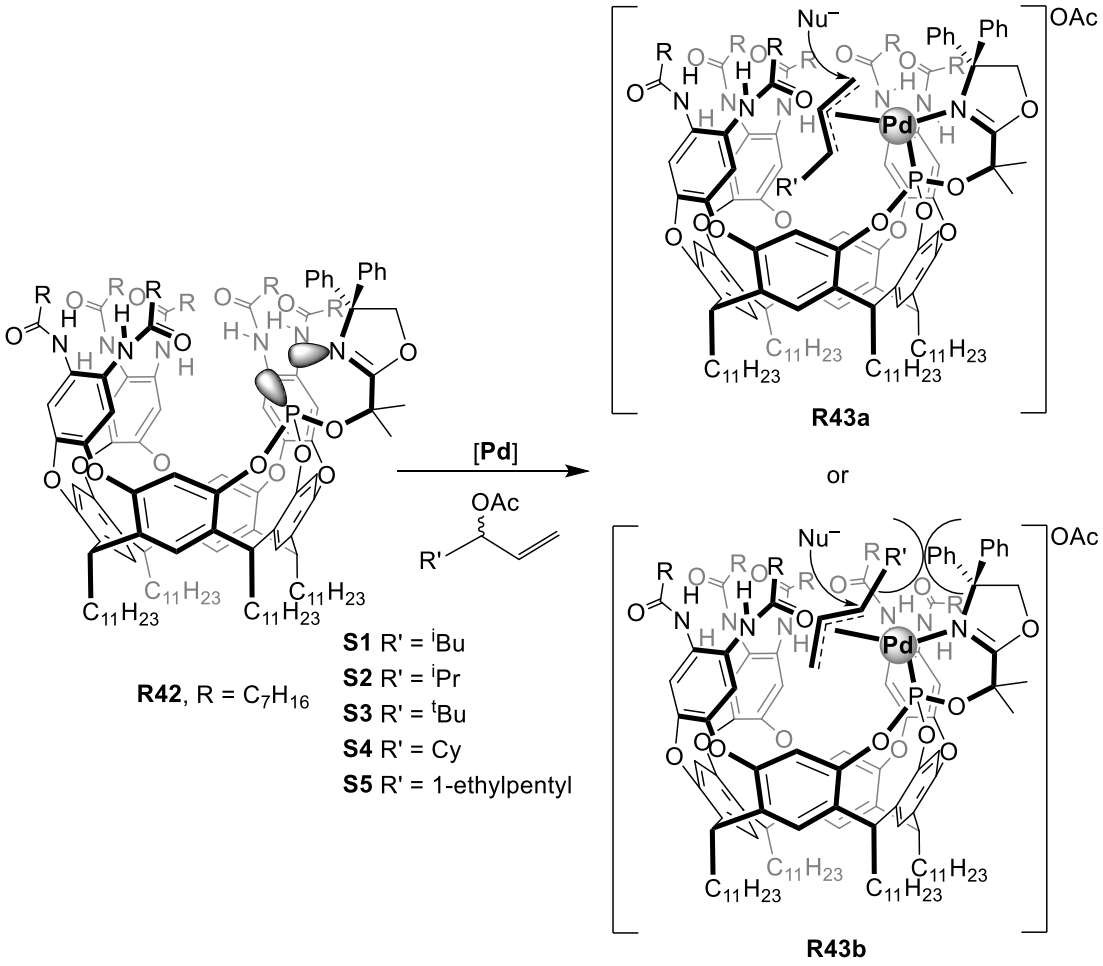

Scheme 16. Resorcin[4]arene-based ligand **R42** controls the allylic alkylation of various substrates.[65]

For references, see page 59.

In 2010, Harvey and Jugé synthesized the first *P*-chirogenic aminophosphane-phoshinite ligand comprising an upper rim-functionalized calix[4]arene platform (Scheme 17).[66] The Rh(I) complex derived from this ligand was used as a catalyst for the asymmetric hydrogenation of various prochiral olefin substrates (Scheme 18), giving rise to excellent activities, and *ee* values as high as 98% were obtained in the case of the (*R*)-*N*-acetylphenlalanine methyl ester substrate, using benzene as the solvent. On the contrary, analogous ligands bearing an isoelectronic but less bulky substituent showed poorer performances. Computer modeling indicated the presence of two different conformers. The one in which the rhodium center is located outside the cavity is slightly more favored than the one with the metal inside. Therefore, it is highly probable that metal and substrate encapsulation is not responsible for enantiodiscrimination, effective enantiodiscrimination is the result of the rather large calix[4]arene platform.

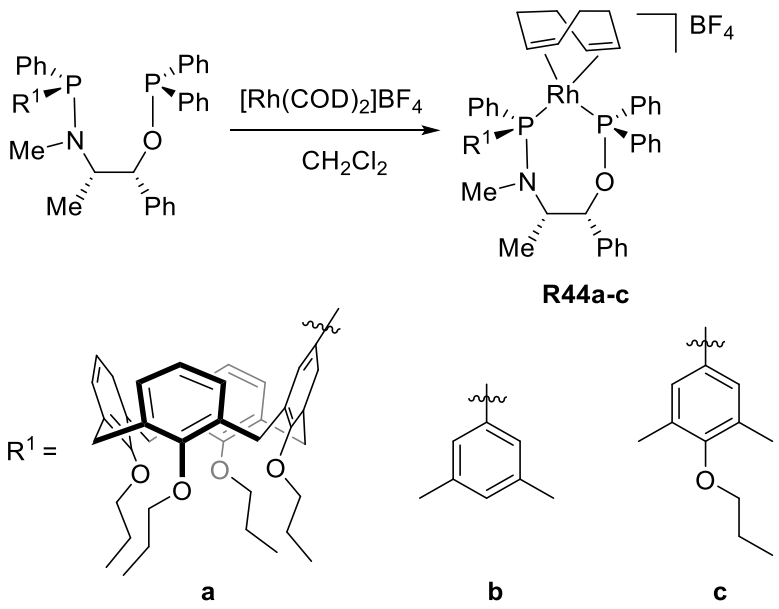

Scheme 17. Preparation of Rh(I) complexes **R44a-c**.

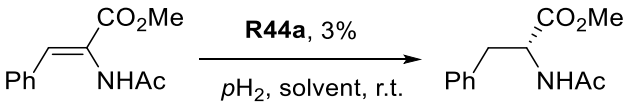

Scheme 18. Asymmetric hydrogenation of methyl 2-acetamidocinnamate catalyzed by **R44a**.[66]

I. 3. 2. Cavity-shaped bidentate ligands equipped with two non-equivalent coordinating arms

For references, see page 59.

The first part of this section will deal with ligands having two different coordinating groups connected to two different positions of the macrocyclic platform. Because the separation between the two donor atoms is usually large, large chelate complexes can form provided the macrocycle is rigid and preorganized enough to avoid noncyclic species.

Woggon reported Ru complexes derived from a modified β-CD with either a *N*-(2-hydroxyethyl)amino (**R45a**) or an *N*-methylamino unit (**R45b**) connected to a CD C-3 atom at the secondary face (Scheme 19).[67] The opening of the CD epoxide starting material with the amine nucleophile resulted in distorted β-CD cavities in which the new altrose unit adopts a $^{1}C_{4}$ conformation and not the standard glucose $^{4}C_{1}$ conformation as revealed by ^{1}H NMR investigations. No more information on the precise structures of the new host molecules could be obtained, notably by X-ray diffraction studies. Furthermore, in **R45a** ligand chelation did involve the amino and hydroxyl groups of the *N*-(2-hydroxyethyl)amino unit as in primary face-modified **R12**,[44] but a much more rigid chelate complex was formed involving the nitrogen atom of the *N*-(2-hydroxyethyl)amino unit and a neighboring 2-OH function belonging to the same altrose unit. The enhanced rigidity of the complexes resulting from this mode of chelation together with the encapsulation of the ketone substrate in the CD hollow is likely to be responsible for the good to excellent enantioselectivities (70% to 98%) in the transfer hydrogenation of challenging aliphatic ketones with sodium formate in water. Indeed, poor chiral induction occurs in organic solvents, a medium in which substrate encapsulation does not take place. Likewise, cavity-free analogs involving chiral aminoalcohol analogs such as ephedrine gave only moderate *ee* values, demonstrating the importance of the CD cavity in the enantiodiscrimination process.

For references, see page 59.

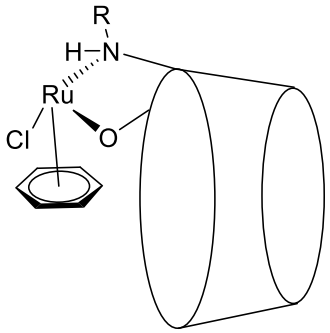

R45a, R = $(CH_2)_2OH$
R45b, R = Me

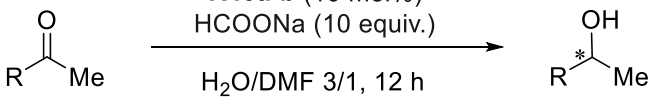

R45a (50 °C), R = Bu, 4-Methylpentyl, 4-Methypentyl-3-enyl, Hexyl, Heptyl, Octyl, 4-ClC_6H_4, 2-phenethyl, yield: 55-92%, enantioselectivity: 70-98%
R45b (25 °C), R = Bu, 4-Methylpentyl-3-enyl, Hexyl, Heptyl, Octyl, Decyl, Cyclohexyl, $CyCH_2$, 4-$^tBuC_6H_4$, 4-ClC_6H_4, 2-phenethyl, yield: 37-92%, enantioselectivity: 77-96%

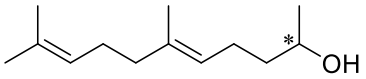

R45a, yield: 35%, enantioselectivity: 98%
R45b, yield: 76%, enantioselectivity: 93%

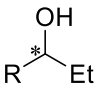

R45b, R = Pent, yield: 61%, enantioselectivity 77%
R = Hex, yield: 55%, enantioselectivity 91%

Scheme 19. Transfer hydrogenation of ketone in the presence of **R45a-b**.[67]

Armspach and Matt[68] described four different hybrid phosphane-phosphite ligands (**R46a-d**) in which two adjacent glucose units of a permethylated α-CD were substituted with two distinct P(III) coordinating units at the CD primary face. Owing to the potential enantioinduction caused by the pseudoinherent chirality of these C_1-symmetric structures, these ligands proved to be excellent chelators and were assessed in the rhodium-catalyzed enantioselective hydrogenation of α-dehydroamino acid esters and hydroformylation of styrene (Scheme 20). Despite the flexibility of the rather large chelate rings, the bulky ligand **R46b** gave rise to *ee* values up to 60%. As the only source of chirality is the CD macrocycle in this system, the chirality of CD is somehow transferred to the chelate ring. However, whether enantiodiscrimination was caused by the inherent chirality of the CD platform and/or by a particular conformation of the metallocycle could not be settled. Moreover, when a stereogenic (*R*)-binaphthyl unit was introduced into the phosphite moiety, the *ee* value reached 92%, whereas enantioselectivities produced by the (*S*) counterpart were much lower (up to 70% *ee*), which indicated a clear match/mismatch relationship. The rhodium-catalyzed

For references, see page 59.

hydroformylation of styrene was also tested using **R46b** in a standard *l*:*b* ratio of 0.3, and displayed moderate *ee* values (up to 50% *ee* in favor of the (*R*) product).

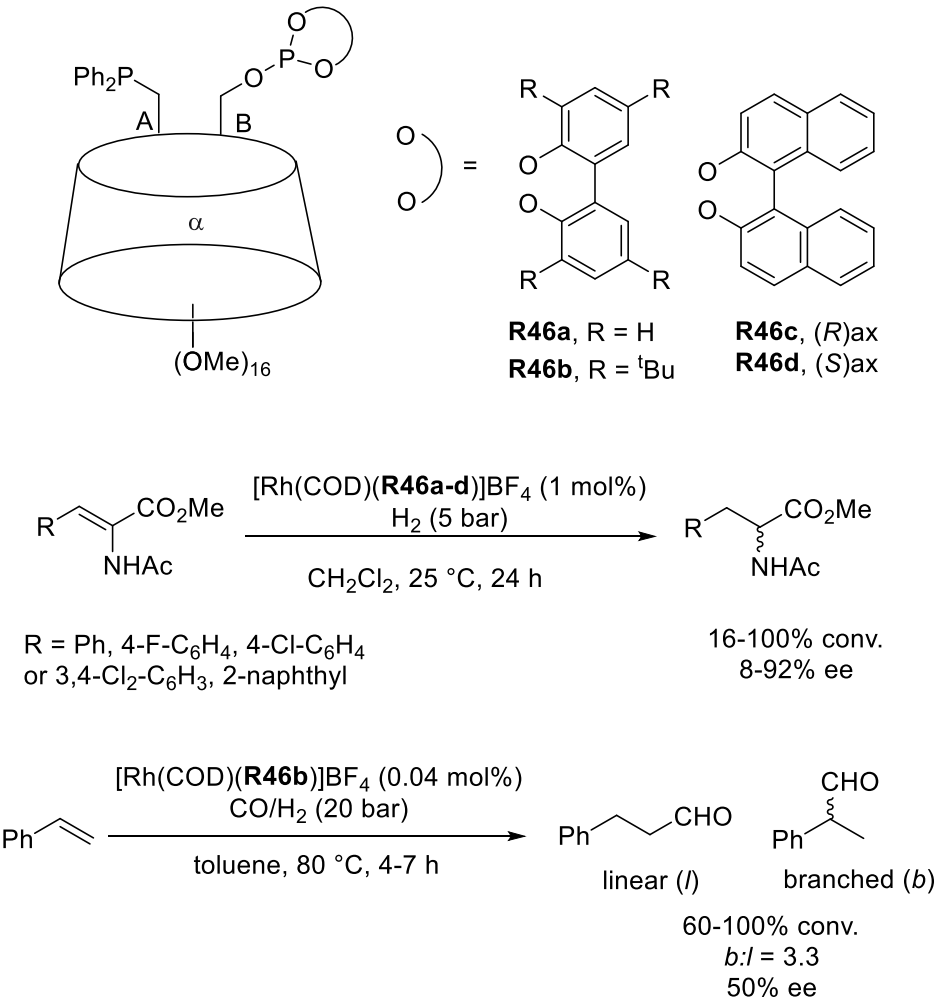

Scheme 20. Rh(I)-catalyzed asymmetric hydrogenation and hydroformylation of olefins using **R46a-d** as ligands.[68]

Kamer et al. synthesized a calix[4]arene-based P,N ligand (**R47**) by grafting a quinoline unit first onto the lower rim of the calix[4]arene platform before reacting the three remaining hydroxyl groups with phosphorus trichloride (Scheme 21).[69] The X-ray crystal structure of this resulting P,N ligand revealed the cone conformation of the calixarene platform, which is ideal for chelation. Indeed, chelate complexes [PdMeCl(**R47**)] and [Rh(CO)Cl(**R47**)] could be formed in high yields when an equimolar amount of metal precursor was used. However, in the presence of excess ligand, the bis-phosphite complex *cis*-[$PtCl_2$(**R47**)$_2$] was formed pointing to the hemilabile behavior of the quinoline unit. Indeed, in the complex [Rh(acac)(CO)(**R47**)], obtained by reacting **R47** with one equivalent of [Rh(acac)$(CO)_2$], the

For references, see page 59.

P,N ligand behaves as a monodentate ligand as only the phosphite unit is coordinated to the metal. This ligand was then tested in three different metal-catalyzed transformations. Under the employed reaction conditions, poor activities were obtained in the Pd-catalyzed CO/ethylene copolymerization, while good regioselectivities towards the branched product were observed in the Pd-catalyzed allylic alkylation of cinnamyl acetate. Ligand **R47** showed low activities and very poor selectivities towards linear aldehydes in the Rh-catalyzed hydroformylation of 1-octene.

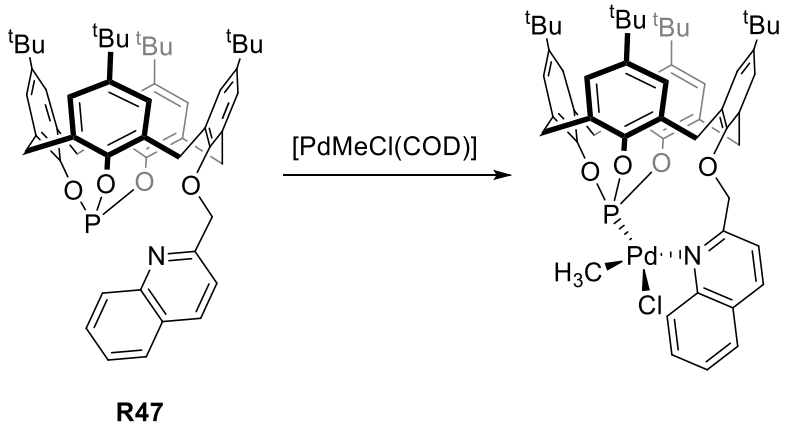

R47

Scheme 21. Preparation of Pd(II) complex from **R47**.

The last part of this section will deal with cavity-shaped chelating ligands having identical pendant coordinating units but that are non-equivalent because of the lack of symmetry of the macrocyclic platform.

Early work by Tabushi demonstrated that β-CDs equipped with two identical histamino pendant arms were able to complex Zn(II) cations,[70] most likely in a chelate fashion. These complexes were shown to behave as efficient carbonic anhydrase models. Although Tabushi's contribution is seminal in the field of metalloenzyme mimics, the complexes at stake are ill-defined due to the lack of adequate analytical tools at that time. In the following, only chelate complexes in which the metal coordination sphere is clearly identified will be discussed.

In 1996, Vecchio, Saviano et al. published a chelating diamine built on a β-CD platform that led to a well-defined platinum(II) chelate complex (**R48**) (Fig 12).[71] The two coordinating primary amines, which have been introduced onto two neighboring glucose units, are close enough to allow the formation of a square-planar *cis*-chelate complex reminiscent of the well-known anticancerous *cis*-platin drug but with higher water solubility. Interestingly the $PtCl_2$ unit is pointing towards the center of the cavity but no clear reason for the encapsulation of the

For references, see page 59.

metal center was given. The ^{1}H NMR spectra clearly show that protons belonging to the metal-capped glucose units have distinctive chemical shifts owing to platinum complexation, in particular for the CH_2N protons which are all upfield shifted except for one, of which the high chemical shift was attributed to cavity inclusion. A circular dichroism (c. d.) study revealed that the chirality of the CD is somewhat transferred to the metal center, which acts here as the chromophore, probably as a result of the very rigid nature of the chelate ring. Indeed, the intensity of the c. d. bands is highly sensitive to the presence of the CD guest molecule 1-adamantol which is known to form strong inclusion complexes with β-CD in water and which is capable here to displace to some extent the chelate plane from the cavity.

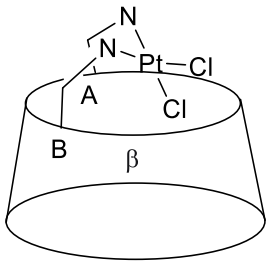

R48

Fig 12. Platinum(II) chelate complex built on a β-CD platform.

In 2002, Jia reported a novel diphosphine ligand $6^{A},6^{B}$-bis(diphenylphosphino)-$6^{A},6^{B}$-dideoxy-permethylated-β-CD (**R49**) (Scheme 22).[52] Because of the torus-like structure of CD and the fact that the two PPh_2 units are located on adjacent glucose units, the two phosphorus atoms are likely to be in close proximity despite a nine-bond separation, as evidenced by the presence of rare through-space P-P couplings ($J_{P,P}$ = 10.2 Hz) revealed by the 2D homonuclear $^{31}P\{^{1}H\}$ COSY spectrum of **R49**. Clearly, the two PPh_2 units should be ideally placed to promote the formation of chelate complexes although no X-ray crystal structure of the diphosphine could be obtained and the exact orientation of the phosphorus lone pairs remains unknown. Treatment of **R49** with $[PtCl_2(COD)]$ or $[Rh(COD)_2]BF_4$ in dichloromethane produced the *cis*-chelate $[PtCl_2$(**R49**)] and [Rh(COD)(**R49**)]BF_4 (**R50**) (Scheme 22) complexes, respectively. Again, the exact position of the metal with respect to the cavity is not known because of the lack of X-ray diffraction data. The Rh complex displayed good catalytic activity for the hydrogenation of various unsaturated carboxylic acids and esters at 1 mol% with *ee* values reaching up to 92%.

For references, see page 59.

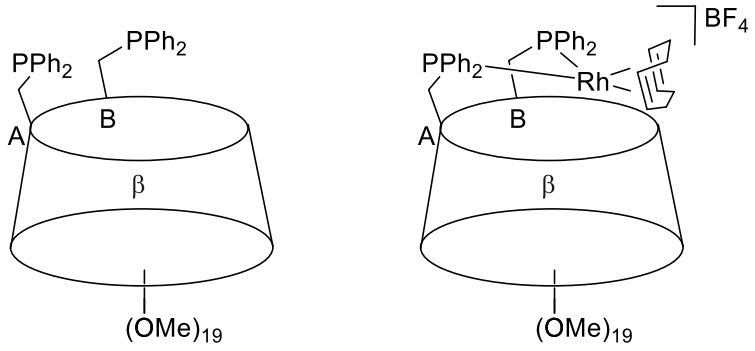

R49 **R50**

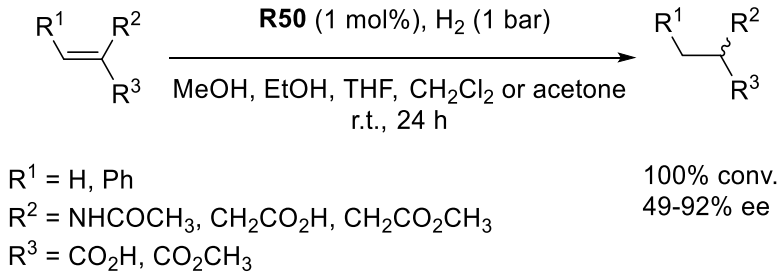

Scheme 22. Rh(I)-catalyzed asymmetric hydrogenation of functional olefins.[52]

Shortly later, larger chelate rhodium complexes were devised by Armspach and Matt from diphosphite ligands **R51**, **R52**, built on an AC or AD difunctionalized α-CD platform, respectively (Scheme 23).[72] The unexpected presence of a singlet in ^{31}P NMR spectrum (δ 127.5 ppm) of the unsymmetrical ligand **R52** showed that the two phosphorus atoms appear as magnetically equivalent. Unlike Jia's diphosphine **R50**, these more flexible bidentate ligands can only form chelate complexes with cationic rhodium precursors, not neutral ones. The cationic rhodium chelate complexes obtained from **R51** and **R52** were tested as catalysts in the hydroformylation of 1-octene and the hydrogenation of prochiral dimethyl itaconate. A TOF up to 1200 mol (1-octene) mol $(Rh)^{-1}$ h^{-1} was obtained in the hydroformylation of 1-octene with standard *l*/*b* selectivity (up to 2). *Ee* values up to 84% were obtained in the hydrogenation of dimethyl itaconate when using the preformed *cis* chelate complex **R53** (Scheme 23), however with much lower activities (17% conv. after 24 h reaction) than to those observed by Jia (see above). A 10-fold increase in activity, though with a very poor enantioselectivity (17% *ee*), was observed for the same reaction when the catalytic reaction was performed by reacting the ligands in situ with $[Rh(COD)_2]BF_4$ without isolating the chelate complexes, but in this case, the presence of a mixture of chelate and non-chelate complex in the reaction mixture is likely. Despite its higher flexibility, chelate complex **R53** is able to give rise to high

For references, see page 59.

enantioselectivity. This work together with that of Jia illustrate the potential of unsymmetrically metal-capped CDs in asymmetric catalysis.

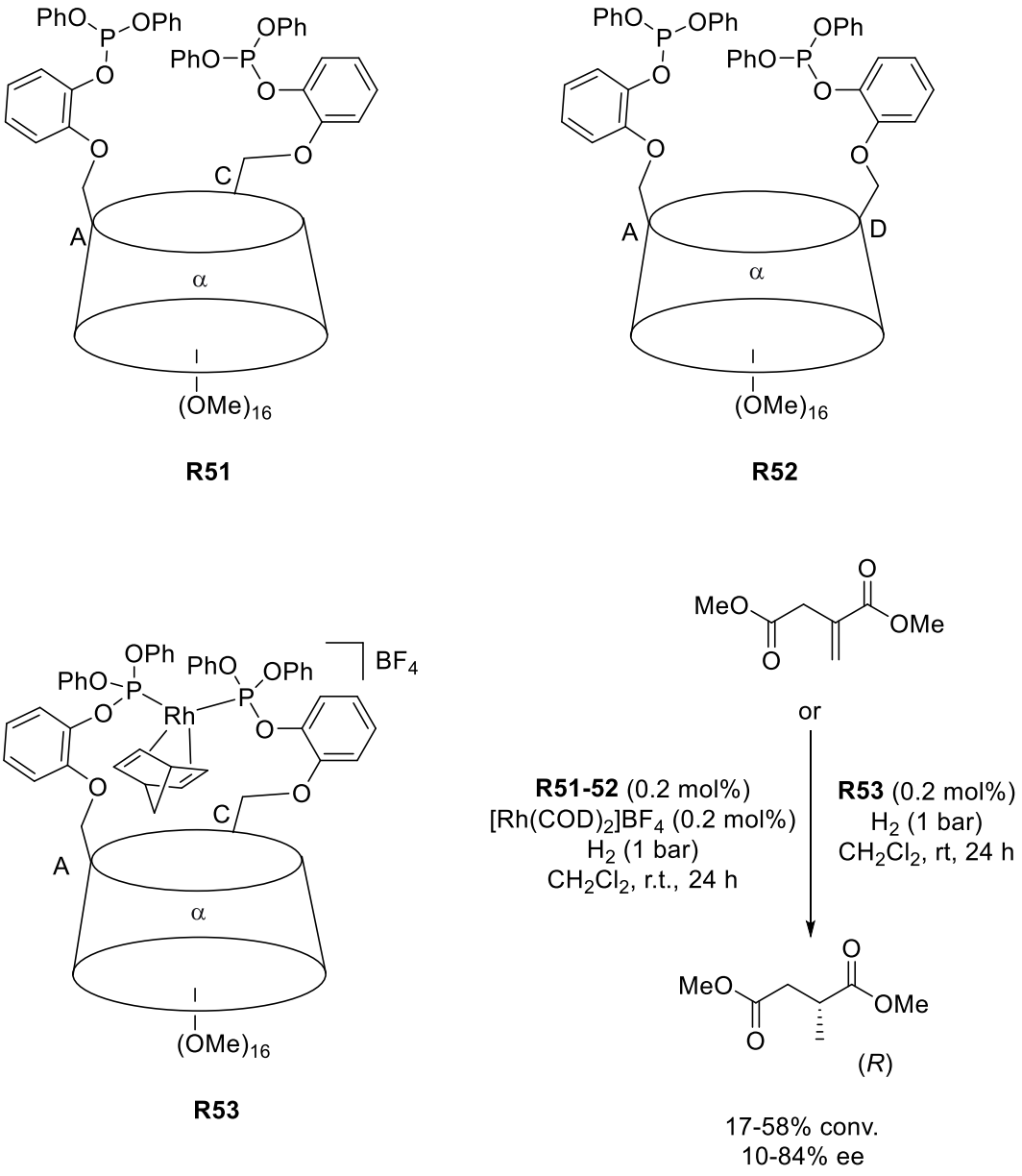

Scheme 23. Diphosphite functionalized α-CDs for Rh(I) catalyzed asymmetric hydrogenation of dimethyl itaconate.[72]

One year later, the synthesis and coordinative properties of another A,C-disubstituted α-CD-derived diphosphine containing two C(5)-linked "CH_2PPh_2" units (**R54**) were reported by the same group (Scheme 24)[73]. This ligand was proven capable of controlling both the first and second coordination spheres of coordinated transition metal ions. The chelate complexes of the ligand are characterized by the presence of P(III) units lying close to the cavity entrance which

For references, see page 59.

leads upon complexation to the partial entrapment of the metal fragment in the CD. With Pd(II), Pt(II), and Rh(I) metal precursors, this diphosphine always forms square planar *trans* chelate complexes. An NMR study revealed that in the case of square planar complexes comprising a chlorido ligand, the M–Cl bond is always maintained inside the CD owing to weak Cl···H-5 interactions, illustrating the ability of permethylated α-CDs to discriminate between a metal-bonded chloride and other, less polarized, M-R bonds.

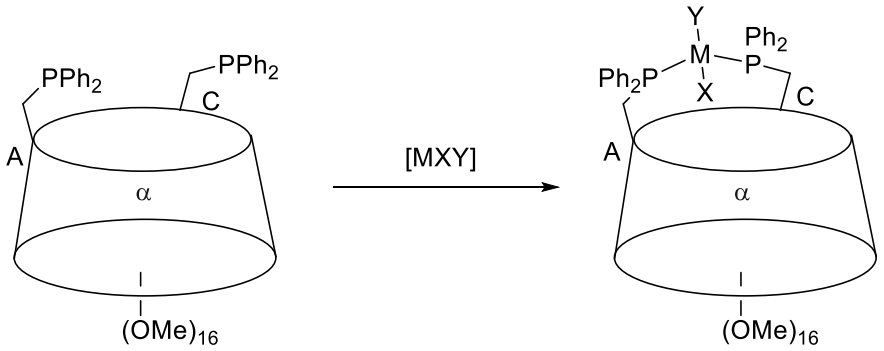

R54

R55a, M = Pd, X = Y = Cl
R55b, M = Pt, X = Y = Cl
R55c, M = Pd, X = Cl, Y = Me
R55d, M = Rh, X = Cl, Y = CO
R55e, M = Rh, X = CO, Y = H

Scheme 24. Chelate complexes **R55a-e** obtained from **R54**.

More recently, Armspach and Matt[74] described a short and convenient synthesis of $6^{A},6^{B}$:$6^{D},6^{E}$-doubly capped β-CD (**R56**) (Scheme 25), and it was shown that double capping is a powerful tool of tetrasubstituting native β-CD, as well as for introducing useful functionalities, in particular donor atoms, on methylated CDs.

For references, see page 59.

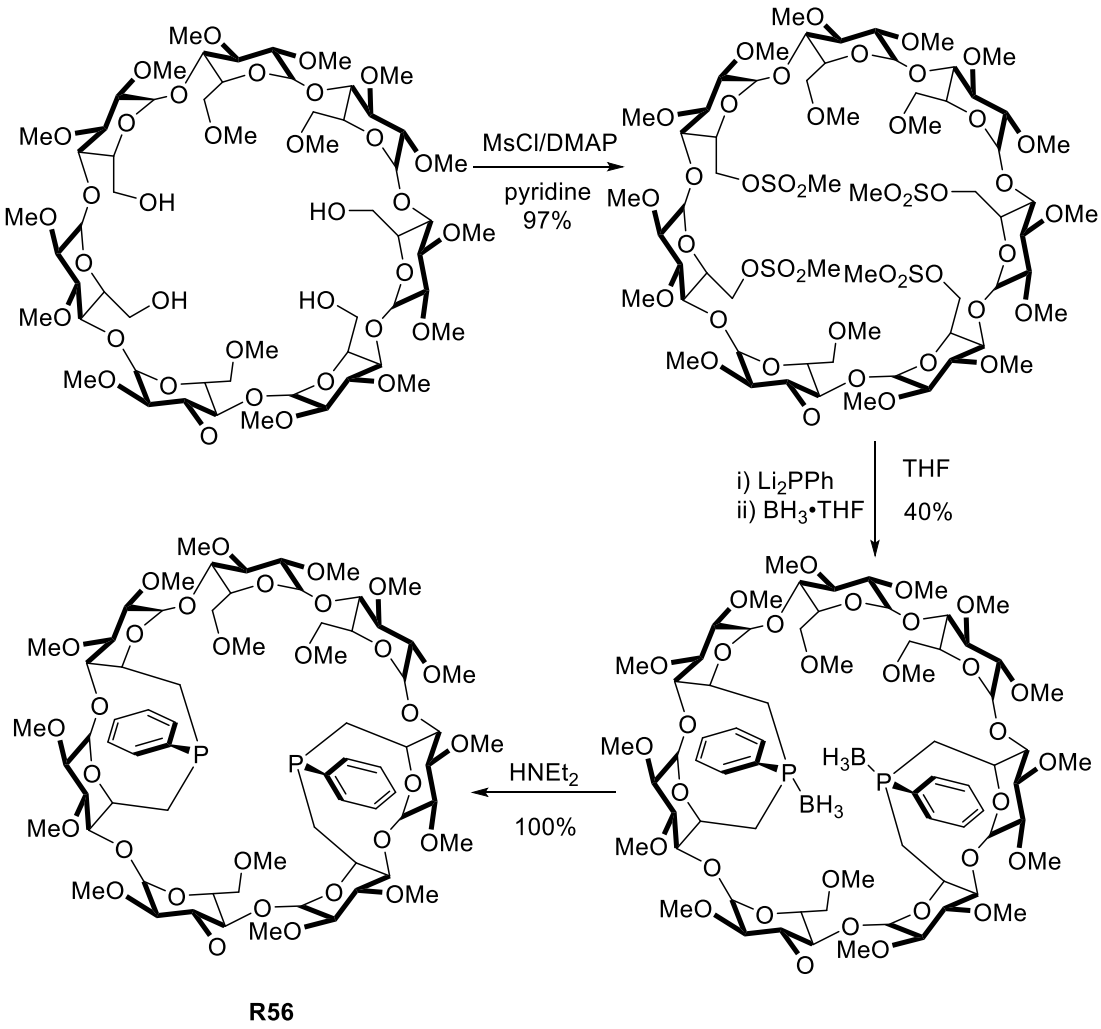

Scheme 25. Synthesis of the $6^A,6^B$:$6^D,6^E$-doubly capped diphosphine **R56**.

Being built on a nonsymmetrical β-CD scaffold, the introverted diphosphine **R56** (**WIDEPHOS**) has two nonequivalent bridging phosphorus atoms[75]. Despite the large separation between the two donor atoms, the ligand still turned out to be suitable for the chelation of a range of transition metals in a *trans* fashion as for C_2-symmetrical α-CD analogs (Scheme 26). However, molecular modeling indicated that the ligand cannot behave as a perfect *trans*-chelator given the rigidity of the P(III) atoms embedded in the nonsymmetrical CD framework, the P-M-P angle reaching a maximum of 160° instead of 180°. The resulting non-optimal *trans* coordination triggers a unique molecular movement, called oschelation, which is best described as an oscillation of the ligand around the coordinated metal during which the two P lone pairs alternately maximize their overlap with the metal d_{x2-y2} orbital (Scheme 27). It is noteworthy that oschelation was also observed with hybrid P,O chelating ligands.[76]

For references, see page 59.

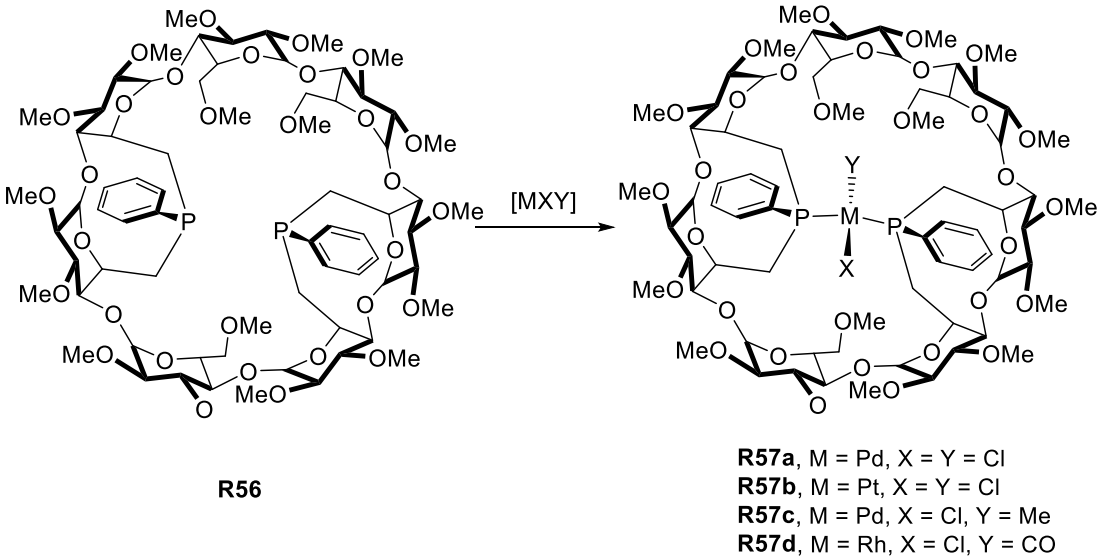

Scheme 26. Chelate complexes **R57a-d** obtained from **R56**.

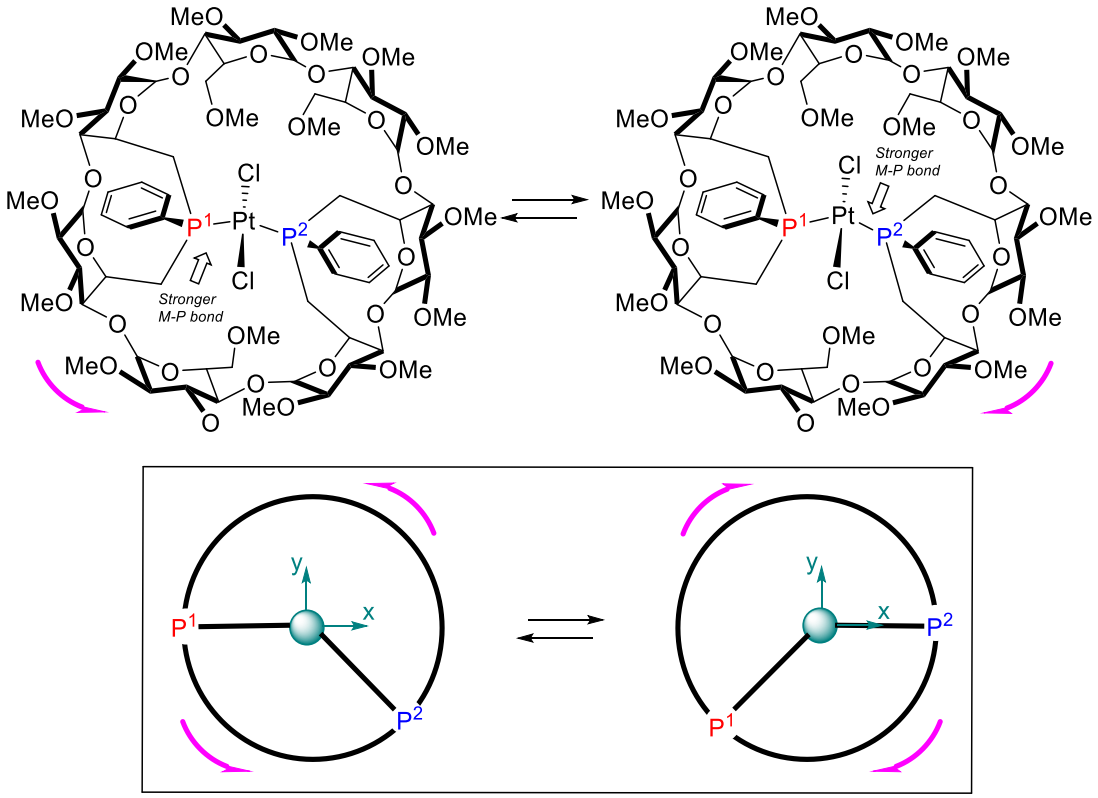

Scheme 27. Balance wheel movement of **R56** in complex **R57b** (view along the CD axis).[76]

Treatment of **R57a** with $[PdCl_2(PhCN)_2]$ led formally to insertion of a $PdCl_2$ fragment into one of the Pd-P bonds of **R57a** (Scheme 28). The resulting complex **R58** crystallized with a water molecule coordinated to one of the Pd atoms. Owing to the geometrical constraints imposed by the CD macrocyclic platform on the metals' first coordination spheres, complex **R58** didn't

For references, see page 59.

display the usual flat or roof structure and therefore preferred to cap a $\{Pd_2Cl_4\}$ unit having only a single chloride bridge. Furthermore, partial oxidation of **R58** by air causes the cleavage of one of its M–P bonds and concomitant oxidation of one phosphorus atom to produce equimolar amounts of complexes **R59** and **R60**. In the former, the oxidized phosphorus atom is replaced by an endohedrally coordinated water molecule hydrogen-bonded both to the P=O group and to a primary methoxy group, while in **R60**, the phosphine oxide moiety is directly coordinated to the metal center via its oxygen atom.

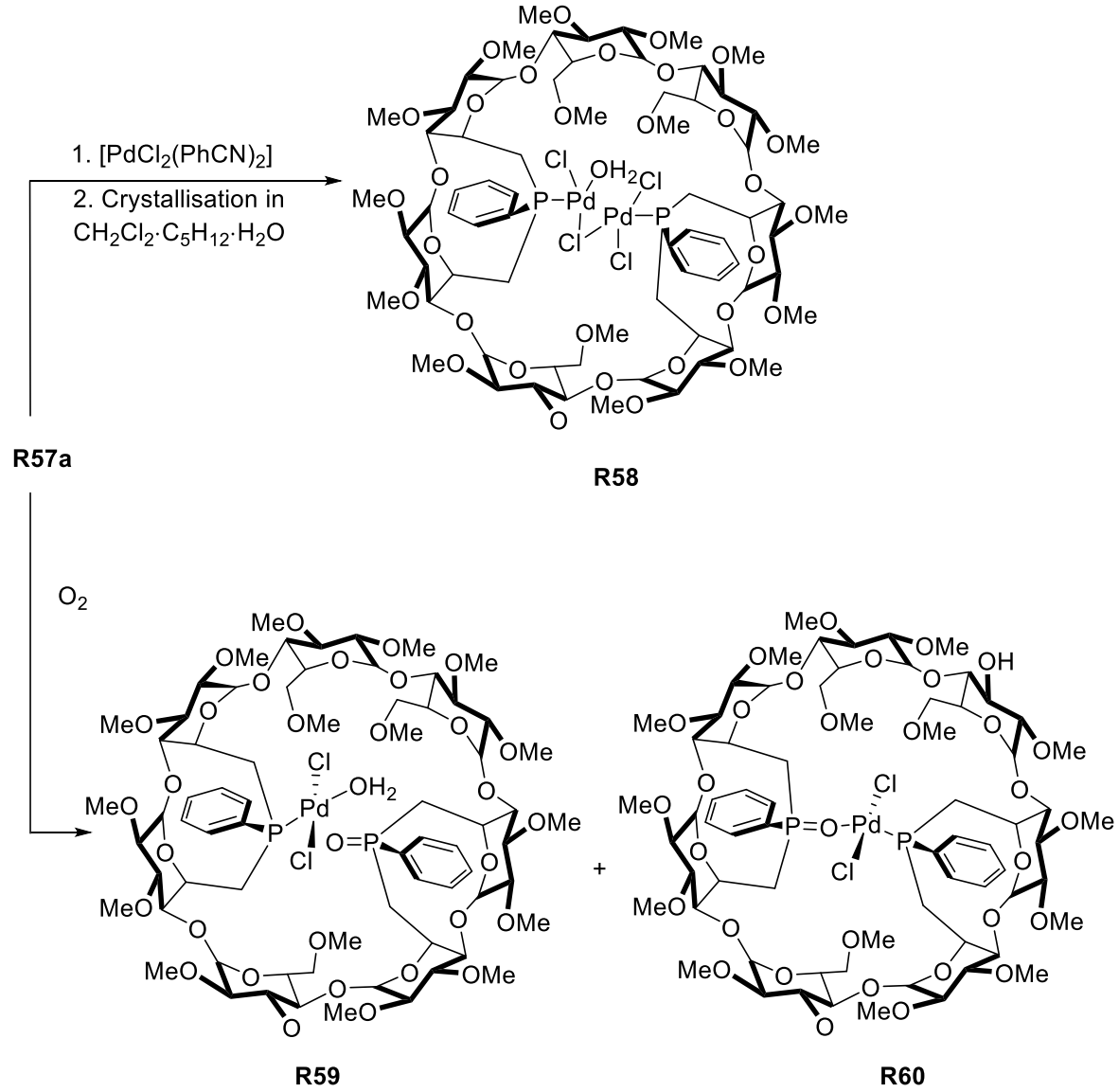

Scheme 28. Phosphorus-metal bond cleavage in complex **R57a**.

A series of calix[4]arenes bearing two phosphorus pendent groups were synthesized by Matt et al.[63b] The enantiomerically pure calixarenes **R62a** and **R63**, which have an AABC

For references, see page 59.

substitution pattern are inherently chiral. Their palladium and rhodium complexes were also prepared. While preformed cationic palladium complexes incorporating ligands **R62a** and **R63** were tested in asymmetric allylic alkylation, their rhodium analogs acted as catalysts for dimethyl itaconate hydrogenation (Scheme 29). Moderate to average *ee* values (25–67%) was observed for all these catalysts. The best results were obtained when the fourth phenolic unit remains unsubstituted as in **R62a** both in terms of activity and enantioselectivity (TOF up to 2000 h^{-1} and 48% *ee* for the hydrogenation of itaconate using [Rh(nbd)(**R62a**/**R63**)]BF_4 (nbd = norbornadiene) as catalyst and a TOF of 30 h^{-1} and 67% ee for the alkylation of 1,3-diphenylprop-2-enyl acetate using [Pd(η^3-2-MeC_3H_4)(**R62a**)]BF_4 as a catalyst. Interestingly, analogous complexes lacking inherent chirality with the two phosphine units in either proximal or distal positions (not drawn) produced much lower enantioselectivities (*ee* values between 0 and 16%) proving that enantiodiscrimination occurs mainly as a result of the inherent chirality of the calix[4]arene platform. This is believed to be the first example of asymmetric catalysis based on metal complexes of inherently chiral calix[4]arenes.

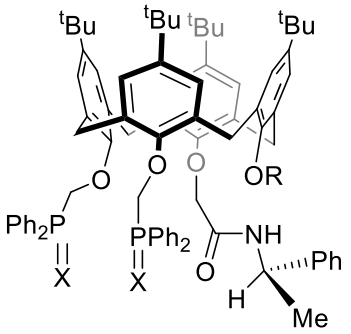

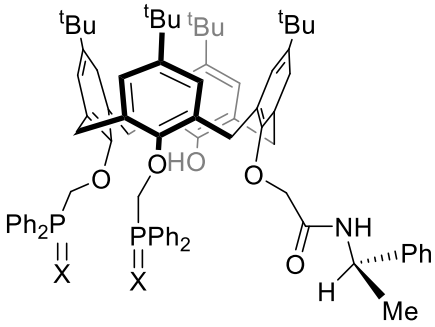

R61a, X = O, R = H
R62a, X = lone pair, R = H
R63, X = lone pair, R = $SiMe_3$

R61b, X = O
R62b, X = lone pair

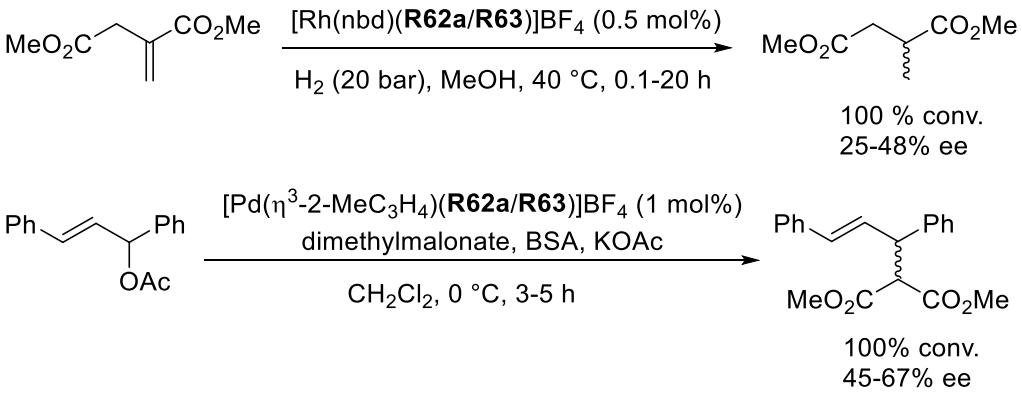

Scheme 29. Asymmetric alkylation and hydrogenation of functional olefins catalyzed by diphosphines derived from chiral calix[4]arene platforms.[63b]

For references, see page 59.

I. 4. Conclusion

Cavity-shaped chelating hybrid ligands have attracted increasing interest in the field of molecular recognition and catalysis, in particular asymmetric catalysis where a chiral environment around the catalytic center can make the difference in terms of selectivity compared to standard cavity-free systems. Although much progress has been made in the last 25 years in this field, cavity-shaped hybrid ligands capable of forcing the coordination of a metal center inside a confined space are not very common, even less so in the catalytically relevant *cis*-chelating mode. Moreover, selectivity in these systems often comes at the expense of activity and ways of boosting both activity and robustness, as well as selectivity, are needed to make these systems truly competitive with existing industrial catalysts. The possibility of sterically differentiating coordination sites involved in catalytic reactions based on these hybrid ligands allowing a strict control of the first and second coordination spheres of the catalytic center should open new opportunities in catalysis that are not reachable with standard ligands. The following chapters describe our contribution to the development of new concepts in homogeneous catalysis that rely on the use of metal confining, cavity-shaped hybrid ligands.

For references, see page 59.

I. 5. References

1. (a) Anastas, P.; Eghbali, N., Green Chemistry: Principles and Practice. *Chem. Soc. Rev.* **2010,** *39*, 301-312. (b) Sheldon, R. A., Fundamentals of green chemistry: efficiency in reaction design. *Chem. Soc. Rev.* **2012,** *41*, 1437-1451.

2. Raynal, M.; Ballester, P.; Vidal-Ferran, A.; van Leeuwen, P. W., Supramolecular catalysis. Part 2: artificial enzyme mimics. *Chem. Soc. Rev.* **2014,** *43*, 1734-1787.

3. Mu, R.; Wang, Z.; Wamsley, M. C.; Duke, C. N.; Lii, P. H.; Epley, S. E.; Todd, L. C.; Roberts, P. J., Application of Enzymes in Regioselective and Stereoselective Organic Reactions. *Catalysts* **2020,** *10*, 832.

4. (a) Schwizer, F.; Okamoto, Y.; Heinisch, T.; Gu, Y.; Pellizzoni, M. M.; Lebrun, V.; Reuter, R.; Köhler, V.; Lewis, J. C.; Ward, T. R., Artificial Metalloenzymes: Reaction Scope and Optimization Strategies. *Chem. Rev.* **2018,** *118*, 142-231. (b) Heinisch, T.; Ward, T. R., Latest Developments in Metalloenzyme Design and Repurposing. *Eur. J. Inorg. Chem.* **2015,** *2015*, 3406-3418.

5. Hackley, B. E.; Plapinger, R.; Stolberg, M.; Wagner-Jauregg, T., Acceleration of the Hydrolysis of Organic Fluorophosphates and Fluorophosphonates with Hydroxamic Acids. *J. Am. Chem. Soc.* **1955,** *77*, 3651-3653.

6. Breslow, R.; Overman, L. E., An "artificial enzyme" combining a metal catalytic group and a hydrophobic binding cavity. *J. Am. Chem. Soc.* **1970,** *92*, 1075-7.

7. Pedersen, C. J., Cyclic polyethers and their complexes with metal salts. *J. Am. Chem. Soc.* **1967,** *89*, 2495-2496.

8. Lehn, J.-M., Supramolecular Chemistry – Scope and Perspectives Molecules, Supermolecules, and Molecular Devices(Nobel Lecture). *Angew. Chem. Int. Ed. Engl.* **1988,** *27*, 89-112.

9. Lehn, J. M.; Sauvage, J. P., Cation and cavity selectivities of alkali and alkaline-earth "cryptates". *J. Chem. Soc. D* **1971,** *0*, 440-441.

10. Cram, D. J., The Design of Molecular Hosts, Guests, and Their Complexes (Nobel Lecture). *Angew. Chem. Int. Ed. Engl.* **1988,** *27*, 1009-1020.

11. Pedersen, C. J., The Discovery of Crown Ethers (Nobel Lecture). *Angew. Chem. Int. Ed. Engl.* **1988,** *27*, 1021-1027.

12. Sauvage, J.-P., From Chemical Topology to Molecular Machines (Nobel Lecture). *Angew. Chem. Int. Ed.* **2017,** *56*, 11080-11093.

13. (a) Iwasawa, T., Recent developments of cavitand-recessed type metal catalysts.

For references, see page 59.

Tetrahedron Lett. **2017,** *58*, 4217-4226. (b) Tan, C.; Chu, D.; Tang, X.; Liu, Y.; Xuan, W.; Cui, Y., Supramolecular Coordination Cages for Asymmetric Catalysis. *Chemistry* **2019,** *25*, 662-672. (c) Kaya, Z.; Bentouhami, E.; Pelzer, K.; Armspach, D., Cavity-shaped ligands for asymmetric metal catalysis. *Coord. Chem. Rev.* **2021,** *445*, 214066. (d) Murray, J.; Kim, K.; Ogoshi, T.; Yao, W.; Gibb, B. C., The aqueous supramolecular chemistry of cucurbit[n]urils, pillar[n]arenes and deep-cavity cavitands. *Chem. Soc. Rev.* **2017,** *46*, 2479-2496.

14. (a) Ewins, A. J., CLXVIII. – The action of phosphorus pentachloride on the methylene ethers of catechol derivatives. Part V. Derivatives of protocatechuyl alcohol and protocatechuonitrile. *J. Chem. Soc., Trans.* **1909,** *95*, 1482-1488. (b) Robinson, G. M., XXX. – A reaction of homopiperonyl and of homoveratryl alcohols. *J. Chem. Soc., Trans.* **1915,** *107*, 267-276.

15. (a) Brotin, T.; Dutasta, J.-P., Cryptophanes and Their Complexes – Present and Future. *Chem. Rev.* **2009,** *109*, 88-130. (b) Hardie, M. J., Recent advances in the chemistry of cyclotriveratrylene. *Chem. Soc. Rev.* **2010,** *39*, 516-527.

16. Gutsche, C. D., *Calixarenes: An Introduction*. Cambrige: Royal Society of Chemistry, **2008**.

17. (a) Arnott, G. E., Inherently Chiral Calixarenes: Synthesis and Applications. *Chemistry* **2018,** *24*, 1744-1754. (b) Wang, M.-X., Nitrogen and Oxygen Bridged Calixaromatics: Synthesis, Structure, Functionalization, and Molecular Recognition. *Acc. Chem. Res.* **2012,** *45*, 182-195.

18. (a) Freeman, W. A.; Mock, W. L.; Shih, N. Y., Cucurbituril. *J. Am. Chem. Soc.* **1981,** *103*, 7367-7368. (b) Behrend, R.; Meyer, E.; Rusche, F., I. Ueber Condensationsproducte aus Glycoluril und Formaldehyd. *Justus Liebigs Ann. Chem.* **1905,** *339*, 1-37.

19. Biedermann, F.; Vendruscolo, M.; Scherman, O. A.; De Simone, A.; Nau, W. M., Cucurbit[8]uril and Blue-Box: High-Energy Water Release Overwhelms Electrostatic Interactions. *J. Am. Chem. Soc.* **2013,** *135*, 14879-14888.

20. (a) Barrow, S. J.; Kasera, S.; Rowland, M. J.; del Barrio, J.; Scherman, O. A., Cucurbituril-Based Molecular Recognition. *Chem. Rev.* **2015,** *115*, 12320-12406. (b) Isaacs, L., Stimuli Responsive Systems Constructed Using Cucurbit[n]uril-Type Molecular Containers. *Acc. Chem. Res.* **2014,** *47*, 2052-2062. (c) Vallavoju, N.; Sivaguru, J., Supramolecular photocatalysis: combining confinement and non-covalent interactions to control light initiated reactions. *Chem. Soc. Rev.* **2014,** *43*, 4084. (d) Ni, X.-L.; Xiao, X.; Cong, H.; Liang, L.-L.; Cheng, K.; Cheng, X.-J.; Ji, N.-N.; Zhu, Q.-J.; Xue, S.-F.; Tao, Z., Cucurbit[n]uril-based coordination chemistry: from simple coordination complexes to novel poly-dimensional

For references, see page 59.

coordination polymers. *Chem. Soc. Rev.* **2013,** *42*, 9480. (e) Lü, J.; Lin, J.-X.; Cao, M.-N.; Cao, R., Cucurbituril: A promising organic building block for the design of coordination compounds and beyond. *Coord. Chem. Rev.* **2013,** *257*, 1334-1356. (f) Ni, X.-L.; Xiao, X.; Cong, H.; Zhu, Q.-J.; Xue, S.-F.; Tao, Z., Self-Assemblies Based on the "Outer-Surface Interactions" of Cucurbit[n]urils: New Opportunities for Supramolecular Architectures and Materials. *Acc. Chem. Res.* **2014,** *47*, 1386-1395.

21. Dodziuk, H., *Cyclodextrins and Their Complexes: chemistry, analytical methods, applications*. Warsaw: John Wiley & Sons, **2006**.

22. Szejtli, J., Introduction and General Overview of Cyclodextrin Chemistry. *Chem. Rev.* **1998,** *98*, 1743-1754.

23. Connors, K. A., The Stability of Cyclodextrin Complexes in Solution. *Chem. Rev.* **1997,** *97*, 1325-1358.

24. Crini, G., Review: A History of Cyclodextrins. *Chem. Rev.* **2014,** *114*, 10940-10975.

25. (a) Harada, A.; Takashima, Y.; Nakahata, M., Supramolecular Polymeric Materials via Cyclodextrin–Guest Interactions. *Acc. Chem. Res.* **2014,** *47*, 2128-2140. (b) Molnár, Á., Synthetic Application of Cyclodextrins in Combination with Metal Ions, Complexes, and Metal Particles. *ChemCatChem* **2020,** *13*, 1424-1474. (c) Macaev, F.; Boldescu, V., Cyclodextrins in Asymmetric and Stereospecific Synthesis. *Symmetry* **2015,** *7*, 1699-1720. (d) Menuel, S.; Bertaut, E.; Monflier, E.; Hapiot, F., Cyclodextrin-based PNN supramolecular assemblies: a new class of pincer-type ligands for aqueous organometallic catalysis. *Dalton Trans.* **2015,** *44*, 13504-13512. (e) Jouffroy, M.; Armspach, D.; Matt, D., Cyclodextrin and phosphorus(III): a versatile combination for coordination chemistry and catalysis. *Dalton Trans.* **2015,** *44*, 12942-12969. (f) Hapiot, F.; Bricout, H.; Tilloy, S.; Monflier, E., Functionalized Cyclodextrins as First and Second Coordination Sphere Ligands for Aqueous Organometallic Catalysis. *Eur. J. Inorg. Chem.* **2012,** *2012*, 1571-1578. (g) Hapiot, F.; Tilloy, S.; Monflier, E., Cyclodextrins as supramolecular hosts for organometallic complexes. *Chem. Rev.* **2006,** *106*, 767-81. (h) Delbianco, M.; Bharate, P.; Varela-Aramburu, S.; Seeberger, P. H., Carbohydrates in Supramolecular Chemistry. *Chem. Rev.* **2016,** *116*, 1693-752.

26. Ogoshi, T.; Kanai, S.; Fujinami, S.; Yamagishi, T.-A.; Nakamoto, Y., para-Bridged Symmetrical Pillar[5]arenes: Their Lewis Acid Catalyzed Synthesis and Host–Guest Property. *J. Am. Chem. Soc.* **2008,** *130*, 5022-5023.

27. (a) Xue, M.; Yang, Y.; Chi, X.; Zhang, Z.; Huang, F., Pillararenes, A New Class of Macrocycles for Supramolecular Chemistry. *Acc. Chem. Res.* **2012,** *45*, 1294-1308. (b) Ogoshi, T.; Yamagishi, T. A.; Nakamoto, Y., Pillar-Shaped Macrocyclic Hosts Pillar[n]arenes: New

For references, see page 59.

Key Players for Supramolecular Chemistry. *Chem. Rev.* **2016,** *116*, 7937-8002. (c) Ogoshi, T.; Kakuta, T.; Yamagishi, T. A., Applications of Pillar[n]arene-Based Supramolecular Assemblies. *Angew. Chem. Int. Ed. Engl.* **2019,** *58*, 2197-2206.

28. García-Simón, C.; Gramage-Doria, R.; Raoufmoghaddam, S.; Parella, T.; Costas, M.; Ribas, X.; Reek, J. N. H., Enantioselective Hydroformylation by a Rh-Catalyst Entrapped in a Supramolecular Metallocage. *J. Am. Chem. Soc.* **2015,** *137*, 2680-2687.

29. (a) Han, Y.; Liu, W.; Huang, J.; Qiu, S.; Zhong, H.; Liu, D.; Liu, J., Cyclodextrin-Based Metal-Organic Frameworks (CD-MOFs) in Pharmaceutics and Biomedicine. *Pharmaceutics* **2018,** *10*. (b) Mouarrawis, V.; Plessius, R.; van der Vlugt, J. I.; Reek, J. N. H., Confinement Effects in Catalysis Using Well-Defined Materials and Cages. *Front Chem.* **2018,** *6*, 623.

30. Chughtai, A. H.; Ahmad, N.; Younus, H. A.; Laypkov, A.; Verpoort, F., Metal–organic frameworks: versatile heterogeneous catalysts for efficient catalytic organic transformations. *Chem. Soc. Rev.* **2015,** *44*, 6804-6849.

31. (a) Furukawa, H.; Cordova, K. E.; O'Keeffe, M.; Yaghi, O. M., The chemistry and applications of metal-organic frameworks. *Science* **2013,** *341*, 1230444. (b) Li, H.; Shi, L.; Li, C.; Fu, X.; Huang, Q.; Zhang, B., Metal-Organic Framework Based on alpha-Cyclodextrin Gives High Ethylene Gas Adsorption Capacity and Storage Stability. *ACS Appl. Mater. Interfaces* **2020,** *12*, 34095-34104. (c) Canivet, J.; Aguado, S.; Schuurman, Y.; Farrusseng, D., MOF-supported selective ethylene dimerization single-site catalysts through one-pot postsynthetic modification. *J. Am. Chem. Soc.* **2013,** *135*, 4195-4198. (d) Chaemchuen, S.; Kabir, N. A.; Zhou, K.; Verpoort, F., Metal–organic frameworks for upgrading biogas via CO_2 adsorption to biogas green energy. *Chem. Soc. Rev.* **2013,** *42*, 9304. (e) Kreno, L. E.; Leong, K.; Farha, O. K.; Allendorf, M.; Van Duyne, R. P.; Hupp, J. T., Metal–Organic Framework Materials as Chemical Sensors. *Chem. Rev.* **2012,** *112*, 1105-1125. (f) Horcajada, P.; Gref, R.; Baati, T.; Allan, P. K.; Maurin, G.; Couvreur, P.; Férey, G.; Morris, R. E.; Serre, C., Metal–Organic Frameworks in Biomedicine. *Chem. Rev.* **2012,** *112*, 1232-1268. (g) Kurmoo, M., Magnetic metal–organic frameworks. *Chem. Soc. Rev.* **2009,** *38*, 1353. (h) Nasalevich, M. A.; Becker, R.; Ramos-Fernandez, E. V.; Castellanos, S.; Veber, S. L.; Fedin, M. V.; Kapteijn, F.; Reek, J. N. H.; Van Der Vlugt, J. I.; Gascon, J., Co@NH_2-MIL-125(Ti): cobaloxime-derived metal–organic framework-based composite for light-driven H_2 production. *Energy Environ. Sci.* **2015,** *8*, 364-375.

32. Lehn, J.-M., *Supramolecular Chemistry: concepts and perspectives*. Weinheim: Wiley, **1995**.

33. Davis, H. J.; Ward, T. R., Artificial Metalloenzymes: Challenges and Opportunities. *ACS*

For references, see page 59.

Cent. Sci. **2019,** *5*, 1120-1136.

34. Danopoulos, A. A.; Braunstein, P., Ligand Control of the Metal Coordination Sphere: Structures, Reactivity and Catalysis. *Oil Gas Sci Technol* **2016,** *71*, 24.

35. (a) Stradiotto, M.; Lundgren, R., *Ligand Design in Metal Chemistry: Reactivity and Catalysis*. UK: John Wiley & Sons, **2016**. (b) Potier, J.; Menuel, S.; Rousseau, J.; Tumkevicius, S.; Hapiot, F.; Monflier, E., Multifunctional cyclodextrin-based N,N-bidentate ligands for aqueous Heck arylation. *Appl. Catal. A: Gen.* **2014,** *479*, 1-8. (c) Debata, N. B.; Tripathy, D.; Chand, D. K., Self-assembled coordination complexes from various palladium(II) components and bidentate or polydentate ligands. *Coord. Chem. Rev.* **2012,** *256*, 1831-1945.

36. Braunstein, P.; Naud, F., Hemilability of Hybrid Ligands and the Coordination Chemistry of Oxazoline-Based Systems. *Angew. Chem. Int. Ed.* **2001,** *40*, 680-699.

37. Zhang, W.-H.; Chien, S. W.; Hor, T. S. A., Recent advances in metal catalysts with hybrid ligands. *Coord. Chem. Rev.* **2011,** *255*, 1991-2024.

38. (a) Meeuwissen, J.; Reek, J. N. H., Supramolecular catalysis beyond enzyme mimics. *Nat. Chem.* **2010,** *2*, 615-621. (b) Leenders, S. H.; Gramage-Doria, R.; de Bruin, B.; Reek, J. N., Transition metal catalysis in confined spaces. *Chem. Soc. Rev.* **2015,** *44*, 433-48.

39. Tilloy, S.; Binkowski-Machut, C.; Menuel, S.; Bricout, H.; Monflier, E., Phosphane-Based Cyclodextrins as Mass Transfer Agents and Ligands for Aqueous Organometallic Catalysis. *Molecules* **2012,** *17*, 13062-13072.

40. (a) Bonomo, R. P.; Cucinotta, V.; D'Alessandro, F.; Impellizzeri, G.; Maccarrone, G.; Vecchio, G.; Rizzarelli, E., Conformational features and coordination properties of functionalized cyclodextrins. Formation, stability, and structure of proton and copper(II) complexes of histamine-bearing .beta.-cyclodextrin in aqueous solution. *Inorg. Chem.* **1991,** *30*, 2708-2713. (b) Impellizzeri, G.; Maccarrone, G.; Rizzarelli, E.; Vecchio, G.; Corradini, R.; Marchelli, R., 6-Deoxy-6-N-histamino-β-cyclodextrin Copper(II) Complex, a New Enantioselective Receptor for Aromatic Amino Acids. *Angew. Chem. Int. Ed. Engl.* **1991,** *30*, 1348-1349. (c) Cucinotta, V.; D'Alessandro, F.; Impellizzeri, G.; Vecchio, G., The copper(II) complex with the imidazole-bound histamine derivative of β-cyclodextrin as a powerful chiral discriminating agent. *J. Chem. Soc., Chem. Commun.* **1992,** 1992, 1743-1745. (d) Bonomo, R. P.; Cucinotta, V.; Allessandro, F. D.; Impellizzeri, G.; Maccarrone, G.; Rizzarelli, E.; Vecchio, G., Coordination properties of 6-deoxy-6-[1-(2-amino) ethylamino]-?-cyclodextrin and the ability of its copper(II) complex to recognize and separate amino acid enantiomeric pairs. *J. Incl. Phenom. Macrocycl. Chem.* **1993,** *15*, 167-180.

41. Marcella Bonchio, T. C., Fulvio Di Furia, Roberto Fomasier, selective Oxidation of

For references, see page 59.

Thioanisole in Water by Hydrogen Peroxide Catalyzed by Mo(VI) in the Presence of /7-Cyclodextrin-Based Ligands Supramolecular Catalysis:. *J. Org. Chem.* **1995,** *60*, 5986-5988.

42. (a) Brown, S. E.; Coates, J. H.; Easton, C. J.; Lincoln, S. F., Metallocyclodextrins of 6A-(3-aminopropylamino)-6A-deoxy-β-cyclodextrin: their formation and enantioselective complexation of (R)- and (S)-tryptophan anions in aqueous solution. *J. Chem. Soc., Faraday Trans.* **1994,** *90*, 739-743. (b) Brown, S. E.; Coates, J. H.; Easton, C. J.; van Eyk, S. J.; Lincoln, S. F.; May, B. L.; Stile, M. A.; Whalland, C. B.; Williams, M. L., Tryptophan anion complexes of β-cyclodextrin (cyclomaltaheptaose), an aminopropylamino-β-cyclodextrin and its enantioselective nickel(II) complex. *J. Chem. Soc., Chem. Commun.* **1994,** 1994, 47-47.

43. Potter, C. F.; Russell, N. R.; McNamara, M., Spectroscopic Characterisation of Metallo-Cyclodextrins for Potential Chiral Separation of Amino Acids and L/D-DOPA. *J. Incl. Phenom. Macrocycl. Chem.* **2006,** *56*, 395-403.

44. Schlatter, A.; Kundu, M. K.; Woggon, W. D., Enantioselective reduction of aromatic and aliphatic ketones catalyzed by ruthenium complexes attached to beta-cyclodextrin. *Angew. Chem. Int. Ed. Engl.* **2004,** *43*, 6731-6734.

45. Shen, H. M.; Ji, H. B., Amino alcohol-modified beta-cyclodextrin inducing biomimetic asymmetric oxidation of thioanisole in water. *Carbohydr. Res.* **2012,** *354*, 49-58.

46. Shen, H.-M.; Ji, H.-B., Cyclodextrin–[$RuCl_2$(Arene)]2 conjugates: another way to enhance the enantioselectivity of aromatic ketones reduction by aromatic ligands' volume. *Tetrahedron* **2013,** *69*, 8360-8367.

47. Reetz, M. T.; Rudolph, J., Synthesis of a phosphine-modified cyclodextrin and its rhodium complex. *Tetrahedron: Asymmetry* **1993,** *4*, 2405-2406.

48. Reetz, M. T.; Rudolph, J.; Goddard, R., Diastereotopic group recognition in the solid state - A unique intramolecular β-cyclodextrin inclusion complex. *Can. J. Chem.* **2001,** *79*, 1806-1811.

49. Reetz, M. T.; Kostas, I. D.; Waldvogel, S. R., Synthesis of a gold(I) complex with a (thio)phosphine-modified β-cyclodextrin. *Inorg. Chem. Commun.* **2002,** *5*, 252-254.

50. Yang, C.; Wong, Y. T.; Li, Z.; Krepinsky, J. J.; Jia, G., Synthesis of β-Cyclodextrin-Functionalized (2S,4S)-(−)-4-(Diphenylphosphino)-2-(diphenylphosphinomethyl)pyrrolidine Ligands and Their Rhodium and Platinum Complexes. *Organometallics* **2001,** *20*, 5220-5224.

51. (a) Tillack, A.; Michalik, D.; Koy, C.; Michalik, M., Catalytic asymmetric hydrosilylation of butadiynes: A new synthesis of optically active allenes. *Tetrahedron Lett.* **1999,** *40*, 6567-6568. (b) Achiwa, K., Asymmetric hydrogenation with new chiral functionalized bisphosphine-rhodium complexes. *J. Am. Chem. Soc.* **1976,** *98*, 8265-8266.

For references, see page 59.

52. Wong, Y. T.; Yang, C.; Ying, K.-C.; Jia, G., Synthesis of a Novel β-Cyclodextrin-Functionalized Diphosphine Ligand and Its Catalytic Properties for Asymmetric Hydrogenation. *Organometallics* **2002,** *21*, 1782-1787.

53. Ohga, Y.; Iitaka, Y.; Achiwa, K., The Crystal Structure of Cycloocta-1,5-Diene-4-Diphenylphosphino-2-Diphenylphosphinomethylpyrrolidine(PPM)-Rhodium(I) Perchlorate. *Chem. Lett.* **1980,** *9*, 861-864.

54. Milovic, N. M.; Badjic, J. D.; Kostic, N. M., Conjugate of palladium(II) complex and beta-cyclodextrin acts as a biomimetic peptidase. *J. Am. Chem. Soc.* **2004,** *126*, 696-697.

55. Zhang, G.; Luan, Y.; Han, X.; Wang, Y.; Wen, X.; Ding, C.; Gao, J., A palladium complex with functionalized β-cyclodextrin: a promising catalyst featuring recognition abilities for Suzuki–Miyaura coupling reactions in water. *Green Chem.* **2013,** *15*, 2081-2085.

56. Zhang, G.; Wang, Y.; Wen, X.; Ding, C.; Li, Y., Dual-functional click-triazole: a metal chelator and immobilization linker for the construction of a heterogeneous palladium catalyst and its application for the aerobic oxidation of alcohols. *Chem. Commun.* **2012,** *48*, 2979.

57. Shinde, V.; Jeong, D.; Jung, S., An Amino-Chain Modified β-cyclodextrin: A Supramolecular Ligand for $Pd(OAc)_2$ Acceleration in Suzuki–Miyaura Coupling Reactions in Water. *Catalysts* **2019,** *9*, 111.

58. Luo, K.; Zhang, L.; Yang, R.; Jin, Y.; Lin, J., Picolinamide modified beta-cyclodextrin/Pd (II) complex: Asupramolecular catalyst for Suzuki-Miyaura coupling of aryl, benzyl and allyl halides with arylboronic acids in water. *Carbohydr Polym.* **2018,** *200*, 200-210.

59. Guo, Y.; Li, J.; Zhao, F.; Lan, G.; Li, L.; Liu, Y.; Si, Y.; Jiang, Y.; Yang, B.; Yang, R., Palladium-modified functionalized cyclodextrin as an efficient and recyclable catalyst for reduction of nitroarenes. *Rsc. Adv.* **2016,** *6*, 7950-7954.

60. Khan, R. I.; Pitchumani, K., Water-Soluble Palladium Complex of N′-(pyridin-2-yl)propane-1,3-diamine modified β-Cyclodextrin: An efficient Catalyst for Transfer Hydrogenation of Carbonyl Compounds. *ACS Sustain. Chem. Eng.* **2018,** *6*, 16130-16138.

61. Li, H.; Li, F.; Zhang, B.; Zhou, X.; Yu, F.; Sun, L., Visible light-driven water oxidation promoted by host-guest interaction between photosensitizer and catalyst with a high quantum efficiency. *J. Am. Chem. Soc.* **2015,** *137*, 4332-4335.

62. Sechet, D.; Kaya, Z.; Phan, T. A.; Jouffroy, M.; Bentouhami, E.; Armspach, D.; Matt, D.; Toupet, L., Aza-capped cyclodextrins for intra-cavity metal complexation. *Chem. Commun. (Camb)* **2017,** *53*, 11717-11720.

63. (a) Creaven, B. S.; Donlon, D. F.; McGinley, J., Coordination chemistry of calix[4]arene derivatives with lower rim functionalisation and their applications. *Coord. Chem. Rev.* **2009,**

For references, see page 59.

253, 893-962. (b) Dieleman, C.; Steyer, S.; Jeunesse, C.; Matt, D., Diphosphines based on an inherently chiral calix[4]arene scaffold: synthesis and use in enantioselective catalysis. *J. Chem. Soc., Dalton Trans.* **2001,** *2001*, 2508-2517. (c) Lo, P.; Wong, M., Extended Calix[4]arene-Based Receptors for Molecular Recognition and Sensing. *Sensors* **2008,** *8*, 5313-5335. (d) Joseph, R.; Rao, C. P., Ion and Molecular Recognition by Lower Rim 1,3-Di-conjugates of Calix[4]arene as Receptors. *Chem. Rev.* **2011,** *111*, 4658-4702.

64. Lucking, U.; Chen, J.; Rudkevich, D. M.; Rebek, J., Jr., A self-folding metallocavitand. *J. Am. Chem. Soc.* **2001,** *123*, 9929-9934.

65. Gibson, C.; Rebek, J., Jr., Recognition and catalysis in allylic alkylations. *Org. Lett.* **2002,** *4*, 1887-1890.

66. Khiri, N.; Bertrand, E.; Ondel-Eymin, M.-J.; Rousselin, Y.; Bayardon, J.; Harvey, P. D.; Jugé, S., Enantioselective Hydrogenation Catalysis Aided by a σ-Bonded Calix[4]arene to a P-Chirogenic Aminophosphane Phosphinite Rhodium Complex. *Organometallics* **2010,** *29*, 3622-3631.

67. Schlatter, A.; Woggon, W.-D., Enantioselective Transfer Hydrogenation of Aliphatic Ketones Catalyzed by Ruthenium Complexes Linked to the Secondary Face of β-Cyclodextrin. *Adv. Synth. Catal.* **2008,** *350*, 995-1000.

68. Jouffroy, M.; Sémeril, D.; Armspach, D.; Matt, D., Phosphane-Phosphite Chelators Built on a α-Cyclodextrin Scaffold: Application in Rh-Catalysed Asymmetric Hydrogenation and Hydroformylation. *Eur. J. Org. Chem.* **2013,** *2013*, 6069-6077.

69. Marson, A.; Ernsting, J. E.; Lutz, M.; Spek, A. L.; van Leeuwen, P. W.; Kamer, P. C., A novel hemilabile calix[4],quinoline-based P,N-ligand: coordination chemistry and complex characterisation. *Dalton Trans.* **2009,** *2009*, 621-633.

70. Tabushi, I.; Kuroda, Y.; Mizutani, T., Functionalized cyclodextrins as artificial receptors. *Tetrahedron* **1984,** *40*, 545-552.

71. (a) Cucinotta, V.; Grasso, G.; Pedotti, S.; Rizzarelli, E.; Vecchio, G.; Di Blasio, B.; Isernia, C.; Saviano, M.; Pedone, C., A Platinum(II) Diamino-β-cyclodextrin Complex: A Crystallographic and Solution Study. Synthesis and Structural Characterization of a Platinum(II) Complex of 6A,6B-Diamino-6A,6B-dideoxycyclomaltoheptaose. *Inorg. Chem.* **1996,** *35*, 7535-7540. (b) Di Blasio, B.; Galdiero, S.; Saviano, M.; Pedone, C.; Benedetti, E.; Rizzarelli, E.; Pedotti, S.; Vecchio, G.; Gibbons, W. A., Synthesis and structural characterization of 6I,6II-diamino-6I,6II-dideoxy-cyclomaltoheptaose, a difunctionalized β-cyclodextrin. *Carbohydr. Res.* **1996,** *282*, 41-52.

72. Engeldinger, É.; Armspach, D.; Matt, D.; Toupet, L.; Wesolek, M., Synthesis of large

For references, see page 59.

chelate rings with diphosphites built on a cyclodextrin scaffold. Unexpected formation of 1,2-phenylene-capped α-cyclodextrins. *C. R. Chim.* **2002,** *5*, 359-372.

73. Engeldinger, E.; Armspach, D.; Matt, D.; Jones, P. G., Cyclodextrin Phosphanes as First and Second Coordination Sphere Cavitands. *Eur. J. Chem.* **2003,** *9*, 3091-3105.

74. Gramage-Doria, R.; Rodriguez-Lucena, D.; Armspach, D.; Egloff, C.; Jouffroy, M.; Matt, D.; Toupet, L., Regioselective Double Capping of Cyclodextrin Scaffolds. *Eur. J. Chem.* **2011,** *17*, 3911-3921.

75. Gramage-Doria, R.; Armspach, D.; Matt, D.; Toupet, L., Non-conventional coordination of cavity-confined metal centres. *Dalton Trans.* **2012,** *41*, 8786-96.

76. Gramage-Doria, R.; Armspach, D.; Matt, D.; Toupet, L., A Cavity-Shaped Diphosphane Displaying "Oschelating" Behavior. *Angew. Chem.* **2011,** *123*, 1592-1597.

For references, see page 59.

Chapter II[†]

Synthesis and characterization of a cavity-shaped, *cis*-chelating P,N ligand and its cavity-free analog – Study of their coordination behavior towards d^8 and d^{10} metal cations

[†] Part of the work in this chapter has been published in *Dalton Trans.*, **2022**, *51*, 11226-11230

II. 1. Introduction

Cyclodextrins (CDs) are cyclic oligosaccharides produced from starch by enzymatic conversion, consisting of D-(+)-glucopyranosyl units connected by α-1,4-glycosidic bonds.[1] Typical commercial CDs contain a number of glucose monomers ranging from six (α-CD), seven (β-CD), to eight (γ-CD) units.[2] The most striking feature of CDs is their unique cone-shaped cavity, which displays a hydrophobic inner wall and a hydrophilic outer surface. The former is responsible for the formation of inclusion complexes with a wide range of hydrophobic compounds in water, and their steric and electronic environment can be profoundly altered as a result of encapsulation.[3] Moreover, thanks to the numerous hydroxyl groups lying at the CD narrow and wide rim – the so-called primary and secondary faces respectively, various functional groups can be introduced at a given positon on both faces, thus altering the physical and chemical properties of CD and making them functional molecules with given characteristics.[4] Because of the presence of a restricted space within the CD core and their exceptional host-guest properties in aqueous solution, many modified CDs acting as "enzyme mimics" have been developed with the aim of achieving efficient and selective transformations working under mild reaction conditions in environmentally friendly media such as water.[5] However, modified CDs targeting more industrially-relevant, transition metal-catalyzed reactions[6] that have a broader scope than traditional CD-based enzyme mimics are still relatively rare and there is a need to explore new types of metal confining ligands that are suited for these transformations.

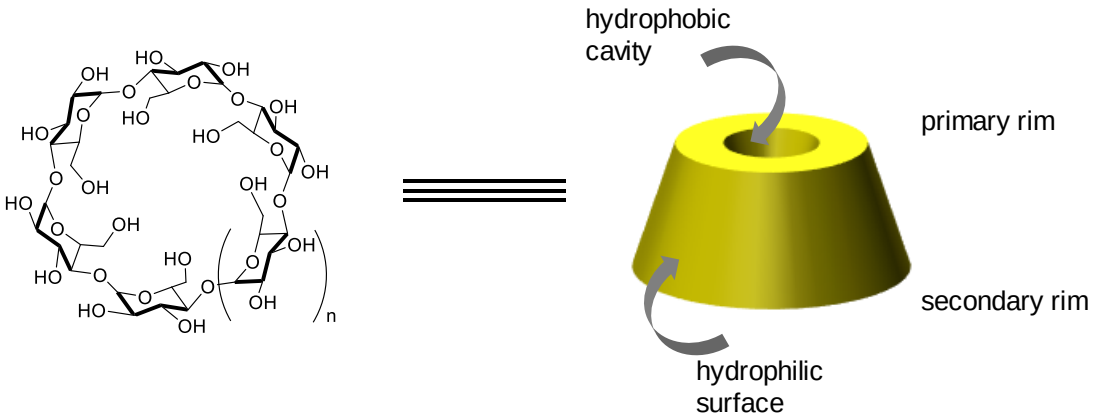

Fig 1. Schematic representation of cyclodextrins.

For references, see page 120.

In this respect, hybrid ligands containing two or more different types of donor groups have attracted increasing attention.[7] Unsymmetrical bidentate ligands with a hard nitrogen and a soft phosphorus donor atom, referred to as P,N ligands hereafter, able to chelate a metal center and give rise to a wide chemical and structural diversity, have been extensively studied in transition metal coordination chemistry and in homogeneous catalysis.[8] In particular, the heterofunctional systems often display unique dynamic features related to the hemilability of the nitrogen donor, which usually results in specific and often enhanced reactivity of their transition metal complexes.[7a,9] Furthermore, the electronic and steric properties of the nitrogen and phosphorus donor moieties can be easily modified, thus increasing their scope in terms of coordinating and catalytic properties.[8a-f,8h,8i]

When it comes to CD-based ligands, the incorporation of bridging coordinating groups within the macrocyclic structure of CDs has allowed access to high-performance ligands in asymmetric metal catalysis. For example, introverted phosphinocyclodextrins (**HUGPHOS-1** and **HUGPHOS-2**) designed by Armspach and Matt have been used in asymmetric hydroformylation of styrene and in asymmetric cycloisomerisation of 1,6-enynes.[10] It was previously shown that a bridging unit consisting of a single donor atom like phosphorus or nitrogen linking two adjacent glucose units is sufficiently rigid to force the donor atom lone pair to point towards the CD interior and upon metal complexation force a metal center to reside inside the cavity.[11] The latter feature is prone to produce high chemo-, regio-, and/or enantioelectivity in metal catalysis if the receptor is optically active (see Chapter 1).[12] To date, most ligands used in catalysis are *cis*-chelating, because the catalytic cycle of many reactions, such as C–C and C–N coupling reactions involves a *cis* arrangement of the reactive entities around the metal center. This particular geometry can be imposed by *cis*-chelating ligands, including hybrid ones. In this chapter, we will focus on the preparation of the first *cis*-chelating P,N ligand (**L1**) derived from CD capable of confining a metal center and describe various complexes in which a transition metal is deeply buried.

For references, see page 120.

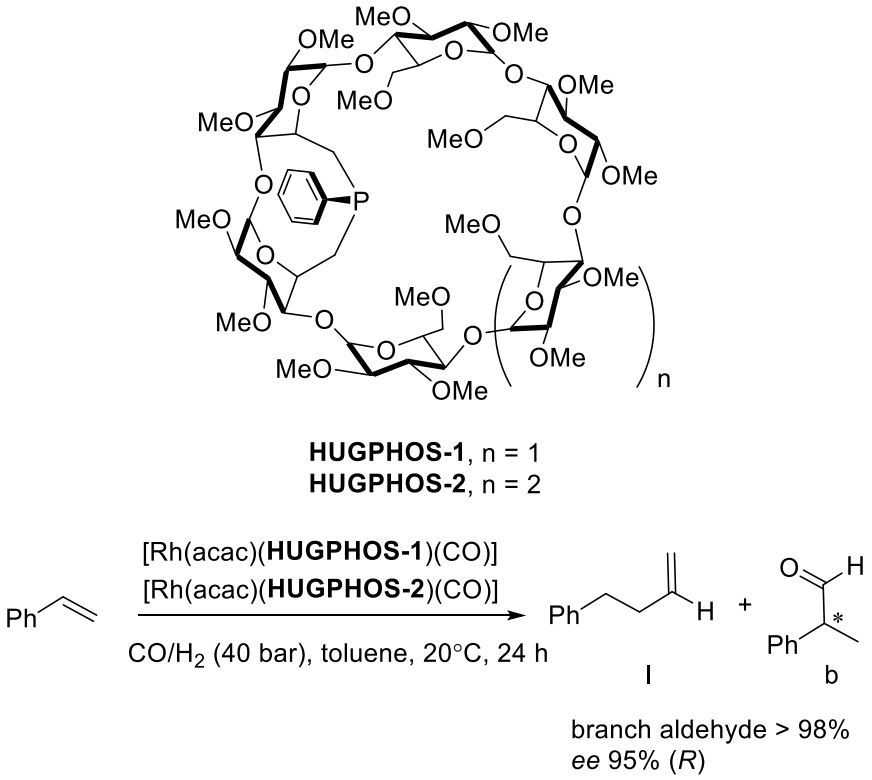

Scheme 1. Use of phosphinocyclodextrins (**HUGPHOS-1** and **HUGPHOS-2**) in Rh-catalyzed asymmetric hydroformylation of styrene.

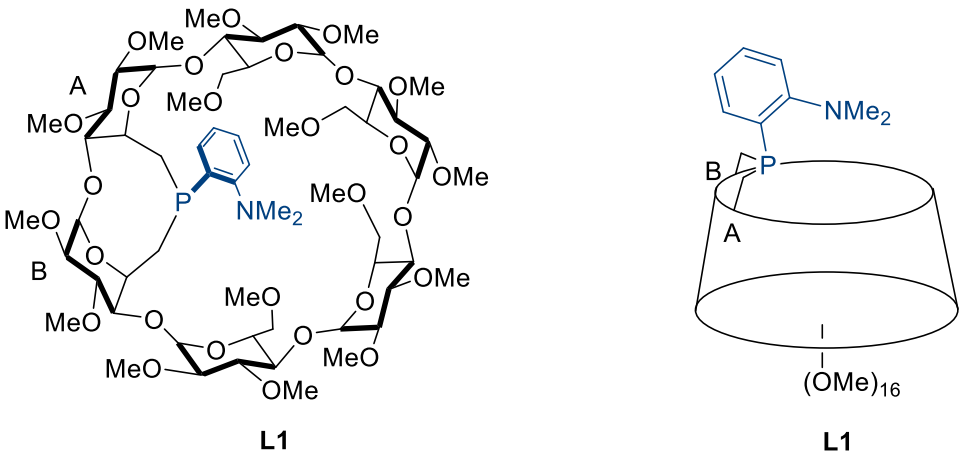

Fig 2. Two different representations of the cavity-shaped P,N ligand **L1**.

II. 2. Results and discussion

II. 2. 1. Preliminary studies

For references, see page 120.

The bidentate P,N ligand **L1** was prepared by capping the known dimesylate **1b** with a P,N coordinating unit. The procedure for preparing **1b** has already been reported by our group, and is detailed in Scheme 2.[13]

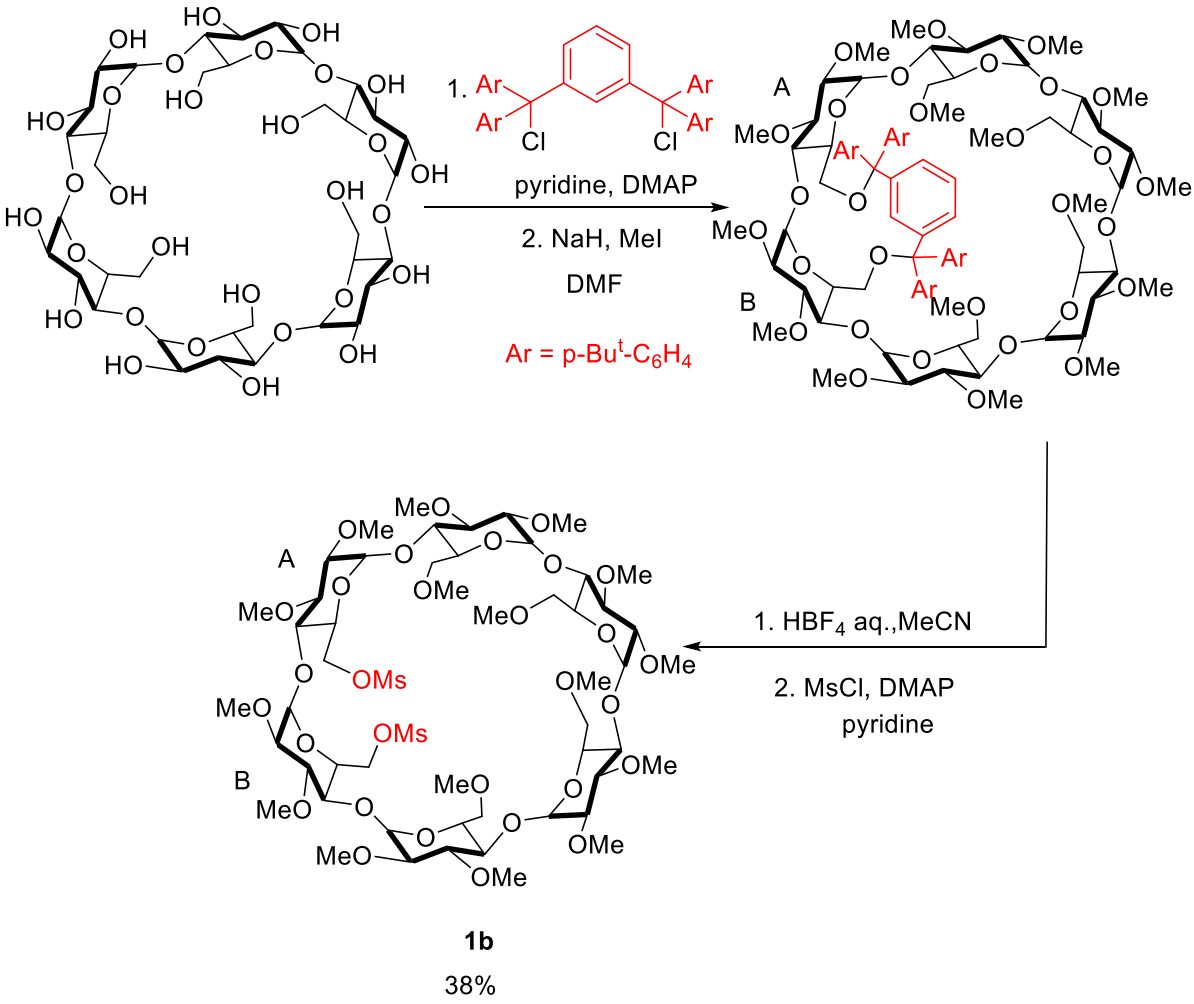

Scheme 2. Formation of α-CD-based dimesylate **1b**.

The commercial α-CD was first capped with 1,3-bis[bis(4-tert-butylphenyl)chloromethyl]benzene. The resulting 6^A, 6^B-briged CD was not isolated, but directly treated with excess MeI/NaH in order to methylate the remaining hydroxyl groups before being deprotected with aqueous HBF_4 in MeCN to afford diol **1a**.

For references, see page 120.

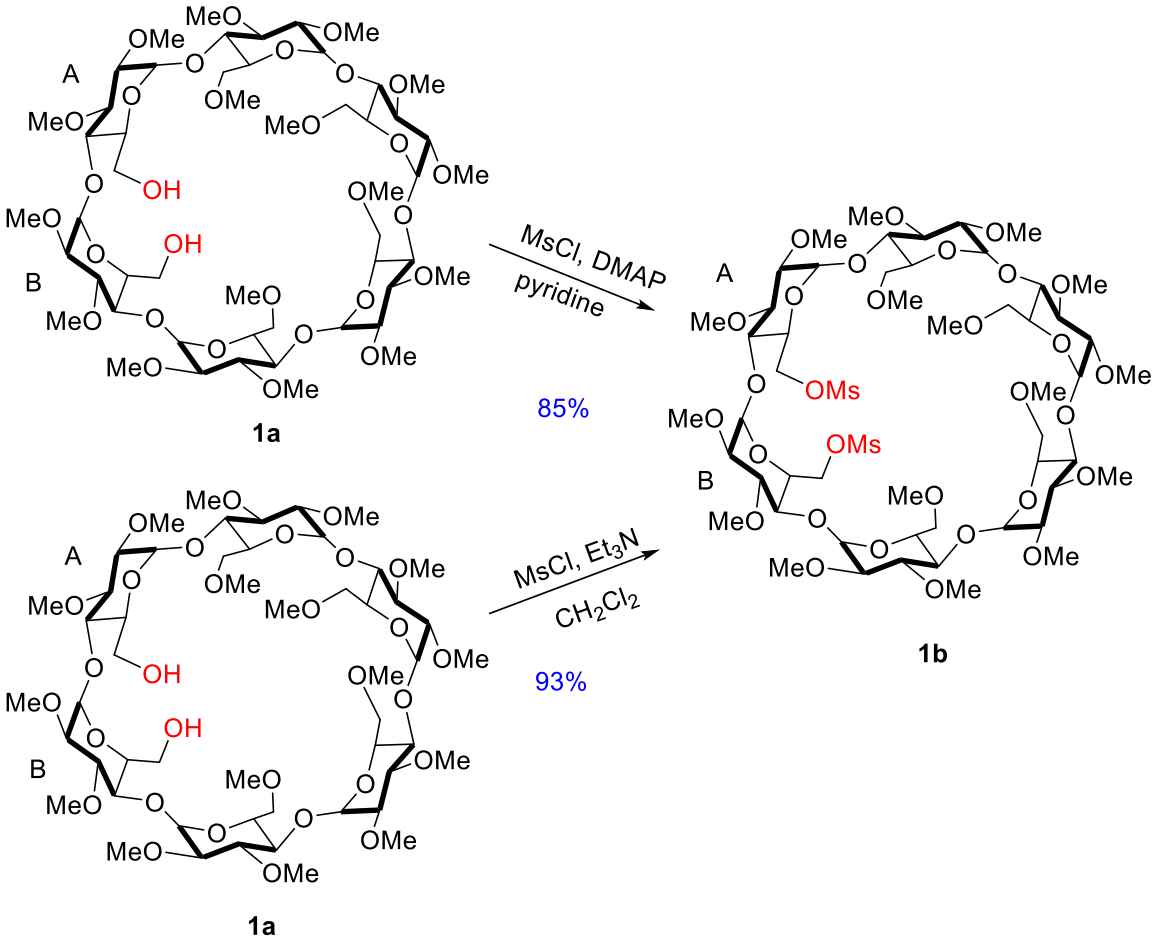

Scheme 3. Optimization of the synthesis of dimesylate **1b**.

The usual reaction pathway for accessing dimesylate **1b** consists in reacting diol **1a** with MsCl and DMAP in pyridine.[14] As a reaction solvent and base, pyridine has a high boiling point, is highly toxic and difficult to remove totally. As a result, dimesylate **1b** prepared in this way usually contains traces of pyridine even after chromatographic purification, which may have unfortunate consequences on subsequent reactions. Therefore a new procedure was developed by replacing pyridine with NEt_3 as a base in order to synthesize dimesylate **1b** with CH_2Cl_2 as the solvent.[15] With this new pathway in hand, there was no problem of residual base, and the yield also increased significantly, from 85% to 93%.

The synthesis of the targeted P,N bidentate ligand **L1** also involved the preparation of 2-(*N*,*N*-dimethylamino)phenylphosphine **2**.

For references, see page 120.

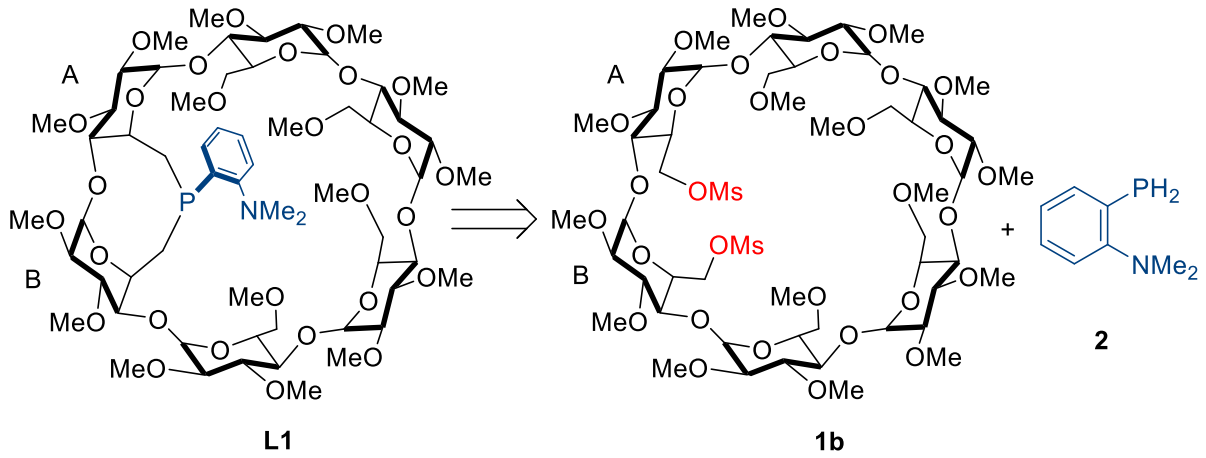

Scheme 4. Retrosynthetic analysis for P,N bidentate ligand **L1**.

The preparation of alkyl or aryl substituted primary phosphines commonly involves the reduction of phosphonates using lithium aluminum hydride[16]. Phosphonate **3** was therefore synthesized first to obtain phosphine **2**. According to the literature, two different methods can be used for preparing **3** (Scheme 5). Both of them use 2-bromoaniline as starting material. In method 1, 2-bromoaniline was firstly methylated with MeI under basic conditions[17] and then the *N*-methylated product ortho-lithiated with *n*-BuLi. The resulting anion reacted with diethyl chlorophosphite[18] to form diethyl [2-(*N*,*N*-dimethylamino)phenyl]phosphonate **3**. The overall yield from 2-bromoaniline is 38%. However, the nucleophilic substitution step produces some over-alkylated side products that are difficult to separate from the desired product and lower the yield. In method 2, which we developed in part, a Stelzer procedure[19] was used to perform a Pd-catalyzed P–C coupling reaction between 2-bromoaniline and diethyl phosphite ($HPO(OEt)_2$). This step was then followed by the *N*,*N*-dimethylation of the primary amine group to give **3**. Compared to method 1, method 2 gives a much higher yield (overall yield from 2-bromoaniline: 86%) and the targeted product was more easily separated from the reaction mixture.

For references, see page 120.

Method 1

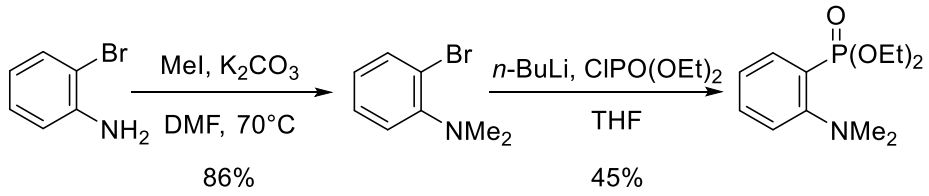

3

Method 2

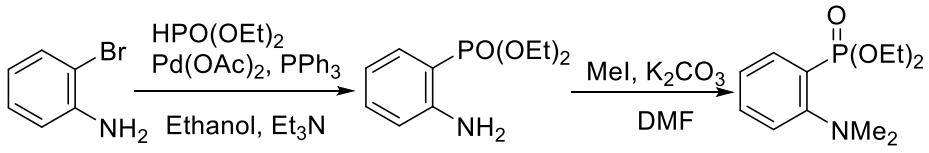

3

Scheme 5. The two methods used for the synthesis of the phosphonate **3**.

The primary phosphine **2** has already been characterized by $^{31}P\{^{1}H\}$ and $^{13}C\{^{1}H\}$ NMR although its synthesis is not described in the literature[20]. The phosphonate **3** was reduced by $LiAlH_4$ in the presence of Me_3SiCl to yield **2** according to the literature.[18] Under those reaction conditions, Me_3SiCl was first added to a suspension of $LiAlH_4$ in THF at -78 °C. The reaction was then allowed to reach room temperature and stirred for 2 h. A solution of **3** in THF was finally transfered by cannula to the mixture at -30 °C and the mixture was stirred for 2 h at room temperature. The crude solution should be used in the next step without further purification since **2** is easily oxidized. Even if the initial conditions used for the reduction produced the expected product (single peak at -128.8 ppm in the $^{31}P\{^{1}H\}$ NMR spectrum), a number of side products were also formed.

For references, see page 120.

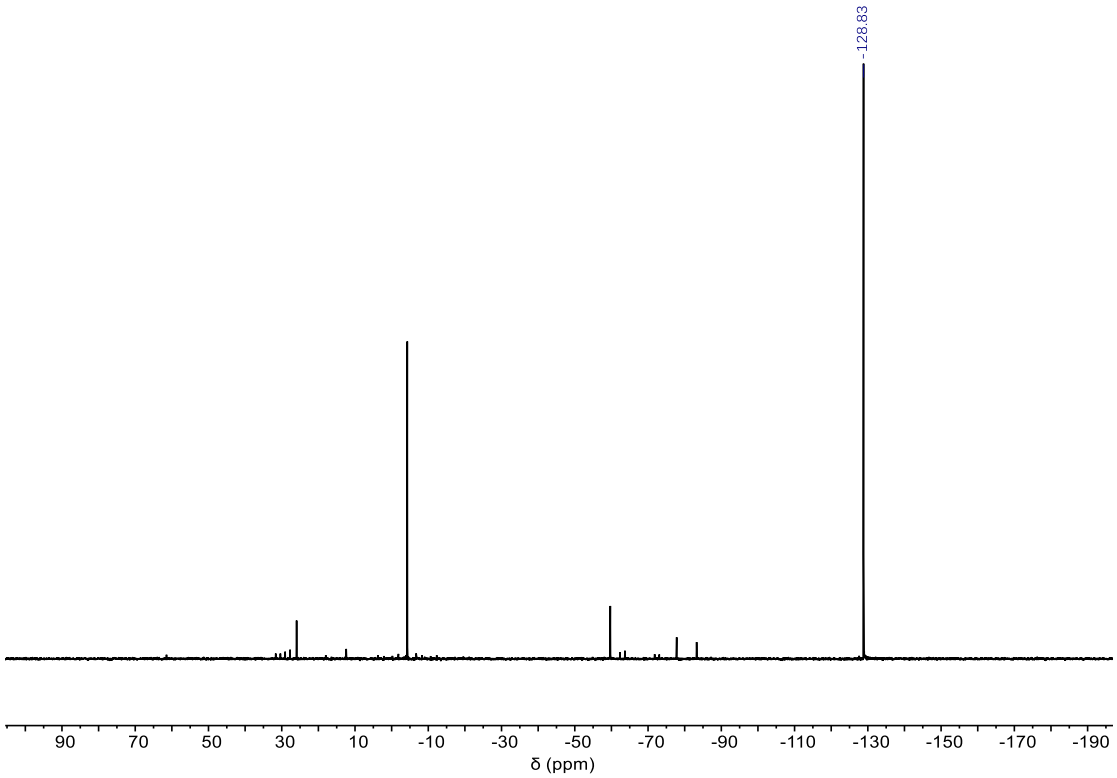

Fig 3. $^{31}P\{^{1}H\}$ NMR spectrum (in $CDCl_3$) of **2**.

In order to access a cleaner primary phosphine, two different reaction temperatures, namely 0 °C and -30 °C, were tested after addition of the reducing agent to the phosphonate. The reaction was over after 2 h at room temperature or at 0 °C, whereas at -30 °C, it was not complete after 4 h. Most of the phosphonate was still present but impurities already started to form under those reaction conditions, as monitored by the $^{31}P\{^{1}H\}$ NMR (Fig 4). It was observed that performing the reduction at lower temperature can limit the formation of side-products.

For references, see page 120.

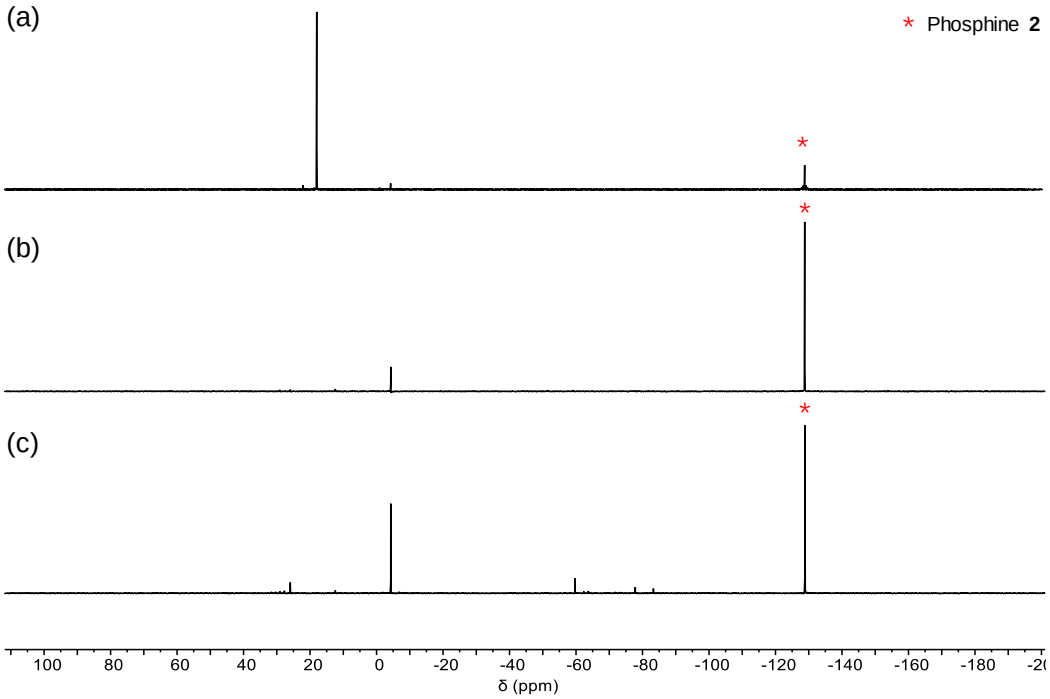

Fig 4. $^{31}P\{^{1}H\}$ NMR spectrum (in $CDCl_3$) of the reaction mixture containing **2** when the reaction was conducted: (a) at -30 °C for 3 h; (b) at 0 °C for 2 h; or (c) at room temperature for 2h.

The influence of the reaction time was also studied. The reaction was conducted at 0 °C for 1 h, 1.5 h, and 2 h, respectively. The results showed that complete conversion could be achieved after 1.5 h with minimal amounts of side-products being formed. The optimal reaction conditions we came up with for the synthesis of **2** are described below:

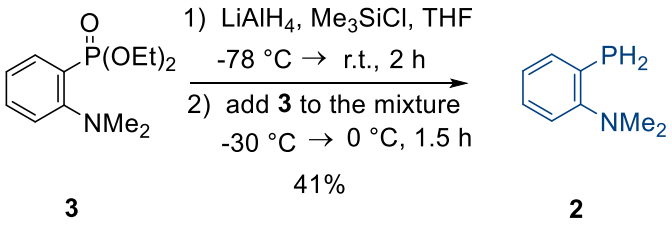

3 **2**

Scheme 6. Optimized conditions for the synthesis of **2**.

II. 2. 2. Synthesis of P,N bidentate ligands

The primary phosphine **2** and the dimesylate **1b** must be fully dried before engaging them in the synthesis of ligand **L1** as CD-entrapped water molecules lead to the hydrolysis of

For references, see page 120.

dimesylate **1b** in the presence of *n*-BuLi. **2** was deprotonated with *n*-BuLi and then reacted with **1b** to afford α-CD-based P,N bidentate ligand **L1** in 63% yield.

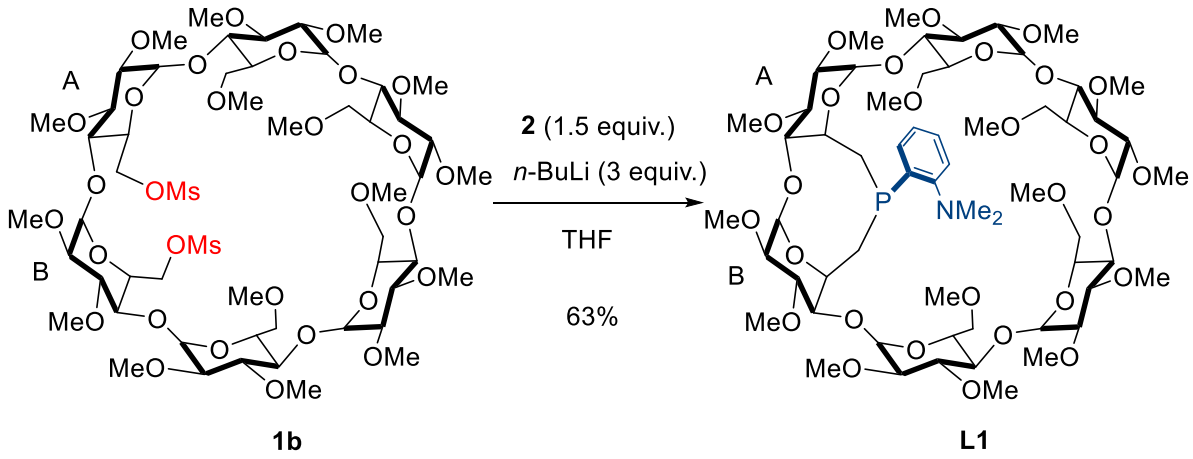

Scheme 7. Synthesis of CD-based P,N bidentate ligand **L1**.

Despite its ^{31}P NMR chemical shift suggesting an electron-rich phosphorus atom, ligand **L1** (δ_{31P} = -28.4 ppm) is remarkably air-stable when compared to the analogous phosphine lacking the NMe_2 unit (δ_{31P} = -16.2 ppm) to the extent that it could be purified by standard column chromatography on silica without any noticeable oxidation. As for monophosphine analogs (**HUGPHOS-1** and **HUGPHOS-2**), only the diastereomer in which the phosphorus lone pair is pointing towards the cavity interior could be detected in the reaction mixture (see coordination properties below). The ligand was fully characterized thanks to NMR spectroscopy, including 2D COSY, TOCSY, ROESY and (^{1}H,^{13}C)-HSQC spectra, mass spectrometry and elemental analysis.

For comparison, the cavity-free analog **L2**[21] was also synthesized from 2-bromo-*N*,*N*-dimethylaniline by *ortho*-lithiation followed by nucleophilic substitution of chlorodiethylphosphine, and isolated in 40% yield. Resistance to oxidation was also observed for **L2** (δ_{31P} = -25.1 ppm) as in analogous P,N ligands of the Me-DalPhos family[22].

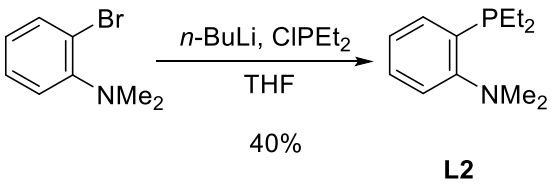

Scheme 8. Synthesis of the cavity-free P,N bidentate ligand **L2**.

For references, see page 120.

II. 2. 3. Synthesis of metal complexes derived from P,N bidentate ligands

II. 2. 3. 1. Synthesis of metal complexes derived from CD-based P,N ligand L1

The palladium complexes **4** and **5** were obtained by reacting CD ligand **L1** with one equivalent of [$PdCl_2$(COD)] or [PdMeCl(COD)] (COD = 1,5-cyclooctadiene) respectively in deoxygenated CH_2Cl_2. The two chelate Pd(II) complexes **4** and **5** were isolated in 82% and 58% yield respectively after chromatographic purification on silica. The ^{1}H and $^{31}P\{^{1}H\}$ NMR spectra in $CDCl_3$ of complexes **4** and **5** together with ligand **L1** are shown in Fig 5 and Fig 6. Again, full NMR assignment was performed using the same 2D NMR experiments as above. Increasing the ligand/metal ratio did not produce any other complexes, in particular bis(phosphine) complexes. Instead, the ligand in excess remained unreacted (Fig 7).

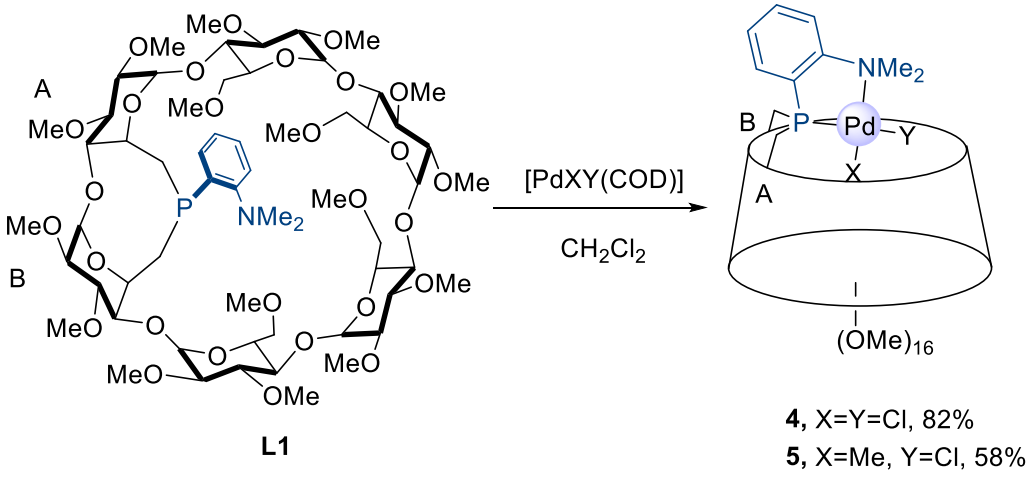

Scheme 9. The synthesis of Pd(II) complexes **4** and **5** derived from **L1**.

For references, see page 120.

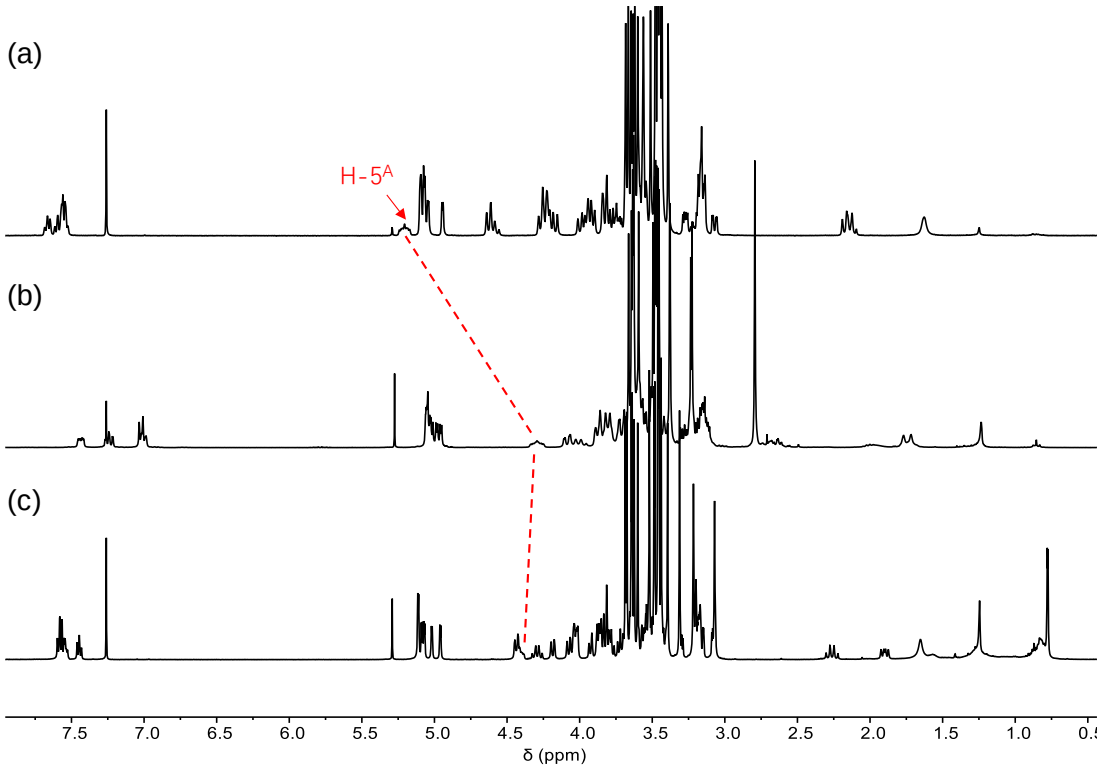

Fig 5. ^{1}H NMR spectra in $CDCl_3$ of: (a) **4**, (b) **L1**, (c) **5**.

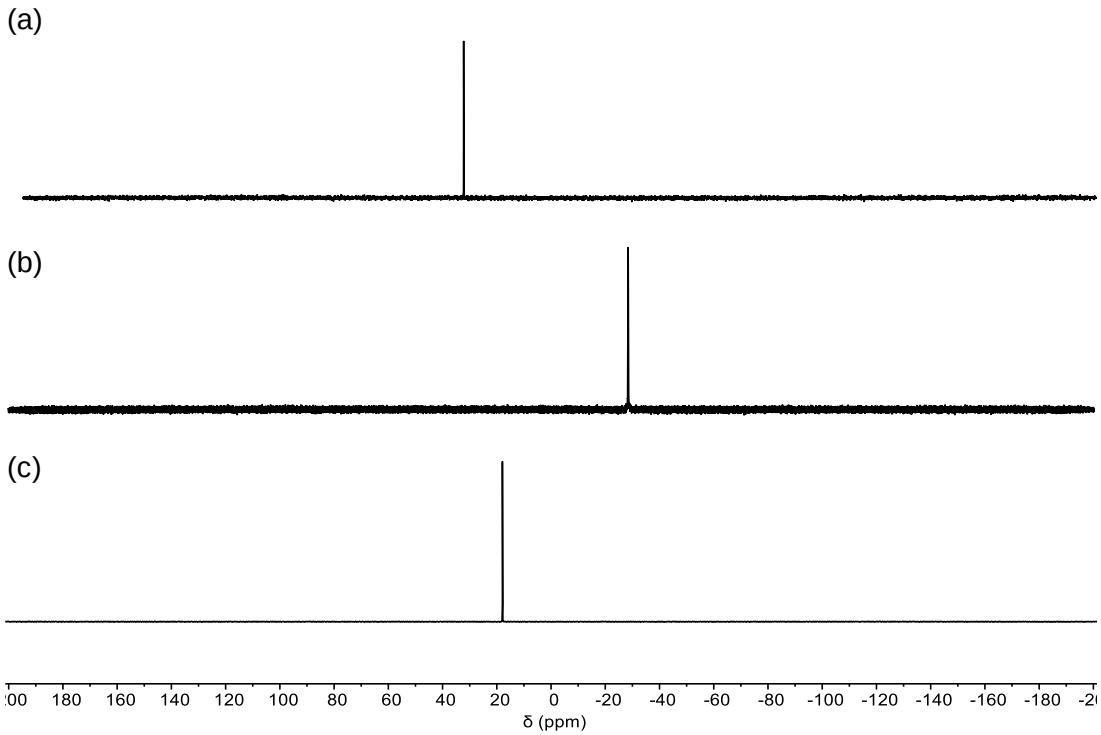

Fig 6. $^{31}P\{^{1}H\}$ NMR spectra in $CDCl_3$ of: (a) **4**, (b) **L1**, (c) **5**.

For references, see page 120.

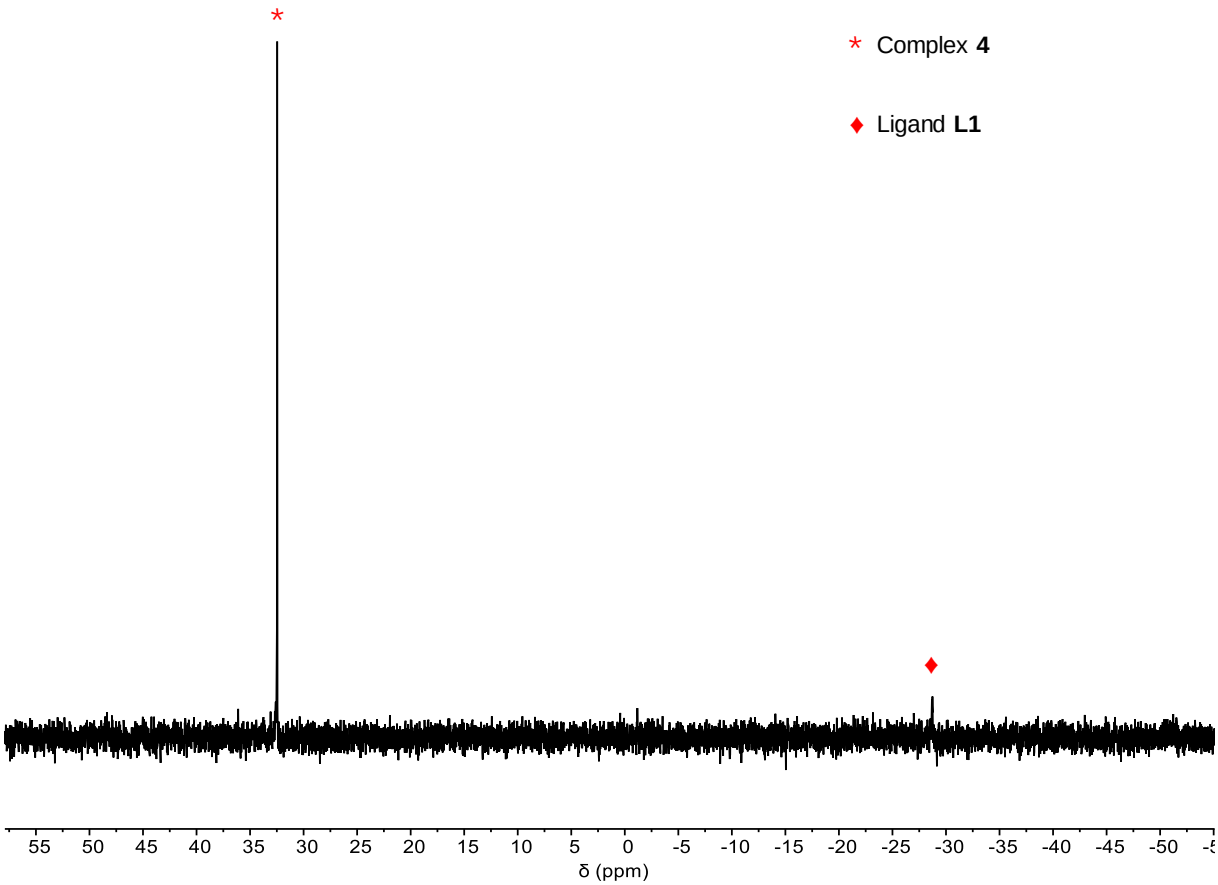

Fig 7. $^{31}P\{^{1}H\}$ NMR spectra of crude complex **4** in the presence of excess ligand **L1** (1.2 equiv.).

The ^{31}P chemical shifts lie in the expected range (δ_{31P} = 32.5 ppm and 17.9 ppm for **4** and **5**, respectively), and both Pd(II) complexes display a large downfield shift compared to the free ligand **L1** (δ_{31P} = -28.4 ppm), indicating coordination of phosphorus to the metal center. As previously reported for CD-encapsulated M–X units, the inner-cavity H-5 proton of capped glucose unit A in **4** is usually downfield shifted (δ_H = 5.19 ppm *vs* 4.31 for ligand **L1**), as a result of weak CH•••Cl H-bonding within the CD hollow. On the contrary, in the case of **5**, no such large downfield shift was observed (δ_H = 4.41 ppm for H-5^A), indicating that the chlorido ligand is not included in the CD cavity unlike its $PdCl_2$ counterpart as evidenced by a ROESY experiment. Indeed, the PdMe signal, which resonates as a doublet at 0.78 ppm ($^3J_{H,P}$ = 2.5 Hz), gave rise to cross-peaks corresponding to through-space correlations involving all inner-cavity H-5 protons (Fig 8). The orientation of the methyl ligand is not a result of its affinity for the α-CD inner-space but rather of the larger *trans* influence of phosphine and methyl over amine and chlorido with the donor groups with the largest *trans* influence, namely methyl and phosphine, avoiding a mutually *trans* position.[23] Therefore the methyl group can only be *cis* to

For references, see page 120.

phosphorus and inside the CD cavity, whereas the chlorido ligand has to be *trans* to the phosphorus donor atom and outside the cavity. Both the deshielded H-5 proton in **4** and ROESY cross-peaks involving inner-cavity H-5 protons and the Pd-Me group in **5** prove that the P,N ligand **L1** is indeed metal confining in solution. Such a feature was also confirmed in the solid state by the crystal structure determination of **4** (Fig 9). The single crystal of complex **4** was obtained by slow diffusion of *n*-pentane into a butanone solution of **4**.

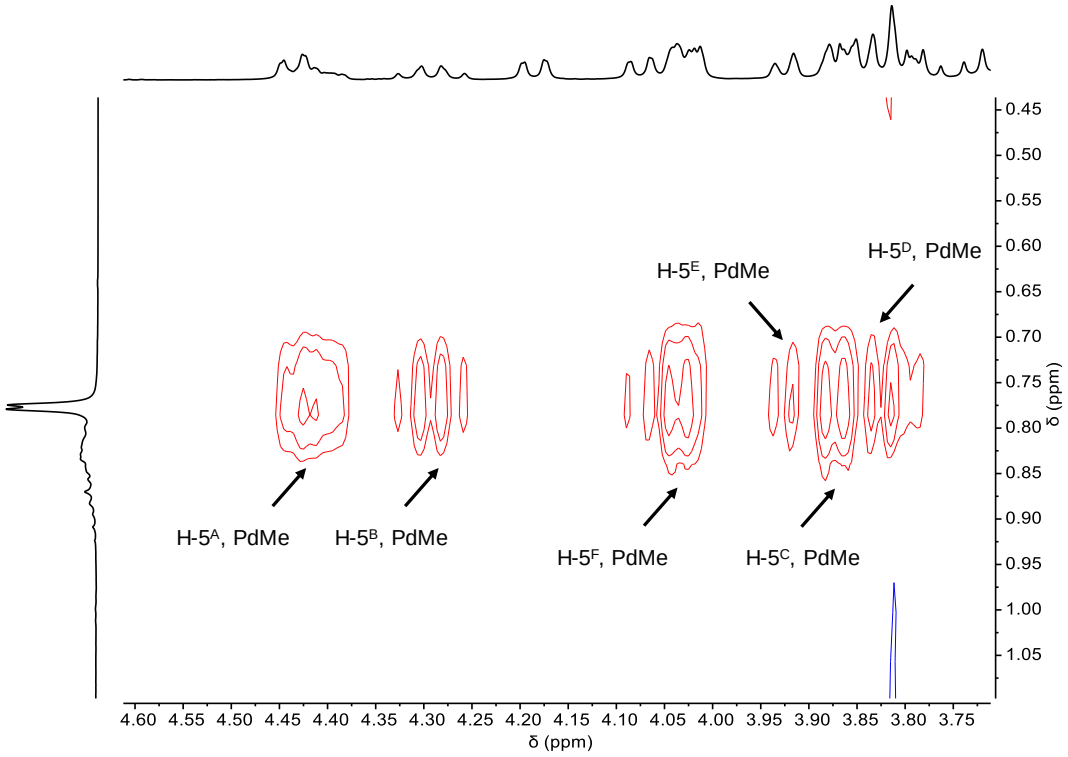

Fig 8. Part of the ROESY spectrum of complex **5** revealing the correlations between Pd-Me protons and the inner-cavity H-5 protons of the CD unit.

For references, see page 120.

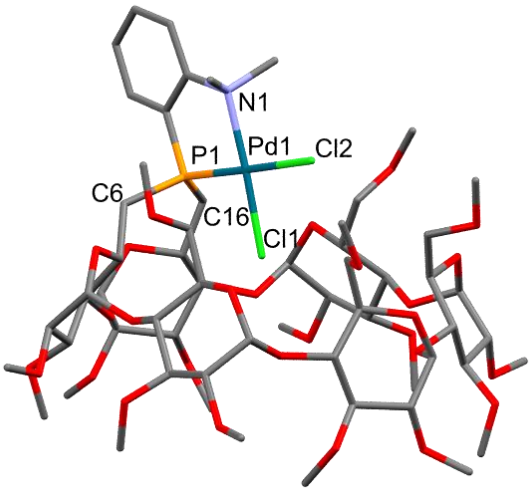

Fig 9. View of the X-ray crystal structure of complex **4**. Hydrogen atoms and solvent molecules are omitted for clarity. Important bond lengths (Å) and angles (°) for complex **4**: N1-Pd1: 2.125 (4), P1-Pd1: 2.1947 (14), Pd1-Cl1: 2.2949 (14), Pd1-Cl2: 2.3676 (15), P1-C6: 1.837 (5), P1-C16: 1.836 (5), N1-Pd1-P1: 86.83 (12), N1-Pd1-Cl1: 175.19 (13), N1-Pd1-Cl2: 92.05 (12), P1-Pd1-Cl1: 88.49 (5), P1-Pd1-Cl2: 178.87 (6), Cl1-Pd1-Cl2: 92.63 (6), C6-P1-Pd1: 116.12 (17), C16-P1-Pd1: 116.74 (17), C6-P1-C16: 112.7 (2).

Complex **4** shows a square planar geometry, consistent with its diamagnetic. This structure also reveal a cis-chelated $PdCl_2$ unit seating just above the CD cavity and nearly perpendicular to the macrocyclic structure (angle between CD O-4 atoms plane and $PNPdCl_2$ plane is 86.05°). As expected from the solution studies, one of the two chlorido ligands is included in the cavity and displays a short contact with the H-5 proton of bridging unit A (2.840 Å). The second chlorido ligand clearly points outside the cavity and is at a significantly longer distance from the palladium (2.368 Å) than the encapsulated one (2.295 Å). This is expected as a result of the larger *trans* influence of the phosphorus donor atom.

The corresponding nickel(II) complex **6** was also obtained by reacting ligand **L1** with one equivalent of [$NiBr_2$(DME)] (DME = 1,2-dimethoxymetane) in deoxygenated CH_2Cl_2. Unlike its $PdCl_2$ analog **4**, this complex was found to be unstable on silica and therefore could not be purified by column chromatography. Instead, a pure sample of the complex was isolated in 65% yield by crystallization from a benzene/*n*-pentane mixture.

For references, see page 120.

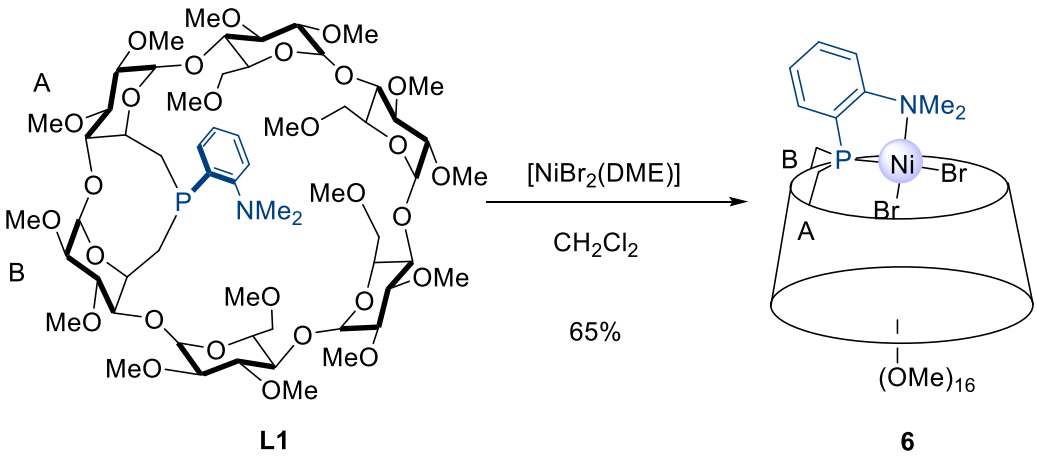

Scheme 10. Synthesis of the Ni(II) complex **6** derived from **L1**.

Single crystals of complex **6** were obtained by slow diffusion of *n*-pentane into a benzene and X-ray diffraction analysis established the molecular structure of the complex (Fig 10).

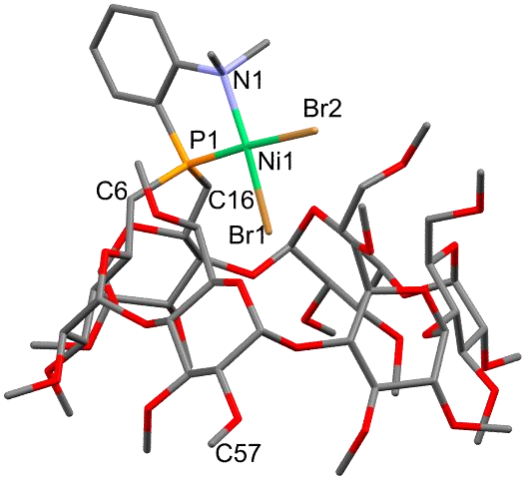

Fig 10. View of the X-ray crystal structure of complex **6**. Hydrogen atoms and solvent molecules are omitted for clarity. One methyl (C57) is disordered over two positions. Important bond lengths (Å) and angles (°) for complex **4**: N1-Ni1: 2.007 (6), P1-Ni1: 2.1263 (15), Ni1-Br1: 2.3063 (10), Ni1-Br2: 2.3807 (9), P1-C6: 1.850 (6), P1-C16: 1.834 (6), N1-Ni1-P1: 88.53 (15), N1-Ni1-Br1: 171.95 (16), N1-Ni1-Br2: 95.01 (15), P1-Ni1-Br1: 84.06 (5), P1-Ni1-Br2: 176.45 (6), Br1-Ni1-Br2: 92.40 (3), C6-P1-Ni1 : 118.18 (18), C16-P1-Ni1: 116.70 (17), C6-P1-C16: 113.1 (3).

This nickel complex also displays a *cis*-chelating ligand and its square planar is closely related to that of the $PdCl_2$ analog **4**. Noticeably, as in the case of **4**, the two halido ligands experience

For references, see page 120.

very different steric environments, a very rare feature in metal confining ligands that could have a great impact on catalytic properties.[24] Moreover, in the Pd complex **4**, the $PNMX_2$ unit is slightly more included in the cavity than in its Ni counterpart **6** (angle between CD O-4 atoms and the C6-P1-C16 planes = 50.27° *vs.* 54.82°, respectively), probably because the MX_2 unit is larger in **4** than in **6**. Despite the fact that complex **6** has a square-planar geometry and should therefore behave as a diamagnetic species in the solid state, its $^{31}P\{^1H\}$ NMR spectrum was quite broad at room temperature. A variable temperature NMR study shows that the $^{31}P\{^1H\}$ spectrum of **6** sharpens gradually upon decreasing the temperature (sharp single at δ_{31P} = 10.4 ppm at 213 K) with no significant change of the chemical shift. Line broadening at room temperature is rather common with this type of complexes.[24]

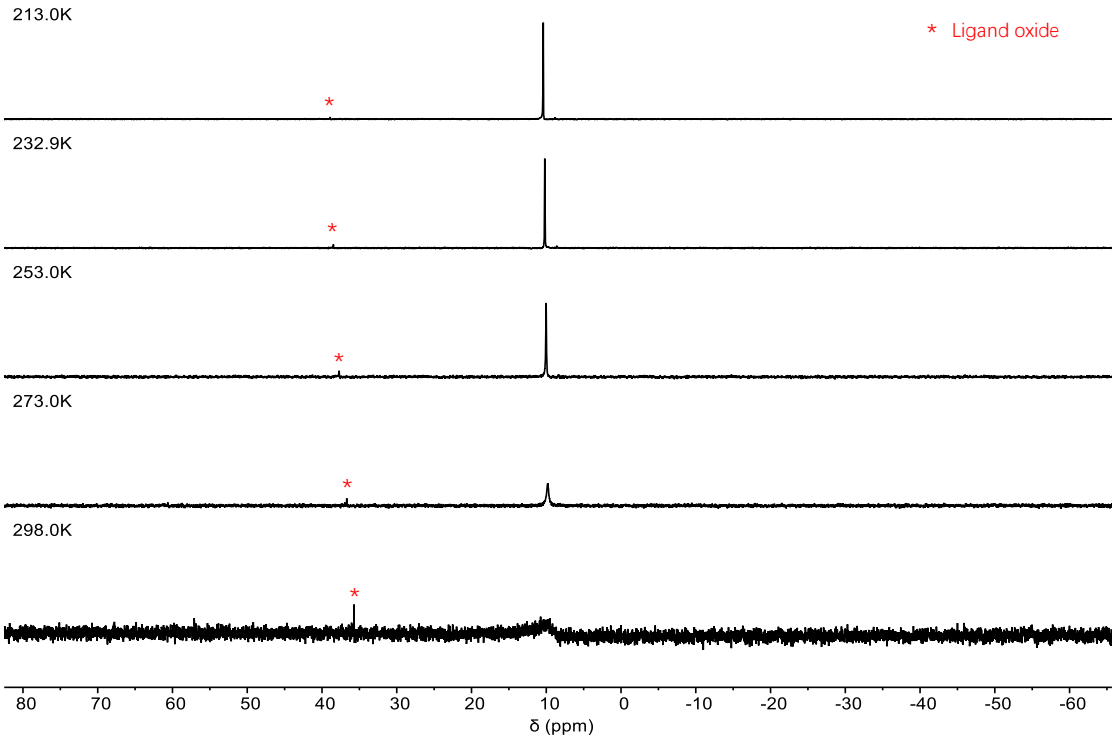

Fig 11. $^{31}P\{^1H\}$ VT NMR study of **6** in CD_2Cl_2.

The gold(I) complex **7** was also synthesized by reacting **L1** with [AuCl(tht)] (tht = tetrahydrothiophene) in deoxygenated CH_2Cl_2.

For references, see page 120.

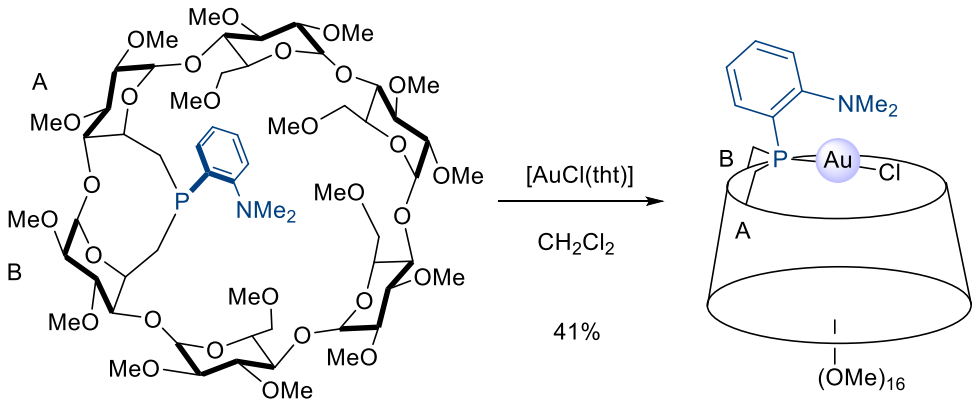

L1 **7**

Scheme 11. Synthesis of the Au(I) complex **7** derived from **L1**.

The ^{1}H NMR spectrum of **7** shows that the chemical shift of H-5 is not much affected by metal complexation (δ_H = 4.29 ppm *vs* 4.31 ppm for **L1**), which is a clear indication of the absence of chloride inclusion in the CD cavity. Single crystals could be obtained by slow diffusion of *n*-pentane into a benzene solution of **7**, allowing a determination of its molecular structure by X-ray diffraction analysis (Fig 14). Unlike its d^8 counterparts, the d^{10} metal cation is not chelated by the ligand but is bonded to the phosphorus atom only, leaving the NMe_2 unit uncoordinated above the encapsulated metal center. This is consistent with the NMR analysis in solution. The structure of this Au(I) complex proves that it is the phosphorus donor atom that imposes the overall orientation of the metal with the respect to the cavity and not the tertiary amine.

For references, see page 120.

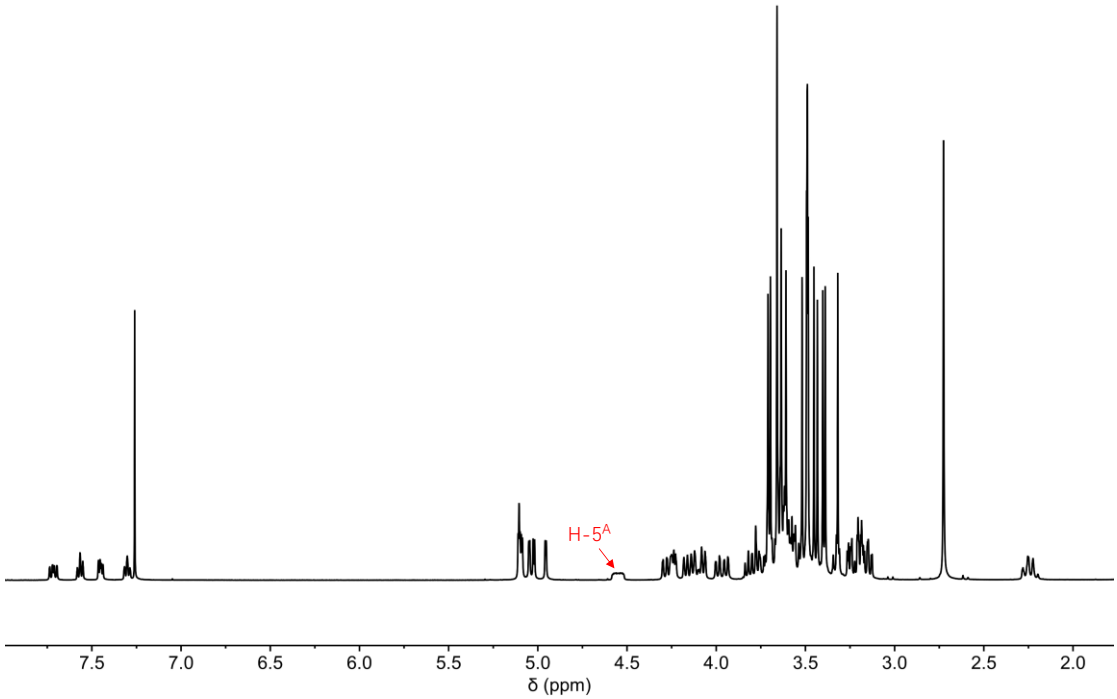

Fig 12. ^{1}H NMR spectrum in $CDCl_3$ of **7**.

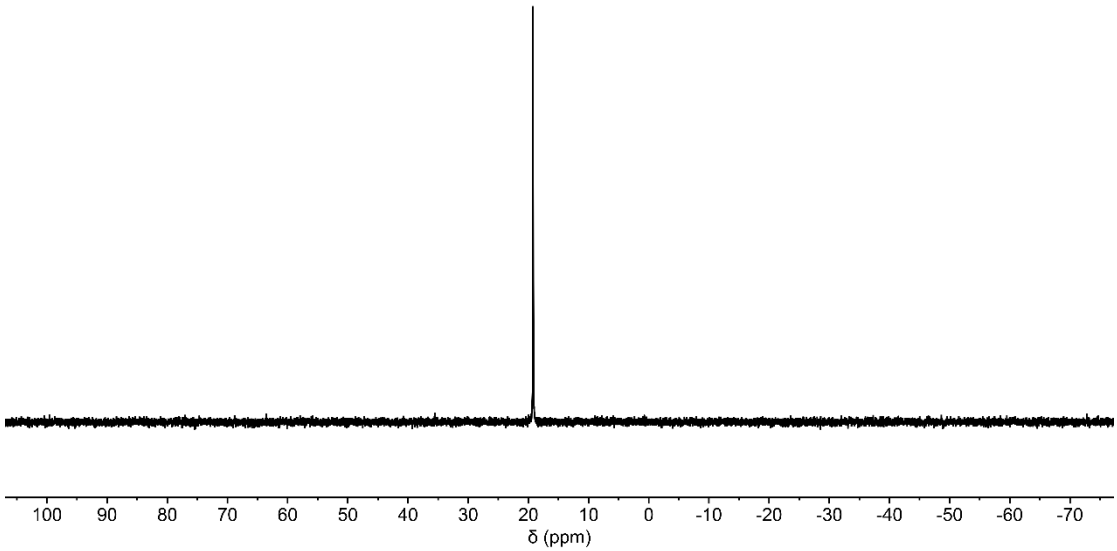

Fig 13. $^{31}P\{^{1}H\}$ NMR spectrum in $CDCl_3$ of **7**.

For references, see page 120.

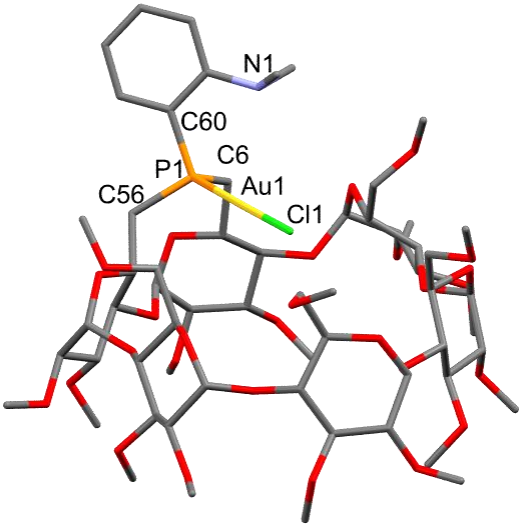

Fig 14. View of the X-ray crystal structure of complex **7**. Hydrogen atoms and solvent molecules are omitted for clarity. Important bond lengths (Å) and angles (°) for complex **7**: P1-Au1: 2.2329 (18), Au1-Cl1: 2.2755 (19), C6-P1: 1.837 (8), C56-P1: 1.846 (8), C6-P1-Au1: 111.8 (3), C56-P1-Au1: 111.4 (2), C60-P1-C56: 102.7 (4), C60-P1-Au1: 116.7 (3), P1-Au1-Cl1: 178.16 (7).

Finally, it should be mentioned that in every aforementioned crystal structures, the CD unit has an undistorted, overall circular shape, all glucose units adopting the standard $^4C_1$ conformation.

II. 2. 3. 2. Synthesis of metal complexes derived from cavity-free P,N ligand L2

In order to investigate the influence of the CD cavity on the metal coordination and catalytic properties, a cavity-free P,N ligand (**L2**) with the same electronic properties as ligand **L1** was also prepared and coordinated to d^8 transition metal cations. Unlike CD-based P,N ligand **L1**, the reaction of cavity-free P,N ligand **L2** with one equivalent of [$PdCl_2$(COD)] in deoxygenated CH_2Cl_2 produced a 9:1 mixture of chelate complex **8** and cationic bis(phosphine) complex **9**. As expected, raising the ligand/metal ratio to 2:1 caused the proportion of complex **9** to significantly increase, with a **8**:**9** ratio up to 3:7. The $^{31}P\{^1H\}$ NMR spectrum of **8** show a singlet at 62.1 ppm, whereas **9** show two doublets at 56.0 ($^2J_{P,P}$ = 13.1 Hz) and 21.9 ($^2J_{P,P}$ = 13.3 Hz) ppm. In stark contrast with **L2**, when [$PdCl_2$(COD)] was treated with an excess of ligand **L1**, only the chelate complex **4** and unreacted free ligand **L1** were found in the reaction mixture. This shows clearly that the presence of the cavity has a strong influence on the coordinating properties of the ligand. Because of the sheer bulk of its macrocyclic structure, **L1** is not able to coordinate the metal center twice unlike cavity-free **L2**. This is reminiscent

For references, see page 120.

of the monophosphines **HUGPHOS-1** and **HUGPHOS-2** which are also incapable of forming bis(phosphine) complexes for the same reason.

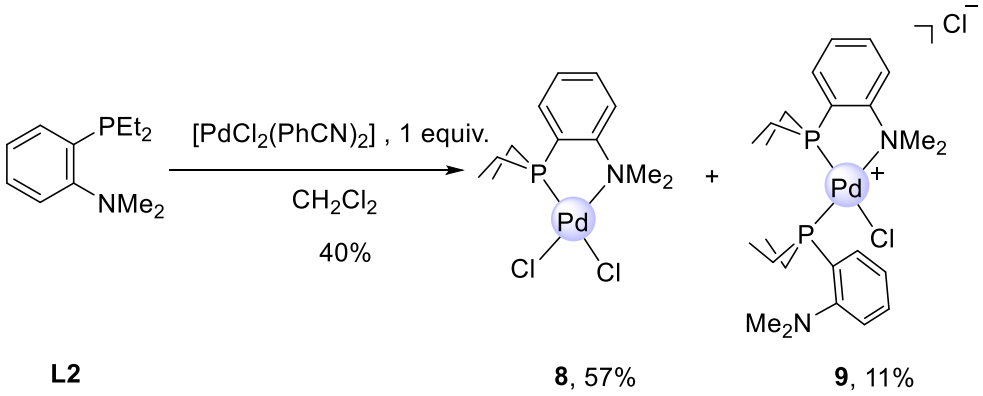

Scheme 12. Synthesis of Pd(II) complexes **8** and **9** derived from **L2**.

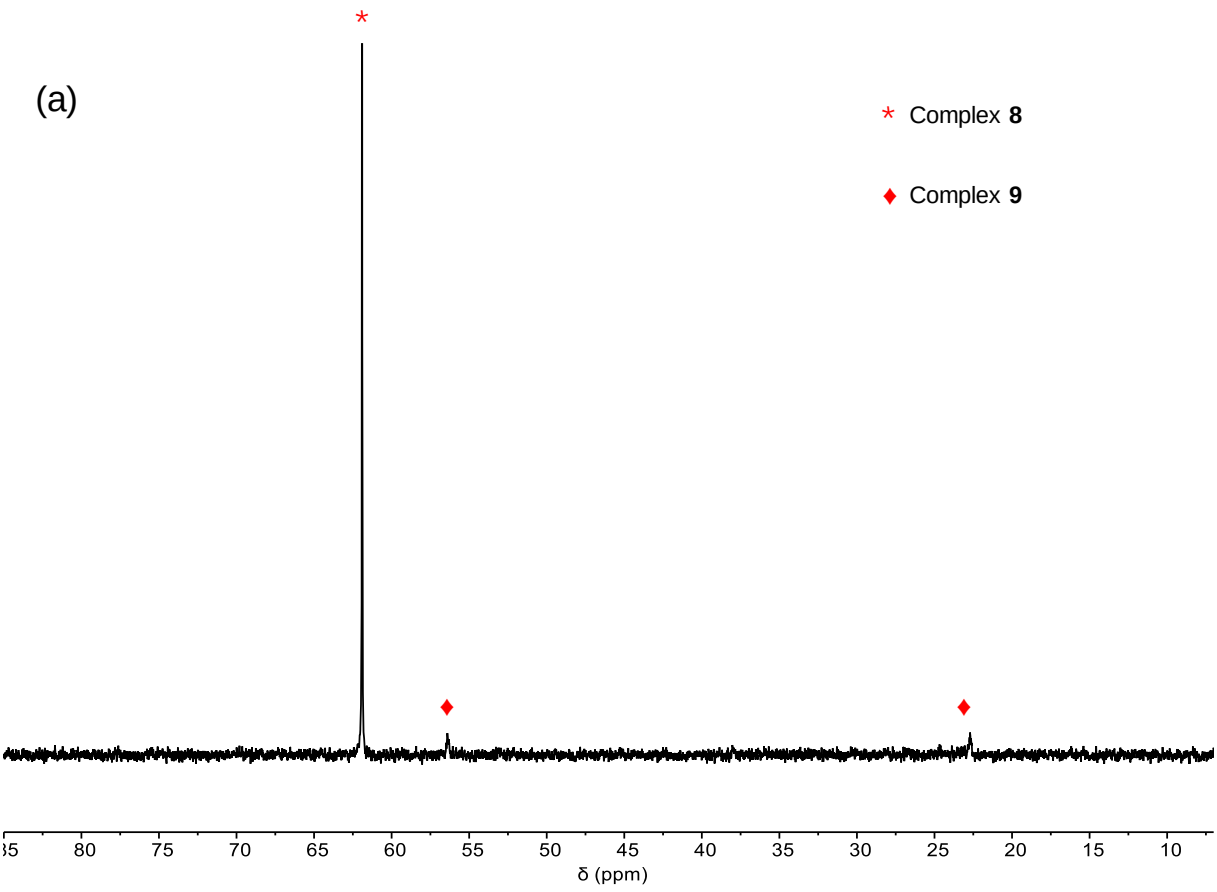

For references, see page 120.

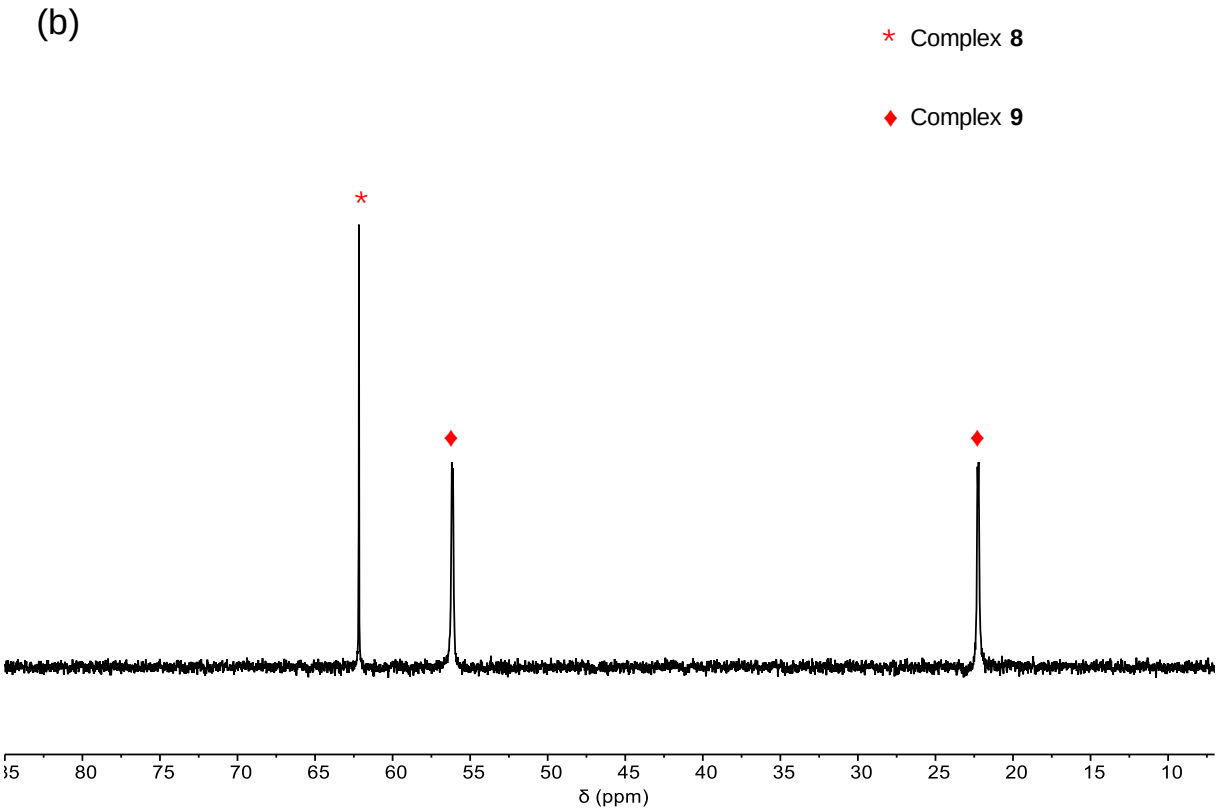

Fig 15. $^{31}P\{^{1}H\}$ NMR spectra of crude mixtures of complexes **8**/**9** with a metal/ligand ratio of: (a) 1:1, (b) 1:2, respectively

The crystal structures of both **8** and **9** were established by X-ray diffraction analysis. The structure of cationic **9** clearly shows that two phosphines but only one tertiary amine are coordinated to palladium.

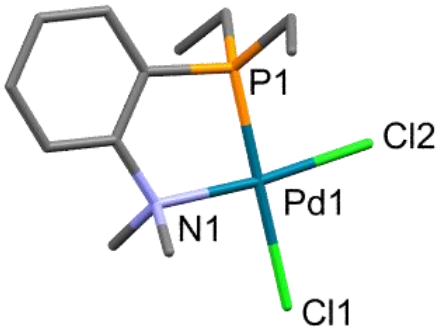

Fig 16. View of the X-ray crystal structure of complex **8**. Hydrogen atoms and solvent molecules are omitted for clarity. Important bond lengths (Å) and angles (°) for complex **8**: N1-Pd1: 2.111 (3), P1-Pd1: 2.1857 (9), Pd1-Cl1: 2.4087 (9), Pd1-Cl2: 2.2982 (9), N1-Pd1-P1:

For references, see page 120.

86.68 (8), N1-Pd-Cl1: 94.33 (8), N1-Pd1-Cl2: 173.76 (8), P1-Pd1-Cl1: 178.61 (3), P1-Pd1-Cl2: 87.20 (3).

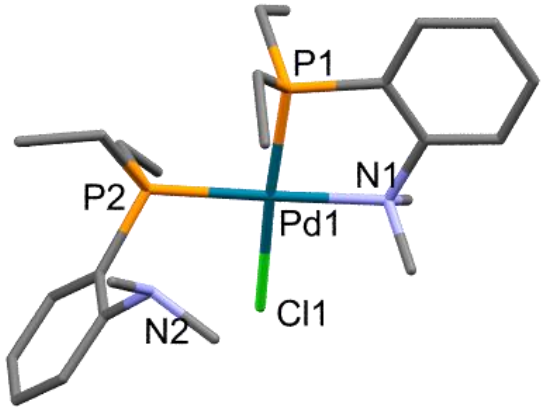

Fig 17. View of the X-ray crystal structure of complex **9**. Hydrogen atoms, solvent molecules and chlorido anion are omitted for clarity. Important bond lengths (Å) and angles (°) for complex **9**: N1-Pd1: 2.185 (5), P1-Pd1: 2.2326 (15), P2-Pd1: 2.2724 (14), Pd1-Cl1: 2.3728 (14), N1-Pd1-P1: 84.71 (17), N1-Pd1-P2: 177.17 (18), N1-Pd1-Cl1: 91.36 (17), P1-Pd1-P2: 95.45 (5), P1-Pd1-Cl1: 174.40 (6), P2-Pd1-Cl1: 88.28 (5).

A variable temperature NMR study (VT NMR) was conducted for **9** in the temperature range from 273 K to 323 K in $CDCl_3$. Both ^{1}H and $^{31}P\{^{1}H\}$ VT NMR experiments revealed that line broadening occurred as the temperature increased from 273 K to 323K. It is therefore reasonable to suppose that a fluxional behavior involving the slow coordination and decoordination of the weaker nitrogen donor atoms of the NMe_2 units takes place on the NMR time scale, as described in Scheme 13.

For references, see page 120.

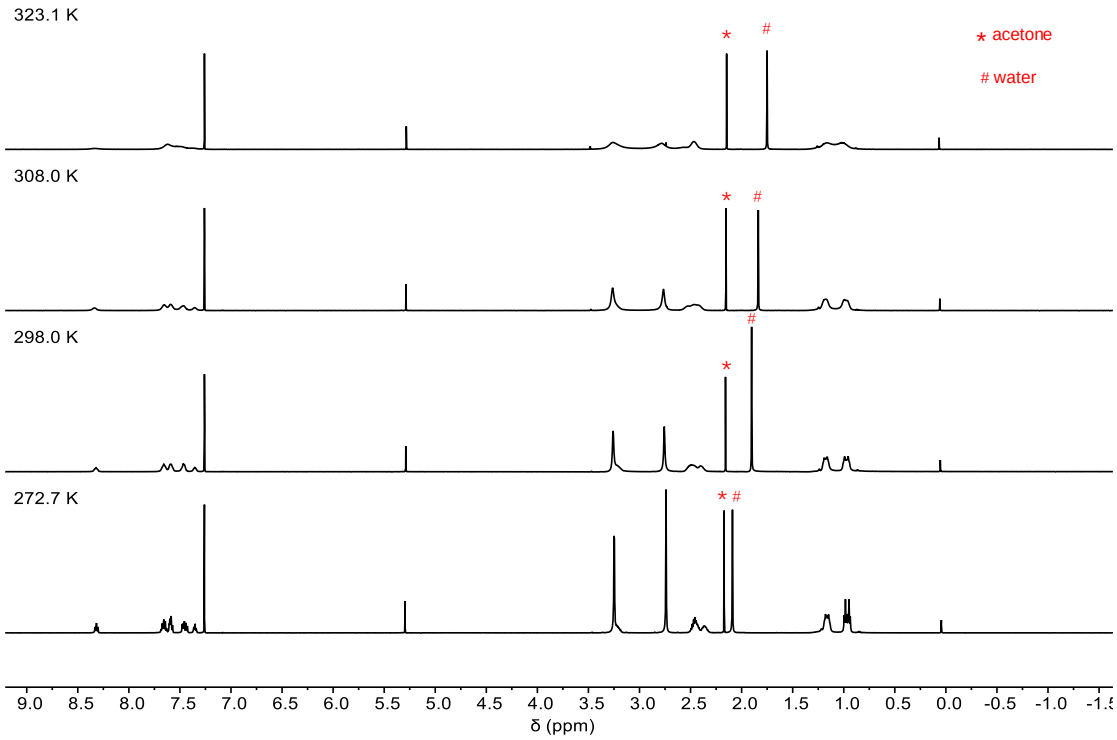

Fig 18. ^{1}H VT NMR spectra of **9** in $CDCl_3$.

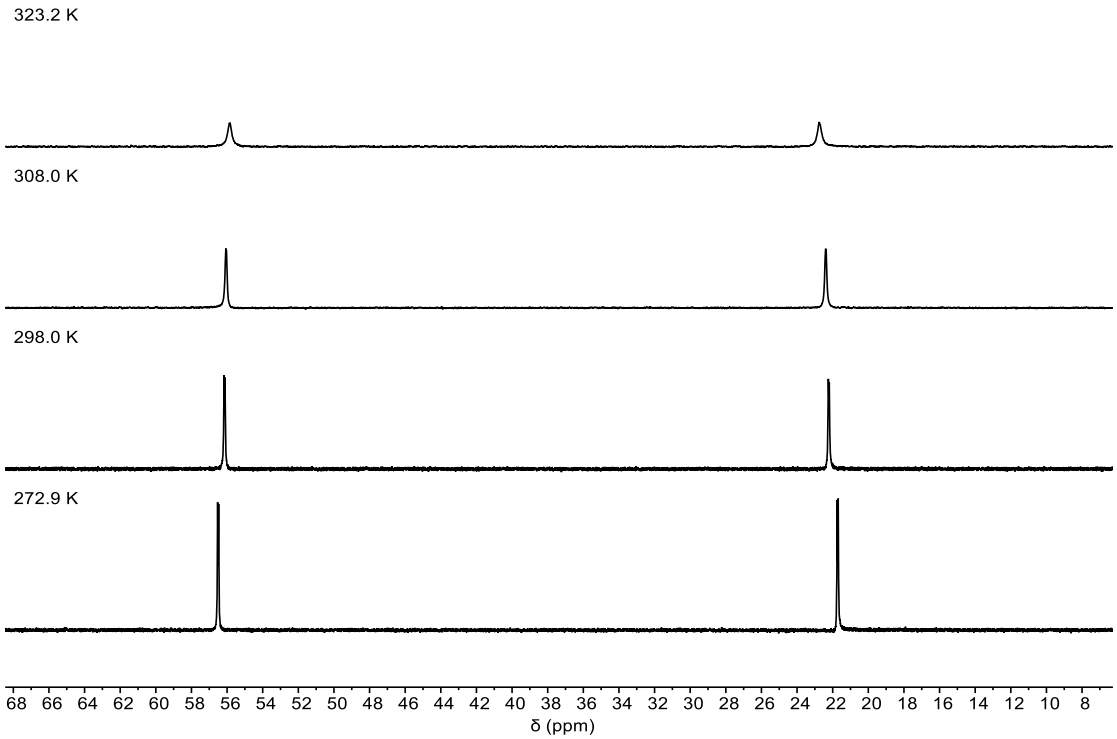

Fig 19. $^{31}P\{^{1}H\}$ VT NMR spectra of **9** in $CDCl_3$.

For references, see page 120.

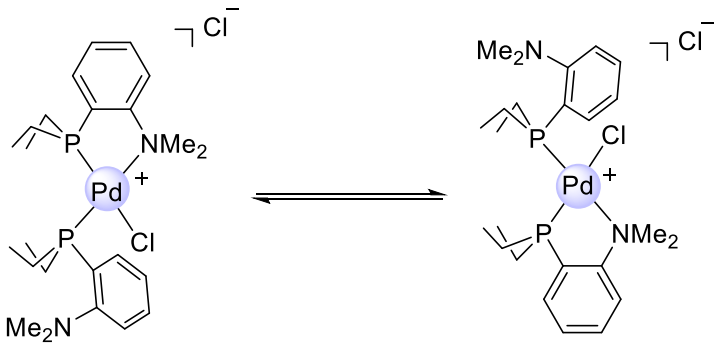

Scheme 13. Postulated coordination and decoordination processes taking place in **9**.

Surprisingly, the reaction of [PdMeCl(COD)] with either one or two equiv. of **L2** in CH_2Cl_2 gave only the neutral chelate complex **10** and unreacted ligand when **L2** was added in excess. But upon bringing the reaction mixture in CH_3OD, a complex mixture of at least three species in equilibrium was formed, amongst which cationic **11** appeared to be the major one together with significant amounts of neutral chelate complex **10**. Despite the fact that the cationic complex **11** could not be isolated from the mixture, the formation of this bis(phosphine) complex was inferred from the ESI-HRMS spectra, which shows intense peaks at *m/z* 539.1928 and 561,1375, corresponding to the $[M\text{-Cl}]^+$ and $[M\text{-Me}]^+$ ions, respectively. It was then hypothesized that in such a polar solvent, the cationic bis(phosphine) species **11** is favored in the absence of steric protection provided by the CD cavity.

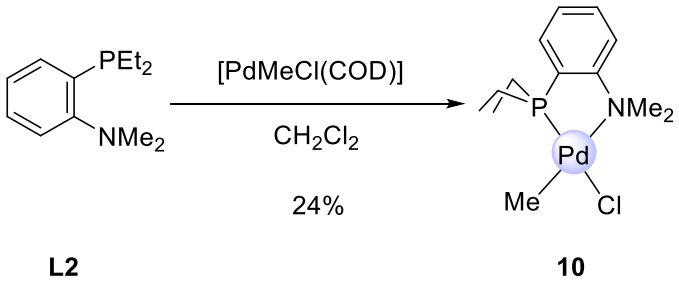

Scheme 14. Synthesis of Pd(II) complex **10** derived from **L2**.

For references, see page 120.

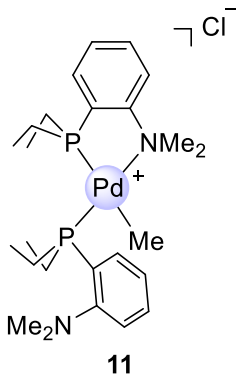

11

Fig 20. Molecular structure of complex **11**.

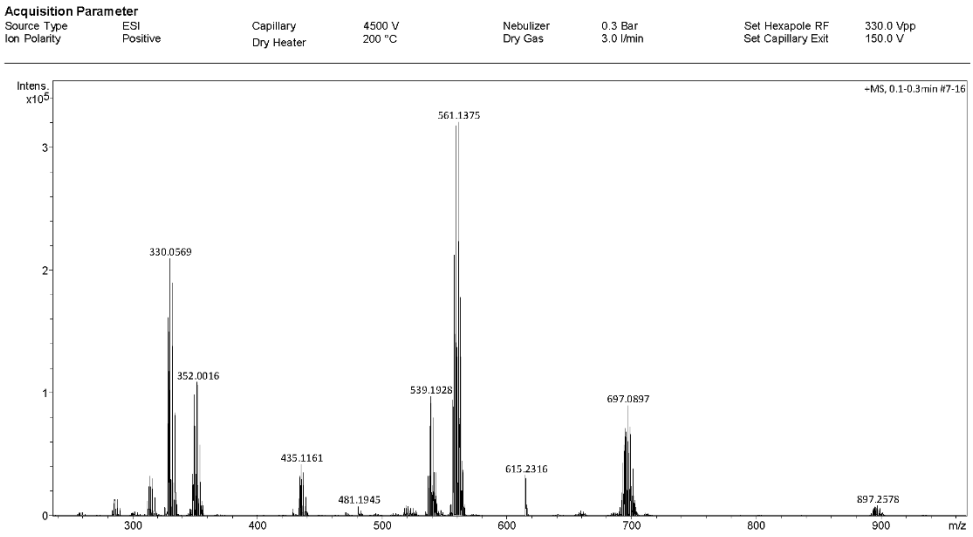

Fig 21. ESI-MS spectrum of the mixture of complexes including **11**.

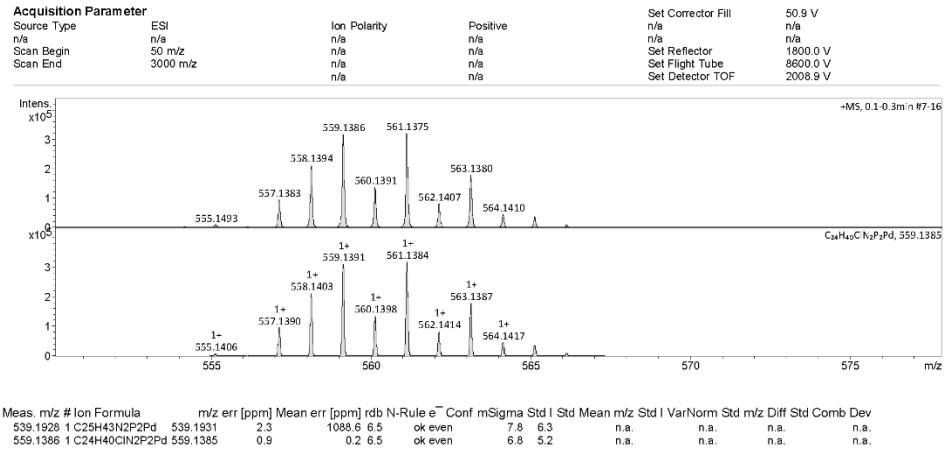

Meas. m/z	#	Ion Formula	m/z err [ppm]	Mean err [ppm]	rdb	N-Rule	e⁻ Conf	mSigma	Std I	Std Mean m/z	Std I	VarNorm Std m/z	Diff Std Comb	Dev
539.1928	1	C25H43N2P2Pd	539.1931	2.3	1088.6	6.5	ok	even	7.8	6.3	n.a.	n.a.	n.a.	n.a.
559.1386	1	C24H40ClN2P2Pd	559.1385	0.9	0.2	6.5	ok	even	6.8	5.2	n.a.	n.a.	n.a.	n.a.

Fig 22. Partial ESI-MS spectrum of **11**.

For references, see page 120.

Single crystals were obtained by slow diffusion of *n*-hexane into a solution of **10** in dichloromethane. As shown in Fig 23, the methyl group is located *cis* to the phosphorus donor atom as a result of the *trans* influence of phosphorus, a feature also observed in cavity-shaped complex **5**.

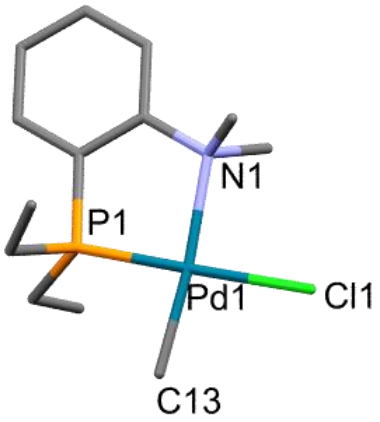

Fig 23. View of the X-ray crystal structure of complex **10**. Hydrogen atoms and solvent molecules are omitted for clarity. Important bond lengths (Å) and angles (°) for complex **10**: N1-Pd1: 2.212 (2), P1-Pd1: 2.1724 (8), Cl1-Pd1: 2.4002 (7), Pd1-C13: 2.050 (3), C13-Pd1-N1: 174.16 (11), C13-Pd1-P1: 87.56 (10), C13-Pd1-Cl1: 93.17 (9), N1-Pd1-Cl1: 92.60 (6), P1-Pd1-N1: 86.70 (6), P1-Pd1-Cl1: 178.02 (3).

A Ni(II) complex **12** based on this cavity-free ligand **L2** was also synthesized by reaction of **L2** with one equivalent of [$NiBr_2$(DME)] in deoxygenated CH_2Cl_2. The formation of a bis(phosphine) complex was not observed, as already noticed by Levason[25] with very similar Ni(II) complexes. Single crystals of complex **12** could be obtained by slow diffusion of *n*-hexane into a solution of **12** in dichloromethane. The X-ray crystal structure of **12** is shown in Fig 24.

For references, see page 120.

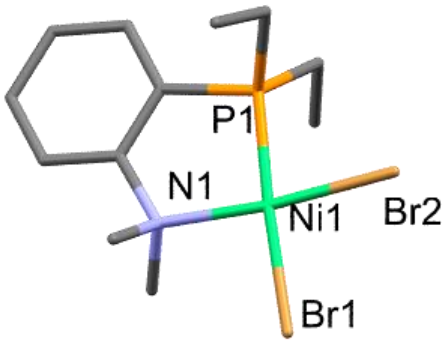

Fig 24. View of the X-ray crystal structure of complex **12**. Hydrogen atoms and solvent molecules are omitted for clarity. Important bond lengths (Å) and angles (°) for complex **12**: N1-Ni1: 2.010 (3), P1-Ni1: 2.1248 (10), Ni1-Br1: 2.3626 (5), Ni1-Br2: 2.3122 (6), N1-Ni1-P1: 88.63 (9), N1-Ni1-Br1: 94.48 (8), N1-Ni1-Br2: 173.87 (9), P1-Ni1-Br1: 176.73 (3), P1-Ni1-Br2: 85.25 (3), Br1-Ni1-Br2: 91.64 (2).

Again, this cavity-free nickel complex **12** and cavity-shaped analog **6** show similar behavior to. Despite being square planar and therefore diamagnetic, the $^{31}P\{^{1}H\}$ NMR spectrum of **12** recorded in CD_2Cl_2 display a very broad singlet at room temperature. However, as for cavity-shaped complex **6**, the ^{31}P signal sharpens upon cooling and is well defined at 213 K (δ_{31P} = 10.5 ppm).

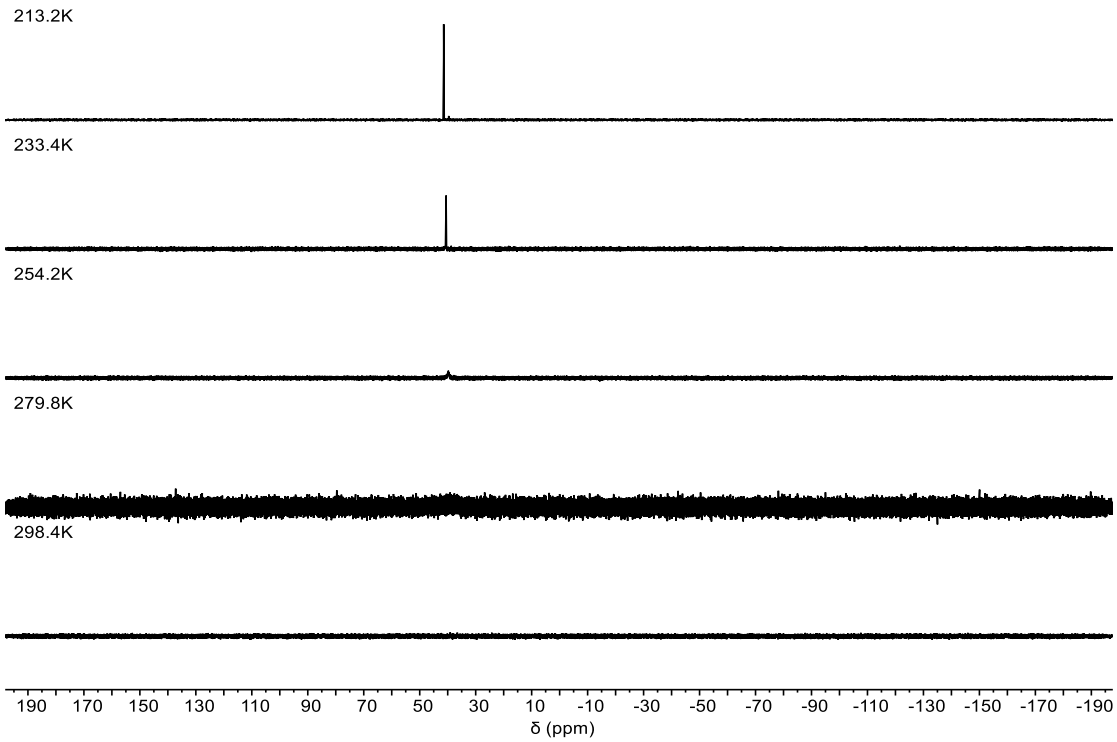

Fig 25. $^{31}P\{^{1}H\}$ VT NMR study of **12** in CD_2Cl_2.

For references, see page 120.

In order to investigate the effect of the CD cavity on the ligand electronic properties, UV-vis spectra of the CD-based and cavity-free metal complexes were recorded in CH_2Cl_2 at room temperature. The UV-vis spectra of nickel and palladium complexes are shown in Fig 26 and Fig 27, respectively. The UV-vis spectra of the two nickel complexes **6** and **12** display a shoulder at 290-350 nm, and two bands with maximum absorption at 401, 536 nm and 384, 528 nm for **6** and **12**, respectively, whereas the UV-vis spectra of palladium complexes **4** and **8** show two bands at 295, 351 nm and 275, 345 nm for **4** and **8**, respectively, in addition to the usual π-π* absorption at wavelengths below 270 nm. In the case of nickel complexes, the bands at around 390 and 530 nm maximum absorption correspond respectively to metal-to-ligand charge transfer (MLCT) and metal-centered d-d transitions. The fact that in both Pd and Ni complexes, a small redshift, in particular for the MLCT bands, is observed on going from the cavity-free to the cavity-shaped complexes indicates that the presence of the CD macrocyclic structure alters to some extent the electronic environment of the metal center. This is surprising since in the solid state (see X-ray structures above in Fig 9, 10, 16 and 24), both cavity-free and cavity-shaped complexes of d^8 metals have a very similar first coordination sphere, the only significant difference between the two types of complexes being an elongation of the external Ni–Br bond by ca. 0.02 Å on going from **12** to **6** and a shortening of the corresponding M–X bond by ca. 0,04 Å on going from Pd complexes **8** to **4.**

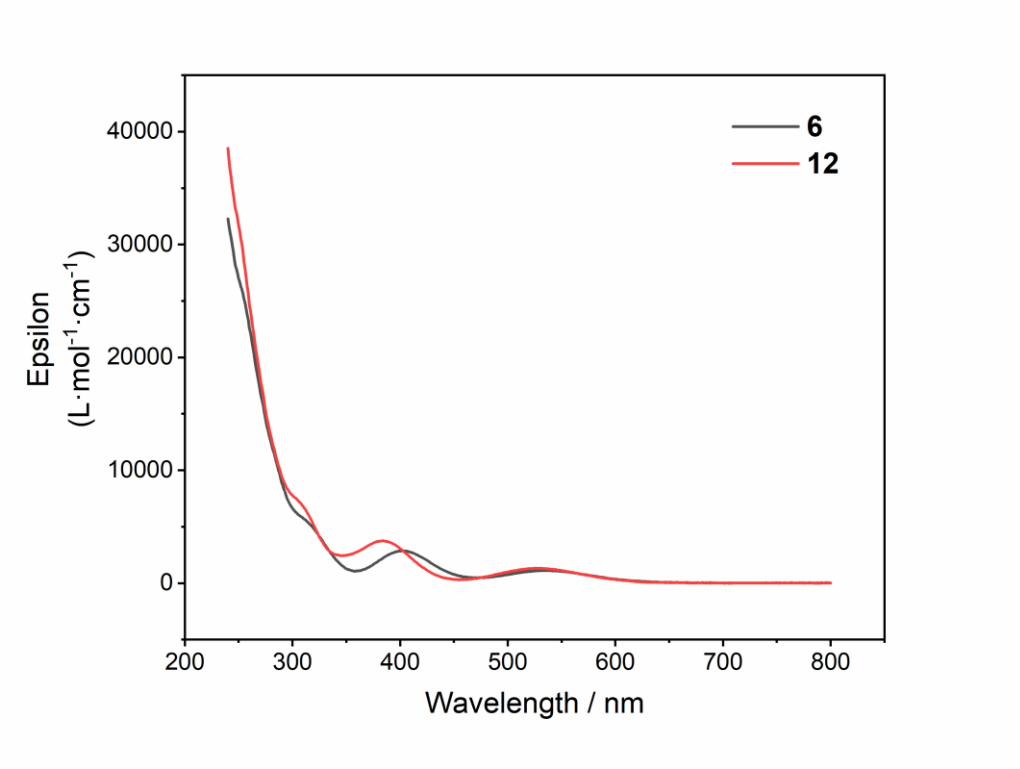

Fig 26. UV-vis spectra of nickel complexes **6** (black) and **12** (red).

For references, see page 120.

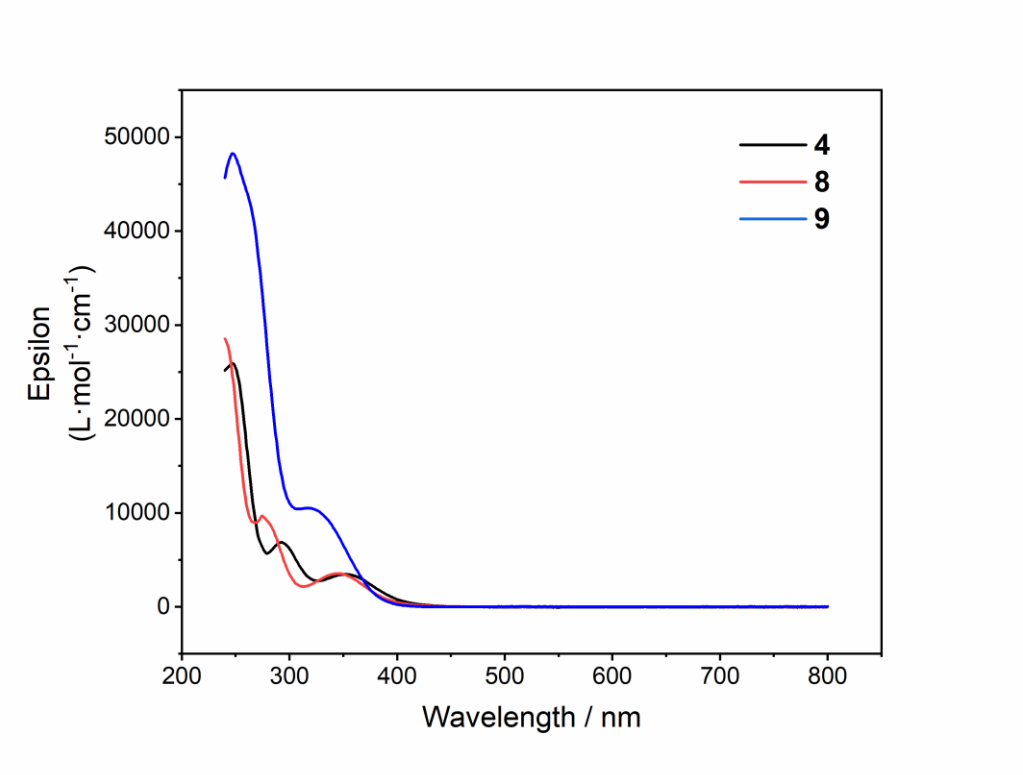

Fig 27. UV-vis spectra of palladium complexes **4** (black), **8** (red) and **9** (blue).

II. 3. Conclusion

In conclusion, the CD-based P,N bidentate ligand **L1** was prepared by bridging two adjacent glucose units of an AB difunctionalized α-CD platform with a *cis*-chelating P,N coordinating unit. In this rigid bridging unit, the phosphorus lone pair is directed towards the CD interior and forces a coordinated metal center to be located just above the narrow rim of the CD torus, thus allowing perfect control of the first metal coordination sphere. In the corresponding square-planar $PdCl_2$ and $NiBr_2$ *cis*-chelate complexes, the two halido ligands are sterically differentiated, one being inside the cavity and the other pointing outside, as demonstrated by NMR spectroscopy and X-ray diffraction analysis. The methyl ligand in the analogous PdMeCl complex was found to be inside the cavity because of the *trans* influence of phosphorus. Moreover, the single crystal structure of the linear AuCl complex revealed that phosphorus, but not nitrogen, is coordinated to gold and it is the phosphorus donor atom that forces the metal to be included in the cavity. For comparison, an analogous cavity-free P,N bidentate ligand (**L2**) was prepared and its coordination properties towards d^8 cations (Ni(II) and Pd(II)) were investigated. It was proven that the steric hindrance provided by the CD cavity is able to prevent the formation of bis(phosphine) complexes and promote exclusively the formation of 1:1 ligand/metal complexes. A UV-vis study showed that the presence of the macrocyclic

For references, see page 120.

moiety has an effect on the electronic properties of the complexes. It will of course be interesting to examine whether the very different steric environments experienced by the metal in cavity-shaped and cavity-free complexes will have an impact on catalytic reactions, in particular ethylene oligomerization (see Chapter 4).

II. 4. Experimental part

II. 4. 1. General procedures

All reactions and manipulations were carried out under an inert atmosphere (nitrogen or argon) using standard Schlenk techniques. All glassware was stored in the oven prior to use under an inert atmosphere of gas (Argon). All commercial reagents were used as supplied unless otherwise stated. Solvents were dried by conventional methods and distilled immediately prior to use. Deuterated solvents were passed through a 5 cm-thick alumina column and stored under nitrogen over molecular sieves (4 Å). Column chromatography was performed on silica gel 60 (particle size 40-63 µm, 230-240 mesh). Routine ^{1}H, $^{31}P\{^{1}H\}$ and $^{13}C\{^{1}H\}$ NMR spectra were recorded on Bruker FT instruments (AVANCE 300, 400, 500, 600 spectrometers) at room temperature unless otherwise stated. ^{1}H NMR spectral data were referenced to residual protiated solvents (δ = 7.26 ppm for $CDCl_3$, 7.15 ppm for C_6D_6 and 5.32 ppm for CD_2Cl_2), $^{13}C\{^{1}H\}$ chemical shifts are reported relative to deuterated solvents (δ = 77.16 ppm for $CDCl_3$, 128.02 ppm for C_6D_6 and 53.84 ppm for CD_2Cl_2) and the $^{31}P\{^{1}H\}$ NMR data are given relative to external H_3PO_4. Mass spectra were recorded on a Bruker MicroTOF spectrometer (ESI-TOF) using CH_2Cl_2, CH_3CN or CH_3OH as the solvent. Elemental analyses were performed by the Service de Microanalyse, Institut de Chimie UMR 7177, Strasbourg. Melting points were determined with a Buchi 535 capillary melting point apparatus. In this chapter, the cyclodextrins are depicted as seen from the secondary face, the glucose units following counterclockwise squence in the order: A, B, C, D, E, F. The numbering of the atoms within a glucose unit is as follows:

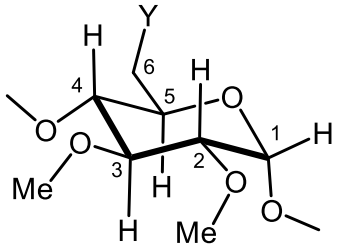

For references, see page 120.

II. 4. 2. Synthesis and characterization

Diethyl [2-(*N*,*N*-dimethylamino)phenyl]phosphonate (3)[26]

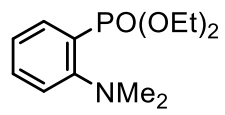

Diethyl 2-amino-1-phenylphosphonate[27] (0.53 g, 2.31mmol), anhydrous K_2CO_3 (1.60 g, 11.56 mmol), methyl iodide (0.72 mL, 11.56 mmol) and dry DMF (5 mL) were placed in a 25 mL flask equipped with a condenser and stirred at 70 °C overnight. The reaction was cooled to room temperature before adding distilled H_2O (15 mL). The mixture was extracted with Et_2O (20 mL). The resulting aqueous layer was then further extracted with Et_2O (3 × 20 mL). The combined organic layers were washed with brine (3 × 15 mL), dried over $MgSO_4$ before being evaporated to dryness. The crude was then subjected to column chromatography (SiO_2; AcOEt/PE, 80/20, *v/v*) to afford **3** (0.51 g, 86%) as a yellow oil. R_f (SiO_2, AcOEt/PE , 90/10 , *v/v*) = 0.26; ^{1}H NMR (400 MHz, $CDCl_3$, 25 °C): δ = 1.35 (t, ^3J = 7.1 Hz, 6H, OCH_2CH_3), 2.79 (s, 6H, NMe_2), 4.16 (m, 4H, OCH_2CH_3), 7.12 (m, 1H, aromatic H), 7.25 (m, 1H, aromatic H), 7.47 (m, 1H, aromatic H), 7.81 (m, 1H, aromatic H); ^{31}P{^{1}H} NMR (121 MHz, $CDCl_3$, 25 °C): δ = 18 ppm. All spectral data are consistent with the literature values.[26]

2-(*N*,*N*-Dimethylamino)phenylphosphine (2)[28]

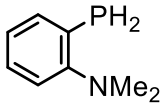

Pure Me_3SiCl (2.36 mL, 18.6 mmol) was added to a suspension of $LiAlH_4$ (0.71 g, 18.6 mmol) in THF (20 mL) at -78 °C. The reaction mixture was allowed to reach room temperature and stirred for 2 h. A solution of phosphonate **3** (1.60 g, 6.2 mmol) in THF (6 mL) was then transfered to the mixture at -30 °C by cannula and stirring was mainntained for 1.5 h at 0 °C. The solvent was removed *in vacuo* and the residue was extracted with NaOH/Et_2O under argon to avoid phosphine oxidation. The organic layer was dried over $MgSO_4$. The solvent was finally removed under vacuum to afford the primary phosphine **2** (0.56 g, 58%) as a colourless oil. The crude was used for the synthesis of **5** without further purification. R_f (SiO_2, AcOEt/PE, 70/30, *v/v*) = 0.95; ^{1}H NMR (400 MHz, $CDCl_3$, 25 °C): δ = 2.73 (s, 6H, NMe_2), 3.91 (d, 2H, $^1J_{PH}$ = 204 Hz, PH_2), 6.98 (m, 1H, aromatic H), 7.12 (m, 1H, aromatic H), 7.27 (m, 1H, aromatic H), 7.48 (m, 1H, aromatic H); ^{31}P{^{1}H} NMR (161 MHz, $CDCl_3$, 25 °C): δ = -128 ppm. HRMS (ESI-TOF) for $C_8H_{12}NP$: *m/z* (%):154.0782 (100) [M + H]$^+$. All spectral data are consistent with the literature values.[28]

6^A,6^B-Dideoxy-6^A,6^B[(*R*)-2-(*N*,*N*-dimethylamino)phenylphosphinidene]-2^A,2^B,2^C,2^D,2^E,2^F, 3^A,3^B,3^C,3^D,3^E,3^F, 6^C,6^D,6^E,6^F-hexadeca-O-methyl-α-cyclodextrin (L1)

For references, see page 120.

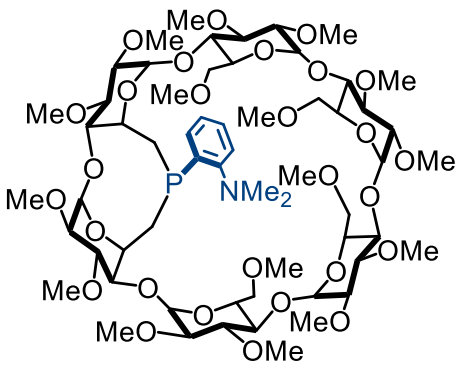

A solution of *n*-BuLi in hexane (1.6 M, 0.28 mL, 0.44 mmol) was added dropwise to a stirred solution of fully dried phosphine **2** (0.034 g, 0.22 mmol) in 4 mL of THF at -78 °C. The mixture was then allowed to reach room temperature over a period of 1 h. The solution was cooled again to -78 °C and then added dropwise to a solution of fully dried dimesylate **1** (0.2 g, 0.15 mmol) in THF (10 mL) via a cannula. The orange solution was stirred for 12 h at room temperature. The solvent was removed *in vacuo* and excess phosphide was protonated with MeOH (2 mL). The suspension was then evaporated to dryness to afford a colourless solid, which was subjected to chromatography over a short plug of silica (SiO_2; CH_2Cl_2/MeOH, 9/1, *v/v*). Finally, the filtrate was evaporated to dryness *in vacuo* and the resulting residue was subjected again to column chromatography (SiO_2; CH_2Cl_2/MeOH, 97:3, *v/v*) to afford pure **L1** (0.122 g, 63%) as a colourless solid. M.p. = 101-103 °C. ^{1}H NMR (400 MHz, $CDCl_3$, 25 °C): δ (assignment by COSY and HSQC) = 1.73 (m,1H, H-6a^B), 1.75 (m, 1H, H-6a^A), 2.68 (m, 1H, H-6b^B), 2.80 (s, 6H, NMe_2), 3.14 (m, 1H, H-6b^A), 3.23 (s, 3H, OMe), 3.24 (s, 3H, OMe), 3.38 (s, 6H, OMe), 3.46 (s, 3H, OMe), 3.47 (s, 3H, OMe), 3.48 (s, 3H, OMe), 3.49 (s, 6H, OMe), 3.50 (s, 3H, OMe), 3.60 (s, 3H, OMe), 3.63 (s, 6H, OMe), 3.64 (s, 3H, OMe), 3.65 (s, 3H, OMe), 3.67 (s, 3H, OMe), 3.11–3.90 (29H, H-2, H-3, H-4, H-5, H-6), 4.01 (m, 1H, H-5^B), 4.09 (dd, 1H, $^2J_{H\text{-}6a,\ H\text{-}6b}$ = 2.0 Hz, $^2J_{H6\text{-}H5}$ = 10.6 Hz, H-6), 4.30 (m, 1H, H-5^A), 4.96 (d, 1H, $^3J_{H1\text{-}H2}$ = 2.8 Hz, H-1), 4.99 (d, 1 H, $^3J_{H1\text{-}H2}$ = 2.9 Hz, H-1), 5.02 (d, 1H, $^3J_{H1\text{-}H2}$ = 4.0 Hz, H-1), 5.05 (d, 1H, $^3J_{H1\text{-}H2}$ = 4.2 Hz, H-1), 5.06-5.07 (2H, H-1), 7.01-7.44 (4H, aromatic H); ^{13}C{^{1}H} NMR (100.6 MHz, $CDCl_3$, 25 °C): δ (assignment by HSQC) = 27.38 (C-6$^{A\text{ or }B}$), 34.08 (C-6$^{A\text{ or }B}$), 46.10, 46.16 (-N(CH_3)$_2$), 57.58, 57.96 [x5], 58.95, 59.04, 59.07, 59.15, 61.77 [x3], 61.87, 62.05, 62.18 (OMe), 70.27, 71.02 (C-6), 71.05 (C-5), 71.28 (C-6), 71.32, 71.40, 71.46 (C-5), 71.56 (C-6), 72.90, 73.20 (C-5), 81.28 [x4], 81.43, 81.56 [x2], 81.66, 81.83 [x2], 82.14, 82.37 [x2], 82.52, 82.71, 83.47, 87.87, 89.18 (C-2, C-3, C-4), 97.51, 99.35, 100.01, 100.19, 100.28, 100.63 (C-1), 118.69, 123.65, 129.85, 133.48 (aromatic C), 135.12 (d, $^1J_{P,C}$ = 19.1 Hz, aromatic C), 157.27(d, $^2J_{P,C}$ = 12.2 Hz, aromatic C); ^{31}P{^{1}H} NMR (121 MHz , $CDCl_3$, 25 °C): δ = -28.4 ppm; elemental analysis (%) calcd for $C_{60}H_{100}NO_{28}P{\bullet}H_2O$: C 54.09, H 7.72, N 1.05, found: C 54.13, H 7.64, N 0.97; MS (ESI-TOF) for $C_{60}H_{100}NO_{28}P$: *m/z* (%): 1314.63 (100) [*M* + H]$^+$.

***N*,*N*-dimethyl-2-diethylphosphinoaniline (L2)**[29]

For references, see page 120.

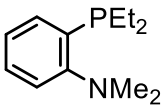

A Schlenk tube filled with argon was charged with 2-bromo-*N*,*N*-dimethylaniline (0.32 g, 1.60 mmol) in THF (3 mL). The solution was cooled at -78 °C and *n*-BuLi (1.92 mmol, 1.2 equiv.) was added dropwise. The mixture was allowed to rise slowly to room temperature. Et_2PCl (0.2 g, 1.60 mmol) was then added to the mixture at 0 °C which was stirred overnight at room temperature. The solvent was removed *in vacuo*. The residue was suspended in DCM and filtered through Celite. Removal of the solvent under reduced pressure afforded the crude filtrate which was purified by column chromatography (SiO_2; PE/DCM, 50/50, *v/v*) to afford **10** as a pale-yellow oil (0.135 g, 40%). ^{1}H NMR (500 MHz, $CDCl_3$, 25 °C): δ = 0.98 (t, ^3J = 7.5 Hz, 3H, PCH_2CH_3), 1.03 (t, ^3J = 7.5 Hz, 3H, PCH_2CH_3), 1.69 (m, 4H, PCH_2CH_3), 2.75 (m, 6H, NMe_2), 7.09 (m, 1H, aromatic H), 7.14 (m, 1H, aromatic H), 7.25-7.34 (2H, aromatic H), ^{31}P{^{1}H} NMR (121 MHz, $CDCl_3$, 25 °C): δ = -25.05 ppm. HRMS (ESI-TOF) for $C_{12}H_{20}NP$: *m/z* (%): 210.1406 (100) $[M + H]^+$. All spectral data are consistent with the literature values.[29]

Dichloro[{6^A,6^B-Dideoxy-6^A,6^B-[(*R*)-2-(*N*,*N*-dimethylaminophenyl)phosphinidene]-2^A,2^B,2^C,2^D,2^E,2^F,3^A,3^B,3^C,3^D,3^E,3^F,6^C,6^D,6^E,6^F-hexadeca-O-methyl-α-cyclodextrin})-κ^{2}P,N] palladium(II) (4)

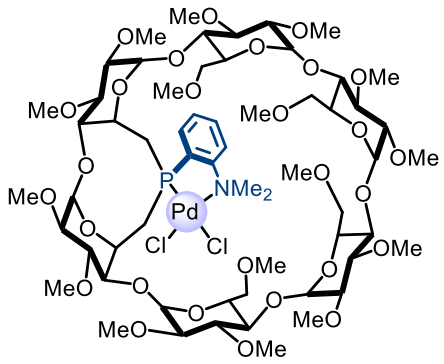

A solution of $[PdCl_2(COD)]$ (0.108 g, 0.38 mmol) in CH_2Cl_2 (4 mL) was added dropwise to a solution of **L1** (0.5 g, 0.38 mmol) in CH_2Cl_2 (4 mL) The reaction mixture was stirred for 2 h at room temperature and then evaporated to dryness under reduced pressure. The resulting yellow residue was subjected to column chromatography (SiO_2, CH_2Cl_2/MeOH, 97/3, *v/v*) to afford pure **4** (0.465 g, 82%) as a yellow solid. A crystalline material was obtained by slow diffusion of *n*-pentane into a butanone solution of **4**. ^{1}H NMR (500 MHz, $CDCl_3$, 25 °C): δ (full assignment by COSY and HSQC) = 2.14 (m, 2H, H-6$^{A\text{ or }B}$), 3.06 (dd, 1H, $^3J_{H2\text{-}H3}$ = 10.1 Hz, $^3J_{H2\text{-}H1}$ = 2.9 Hz, H-2), 3.11–3.19 (4H, H-2), 3.21 (1H, H-6$^{A\text{ or }B}$), 3.26 (dd, 1H, $^3J_{H2\text{-}H3}$ = 9.3 Hz, $^3J_{H2\text{-}H1}$ = 4.2 Hz, H-2), 3.37 (s, 3H, OMe), 3.41 (s, 3H, OMe), 3.43 (s, 6H, NMe_2), 3.44 (s, 6H, OMe), 3.44 (s, 3H, OMe), 3.45 (s, 3H, OMe), 3.46 (s, 6H, OMe), 3.50 (s, 3H, OMe), 3.55 (s, 3H, OMe), 3.58 (s, 3H, OMe), 3.60 (s, 3H, OMe), 3.61 (s, 3H, OMe), 3.63 (s, 3H, OMe), 3.65 (s, 3H, OMe), 3.67 (s, 3H, OMe), 3.35–3.85 (15H, H-3, H-4, H-6), 3.87–3.95 (3H, H-5, H-6), 3.98 (d, 1H, *J* = 11.4 Hz, H-6), 4.15 (d, 1H, *J* = 11.1 Hz, H-6), 4.18–4.28 (4H, H-5, H-6), 4.56 (m, 1H H-5$^{A\text{ or }B}$, H-6 4.59 (m, 1H, H-5$^{A\text{ or }B}$), 4.93 (d, 1H, *J* = 3.1 Hz, H-1), 5.03 (d,

For references, see page 120.

1H, J = 2.6 Hz, H-1), 5.06 (2H, H-1), 5.08 (2H, H-1), 5.19 (m, 1H, H-5$^{A\text{ or }B}$), 7.51–7.68 (4H, aromatic H) ppm; $^{13}C\{^{1}H\}$ NMR (100.6 MHz, $CDCl_3$, 25 °C): δ (assignment by HSQC) = 31.62 (d, $^{1}J_{C6\text{-}P}$ = 32.6 Hz, C-6$^{A\text{ or }B}$), 41.15 (d, $^{1}J_{C6\text{-}P}$ = 28.0 Hz, C-6$^{A\text{ or }B}$), 55.21, 55.48, 57.42, 57.53, 57.68 (OMe), 57.79, 57.82 (NMe_2), 57.90, 59.13 [x2], 59.31, 59.43, 61.78, 61.84, 61.95 [x2], 62.27, 62.55 (OMe), 65.69 (d, $^{2}J_{C5\text{-}P}$ = 6.1 Hz, C-5$^{A\text{ or }B}$), 67.35 (C-5$^{A\text{ or }B}$), 70.02, 70.64, 70.82, 71.01 (C-5), 71.46, 72.03, 72.28, 72.97 (C-6), 80.03, 81.09, 81.13, 81.29, 81.44, 81.52, 81.67, 81.98, 82.07 [x2], 82.28 [x3], 82.55, 82.59, 82.62, 87.96, 90.07 (C-2, C-3, C-4), 98.14, 99.68, 99.99, 100.11, 100.65, 101.32 (C-1), 122.00 (d, $^{2}J_{P,C}$ = 11.7 Hz, aromatic C), 130.89 (d, $^{3}J_{P,C}$ = 6.6 Hz, aromatic C), 131.52 (aromatic C), 131.60 (d, $^{1}J_{P,C}$ = 47.1 Hz, aromatic C), 134.60 (aromatic C), 159.32 (d, $^{2}J_{P,C}$ = 16.2 Hz, aromatic C); $^{31}P\{^{1}H\}$ NMR (121 MHz, $CDCl_3$, 25 °C): δ = 32.5 ppm; elemental analysis (%) calcd for $C_{60}H_{100}Cl_2NO_{28}PPd$•0.15 CH_2Cl_2: C 48.02, H 6.72, N 0.93, found: C 47.71, H 6.82, N 0.94; MS (ESI-TOF) for $C_{60}H_{100}Cl_2NO_{28}PPd$: *m/z* (%): 1456.49 (100) $[M - Cl]^+$.

Methylchloro[{6^{A},6^{B}-Dideoxy-6^{A},6^{B}-[(*R*)-2-(*N*,*N*-dimethylaminophenyl)phosphinidene]-2^{A},2^{B},2^{C},2^{D},2^{E},2^{F},3^{A},3^{B},3^{C},3^{D},3^{E},3^{F},6^{C},6^{D},6^{E},6^{F}-hexadeca-O-methyl-α-cyclodextrin})-κ^{2}P,N]palladium(II) (5)

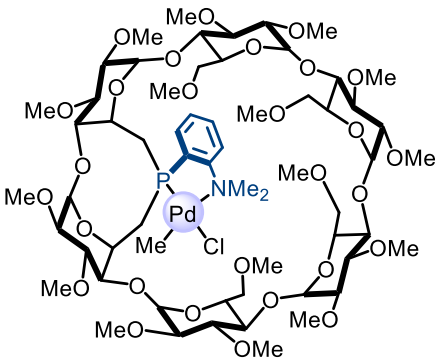

To a solution of **L1** (0.298 g, 0.22 mmol) in CH_2Cl_2 (2 mL) was added dropwise a solution of PdMeCl(COD) (0.060 g, 0.22 mmol) in CH_2Cl_2. The reaction mixture was stirred for 2 h at room temperature. The solution was concentrated under reduced pressure and the resulting yellow residue was subjected to column chromatography (SiO_2, CH_2Cl_2/MeOH, 97/3, *v/v*) to afford pure **5** (yield: 0.197 g, 59%) as a pale yellow solid; R_f (SiO_2, CH_2Cl_2/MeOH, 95:5, *v/v*) = 0.28; m.p. dec. >250 °C; ^{1}H NMR (500 MHz, $CDCl_3$, 25 °C): δ (assignment by combined COSY, ROESY, TOCSY and HSQC) = 0.78 (d, 3H, $^{3}J_{HP}$ = 2.5 Hz, -PdMe), 1.90 (m, 1H, H-6a^{A}), 2.26 (m, 1H, H-6a^{B}), 3.07 (s, 3H, -NMe), 3.08 (m, 1H, H-2^{A}), 3.15-3.19 (4H, H-2^{C,D,E,F}), 3.20 (2H, H-4^{A,B}), 3.22 (s, 3H, -NMe), 3.30 (m, 1H, H-2^{B}), 3.31 (s, 3H, OMe), 3.43 (2H, H-6b^{A,B}), 3.44 (m, 1H, H-3^{C}), 3.44 (s, 3H, OMe), 3.46 (12H, OMe), 3.48 (s, 3H, OMe), 3.49 (s, 3H, OMe), 3.51 (2H, H-3^{A,B}), 3.52(s, 3H, OMe), 3.56 (m, 3H, H-3^{D,E,F}), 3.60 (s, 3H, OMe), 3.62 (s, 3H, OMe), 3.64 (s, 6H, OMe), 3.65 (1H, H-4^{C}), 3.67 (s, 3H, OMe), 3.69 (s, 3H, OMe), 3.72 (m, 1H, H-4^{F}), 3.80 (m, 3H, H-4^{D}, H-6a^{C,D}), 3.81 (m, 1H, H-5^{D}), 3.86 (2H, H-4^{E}, H-6a^{E}), 3.88 (m, 1H, H-5^{C}), 3.92 (m, 2H, H-5^{E}), 4.02 (m, 1H, H-5^{F}), 4.03 (m, 2H, H-6b^{D}, H-6a^{F}), 4.07 (m, 1H,

For references, see page 120.

H-6b^{C}), 4.19 (m, 1H, H-6b^{E}), 4.29 (m, 1H, H-5^{B}), 4.41 (m, 1H, H-5^{A}), 4.44 (m, 1H, H-6b^{F}), 4.96 (d, $^{3}J_{H\text{-}2,H\text{-}1}$ = 3.4 Hz, 1H, H-1^{C}), 5.02 (d, $^{3}J_{H\text{-}2,H\text{-}1}$ = 3.1 Hz, 1H, H-1^{A}), 5.07 (d, $^{3}J_{H\text{-}2,H\text{-}1}$ = 3.2 Hz, 1H, H-1^{D}), 5.09 (d, $^{3}J_{H\text{-}2,H\text{-}1}$ = 4.4 Hz, 1H, H-1^{B}), 5.11 (2H, H-1$^{E,\ F}$), 7.45 (m, 1H, H-5$_{arom}$), 7.56 (m, 3H, H-3$_{arom}$, 4$_{arom}$, 6$_{arom}$) ppm; $^{13}C\{^{1}H\}$ NMR (126 MHz, $CDCl_3$, 25 °C): δ (assignment by HSQC) = -12.06 (d, $^{2}J_{p,c}$ = 4.4 Hz, PdMe), 30.08 (m, C-6^{A}), 40.72 (d, C-6^{B}), 51.33, 51.78 (-NMe$_2$), 57.58, 57.69, 57.73, 57.91, 57.97, 57.99 (OMe-2), 59.24, 59.27, 59.30, 59.37 (OMe-6), 61.78, 61.80, 61.91, 61.98, 62.24, 62.57 (CH_3O-3), 65.67 (d, $^{2}J_{P,C}$ = 6.7, C-5^{A}), 68.58 (d, $^{2}J_{P,C}$ = 4.6, C-5^{B}), 71.16, 70.71, 71.42, 70.93 (C-5^{C,D,E,F}), 71.44, 71.68, 71.92, 72.49 (C-6^{C,D,E,F}), 81.46, 82.51, 82.11 [x4], 80.42, 82.63, 81.63, 81.15 [x3], 81.57, 81.93 (C-2, C-3, C-4^{C,D,E,F}), 88.03 (C-4^{A}), 89.80 (C-4^{B}), 98.09, 99.87, 99.92, 100.41, 100.82, 101.33 (C-1), 122.72 (d, $^{2}J_{P,C}$ = 9.9 Hz, C-6$_{arom}$), 129.25 (d, $^{2}J_{P,C}$ = 6.1 Hz, C-5$_{arom}$), 131.68 (s, C-4$_{arom}$), 133.30 (s, C-3$_{arom}$), 133.80 (m, C-1$_{arom}$), 158.19 (m, C-2$_{arom}$) ppm; $^{31}P\{^{1}H\}$ NMR (162 MHz, $CDCl_3$, 25 °C): δ = 17.9 ppm; elemental analysis (%) calcd for $C_{61}H_{103}ClNO_{28}PPd$: C 49.80, H 7.06, N 0.95, found: C 49.79, H 7.22, N 0.91; MS (ESI-TOF) for $C_{61}H_{103}ClNO_{28}PPd$: *m/z* (%): 1434.54 (100) $[M - Cl]^{+}$.

Dibromo-[{6^{A},6^{B}-Dideoxy-6^{A},6^{B}-[(*R*)-2-(*N*,*N*-dimethylamino)phenylphosphinidene]-2^{A}, 2^{B},2^{C},2^{D},2^{E},2^{F},3^{A},3^{B},3^{C},3^{D},3^{E},3^{F},6^{C},6^{D},6^{E},6^{F}-hexadeca-O-methyl-α-cyclodextrin}-κ^{2}P,N] nickel(II) (6)

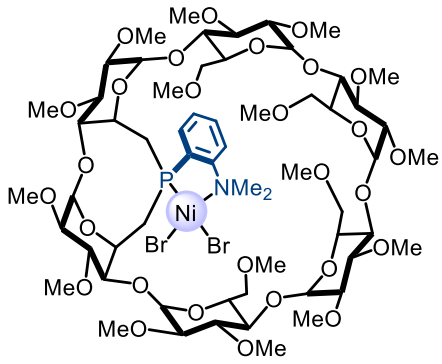

To a solution of **L1** (0.271 g, 0.21 mmol) in CH_2Cl_2 (10 mL) was added dropwise a solution of [$NiBr_2$(DME)] (0.073 g, 0.21 mmol) in CH_2Cl_2. The reaction mixture was stirred for 2 h at room temperature. The solution was evaporated to dryness under reduced pressure. The resulting violet residue was redissolved with benzene and then filtered through a pad of Celite. The filtrate was evaporated *in vacuo* to afford **6** as a violet solid (0.205 g, 64.7%). A crystalline material was obtained by slow diffusion of *n*-pentane into a benzene solution of **6**. ^{1}H NMR (500 MHz, CD_2Cl_2, 25 °C): δ (assignment by COSY and HSQC) = 2.96-4.13 (27H, H-2, H-3, H-4, H-5^{C,D,E,F}, H-6), 3.38 (s, 3H, OMe), 3.39 (s, 3H, OMe), 3.44 (s, 3H, OMe), 3.45(s, 6H, OMe), 3.45 (s, 3H, OMe), 3.46 (s, 3H, OMe), 3.50 (s, 3H, OMe), 3.53 (s, 3H, OMe), 3.55 (s, 3H, OMe), 3.56 (s, 3H, OMe), 3.56 (s, 3H, OMe), 3.57 (s, 3H, OMe), 3.58 (s, 3H, OMe), 3.59 (s, 3H, OMe), 3.61 (s, 3H, OMe), 4.36 (m, 2H, H-5$^{A\ or\ B}$, H-6), 4.47 (d, 1H, *J* = 10.9 Hz, H-6), 4.95 (1H, $^{3}J_{H1\text{-}H2}$ = 3.4 Hz, H-1), 4.98 (2H, H-1, H-5$^{B\ or\ A}$), 4.99-5.03 (2H, H-1), 5.02 (m, 1H,

For references, see page 120.

H-6), 5.09-5.12 (m, 2H, H-1), 7.29-7.66 (4H, aromatic H), signal for NMe_2 is too broad to be identified; $^{13}C\{^1H\}$ NMR (126 MHz, CD_2Cl_2, 25 °C): δ (assignment by HSQC) = 57.62, 57.65, 57.78, 57.78, 57.79, 57.98, 58.97, 58.98, 59.26, 61.26, 61.53, 61.69, 61.80, 61.83, 62.12, 62.34 (OMe), 67.29, 68.85 (br, C-$5^{A,B}$), 70.65, 71.01, 71.11, 71.33 (C-$5^{C,D,E,F}$), 72.18, 72.55, 72.75, 73.39 (C-$6^{C,D,E,F}$), 80.79, 81.65, 81.69, 81.78, 81.88 [x2], 82.01, 82.14 [x2], 82.38, 82.53, 82.67, 82.73, 82.86, 83.02, 83.53, 88.58, 90.32 (C-2, C-3, C-4), 98.48, 99.92, 99.96, 100.31, 100.42, 101.67 (C-1), 121.75 (br), 128.69, 130.90 (br), 134.24 (aromatic C), C-$6^{A,B}$, NMe_2 and two quaternary aromatic carbons could not be identified because of signal broadness; $^{31}P\{^1H\}$ NMR (243 MHz, CD_2Cl_2, -60 °C): δ = 10.40 ppm; elemental analysis (%) calcd for $C_{60}H_{100}Br_2NO_{28}PNi \cdot 0.25\ C_5H_{12}$: C 47.43, H 6.69, N 0.90, found: C 47.26, H 6.88, N 0.98; MS (ESI-TOF) for $C_{60}H_{100}Br_2NO_{28}PNi$: *m/z* (%): 1452.47 (100) $[M - Br]^+$.

Chloro[{6^A,6^B-Dideoxy-6^A,6^B-[(*R*)-2-(*N*,*N*-dimethylaminophenyl)phosphinidene]-2^A,2^B,2^C,2^D,2^E,2^F,3^A,3^B,3^C,3^D,3^E,3^F,6^C,6^D,6^E,6^F-hexadeca-O-methyl-α-cyclodextrin}-κP]gold(I) (7)

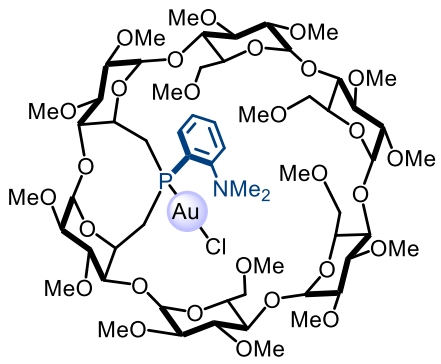

A solution of [AuCl(tht)] (0.042 mg, 0.13 mmol) in CH_2Cl_2 (4 mL) was added dropwise to a solution of **L1** (0.173 g, 0.13 mmol) in CH_2Cl_2 (4 mL). The reaction mixture was stirred for 3 h at room temperature. The solution was evaporated to dryness under reduced pressure and the resulting pale-yellow residue was subjected to column chromatography (SiO_2, CH_2Cl_2/MeOH, 97/3, *v/v*) to afford **7** (0.084 g, 41%) as a pale-yellow solid. A crystalline material was obtained by slow diffusion of *n*-pentane into a benzene solution of **7**. ^1H NMR (500 MHz, $CDCl_3$, 25 °C): δ (assignment by COSY) = 2.17-2.30 (2H, H-$6^{A,\ B}$), 2.73 (s, 6H, NMe_2), 3.25 (m, 1H, H-$4^{A\ or\ B}$), 3.39 (s, 6H, OMe), 3.40 (s, 3H, OMe), 3.43 (s,3H, OMe), 3.45(s, 3H ,OMe), 3,48 (s,3H, OMe), 3.49 (s, 6H, OMe), 3.52 (s, 3H, OMe), 3.54 (m, 1H, H-$6^{A\ or\ B}$), 3.57(m, 1H, H-$6^{A\ or\ B}$), 3.59 (m, 1H, H-$3^{A\ or\ B}$), 3.61 (s, 3H, OMe), 3.64 (s, 6H, OMe), 3.66 (s, 6H, OMe), 3.66 (m, 1H, H-$3^{A\ or\ B}$), 3.70 (s, 3H, OMe), 3.71 (s, 3H, OMe), 3.13-3.85 (27H, H-2, H-3, H-4, H-5, H-6), 4.10 (m, 1H, H-$5^{A\ or\ B}$), 4.56 (m, 1H, H-$5^{A\ or\ B}$), 4.96 (d, 1H, $^3J_{H1\text{-}H2}$ = 3.2 Hz, H-1), 5.02 (d, 1H, $^3J_{H1\text{-}H2}$ = 4.3 Hz, H-1), 5.05 (d, 1H, $^3J_{H1\text{-}H2}$ = 2.9 Hz, H-1), 5.09 (d, 1H, $^3J_{H1\text{-}H2}$ = 3.2 Hz, H-1), 5.11 (m, 2H, H-1), 7.30-7.72 (4H, aromatic H) ppm; $^{13}C\{^1H\}$ NMR (126 MHz, $CDCl_3$, 25°C): δ (assignment by HSQC) = 30.12 (C-$6^{A\ or\ B}$) $^1J_{P,C}$ = 34.0 Hz (d, $^1J_{P,C}$ = 37.8 Hz, C-$6^{A\ or\ B}$), 35.76 (d, $^1J_{P,C}$ = 34.0 Hz, C-$6^{A\ or\ B}$), 47.39 (-NMe_2),

For references, see page 120.

57.57, 57.60, 57.78, 58.00, 58.06, 58.18, 59.22 [x2], 59.30, 59.49, 61.70, 61.83, 61.90, 62.08, 62.16, 62.77 (OMe), 64.67, 70.88 [x2], 71.15, 71.45, 71.70, 71.75, 71.87, 72.87, 73.08 (C-5, C-6^{C,D,E,F}), 80.31, 81.22, 81.26, 81.43, 81.51, 81.63, 81.65, 81.89, 81.98, 82.07, 82.22, 82.24, 82.33, 82.47, 82.81, 82.89, 87.04, 89.66 (C-2, C-3, C-4), 97.88, 99.83, 100.05 100.16, 100.94, 101.12 (C-1), 124.99 (d, $^{3}J_{P,C}$ = 6.0 Hz, aromatic C), 126.72 (d, $^{2}J_{P,C}$ = 11.2 Hz, aromatic C), 128.69 (d, $^{1}J_{P,C}$ = 65.8 Hz, aromatic C), 133.52 (d, $^{2}J_{P,C}$ = 11.8 Hz, aromatic C), 133.66 (d, $^{4}J_{P,C}$ = 2.1 Hz, aromatic C), 158.56 (d, $^{3}J_{P,C}$ = 5.1 Hz, aromatic C) ppm; $^{31}P\{^{1}H\}$ NMR (121 MHz, $CDCl_3$, 25 ˚C): δ = 19.21 (s) ppm; elemental analysis (%) calcd for $C_{60}H_{100}NO_{28}PAuCl$•0.4 CH_2Cl_2: C 45.89, H 6.43, N 0.89, found: C 45.78, H 6.53, N 0.85; MS (ESI-TOF) for $C_{60}H_{100}NO_{28}PAuCl$: *m/z* (%): 1568.54 (100) $[M + Na]^+$.

Dichloro[(*N*,*N*-dimethyl-2-diethylphosphinoaniline)-κ^{2}P,N]palladium(II) (8)

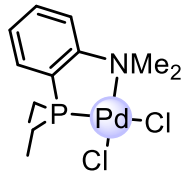

A solution of $[PdCl_2(PhCN)_2]$ (0.126 g, 0.31 mmol) was added to a solution of **L2** (0.066 g, 0.31 mmol) in CH_2Cl_2 (8 mL). The mixture was stirred at room temperature for 20 h and then filtered through Celite. The filtrate was concentrated under reduced pressure and after removal of the solvent under reduced pressure, a yellow solid was obtained which was subjected to column chromatography (SiO_2; CH_2Cl_2/MeOH, 98:2→90:10, *v/v*) to afford two fractions. The first one contained **8** (0.069 g, 58%) and the second one **9** (7 mg, 11%). Recrystallization of **8** was performed by slow diffusion of *n*-pentane into a dichloromethane solution of **8** to afford a yellow crystalline solid (59 mg, 48%). ^{1}H NMR (500 MHz, CD_2Cl_2, 25 °C): δ = 1.17 (t, ^{3}J = 7.5 Hz, 3H, PCH_2CH_3), 1.22 (t, ^{3}J = 7.5 Hz, 3H, PCH_2CH_3), 1.87 (m, 2H, PCH_2CH_3), 2.46 (m, 2H, PCH_2CH_3), 3,42 (s, 6H, NMe_2), 7.58-7.46 (2H, aromatic H), 7.63 (m, 1H, aromatic H), 7.70 (m, 1H, aromatic H). $^{13}C\{^{1}H\}$ NMR (126 MHz, CD_2Cl_2, 25 °C, assignments from HMQC and HMBC): 8.84 (d, $^{2}J_{P,C}$ = 1.3 Hz, PCH_2CH_3), 20.78 (d, $^{1}J_{P,C}$ = 36.5 Hz, PCH_2CH_3), 55.50 (d, $^{3}J_{P,C}$ = 1.0 Hz, NMe_2), 122.57 (d, $^{2}J_{P,C}$ = 11.7 Hz, aromatic C), 126.48 (d, $^{1}J_{P,C}$ = 41.3 Hz, aromatic C), 130.68 (d, $^{3}J_{P,C}$ = 6.5 Hz, aromatic C), 130.80 (aromatic C), 134.94 (d, $^{3}J_{P,C}$ = 2.3 Hz, aromatic C), 162.41 (d, $^{2}J_{P,C}$ = 14.7 Hz, aromatic C); $^{31}P\{^{1}H\}$ NMR (121 MHz, CD_2Cl_2, 25 °C): δ = 62.1 ppm. elemental analysis (%) calcd for $C_{12}H_{20}NPPdCl_2$: C 37.28, H 5.21, N 3.62, found: C 37.26, H 5.24, N 3.46; HRMS (ESI-TOF) for $C_{12}H_{20}Cl_2NPPd$: *m/z* (%): 350.0038 $[M - Cl]^+$.

[Chloro[*N*,*N*-dimethyl-2-diethylphosphinoaniline)-κ^2-P,N][*N*,*N*-dimethyl-2-diethylphosp -hino-aniline)-κ'-P]palladium(II) chloride (9)

For references, see page 120.

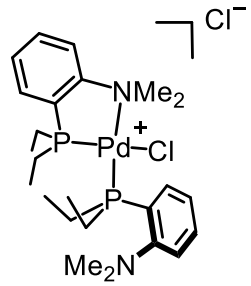

The above procedure was used to prepare the cationic palladium complex **9** from [$PdCl_2(PhCN)_2$] (0.073 g, 0.18 mmol) and **L2** (0.076 g, 0.36 mmol, 2 equiv.) in CH_2Cl_2 (12 mL). Again two fractions were collected. The first one contained **8** (0.020 g, 28 %) and the second one **9** (77 mg, 72%). Yellow single crystals of **9** were obtained by slow diffusion of *n*-pentane into a dichloromethane solution. ^{1}H NMR (500 MHz, $CDCl_3$, 25 °C): δ = 0.95 (br t, 3H, ^3J = 7.5 Hz, PCH_2CH_3), 0.99 (br t, 3H, ^3J = 7.5 Hz, PCH_2CH_3), 1.15 (br t, 3H, ^3J = 7.5 Hz, PCH_2CH_3), 1.19 (br t, 3H, ^3J = 7.5 Hz, PCH_2CH_3), 2.32-2.57 (m, 6H, PCH_2CH_3), 2.76 (s, 6H, NMe_2), 3.09-3.41 (8H, NMe_2, PCH_2CH_3), 7.36 (m, 1H, aromatic H), 7.42-7.50 (2H, aromatic H), 7.55-7.70 (4H, aromatic H), 8.35 (m, 1H, aromatic H); ^{13}C{^{1}H} NMR (126 MHz, CD_2Cl_2, 25 °C, assignments from HMQC and HMBC): 9.12, 9.41 (PCH_2CH_3), 18.79 (d, $^1J_{P,C}$ = 32.3 Hz, PCH_2CH_3), 21.68 (d, $^1J_{P,C}$ = 31.5 Hz, PCH_2CH_3), 47.12, 53.31 (NMe_2), 121.65, 124.41, 126.74, 127.61, 128.10, 131.33, 131.94, 133.15, 133.29, 134.46, 156.54, 158.96 (aromatic C). ^{31}P{^{1}H} NMR (121 MHz, CD_2Cl_2, 25 °C): δ = 56 (d, $^2J_{PP}$ = 13.1 Hz), 21.9 (d, $^2J_{PP}$ = 13.3 Hz) ppm; HRMS (ESI-TOF) for $C_{24}H_{40}Cl_2N_2P_2Pd$: *m/z* (%): 561.1334 [*M* - Cl]$^+$.

Methylchloro[(*N*,*N*-dimethyl-2-diethylphosphinoaniline)-κ^{2}P,N]palladium(II) (10)

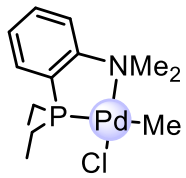

[PdMeCl(COD)] (0.10 g, 0.36 mmol) was added to a solution of **L2** (0.076 g, 0.36 mmol) in CH_2Cl_2 (12 mL). The mixture was stirred at room temperature for 17 h and then filtered through Celite. Concentration under vacuum gave the crude filtrate which was dried under reduced pressure and then purified by column chromatography (SiO_2; DCM/MeOH, 98/2, *v/v*) to afford **10** as a pale yellow solid (0.032 g, 24%). Single crystals of **10** were obtained by slow diffusion of *n*-hexane into a dichloromethane solution. ^{1}H NMR (500 MHz, $CDCl_3$, 25 °C): δ = 0.63 (d, *J* = 2.9 Hz, PdMe), 1.02 (t, ^3J = 7.5 Hz, 3H, PCH_2CH_3), 1.06 (t, ^3J = 7.5 Hz, 3H, PCH_2CH_3), 1.84-2.06 (m, 4H, PCH_2CH_3), 3.09 (s, 6H, NMe_2), 7.40-7.49 (m, 2H, aromatic H), 7.56-7.62 (m, 2H, aromatic H). ^{13}C{^{1}H} NMR (126 MHz, $CDCl_3$, 25 °C, assignments from HMQC and HMBC): -0.93 (d, $^2J_{P,C}$ = 4.8, PdMe), 9.32 (d, $^2J_{P,C}$ = 1.9 Hz, PCH_2CH_3), 20.19 (d, $^1J_{P,C}$ = 32.8 Hz, PCH_2CH_3), 51.45 (NMe_2), 123.07 (d, $^2J_{P,C}$ = 9.3 Hz, aromatic C), 128.75 (d, $^3J_{P,C}$ = 6.0 Hz, aromatic C), 129.30 (d, $^1J_{P,C}$ = 39.3 Hz, aromatic C), 129.99 (aromatic C), 133.27 (d, $^3J_{P,C}$ = 2.5 Hz, aromatic C), 161.30 (d, $^2J_{P,C}$ = 15.5 Hz, aromatic C); ^{31}P{^{1}H} NMR (202 MHz, $CDCl_3$, 25 °C): δ = 44.95 ppm; elemental analysis (%) calcd for $C_{13}H_{23}NPPdCl$•0.4 CH_2Cl_2: C 42.32, H 6.29, N 3.78,

For references, see page 120.

found: C 42.31, H 6.24, N 3.65; HRMS (ESI-TOF) for $C_{13}H_{23}NPPdCl$: *m/z* (%): 330.0597 (100) $[M\text{-}Cl]^+$.

Dibromo[(*N*,*N*-dimethyl-2-diethylphosphinoaniline)-κ^{2}P,N]nickel(II) (12)

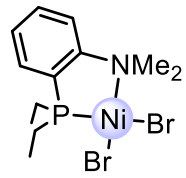

Solid $NiBr_2$ (0.124 g, 0.57 mmol) was added to a solution of **L2** (0.12 g, 0.57 mmol) in CH_2Cl_2 (16 mL) under argon. The reaction mixture was stirred for 22 h at room temperature and filtered through a Celite pad under argon. The filtrate was concentrated to 3-4 mL *in vacuum* and 30 mL Et_2O was added to precipitate a dark red solid. The supernatant was removed with a syringe. The solid was washed with Et_2O and dried under reduced pressure to afford **12** as a dark red solid (0.18 g, 74%). A crystalline material was obtained by slow diffusion of *n*-hexane into a dichloromethane solution of **12**. ^{1}H NMR (600 MHz, CD_2Cl_2, -60 °C): δ = 1.44–1.35 (m, 6H, PCH_2CH_3), 1.64 (dt, ^3J = 15.3, 7.7 Hz, 2H, PCH_2CH_3), 2.35 (dt, ^3J = 15.1, 7.8 Hz, 2H, PCH_2CH_3), 3.13 (s, 6H, NMe_2), 7.41 (m, 3H, aromatic-H), 7.55 (m, 1H, aromatic-H); $^{31}P\{^1H\}$ NMR (243 MHz, CD_2Cl_2, -60 °C): δ = 41.4 ppm; elemental analysis (%) calcd for $C_{12}H_{20}Br_2NNiP$: C 33.69, H 4.71, N 3.27, found: C 33.02, H 4.68, N 3.21; HRMS (ESI-TOF): *m/z* (%): 347.9846 (100) [*M* - Br]$^+$.

II. 4. 3. X-ray crystal structures

Complex **4**. A single crystal suitable for X-ray diffraction analysis was obtained as described in the synthetic procedures. Data were collected at 173(2) K on a Bruker APEX-II CCD diffractometer (Mo-Kα radiation, λ = 0.71073 Å). The structure was solved by direct methods (SHELXS-97) and refined against F2 using the SHELXL-2013 software.[30] The non-hydrogen atoms were refined anisotropically, using weighted full-matrix least-squares on F2. The H-atoms were included in calculated positions and treated as riding atoms using SHELXL default parameters. The crystallographic data are reported in Table 1.

Complexes **6**, **8**, **9**, **10**, **12**. Single crystals suitable for X-ray diffraction analysis obtained as described in the Experimental Part. Data were collected at 120(2) K on a Bruker Bruker PHOTON-III CPAD diffractometer (Mo-Kα radiation, λ = 0.71073 Å). The structure was solved by direct methods (SHELXS-97) and refined against F^2 using the SHELXL-2013 software. The non-hydrogen atoms were refined anisotropically, using weighted full-matrix least-squares on F^2. The H-atoms were included in calculated positions and treated as riding

For references, see page 120.

atoms using SHELXL default parameters. The crystallographic data are reported in Tables 2, 4-7.

Complex **7**. A single crystal suitable for X-ray structure analysis was obtained as described in Experimental Part. Data were collected at 120(2) K on a Bruker Bruker PHOTON-III CPAD diffractometer (Cu-Kα radiation, λ = 1.54178 Å). The structure was solved by direct methods (SHELXS-97) and refined against F^2 using the SHELXL-2013 software. The non-hydrogen atoms were refined anisotropically, using weighted full-matrix least-squares on F^2. The H-atoms were included in calculated positions and treated as riding atoms using SHELXL default parameters. The crystallographic data are reported in Table 3.

For references, see page 120.

Table 1. Crystallographic and structure refinement data for **4** (CCDC 2163655).

Crystal Data	
Crystal size/mm^3	0.25 × 0.12 × 0.1
Empirical formula	$C_{60}H_{100}NO_{28}PCl_2Pd•C_4H_8O$
Formula Weight	1563.78
Crystal system	monoclinic
Space group	$P2_1$
Temperature/K	173(2)
Unit cell parameters	
a/Å	14.9237(6)
b/Å	17.5343(7)
c/Å	15.7250(6)
α/°	90
β/°	101.0630(10)
γ/°	90
V/Å^3	4038.4(3)
Z	2
$D_{(calc)}$ g/cm^3	1.286
F (000)	1652.0
μ/mm^{-1}	0.391

Data Processing and Reduction	
2θ range for data collection/°	3.446 to 56.042
Index ranges	$-19 \leq h \leq 19$, $-20 \leq k \leq 23$, $-20 \leq l \leq 20$
Reflections collected	39896
Independent reflections	18579 [R_{int} = 0.0509, R_{sigma} = 0.0849]
Data / restraints / parameters	18579/2/897
Goodness-of-fit on F^2	0.955
Final R indices [I > 2σ(I)]	R_1 = 0.0478, wR_2 = 0.0893
R indices (all data)	R_1 = 0.0810, wR_2 = 0.0978
Largest diff. peak and hole/eÅ^{-3}	0.53/-0.64
Flack parameter	0.002(11)

For references, see page 120.

Table 2. Crystallographic and structure refinement data for **6** (CCDC 2163663).

Crystal Data	
Crystal size/mm^3	0.3 × 0.2 × 0.15
Empirical formula	$2(C_{60}H_{100}NNiO_{28}PNiBr_2)•5(C_6H_6)•C_5H_{12}$
Formula Weight	3528.49
Crystal system	tetragonal
Space group	$P4_12_12$
Temperature/K	120(2)
Unit cell parameters	
a/Å	17.8671(6)
b/Å	17.8671(6)
c/Å	53.805(2)
α/°	90
β/°	90
γ/°	90
V/Å^3	17176.2(14)
Z	4
$D_{(calc)}$ g/cm^3	1.364
F (000)	7440.0
μ/mm^{-1}	1.252

Data Processing and Reduction	
2θ range for data collection/°	3.79 to 55.792
Index ranges	$-23 \leq h \leq 23$, $-23 \leq k \leq 23$, $-70 \leq l \leq 68$
Reflections collected	277051
Independent reflections	20499 [R_{int} = 0.0618, R_{sigma} = 0.0391]
Data / restraints / parameters	20499/0/919
Goodness-of-fit on F^2	1.040
Final R indices [$I > 2\sigma(I)$]	R_1 = 0.0515, wR_2 = 0.1343
R indices (all data)	R_1 = 0.0741, wR_2 = 0.1474
Largest diff. peak and hole/eÅ^{-3}	0.80/-0.81
Flack parameter	0.016(2)

For references, see page 120.

Table 3. Crystallographic and structure refinement data for **7** (CCDC 2163666).

Crystal Data	
Crystal size/mm^3	0.35 × 0.2 × 0.15
Empirical formula	$C_{60}H_{100}NO_{28}PAuCl•C_6H_6$
Formula Weight	1624.90
Crystal system	monoclinic
Space group	C2
Temperature/K	120(2)
Unit cell parameters	
a/Å	38.308(2)
b/Å	14.1787(8)
c/Å	15.4860(9)
α/°	90
β/°	93.007(2)
γ/°	90
V/Å^3	8399.7(8)
Z	4
$D_{(calc)}$ g/cm^3	1.285
F (000)	3376.0
μ/mm^{-1}	4.367

Data Processing and Reduction	
2θ range for data collection/°	4.62 to 134.642
Index ranges	$-45 \leq h \leq 45$, $-16 \leq k \leq 16$, $-18 \leq l \leq 18$
Reflections collected	108770
Independent reflections	14764 [R_{int} = 0.0684, R_{sigma} = 0.0434]
Data / restraints / parameters	14764/1/901
Goodness-of-fit on F^2	1.149
Final R indices [$I > 2\sigma(I)$]	R_1 = 0.0420, wR_2 = 0.1002
R indices (all data)	R_1 = 0.0430, wR_2 = 0.1012
Largest diff. peak and hole/eÅ^{-3}	1.30/-0.84
Flack parameter	0.171(4)

For references, see page 120.

Table 4. Crystallographic and structure refinement data for **8** (CCDC 2163751).

Crystal Data	
Crystal size/mm^3	0.15 × 0.1 × 0.08
Empirical formula	$C_{12}H_{20}NPPdCl_2$•2($CHCl_3$)
Formula Weight	625.29
Crystal system	monoclinic
Space group	$P2_1/c$
Temperature/K	120(2)
Unit cell parameters	
a/Å	17.0385(7)
b/Å	8.8900(3)
c/Å	32.4365(14)
α/°	90
β/°	92.933(2)
γ/°	90
V/Å^3	4906.8(3)
Z	8
$D_{(calc)}$ g/cm^3	1.693
F (000)	2480.0
μ/mm^{-1}	1.694

Data Processing and Reduction	
2θ range for data collection/°	4.752 to 58.102
Index ranges	$-23 \leq h \leq 23$, $-12 \leq k \leq 11$, $-44 \leq l \leq 44$
Reflections collected	145578
Independent reflections	13078 [R_{int} = 0.1059, R_{sigma} = 0.0475]
Data / restraints / parameters	13078/0/459
Goodness-of-fit on F^2	1.060
Final R indices [$I > 2\sigma(I)$]	R_1 = 0.0423, wR_2 = 0.0784
R indices (all data)	R_1 = 0.0712, wR_2 = 0.0920
Largest diff. peak and hole/eÅ^{-3}	1.28/-1.04

Table 5. Crystallographic and structure refinement data for **9** (CCDC 2163658).

For references, see page 120.

Crystal Data	
Crystal size/mm^3	0.14 × 0.12 × 0.1
Empirical formula	$C_{24}H_{40}N_2P_2PdCl_2$•2(H_2O)
Formula Weight	631.85
Crystal system	orthorhombic
Space group	$Pna2_1$
Temperature/K	120(2)
Unit cell parameters	
a/Å	13.1872(4)
b/Å	11.4097(3)
c/Å	38.4881(11)
α/°	90
β/°	90
γ/°	90
V/Å^3	5791.0(3)
Z	8
$D_{(calc)}$ g/cm^3	1.449
F (000)	2624.0
μ/mm^{-1}	0.959

Data Processing and Reduction	
2θ range for data collection/°	4.234 to 56.032
Index ranges	$-17 \leq h \leq 17$, $-15 \leq k \leq 15$, $-50 \leq l \leq 50$
Reflections collected	94671
Independent reflections	13931 [R_{int} = 0.0609, R_{sigma} = 0.0429]
Data / restraints / parameters	13931/1/611
Goodness-of-fit on F^2	1.069
Final R indices [$I > 2\sigma(I)$]	R_1 = 0.0350, wR_2 = 0.0719
R indices (all data)	R_1 = 0.0464, wR_2 = 0.0783
Largest diff. peak and hole/eÅ^{-3}	2.45/-0.64
Flack parameter	0.341(13)

For references, see page 120.

Table 6. Crystallographic and structure refinement data for **10**.

Crystal Data	
Crystal size/mm^3	0.22 × 0. 2 × 0.18
Empirical formula	$C_{13}H_{23}NPPdCl•CH_2Cl_2$
Formula Weight	451.07
Crystal system	orthorhombic
Space group	Aea2
Temperature/K	120(2)
Unit cell parameters	
a/Å	35.3618(13)
b/Å	15.2642(7)
c/Å	14.4329(6)
α/°	90
β/°	90
γ/°	90
V/Å^3	7790.4(6)
Z	16
$D_{(calc)}$ g/cm^3	1.538
F (000)	3648.0
μ/mm^{-1}	1.438

Data Processing and Reduction	
2θ range for data collection/°	4.052 to 58.302
Index ranges	$-48 \leq h \leq 47$, $-20 \leq k \leq 20$, $-19 \leq l \leq 19$
Reflections collected	80878
Independent reflections	10503 [R_{int} = 0.0224, R_{sigma} = 0.0147]
Data / restraints / parameters	10503/1/371
Goodness-of-fit on F^2	1.136
Final R indices [I > 2σ(I)]	R_1 = 0.0187, wR_2 = 0.0450
R indices (all data)	R_1 = 0.0192, wR_2 = 0.0451
Largest diff. peak and hole/eÅ^{-3}	0.47/-0.69
Flack parameter	0.102(4)

For references, see page 120.

Table 7. Crystallographic and structure refinement data for **12**.

Crystal Data	
Crystal size/mm^3	0.18 × 0.15 × 0.12
Empirical formula	$C_{12}H_{20}NPNiBr_2$
Formula Weight	427.79
Crystal system	triclinic
Space group	P1
Temperature/K	120(2)
Unit cell parameters	
a/Å	7.2760(3)
b/Å	8.6431(3)
c/Å	13.5955(5)
α/°	83.1970(10)
β/°	84.0140(10)
γ/°	71.1770(10)
V/Å^3	801.57(5)
Z	2
$D_{(calc)}$ g/cm^3	1.772
F (000)	424.0
μ/mm^{-1}	6.275

Data Processing and Reduction	
2θ range for data collection/°	5 to 55.84
Index ranges	$-9 \leq h \leq 9$, $-11 \leq k \leq 11$, $-17 \leq l \leq 17$
Reflections collected	54711
Independent reflections	7331 [R_{int} = 0.0369, R_{sigma} = 0.0276]
Data / restraints / parameters	7331/3/315
Goodness-of-fit on F^2	1.077
Final R indices [$I > 2\sigma(I)$]	R_1 = 0.0182, wR_2 = 0.0362
R indices (all data)	R_1 = 0.0203, wR_2 = 0.0376
Largest diff. peak and hole/eÅ^{-3}	0.54/-0.72
Flack parameter	0.014(3)

For references, see page 120.

II. 4. 4. General procedure for determining the glucose units linked by a given capping unit[31]

Our strategy for full structural assignment began with the differentiation between capped and non-capped C-6 carbon atoms by DEPT 135. These appear as two distinct sets of signals. The H-6 protons could then be identified using ^{1}H-^{13}C HMQC. By using TOCSY and COSY, each H-6 proton was correlated to the set of protons belonging to the same glucose residue. The connectivity between individual glucose units was then established via a ROESY experiment showing the proximity between H-4N and H-1N+1 protons (N and N+1 standing for neighboring glucose moieties labelled in the alphabetical order).

For references, see page 120.

II. 5. References

1. Dodziuk, H., *Cyclodextrins and Their Complexes: chemistry, analytical methods, applications*. Warsaw: John Wiley & Sons, **2006**.

2. Szejtli, J., Introduction and General Overview of Cyclodextrin Chemistry. *Chem. Rev.* **1998,** *98*, 1743-1754.

3. Connors, K. A., The Stability of Cyclodextrin Complexes in Solution. *Chem. Rev.* **1997,** *97*, 1325-1358.

4. Crini, G., Review: A History of Cyclodextrins. *Chem. Rev.* **2014,** *114*, 10940-10975.

5. (a) Dong, S. D.; Breslow, R., Bifunctional cyclodextrin metalloenzyme mimics. *Tetrahedron Lett.* **1998,** *39*, 9343-9346. (b) Thompson, Z.; Cowan, J. A., Artificial Metalloenzymes: Recent Developments and Innovations in Bioinorganic Catalysis. *Small* **2020,** *16*, 2000392. (c) Okamoto, Y.; Ward, T. R., Supramolecular Enzyme Mimics. In *Comprehensive Supramolecular Chemistry II*. Amsterdam: Elsevier, **2017**; pp 459-510.

6. (a) Jouffroy, M.; Armspach, D.; Matt, D., Cyclodextrin and phosphorus(III): a versatile combination for coordination chemistry and catalysis. *Dalton Trans.* **2015,** *44*, 12942-12969. (b) Hapiot, F.; Tilloy, S.; Monflier, E., Cyclodextrins as supramolecular hosts for organometallic complexes. *Chem. Rev.* **2006,** *106*, 767-781. (c) Harada, A.; Takashima, Y.; Nakahata, M., Supramolecular Polymeric Materials via Cyclodextrin–Guest Interactions. *Acc. Chem. Res.* **2014,** *47*, 2128-2140. (d) Molnár, Á., Synthetic Application of Cyclodextrins in Combination with Metal Ions, Complexes, and Metal Particles. *ChemCatChem* **2020,** *13*, 1424-1474. (e) Macaev, F.; Boldescu, V., Cyclodextrins in Asymmetric and Stereospecific Synthesis. *Symmetry* **2015,** *7*, 1699-1720. (f) Menuel, S.; Bertaut, E.; Monflier, E.; Hapiot, F., Cyclodextrin-based PNN supramolecular assemblies: a new class of pincer-type ligands for aqueous organometallic catalysis. *Dalton Trans.* **2015,** *44*, 13504-13512. (g) Hapiot, F.; Bricout, H.; Tilloy, S.; Monflier, E., Functionalized Cyclodextrins as First and Second Coordination Sphere Ligands for Aqueous Organometallic Catalysis. *Eur. J. Inorg. Chem.* **2012,** *2012*, 1571-1578. (h) Delbianco, M.; Bharate, P.; Varela-Aramburu, S.; Seeberger, P. H., Carbohydrates in Supramolecular Chemistry. *Chem. Rev.* **2016,** *116*, 1693-1752.

7. (a) Braunstein, P.; Naud, F., Hemilability of Hybrid Ligands and the Coordination Chemistry of Oxazoline-Based Systems. *Angew. Chem. Int. Ed.* **2001,** *40*, 680-699. (b) Zhang, W.-H.; Chien, S. W.; Hor, T. S. A., Recent advances in metal catalysts with hybrid ligands. *Coord. Chem. Rev.* **2011,** *255*, 1991-2024.

8. (a) Margalef, J.; Biosca, M.; De La Cruz Sánchez, P.; Faiges, J.; Pàmies, O.; Diéguez, M.,

For references, see page 120.

Evolution in heterodonor P-N, P-S and P-O chiral ligands for preparing efficient catalysts for asymmetric catalysis. From design to applications. *Coord. Chem. Rev.* **2021,** *446*, 214120. (b) Dwadnia, N.; Roger, J.; Pirio, N.; Cattey, H.; Hierso, J.-C., Input of P, N-(phosphanyl, amino)-ferrocene hybrid derivatives in late transition metals catalysis. *Coord. Chem. Rev.* **2018,** *355*, 74-100. (c) Carroll, M. P.; Guiry, P. J., P,N ligands in asymmetric catalysis. *Chem. Soc. Rev.* **2014,** *43*, 819-833. (d) Ravasio, A.; Boggioni, L.; Tritto, I., Late-Transition Metal Complexes with Mixed NO, NS, NP Chelating Ligands for Olefin Polymerization Catalysis. In *Olefin Upgrading Catalysis by Nitrogen-based Metal Complexes I*, Dordrecht: Springer, **2011**; pp 27-118. (e) Fanfoni, L.; Meduri, A.; Zangrando, E.; Castillon, S.; Felluga, F.; Milani, B., New Chiral P-N Ligands for the Regio- and Stereoselective Pd-Catalyzed Dimerization of Styrene. *Molecules* **2011,** *16*, 1804-1824. (f) Guiry, P. J.; Saunders, C. P., The Development of Bidentate P,N Ligands for Asymmetric Catalysis. *Adv. Synth. Catal.* **2004,** *346*, 497-537. (g) Maggini, S., Classification of P,N-binucleating ligands for hetero- and homobimetallic complexes. *Coord. Chem. Rev.* **2009,** *253*, 1793-1832. (h) F. Speiser, P. B., L. Saussine, Catalytic Ethylene Dimerization and Oligomerization: Recent Developments with Nickel Complexes Containing P, N- Chelating Ligands. *Acc. Chem. Res.* **2005,** *2005*, 784-793. (i) Gavrilov, K. N.; Polosukhin, A. I., Chiral P,N-bidentate ligands in coordination chemistry and organic catalysis involving rhodium and palladium. *Russ. Chem. Rev.* **2000,** *69*, 661-682.

9. (a) Bassetti, M., Kinetic Evaluation of Ligand Hemilability in Transition Metal Complexes. *Eur. J. Inorg. Chem.* **2006,** *2006*, 4473-4482. (b) Morris, R. E.; Brammer, L., Coordination change, lability and hemilability in metal–organic frameworks. *Chem. Soc. Rev.* **2017,** *46*, 5444-5462.

10. (a) Jouffroy, M.; Gramage-Doria, R.; Semeril, D.; Armspach, D.; Matt, D.; Oberhauser, W.; Toupet, L., Phosphinocyclodextrins as confining units for catalytic metal centres. Applications to carbon-carbon bond forming reactions. *Beilstein J. Org. Chem.* **2014,** *10*, 2388-405. (b) Engeldinger, E.; Poorters, L.; Armspach, D.; Matt, D.; Toupet, L., Diastereospecific synthesis of phosphinidene-capped cyclodextrins leading to "introverted" ligands. *Chem. Commun.* **2004,** *2004*, 634-635. (c) Gramage-Doria, R.; Rodriguez-Lucena, D.; Armspach, D.; Egloff, C.; Jouffroy, M.; Matt, D.; Toupet, L., Regioselective Double Capping of Cyclodextrin Scaffolds. *Chem. Eur. J.* **2011,** *17*, 3911-3921. (d) Jouffroy, M.; Armspach, D.; Matt, D.; Osakada, K.; Takeuchi, D., Synthesis of Optically Active Polystyrene Catalyzed by Monophosphine Pd Complexes. *Angew. Chem. Int. Ed.* **2016,** *55*, 8367-8370. (e) Kaya, Z.; Andna, L.; Matt, D.; Bentouhami, E.; Djukic, J.-P.; Armspach, D., A Comparative Study of Confining Ligands Derived from Methylated Cyclodextrins in Gold-Catalyzed

For references, see page 120.

Cycloisomerization of 1,6-Enynes. *Eur. J. Org. Chem.* **2019,** *2019*, 4528-4537.

11. (a) Gramage-Doria, R.; Armspach, D.; Matt, D., Metallated cavitands (calixarenes, resorcinarenes, cyclodextrins) with internal coordination sites. *Coord. Chem. Rev.* **2013,** *257*, 776-816. (b) Leenders, S. H.; Gramage-Doria, R.; de Bruin, B.; Reek, J. N., Transition metal catalysis in confined spaces. *Chem. Soc. Rev.* **2015,** *44*, 433-48. (c) Mouarrawis, V.; Plessius, R.; van der Vlugt, J. I.; Reek, J. N. H., Confinement Effects in Catalysis Using Well-Defined Materials and Cages. *Front Chem.* **2018,** *6*, 623. (d) Matt, D.; Harrowfield, J., Phosphines and other P(III)-derivatives with Cavity-shaped Subunits: Valuable Ligands for Supramolecular Metal Catalysis, Metal Confinement and Subtle Steric Control. *ChemCatChem* **2021,** *13*, 153-168. (e) Orton, G. R. F.; Pilgrim, B. S.; Champness, N. R., The chemistry of phosphines in constrained, well-defined microenvironments. *Chem. Soc. Rev.* **2021,** *50*, 4411-4431.

12. (a) Xu, G.; Leloux, S.; Zhang, P.; Meijide Suárez, J.; Zhang, Y.; Derat, E.; Ménand, M.; Bistri - Aslanoff, O.; Roland, S.; Leyssens, T.; Riant, O.; Sollogoub, M., Capturing the Monomeric (L)CuH in NHC - Capped Cyclodextrin: Cavity - Controlled Chemoselective Hydrosilylation of α,β-Unsaturated Ketones. *Angew. Chem. Int. Ed.* **2020,** *59*, 7591-7597. (b) Kaya, Z.; Bentouhami, E.; Pelzer, K.; Armspach, D., Cavity-shaped ligands for asymmetric metal catalysis. *Coord. Chem. Rev.* **2021,** *445*, 214066. (c) Zhang, P.; Meijide Suárez, J.; Driant, T.; Derat, E.; Zhang, Y.; Ménand, M.; Roland, S.; Sollogoub, M., Cyclodextrin Cavity-Induced Mechanistic Switch in Copper-Catalyzed Hydroboration. *Angew. Chem.* **2017,** *129*, 10961-10965. (d) García-Simón, C.; Gramage-Doria, R.; Raoufmoghaddam, S.; Parella, T.; Costas, M.; Ribas, X.; Reek, J. N. H., Enantioselective Hydroformylation by a Rh-Catalyst Entrapped in a Supramolecular Metallocage. *J. Am. Chem. Soc.* **2015,** *137*, 2680-2687. (e) Jouffroy, M.; Gramage-Doria, R.; Armspach, D.; Sémeril, D.; Oberhauser, W.; Matt, D.; Toupet, L., Confining Phosphanes Derived from Cyclodextrins for Efficient Regio- and Enantioselective Hydroformylation. *Angew. Chem.* **2014,** *126*, 4018-4021. (f) Gadzikwa, T.; Bellini, R.; Dekker, H. L.; Reek, J. N. H., Self-Assembly of a Confined Rhodium Catalyst for Asymmetric Hydroformylation of Unfunctionalized Internal Alkenes. *J. Am. Chem. Soc.* **2012,** *134*, 2860-2863.

13. Armspach, D.; Poorters, L.; Matt, D.; Benmerad, B.; Balegroune, F.; Toupet, L., A new approach to A,B-difunctionalisation of cyclodextrins using bulky 1,3-bis[bis(aryl)chloromethyl]benzenes as capping reagents. *Org. Biomol. Chem.* **2005,** *3*, 2588-92.

14. Armspach, D.; Matt, D., Metal-Capped α-Cyclodextrins: Squaring the Circle. *Inorg. Chem.*

For references, see page 120.

2001, *40*, 3505-3509.

15. Tahtaoui, C.; Parrot, I.; Klotz, P.; Guillier, F.; Galzi, J.-L.; Hibert, M.; Ilien, B., Fluorescent Pirenzepine Derivatives as Potential Bitopic Ligands of the Human M1 Muscarinic Receptor. *J. Med. Chem.* **2004,** *47*, 4300-4315.

16. Katti, K. V.; Pillarsetty, N.; Raghuraman, K., New Vistas in Chemistry and Applications of Primary Phosphines. In *New Aspects in Phosphorus Chemistry III*, Berlin Heidelberg: Springer, **2003**; pp 121-141.

17. Bonnaventure, I.; Charette, A. B., Probing the Importance of the Hemilabile Site of Bis(phosphine) Monoxide Ligands in the Copper-Catalyzed Addition of Diethylzinc to N-Phosphinoylimines: Discovery of New Effective Chiral Ligands. *J. Org. Chem.* **2008,** *73*, 6330-6340.

18. Basra, S.; De Vries, J. G.; Hyett, D. J.; Harrison, G.; Heslop, K. M.; Orpen, A. G.; Pringle, P. G.; Von Der Luehe, K., Efficient asymmetric hydrogenation with rhodium complexes of C1-symmetric 2,5-dimethylphospholane-diphenylphosphines. *Dalton Trans.* **2004,** *2004*, 1901.

19. Machnitzki, P.; Nickel, T.; Stelzer, O.; Landgrafe, C., Novel Syntheses of Mono- and Bisphosphonated Aromatic Phosphanes by Consecutive Pd-Catalyzed P–C Coupling Reactions and Nucleophilic Phosphanylation – X-ray Structure of $Ph_2P–C_6H_4–m\text{-}PO_3Na_2 \cdot 5.5\ H_2O{\cdot}iPrOH$. *Eur. J. Inorg. Chem.* **1998,** *1998*, 1029-1034.

20. Budzelaar, P. H. M.; van Doorn, J. A.; Meijboom, N., Reductive cleavage of the carbon-phosphorus bond with alkali metals. I. Cleavage of functionalised triphenylphosphines; formation of secondary and primary phosphines. *Recueil des Travaux Chimiques des Pays-Bas* **1991,** *110*, 420-432.

21. Mann, F. G.; Watson, H. R., 783. The preparation and quaternisation of o-dimethylamino-phenyldiethylphosphine and an analogous arsine. *J. Chem. Soc. (Resumed)* **1957,** 3945.

22. Lundgren, R. J.; Peters, B. D.; Alsabeh, P. G.; Stradiotto, M., A P,N-Ligand for Palladium-Catalyzed Ammonia Arylation: Coupling of Deactivated Aryl Chlorides, Chemoselective Arylations, and Room Temperature Reactions. *Angew. Chem. Int. Ed.* **2010,** *49*, 4071-4074.

23. Braunstein, P.; Fryzuk, M. D.; Le Dall, M.; Naud, F.; Rettig, S. J.; Speiser, F., Synthesis and structure of Pd(II) complexes containing chelating (phosphinomethyl)oxazoline P,N-type ligands; copolymerisation of ethylene/CO. *J. Chem. Soc., Dalton Trans.* **2000,** *2000*, 1067-1074.

24. Gout, J.; Rat, S.; Bistri, O.; Reinaud, O., Supramolecular Control of Biomimetic Coordination – Zn(II) Cavity Complexes Presenting Two Differentiated Labile Sites in cis

For references, see page 120.

Positions. *Eur. J. Inorg. Chem.* **2014,** *2014*, 2819-2828.

25. Levason, W.; Smith, K. G., Nickel(II) complexes of hybrid nitrogen-phosphorus, nitrogen-arsenic, and nitrogen-antimony ligands. A comparison. *Inorg. Chim. Acta.* **1980,** *41*, 133-141.

26. Xu, F. Y.; Duke, O. M.; Rojas, D.; Eichelberger, H. M.; Kim, R. S.; Clark, T. B.; Watson, D. A., Arylphosphonate-Directed Ortho C-H Borylation: Rapid Entry into Highly-Substituted Phosphoarenes. *J. Am. Chem. Soc.* **2020,** *142*, 11988-11992.

27. Bessmertnykh, A.; Douaihy, C. M.; Muniappan, S.; Guilard, R., Efficient palladium-catalyzed synthesis of aminopyridyl phosphonates from bromopyridines and diethyl phosphite. *Synthesis* **2008,** *2008*, 1575-1579.

28. Budzelaar, P. H. M.; van Doorn, J. A.; Meijboom, N., Reductive cleavage of the carbon-phosphorus bond with alkali metals. I. Cleavage of functionalised triphenylphosphines; formation of secondary and primary phosphines. *Recl. Trav. Chim.* **1991,** *110*, 420-432.

29. Benvenuti, F.; Carlini, C.; Marchionna, M.; Patrini, R.; Raspolli Galletti, A. M.; Sbrana, G., Homogeneous telomerization of 1,3-butadiene with alcohols in the presence of palladium catalysts modified by hybrid chelate ligands. *J. Mol. Catal. A Chem.* **1999,** *140*, 139-155.

30. Sheldrick, G. M., A short history of SHELX. *Acta Crystallographica Section A Foundations of Crystallography* **2008,** *64*, 112-122.

31. Schneider, H. J.; Hacket, F.; Rudiger, V.; Ikeda, H., NMR Studies of Cyclodextrins and Cyclodextrin Complexes. *Chem. Rev.* **1998,** *98*, 1755-1786.

For references, see page 120.

Chapter III

Coordination behavior of cavity-shaped, *cis*-chelating diphosphines towards d^8 cations with two different metal confining environments

III. 1. Introduction

Phosphines are ubiquitous ligands with a wealth of history in coordination chemistry and catalysis.[1] They are considered as soft ligands particularly well suited for coordinating late transition metals and are capable of both σ-donation and π-acidity (back donation). These electronic properties can be easily tuned by varying the substituents (whether alkyl or aryl) at the phosphorus atom, which can also be made stereogenic when equipped with three different groups.[2] Moreover, the steric environment around phosphorus and therefore the coordinated metal, can also be changed at will. Together with the electronic properties of the ligand, steric factors have been shown to have strong impact on metal coordination and the outcome of many catalytic reactions.[3] In the case of chelating diphosphines, the so-called bite angle (Fig 1) is another parameter known to have a strong influence on the coordination of metals and metal-catalyzed reactions.[4] It is therefore no surprise that phosphines and more generally P(III) ligands can be found in numerous industrial processes involving late transition metals, such as the hydroformylation of alkenes, the asymmetric hydrogenation of prochiral alkenes, hydrocyanation of alkenes and many others.[5] CDs equipped with one or several phosphine groups are particularly attractive owing to the fact that the configurationally stable phosphorus atom can be used to force the metal center to be located inside the chiral environment of the CD interior. This specific feature has been shown to have a strong impact on the coordination behavior of the P(III) ligand. In particular, metal confining monophosphines (**HUGPHOS-1** and **HUGPHOS-2**)[6] prevent the formation of bis(phosphine) complexes and promote the formation of undercoordinated species. Such a behavior is key to produce high regioselectivity, stereoselectivity and substrate selectivity in catalytic reactions such as the hydroformylation of vinyl arenes.[6-7] Furthermore, CDs equipped with two widely separated phosphine groups behave as *trans* chelators, in particular when the two phosphorus lone pairs are facing each other and oriented towards the interior of the CD cavity as in the A,B:D,E-capped CDs **TRANSDIP** and **WIDEPHOS**.[8] Unfortunately, both of these diphosphine ligands display *trans*-chelating behavior. The purpose of this chapter is to study the coordination behavior towards catalytically relevant d^8 cations of two *cis*-chelating diphosphine ligands derived from α-CD (Fig 3), previously prepared in our laboratory.[9]

For references, see page 175.

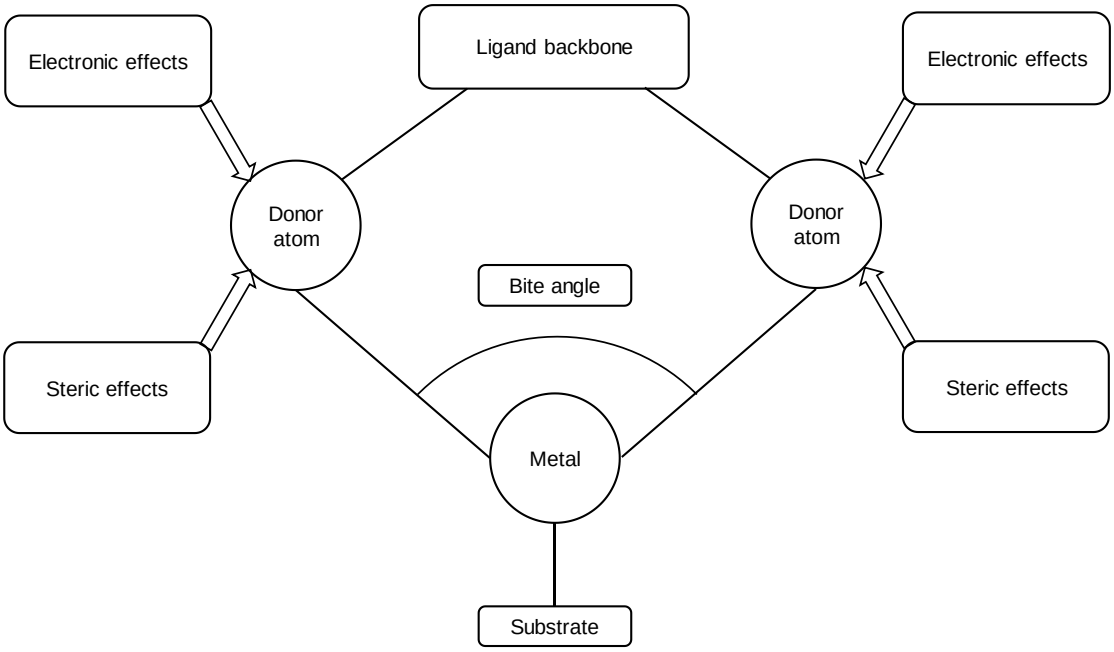

Fig 1. Parameters to be taken into account when designing chelating ligands for catalytic purposes.

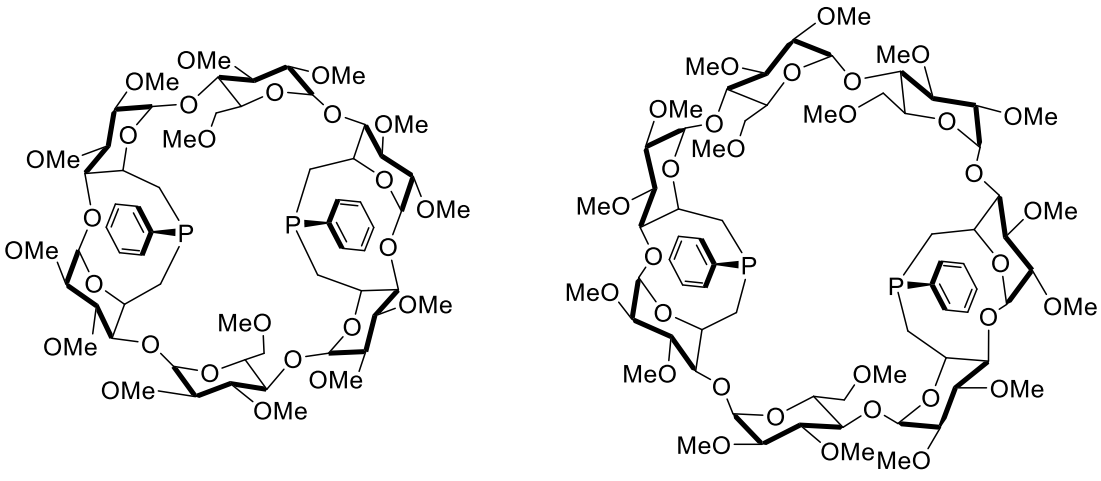

TRANSDIP **WIDEPHOS**

Fig 2. Examples of CD-based *trans*-chelating diphosphine ligands.

For references, see page 175.

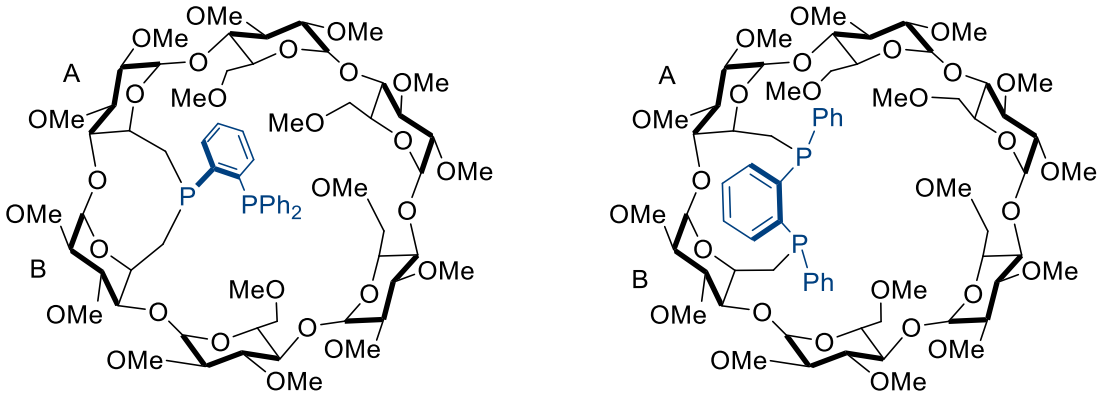

Fig 3. Structures of the metal confining diphosphines studied for metal chelation.

III. 2. Results and discussion

III. 2. 1. Synthesis of α-CD-based diphosphine ligands

The synthesis of **L3** is directly inspired by that of monophosphine **HUGPHOS-1** and ligand **L1**. It consisted in the reaction of dimesylate **1b** with doubly deprotonated phenylphosphine at 25 °C. Similarly, phosphine **L3** was prepared by reacting **1b** with deprotonated diphenylphosphino-2-phosphinobenzene **13**.

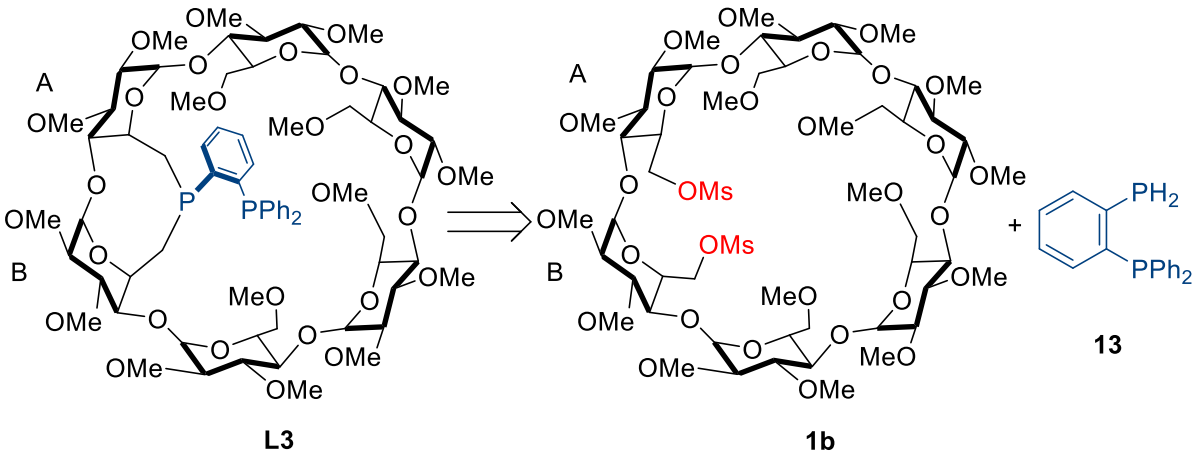

Scheme 1. Retrosynthetic analysis for diphosphine ligand **L3**.

Diphosphine **13** was synthesized according to a procedure described in the literature,[10] which is very similar to the way primary phosphine **2** was prepared. As shown in Scheme 2, the Stelzer method was used to perform a Pd-catalyzed P-C coupling reaction between 2-

For references, see page 175.

bromoiodobenzene and diphenylphosphine[11]. The resulting (2-bromophenyl)diphenylphosphine was then *ortho*-metalated with *n*-BuLi before being reacted with chlorodiethylphosphite to give phosphonate **14** in 58% yield. The latter was subsequently reduced by $LiAlH_4$ in the presence of Me_3SiCl to afford diphosphine **13** in 86% yield. This diphosphine is much less prone to oxidation compared to **2** and could be purified by column chromatography under argon atmosphere. As the two nonequivalent phosphorus atoms are separated by three bonds, their coupling constant is relatively large ($^3J_{PP}$ = 97.9 Hz). The presence of the primary diphosphine was confirmed by the presence of a doublet integrating for two protons at δ_H = 3.90 ppm ($^1J_{PH}$ = 207 Hz, $^4J_{PH}$ = 11.9 Hz).

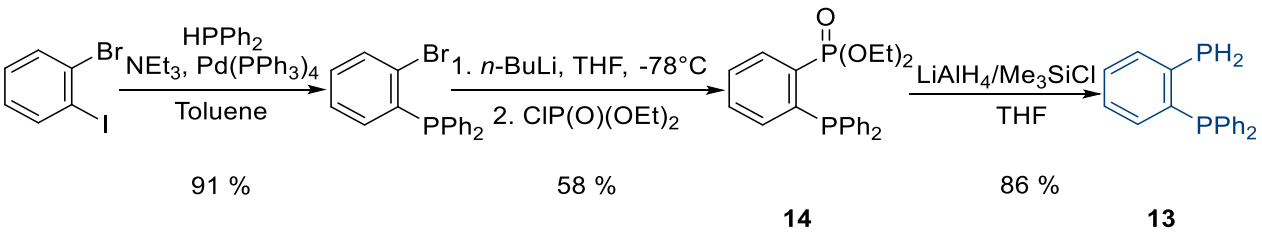

Scheme 2. Synthesis of diphenylphosphino-2-phosphinobenzene **13**.

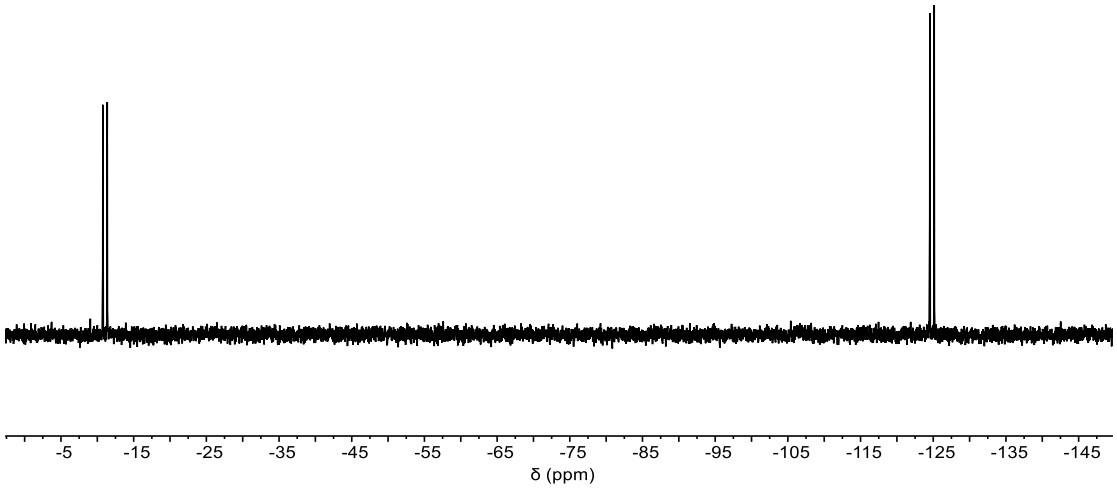

Fig 4. $^{31}P\{^1H\}$ NMR spectrum of diphosphine **13** in $CDCl_3$.

For references, see page 175.

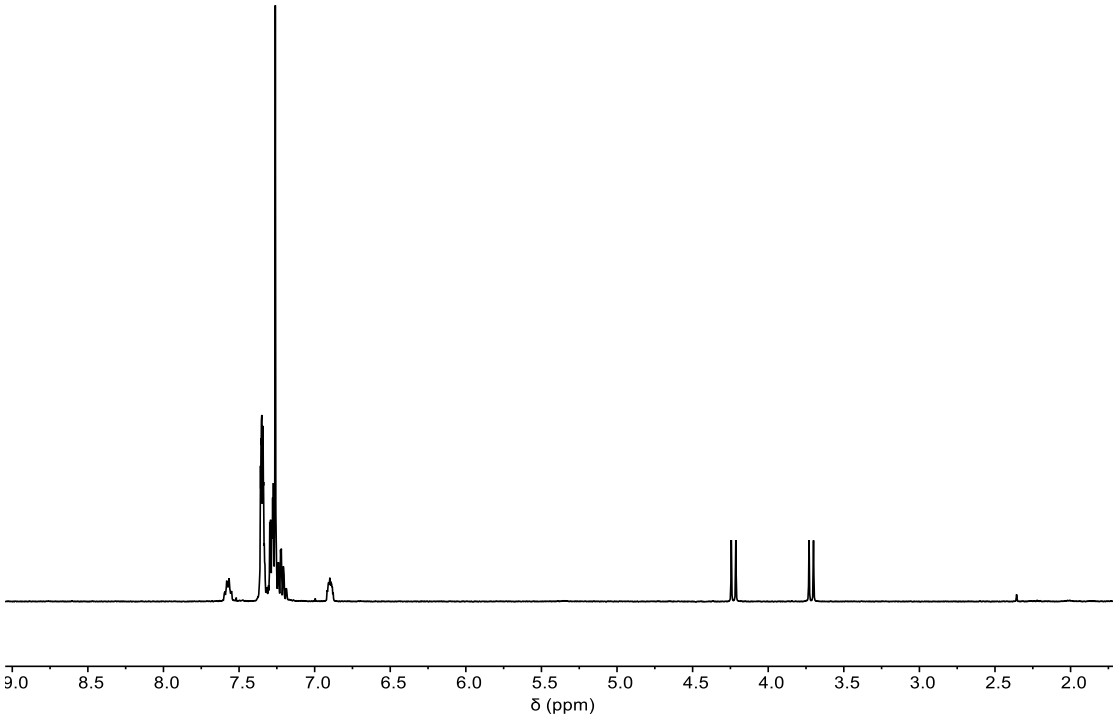

Fig 5. ^{1}H NMR spectrum of diphosphine **13** in $CDCl_3$.

The procedure used for preparing diphosphine ligand **L3** is shown in Scheme 3. The monoanion generated a monoanion by deprotonation of the primary phosphine **13** with 3 equivalents of LDA in THF at -78 °C was added into a solution of dimesylate **1b** in THF at 0 °C and then left to react for 12 h at room temperature. Note that *n*-BuLi was not used in this case to avoid the formation of the dianion which leads to a Smiles-like rearrangement (see below). As for the P,N ligand **L1**, none of the phosphorus atoms is easily oxidized so that purification by column chromatography without particular precaution could be carried out to yield pure ligand **L3** (57% yield).

For references, see page 175.

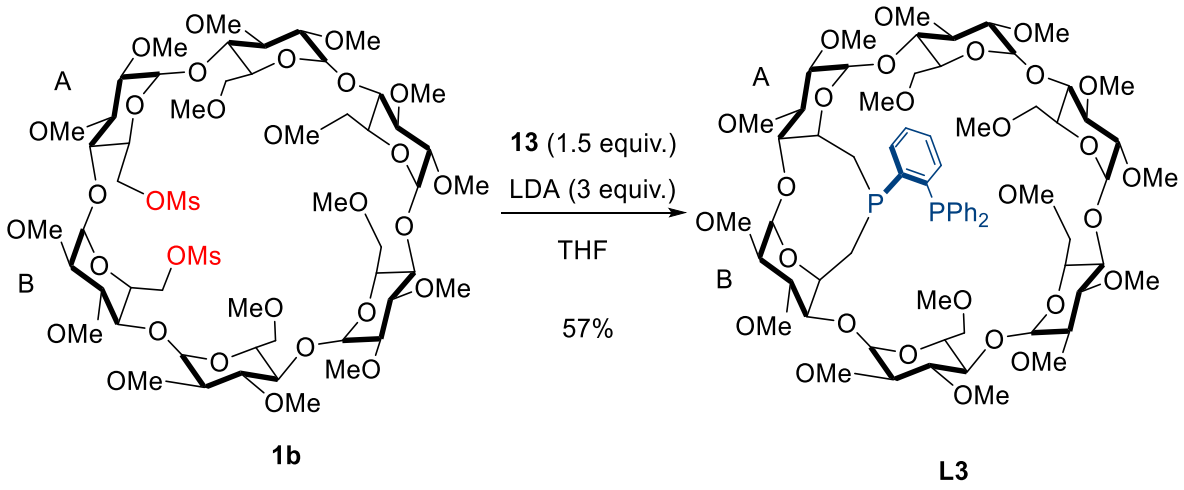

Scheme 3. Synthesis of diphosphine ligand **L3**.

$^{31}P\{^{1}H\}$ NMR spectrum of diphosphine **L3**, named ARMPHOS, comprises two doublets at -28.7 and -14.7 ppm, with a large coupling constant ($^{3}J_{p,p}$ = 167 Hz).

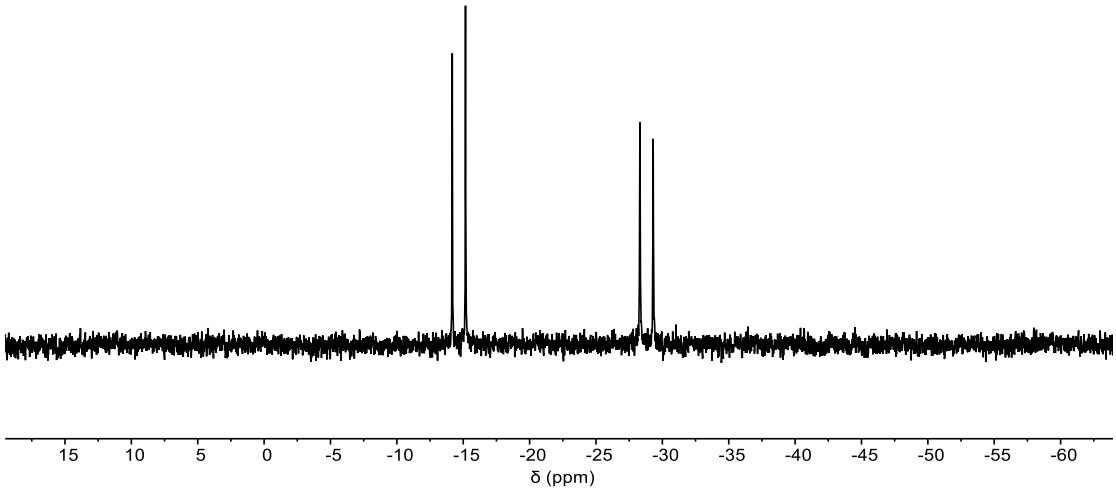

Fig 6. ^{31}P NMR spectrum of diphosphine ligand **L3** in $CDCl_3$.

The synthesis of the second diphosphine ligand **L4** relies on an intramolecular nucleophilic aromatic substitution, which bears some similarities with a Smiles rearrangement.[12]

For references, see page 175.

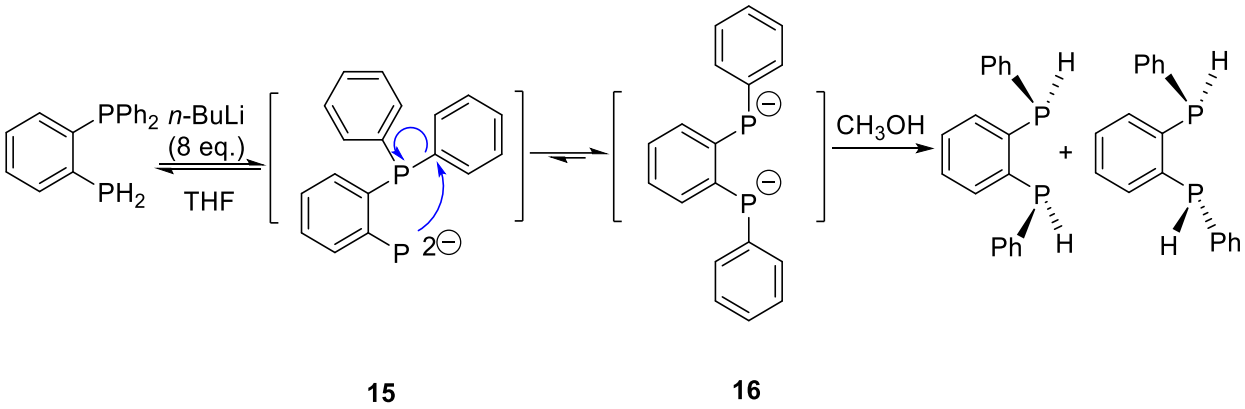

Scheme 4. Mechanism of the new Smiles-like rearrangement in the presence of *n*-BuLi.

In the presence of excess *n*-BuLi, the primary phosphine **13** provided the doubly charged phosphide **15**, which quantitatively isomerized to the secondary diphosphide **16**. This diphosphide is present as three stereoisomers, namely an equimolar mixture of enantiomers (racemic mixture) and a meso compound that is diastereomeric to the pair of enantiomers. When reacted with the dimesylate **1b**, the mixture of doubly charged stereoisomers should lead to a cyclic diphosphine, theoretically present as four diastereoisomers, which are shown in fig 7. These are the diphosphine in which the two phosphorus lone pairs are pointing towards the cavity interior (**a**), two phosphines in which one of the lone pairs is pointing outward and the other inward (**b** and **c**), and a phosphine in which both phosphorus lone pairs are pointing the outside of the CD cavity (**d**).

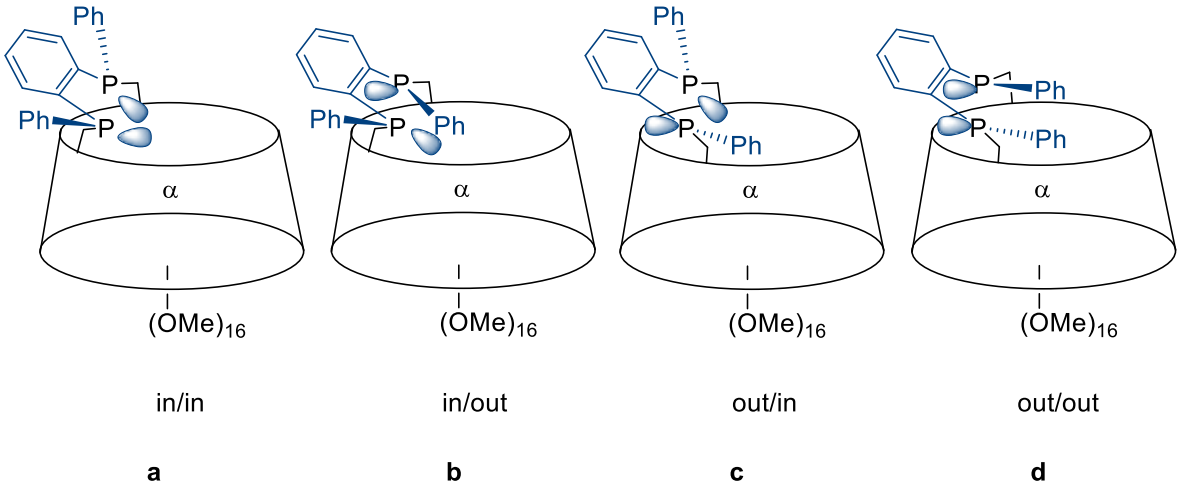

Fig 7. Representation of the four possible diastereomers of diphosphine ligand **L4**.

For references, see page 175.

^{1}H and ^{31}P{^{1}H} NMR spectroscopic analysis of the reaction mixture indicated that only three out of four possible diastereomers were formed. Stereomer **d** cannot form because in this case, the two bulky phenyl groups have to be located in the rather small α-CD cavity, which is not possible for steric reasons. Since the cyclisation probably produced a mixture of the three isomers under kinetic control, the reaction mixture was heated under reflux in mesitylene for 4 h in order to favor the most thermodynamically stable product by simple inversion of the phosphorus at high temperature (T > 135 °C)[13]. After 4 h of heating, the **a**/(**b** + **c**) molar ratio changed from 41/59 to 96/4 and reached an equilibrium, which was confirmed by ^{1}H and ^{31}P{^{1}H} NMR. Finally, the separation of **a** from the **b**/**c** diastereomeric mixture could be achieved by column chromatography on silica. Again, as for **L1** and **L3**, without particular precaution since **L4** is also not very sensitive to oxidation. In the following, **L4** corresponds to stereoisomer **a** only.

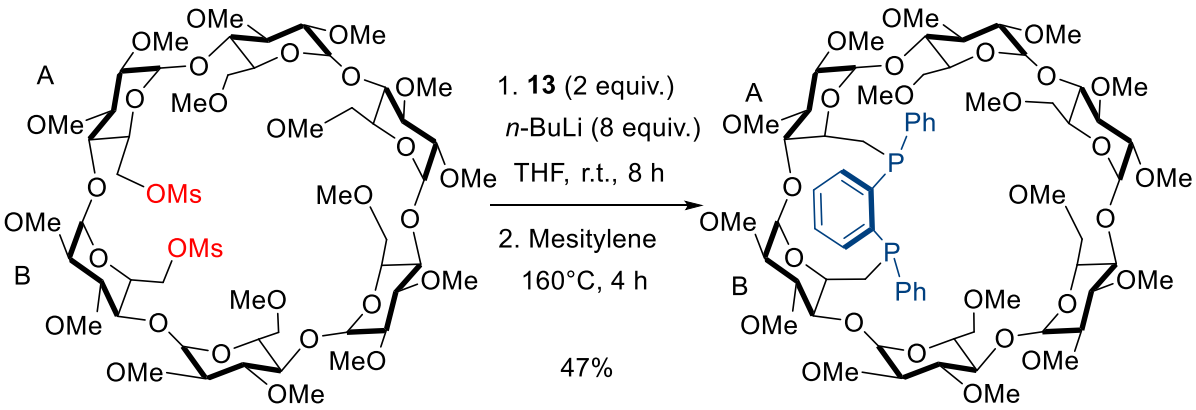

Scheme 5. Synthesis of the diphosphine ligand **L4**.

The optimized procedure for preparing diphosphine **L4**, named DEXPHOS, is detailed in Scheme 5. As for **L3**, the ^{31}P{^{1}H} NMR spectrum of **L4** comprises two doublets at -27.2 and -19.0 ppm (AB spin system) with a coupling constant comparable to that of **L3** ($^{3}J_{P,P}$ = 176 Hz).

For references, see page 175.

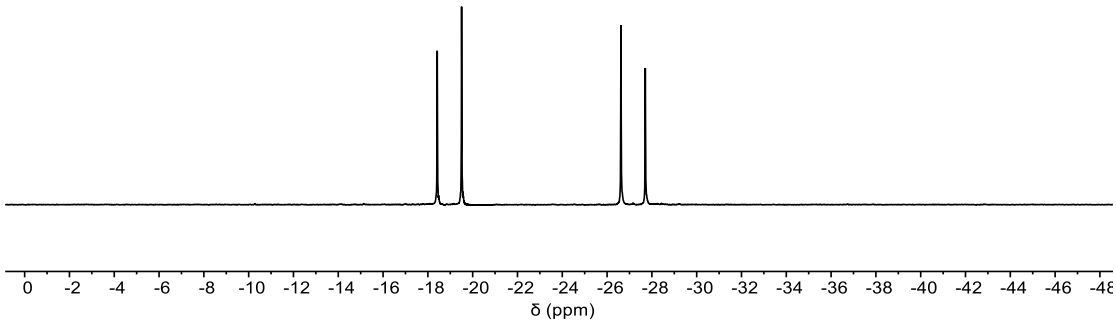

Fig 8. $^{31}P\{^{1}H\}$ NMR spectrum of diphosphine ligand **L4** in $CDCl_3$.

III. 2. 2. Synthesis of metal complexes derived from diphosphines L3 and L4

Although both metal confining, the two ligands have their two phosphorus donor atoms positioned differently with respect to the cavity. For example, in square planar complexes, the coordination plane of **L3** should be perpendicular to that of **L4**. Furthermore, while the two P(III) atoms are electronically equivalent in **L4**, the bridging phosphorus atom **L3** is much more basic than the pendant one. All these features should have major implications on both the coordination and catalytic properties of the diphosphine ligands.

III. 2. 2. 1. Synthesis of metal complexes derived from ARMPHOS (L3)

The corresponding palladium and nickel complexes were synthesized according to the same procedures used for P,N complexes. Accordingly, complex **17** was synthesized in 75% yield by reacting **L3** with one equivalent of $[PdCl_2(COD)]$ in deoxygenated CH_2Cl_2 for 2 h. As for the P,N analog **L1**, only a 1:1 ligand/metal chelate complex was present in the reaction mixture. It is very stable and could be easily purified by column chromatography on silica without particular precaution.

For references, see page 175.

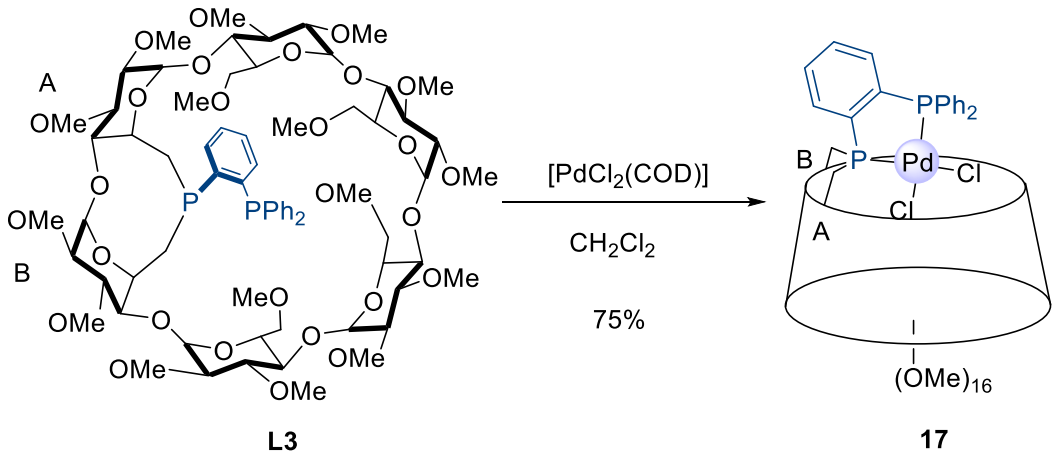

Scheme 6. Synthesis of Pd(II) complex **17** derived from **L3**.

Compared to the free ligand **L3**, the $^{31}P\{^{1}H\}$ chemical shifts of complex **17** are significantly downfield shifted (two doublets at 55.5 and 61.6 ppm, respectively), with a much smaller coupling constant ($^{3+2}J_{P,P}$ = 13.6 Hz) as expected for a palladium chelated by the two phosphorus atoms. As for the palladium complex **4** derived from P,N bidentate ligand **L1**, which has an overall structure similar to that of **L3**, the ^{1}H NMR spectrum of **17** displays downfield-shifted H-5 CD protons, in particular the H-5 proton belonging to the capped glucose unit A (δ_{1H} = 4.21 ppm for **L3** *vs.* 5.30 ppm for **17**), which indicates that the halido ligand is in close contact with these intracavity protons. This feature was also confirmed in the solid state thanks to the X-ray structure of **17** (Fig 11a and 11b). Single crystals suitable for X-ray diffraction could be easily obtained by slow diffusion of *n*-pentane into a solution of **17** in benzene.

For references, see page 175.

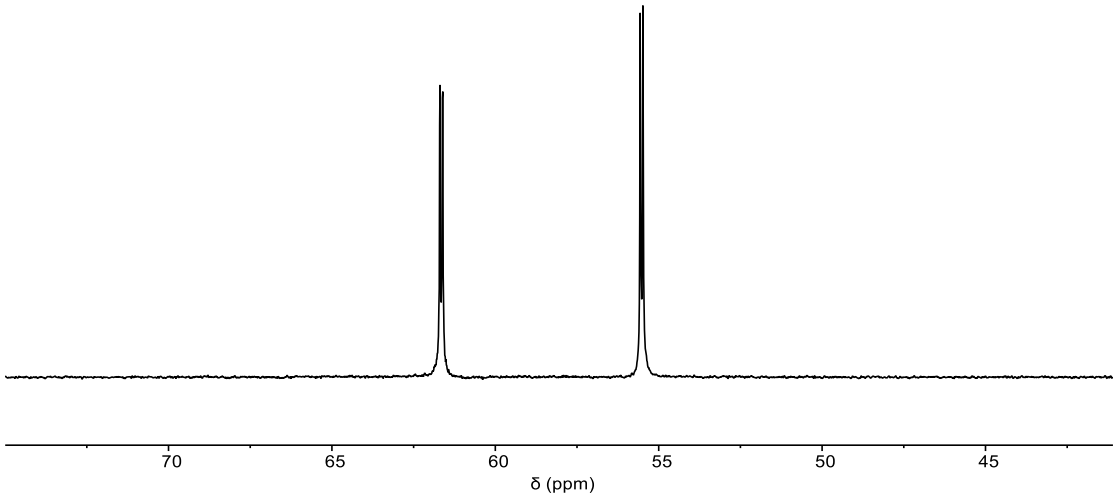

Fig 9. $^{31}P\{^{1}H\}$ NMR spectrum of palladium complex **17** in $CDCl_3$.

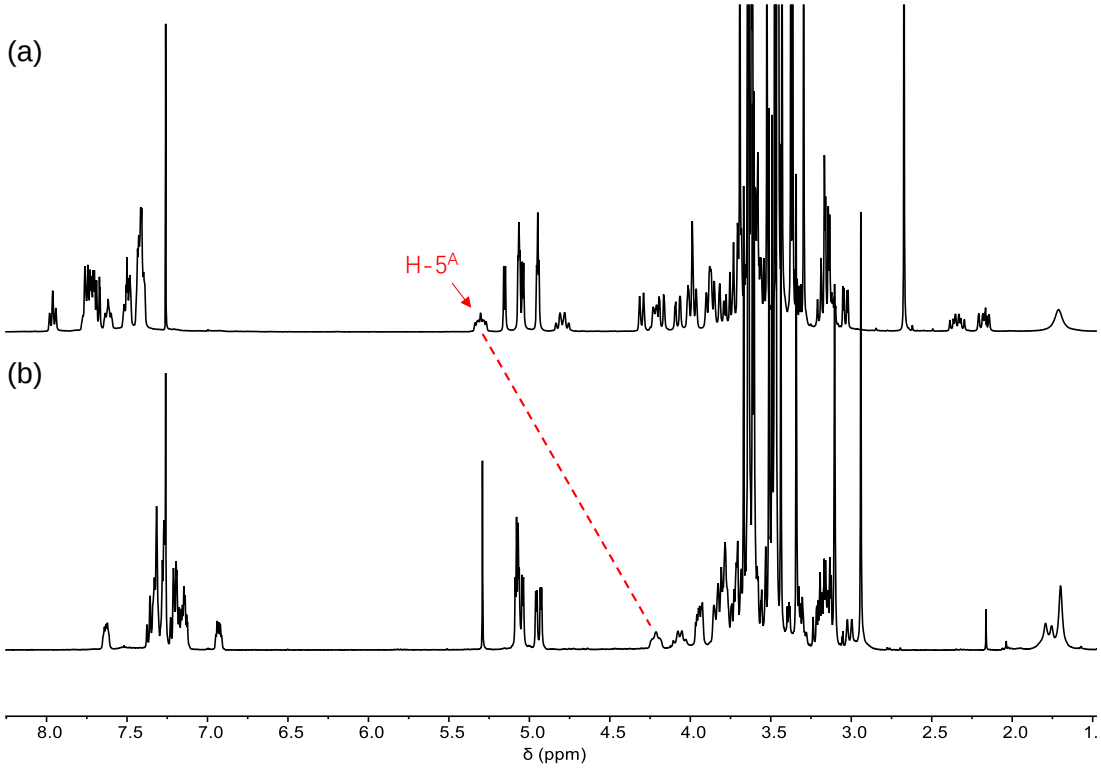

Fig 10. ^{1}H NMR spectra in $CDCl_3$ of: (a) **17**, (b) **L3**.

For references, see page 175.

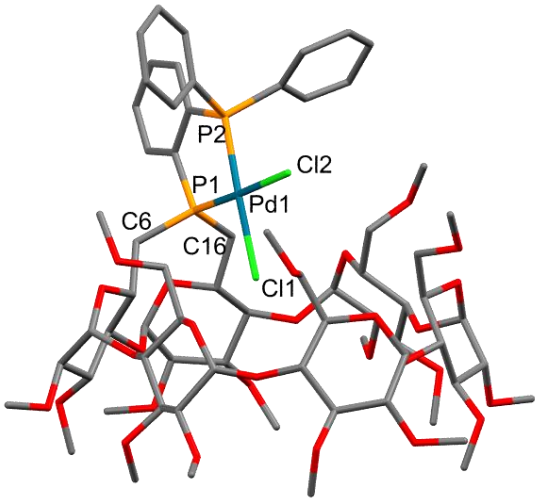

Fig 11a. View of the structure of complex **17a**. Hydrogen atoms and solvent molecules are omitted for clarity. Important bond lengths (Å) and angles (°) for complex **17** which comprises two slightly different structures (**17a** and **17b**) in the unit cell **17a**: P1-Pd1: 2.223 (2), P2-Pd1: 2.224 (2), Pd1-Cl1: 2.3391 (19), Pd1-Cl2: 2.357 (2), C6-P1: 1.837 (9), C16-P1: 1.830 (9), P1-Pd1-P2: 87.18 (7), P1-Pd1-Cl1: 88.46 (8), P1-Pd1-Cl2: 176.03 (10), P2-Pd1-Cl1: 173.19 (8), P2-Pd1-Cl2: 89.89 (8), Cl1-Pd1-Cl2: 94.19 (8), C6-P1-Pd1: 117.8 (3), C16-P1-C6: 113.2 (4), C16-P1-Pd1: 111.3 (3).

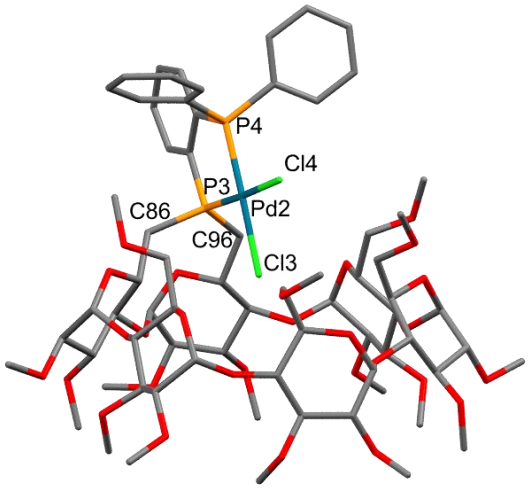

Fig 11b. View of the structure of complex **17b**. Hydrogen atoms and solvent molecules are omitted for clarity. Important bond lengths (Å) and angles (°) for complex **17** which comprises two slightly different structures (**17a** and **17b**) in the unit cell **17b**: P3-Pd2: 2.2187 (18), P4-Pd2: 2.226 (2), Pd2-Cl3: 2.3469 (19), Pd2-Cl4: 2.3481 (19), C86-P3: 1.842 (8), C96-P3: 1.831 (8), P3-Pd2-P4: 87.35 (7), P3-Pd2-Cl3: 88.00 (7), P3-Pd2-Cl4: 177.46 (9), P4-Pd2-Cl3: 175.06 (8), P4-Pd2-Cl4: 90.23 (8), Cl3-Pd2-Cl4: 94.44 (8), C86-P3-Pd2: 114.7 (3), C96-P3-C86: 114.0 (4), C96-P3-Pd2: 113.2 (3).

For references, see page 175.

As shown in Figures 11a and 11b, the crystal structure of complex **17** displays a square planar coordination plane sitting just above the cavity and nearly perpendicular to the O(4) atoms plane of the CD (angle between the $PPMX_2$ unit and O(4) plane is 86.5° and 86.1° for the two CD complexes that are present in the unit cell), a feature that is almost identical to that of d^8 complexes derived from **L1**. However, compared to analogous P,N Pd complex **4** and its bulkier Ni counterpart **6**, the coordination unit, here $PPMCl_2$, is pointing slightly more away from the cavity (angle between the CD O-4 atoms plane and the C6(C86)-P1(P3)-C16(C96) plane is 58.4° on average for **17a**, **17b** *vs.* 50.27° for $PdCl_2$ complex **4** and 54.82° for $NiBr_2$ complex **6**, respectively), probably as a result of the larger size of the PPh_2 unit compared to the NMe_2 group in **L1**. Clearly, the orientation of the bridging P1 atom lone pair is to a certain extent dependent on the size of the nonbridging coordinating group and the MX_2 unit. Again, the phosphorus lone pairs are oriented towards the cavity interior and it is highly likely that the metal center is forced to be located above the cavity by the rigid bridging phosphorus atom P1, the lone pair of which should also be oriented towards the cavity center in ligand **L3** as for the P,N ligand **L1** and the monophosphines **HUGPHOS-1** and **HUGPHOS-2**. As for cavity-shaped P,N complexes, the two halido ligands experience very different steric environments, with one of them located outside the cavity and the other inside. Surprisingly, even if the two P(III) atoms are electronically different, the bridging P(III) atom being more basic than the one in the pendant PAr_3 unit as reflected by the large difference of chemical shifts between the two doublets in the $^{31}P\{^1H\}$ NMR spectrum of **L3** ($\Delta\delta$ = 43.4 ppm), the two Pd-Cl and Pd-P distances in complex **17** are almost identical.

In the same vein, the corresponding PdMeCl isomeric complex **18a**, **18b** were synthesized by treating **L3** with [PdMeCl(COD)] in deoxygenated THF at room temperature. Again, analysis of the crude mixture indicated the presence of only 1:1 ligand/metal complexes, which after purification on standard column chromatography on silica afforded the mixture of complexes **18a**, **18b** in 80% yield. Successful metal complexation was confirmed by the mass spectrum of complexes **18a**, **18b**, which display an intense peal at *m/z* 1635.51, corresponding to the $[M + Na]^+$ cation.

For references, see page 175.

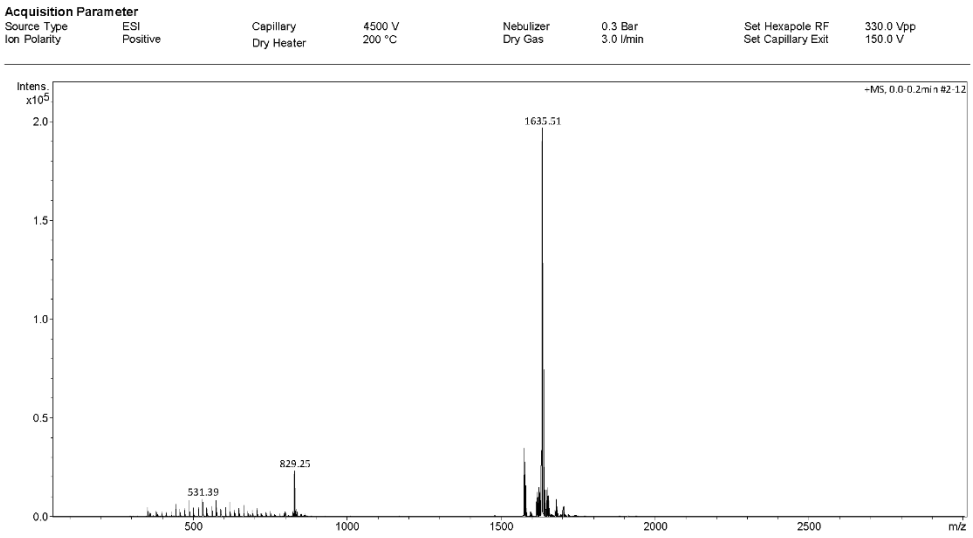

Fig 12. Full ESI-MS spectrum of **18**.

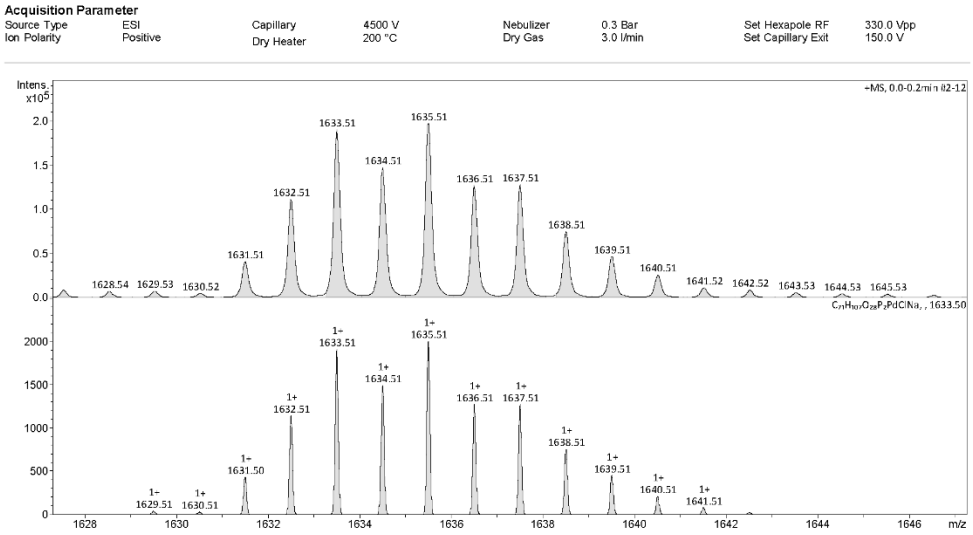

Fig 13. Partial ESI-MS spectrum of **18**.

Careful analysis of the ^{1}H and $^{31}P\{^{1}H\}$ NMR spectra in C_6D_6 of the mixture **18a**, **18b** showed clearly the presence of two different isomers. The $^{31}P\{^{1}H\}$ NMR spectrum comprises two pairs of doublets, each corresponding to one isomer. While for **18a** the two doublets are very close to each other (δ_{31P} = 40.98 and 41.72 ppm with $^{3+2}J_{P,P}$ = 23.6 Hz), the ^{31}P signals in **18b** are much further apart (δ_{31P} = 29.15 and 51.72 ppm with $^{3+2}J_{P,P}$ = 25.7 Hz). The HMQC (^{1}H-^{31}P) experiment (Fig 15) allows us to assign for each compound the more basic bridging phosphorus

For references, see page 175.

atom to the more downfield shifted doublets (41.72 and 51.72 ppm for **18a** and **18b**, respectively).

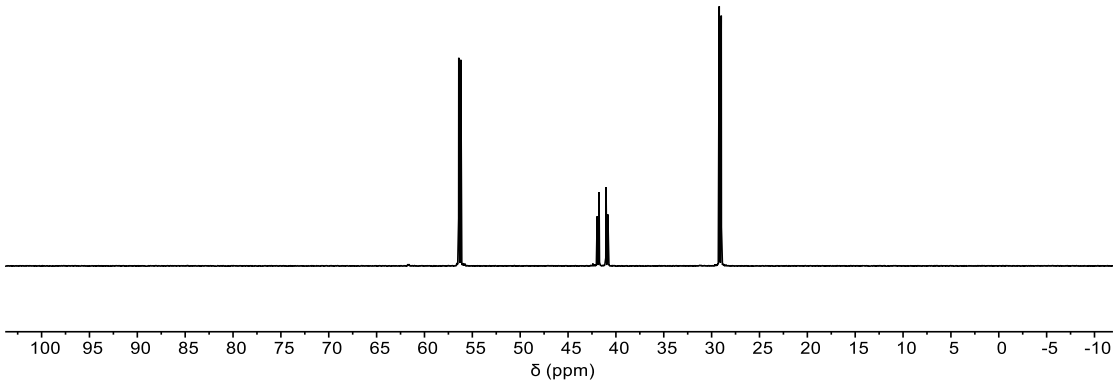

Fig 14. ^{31}P NMR spectrum of the palladium complexes **18a**, **b** in C_6D_6.

Clearly, the PdMeCl complexes **18a**, **b** are *cis*-chelates similar to the $PdCl_2$ analog **17**, but because the two exogeneous ligands (chlorido and methyl) are no longer identical, two different isomers are formed during complexation. The ROESY spectrum of the inseparable mixture **18a**, **b** clearly showed that in the case of **18a**, the Pd-methyl protons correlate strongly with the inner-cavity H-5 protons of several glucose units (Fig 16) and are therefore located in the CD cavity, whereas in the case of **18b**, in which the methyl group is located outside, no such cross-peaks is found. Furthermore, the bridging phosphorus atom in **18b** correlates strongly with the *trans*-disposed palladium-bound methyl protons, whereas the cross-peak was much less intense for the correlation between the same methyl group and the PAr_3 atom, which in **18b** are *cis* to each other. Conversely, in the case of **18a**, the opposite is true in keeping with a methyl group located *trans* to the PAr_3 atom and therefore located inside the CD cavity. This is to be expected because the orbital overlap of the *trans*-disposed methyl group and phosphorus atoms with the metal *d* orbital is much better than when the two donor atoms are *cis* to each other.[14] Indeed, the methyl group in both **18a** and **18b** resonate as a doublet of doublets at δ_{1H} = 1.13 ppm ($^2J_{PtransH}$ = 7.3 Hz and $^2J_{PcisH}$ = 2.5 Hz) and 1.23 ppm ($^2J_{PtransH}$ = 8.7 Hz and $^2J_{PcisH}$ = 3.2 Hz)

For references, see page 175.

with in both cases a much larger coupling constant for the *trans*-arranged P(III) and methyl groups compared to the *cis*-arranged ones. The presence of a very downfield shifted H-5 signal (δ_{1H} = 5.31ppm) belonging to one of the capped glucose units is another proof for the presence of the chlorido ligand inside the CD cavity in **18b**. No such downfield shift was observed upon metal complexation for **18a**, which has its methyl ligand included in the cavity. The ^{1}H NMR spectrum recorded in CD_2Cl_2 indicates that these two isomers are present in a *ca.* 23:77 ratio of **18a**/**18b** at room temperature.

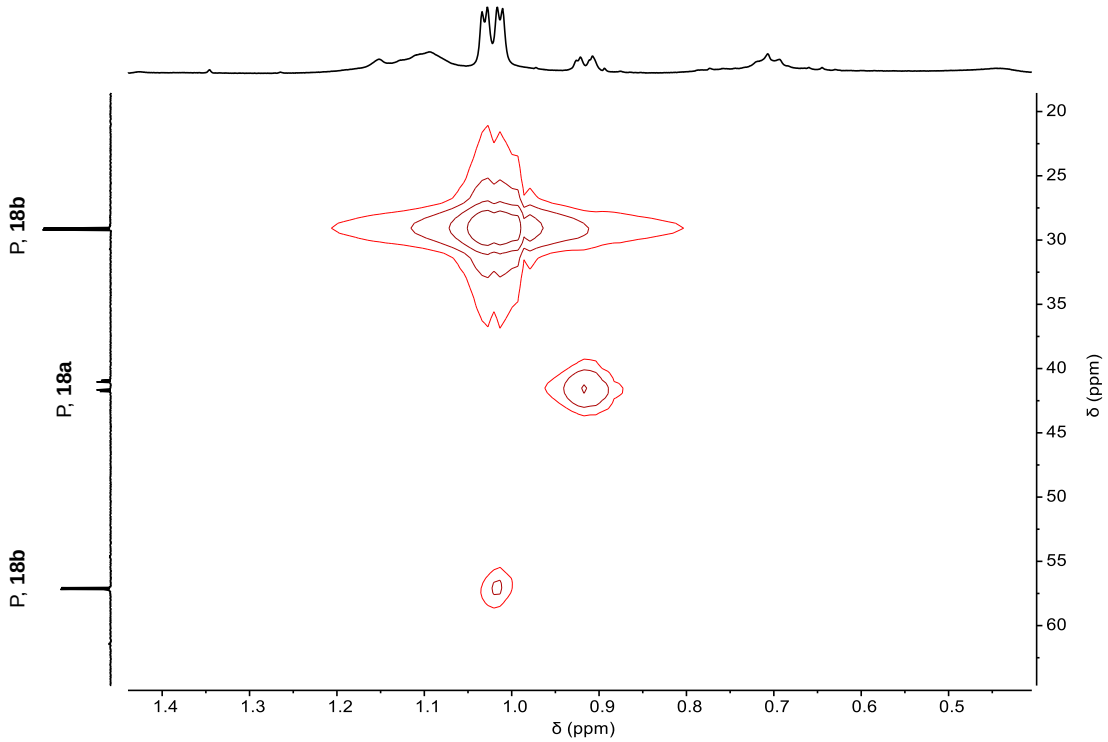

Fig 15. Part of the HMQC (^{1}H-^{31}P) spectrum of the mixture **18a**, **b** revealing the correlations between Pd-Me protons and the phosphorus atoms.

For references, see page 175.

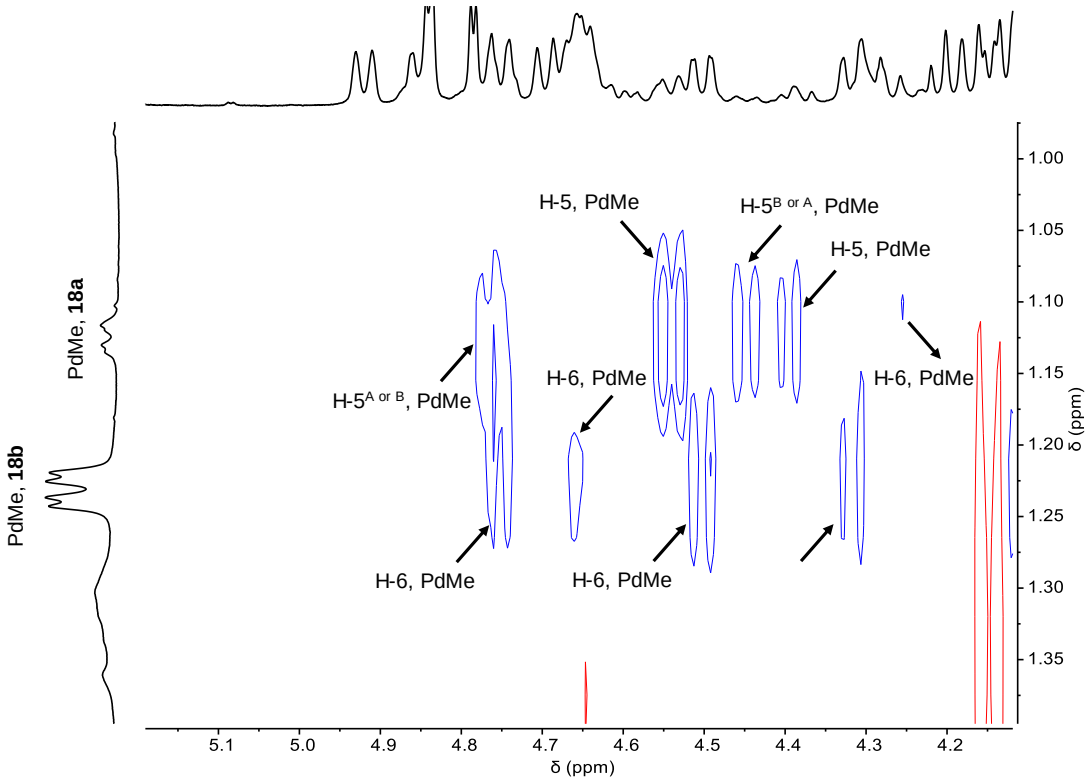

Fig 16. Part of the ROESY spectrum of the **18a**, **b** mixture revealing cross-peaks corresponding to correlations between Pd-Me protons of **18a** and the CD internal H-5 protons as well as correlations between Pd-Me protons of **18b** and CD external H-6 protons.

Bearing in mind that the reaction temperature could affect this isomeric ratio,[15] the complexation was then conducted in the same solvent (THF) at low temperature (-78 °C). However, no change of isomeric ratio was observed at this temperature. Changing the solvent (C_6D_6 to CD_2Cl_2) in which the NMR spectra was recorded did not change the isomeric ratio either. Surprisingly, the **18a**/**18b** ratio varied upon changing the solvent in which the complexation was carried out. When CH_2Cl_2 instead of THF was used as reaction solvent, **18a** was found to become the major isomer and the **18a**/**18b** ratio increased slightly at low temperature (**18a**/**18b** = 68:32 and 80:20 for room temperature and -78 °C, respectively). Moreover, in order to find out whether an equilibrium occurs between isomers **18a** and **18b**, three different reaction mixtures obtained in CH_2Cl_2 at either 25 °C or -78 °C and in THF were analyzed by NMR spectroscopy over a prolonged period of time. The ^{1}H and $^{31}P\{^{1}H\}$ NMR spectra recorded in CD_2Cl_2 showed that the isomeric ratio for both samples left in CD_2Cl_2 solution for up to 7 days did not change, thus indicating the absence of an equilibrium, at least at room temperature. Clearly, these results show that the formation of **18b** is kinetically more favorable than that of **18a**, but the reason why one is formed faster than the other is debatable,

For references, see page 175.

since it is difficult to figure out which factors – electronic or steric – are dominant here given the complexity of the ligand and the small differences of energy at stake.

The Ni(II) complex **19** was also prepared in 86% yield by treating **L3** with [$NiBr_2$(DME)] in deoxygenated CH_2Cl_2. Upon subjecting the reaction mixture to standard column chromatography on silica, it was found that partial halide exchange took place during the purification resulting in the formation of a mixture of $NiBr_2$, $NiCl_2$ and NiBrCl species. This unwanted reaction was clearly identified by $^{31}P\{^1H\}$ NMR spectroscopy. The chloride necessary for the exchange most probably originated from the chlorinated solvent used for the purification (CH_2Cl_2) or from chloride-contaminated silica. To recover pure **19**, the mixture of halide complexes was treated with LiBr in MeOH at room temperature for 2 h.

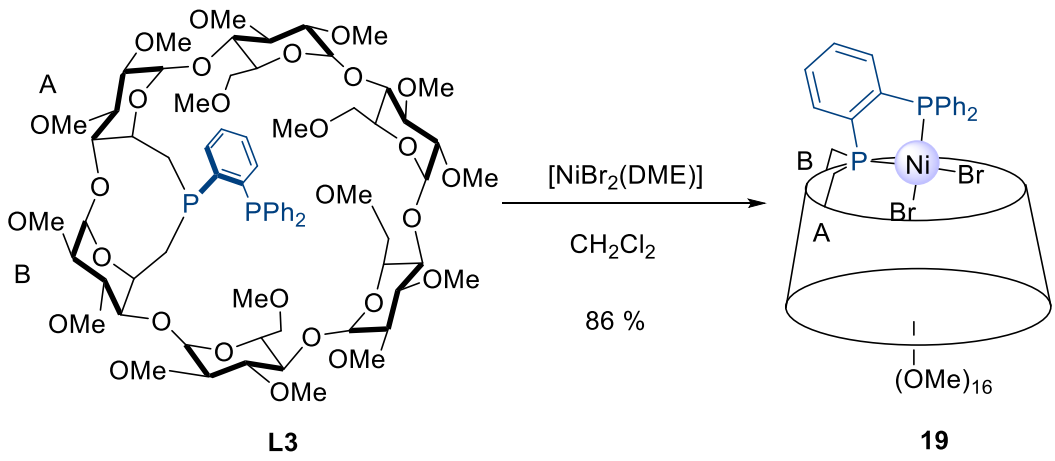

Scheme 7. Synthesis of Ni(II) complex **19** derived from **L3**.

For references, see page 175.

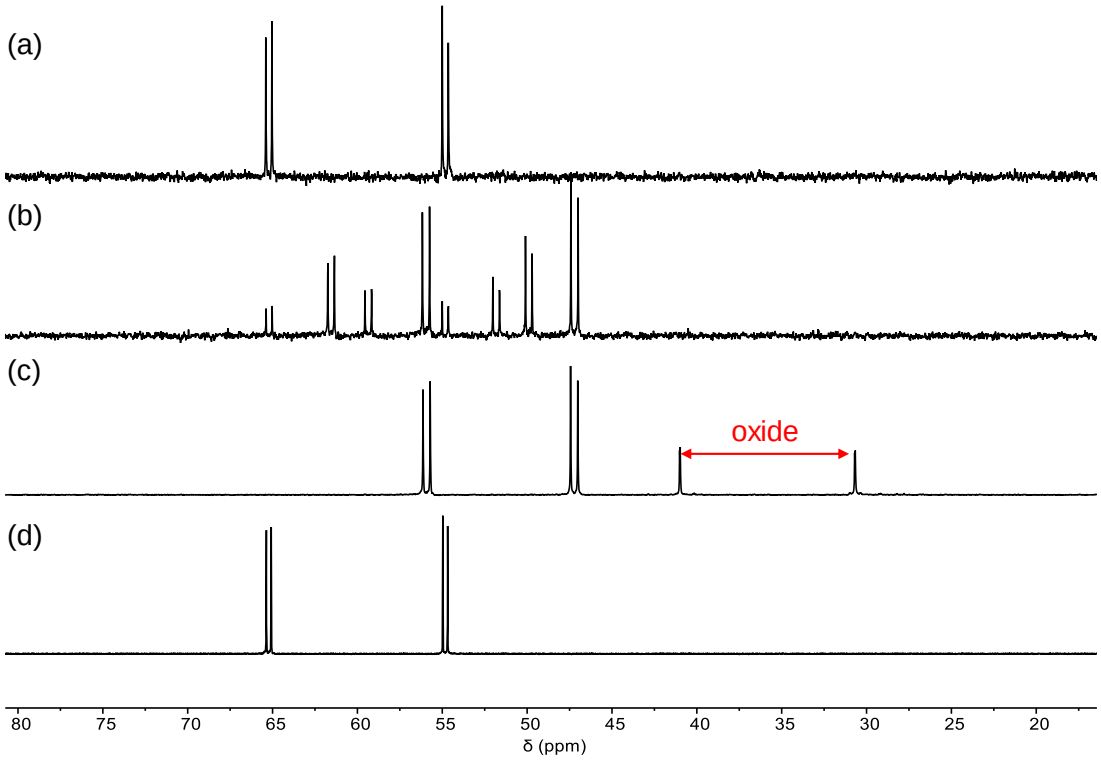

Fig 17. $^{31}P\{^{1}H\}$ NMR spectra in C_6D_6 of: (a) reaction mixture, (b) mixture of complexes after column chromatography, (c) $NiCl_2$ complex, (d) pure **19** obtained after treatment with LiBr.

The $^{31}P\{^{1}H\}$ NMR spectrum also displays downfield-shifted doublets compared to the free ligand (54.83 and 65.22 ppm with a P-P coupling constant $^{3+2}J_{P,P}$ = 57.9 Hz). No single crystal suitable for X-ray diffraction could be obtained, but the ^{1}H and $^{31}P\{^{1}H\}$ NMR spectra of complex **19**, unlike those of the P,N complex **6**, comprises sharp signals and similar features to its $PdCl_2$ analog, indicating that both complexes are diamagnetic with a square planar coordination geometry, with one of the two bromido ligands located inside the CD hollow as revealed again by a downfield-shifted inner-cavity H-5 proton (δ_{1H} of H-5 = 5.21 ppm) (Fig 19), the other pointing outside.

For references, see page 175.

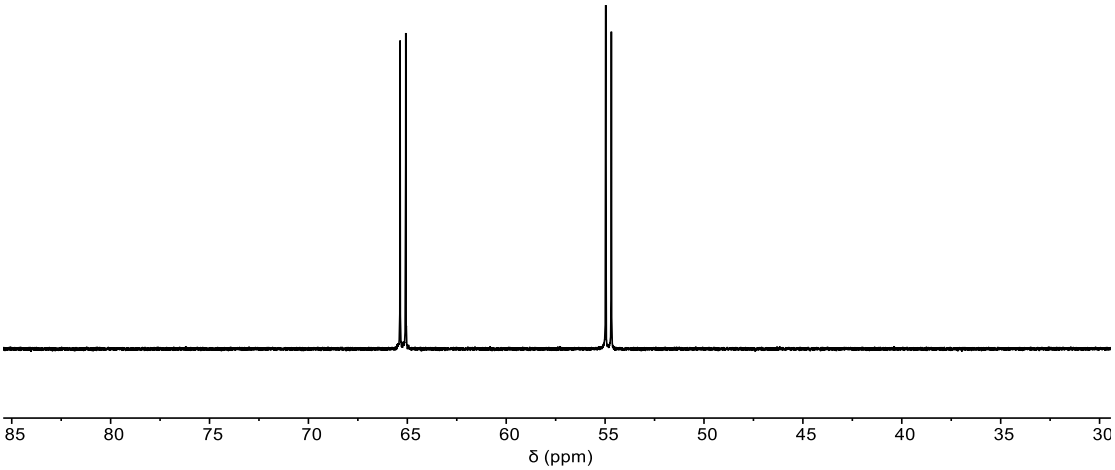

Fig 18. ^{31}P NMR spectrum of the nickel complex **19** in C_6D_6.

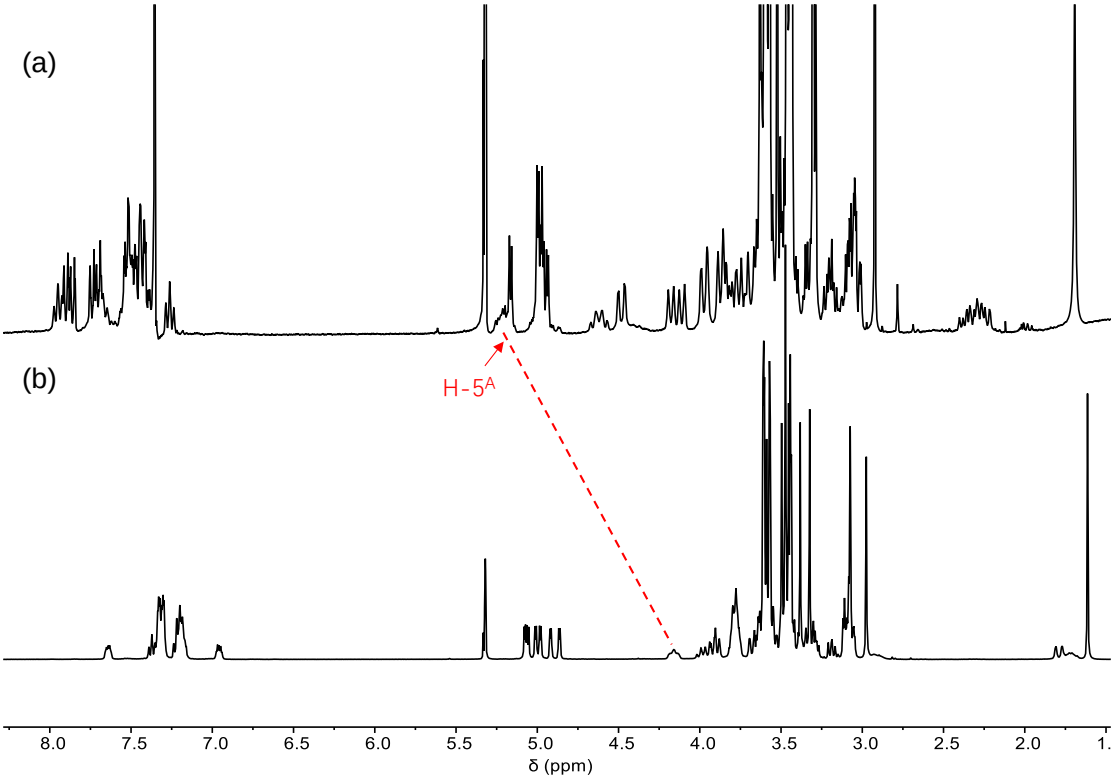

Fig 19. ^{1}H NMR spectra in CD_2Cl_2 of: (a) **19**, (b) **L3**.

For references, see page 175.

III. 2. 2. 2. Synthesis of metal complexes derived from DEXPHOS (L4)

d^8 Complexes based on the second diphosphine ligand **L4** were also prepared. As for P,N ligand **L1** and diphosphine ligand **L3**, **L4** produced only 1:1 ligand/metal complexes. Thus, $[PdCl_2(COD)]$ was reacted with **L4** in deoxygenated CH_2Cl_2 to give the palladium complex **20** in 77% yield.

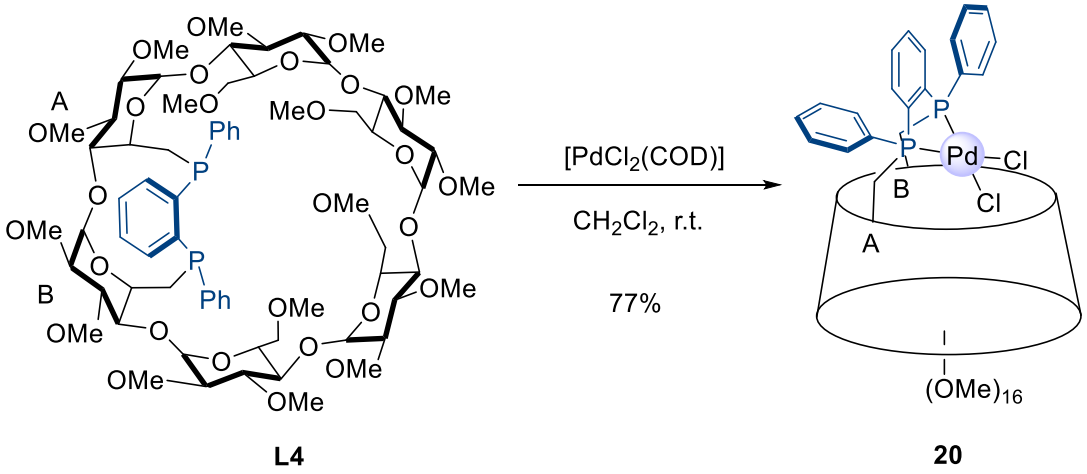

Scheme 8. Synthesis of the Pd(II) complex **20** derived from **L4**.

Again, the $^{31}P\{^1H\}$ NMR spectrum displays signals lying in the expected range, with both doublets significantly downfield shifted compared to those of the free ligand **L4** (62.39 and 68.99 ppm with a P–P coupling constant $^{3+2}J_{P,P}$ = 9.3 Hz).

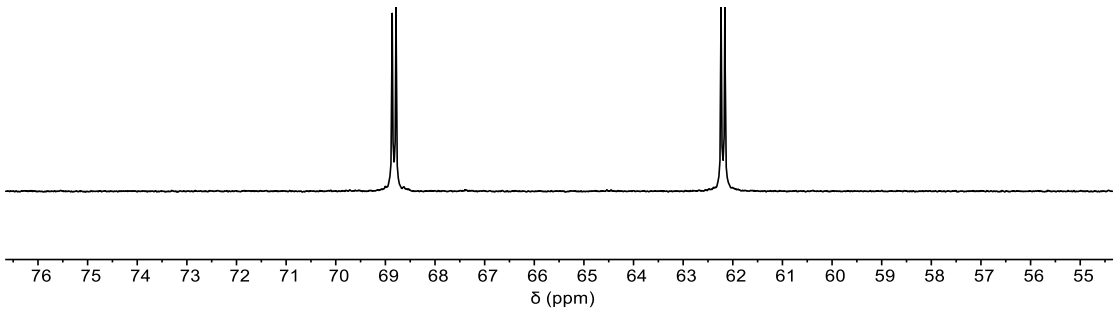

Fig 20. ^{31}P NMR spectrum of the palladium complex **20** in $CDCl_3$.

For references, see page 175.

The signals of the ^{1}H NMR spectrum of **20** (Fig 21) are sharp, indicating as expected that this square planar palladium complex is diamagnetic. As indicated in Fig 21, both H-5 protons of the two bridged glucose units A and B are downfield shifted, but not as much as in the $PdCl_2$ complex derived from **L3** (**17**) ($\Delta\delta_{H\text{-}5A}$ = 0.48 *vs* 1.07 ppm for **20** and **17**, respectively). This shows that none of the two chlorido ligands is as deeply encapsulated in the cavity as one of the chlorido ligands of **17**. Clearly, the $PdCl_2$ unit experiences a radically different environment within **17** and **20** even if these two complexes are equipped with the same α-CD cavity.

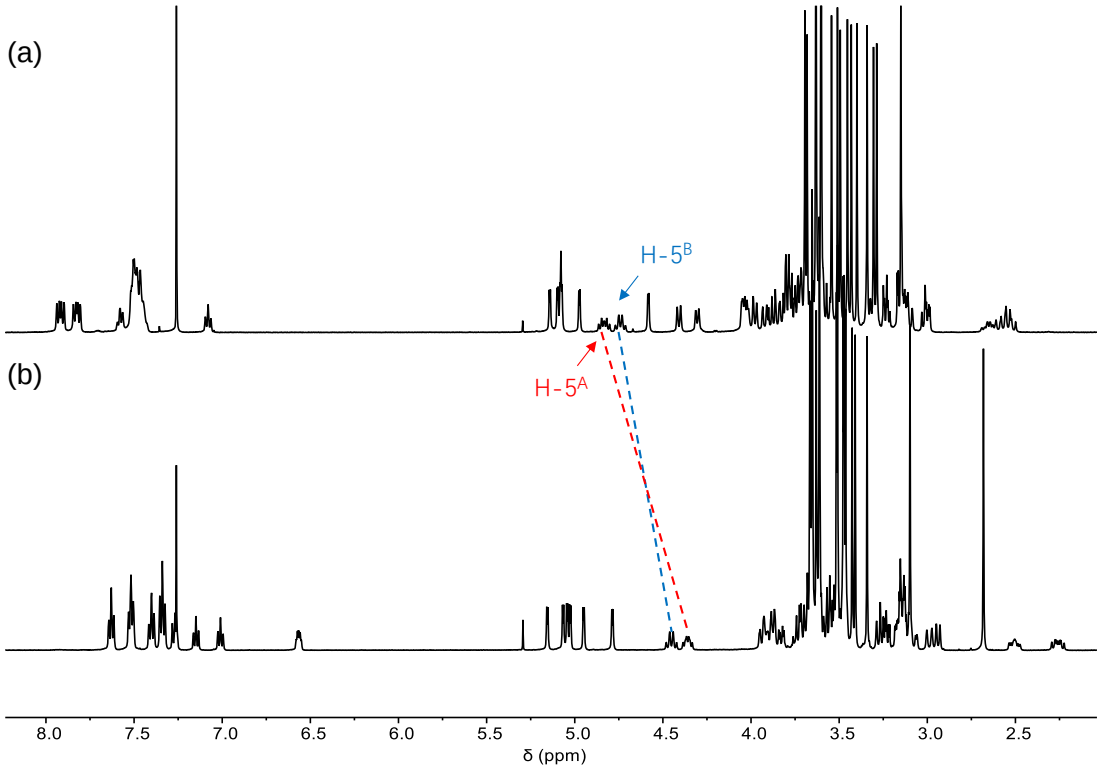

Fig 21. ^{1}H NMR spectra in $CDCl_3$ of: (a) **20**, (b) **L4**.

Single crystals of the $PdCl_2$ chelate complex **20** could be obtained by slow diffusion of *n*-pentane into a solution of **20** in CH_2Cl_2. The X-ray crystal structure of **20** is depicted below in Fig 22.

For references, see page 175.

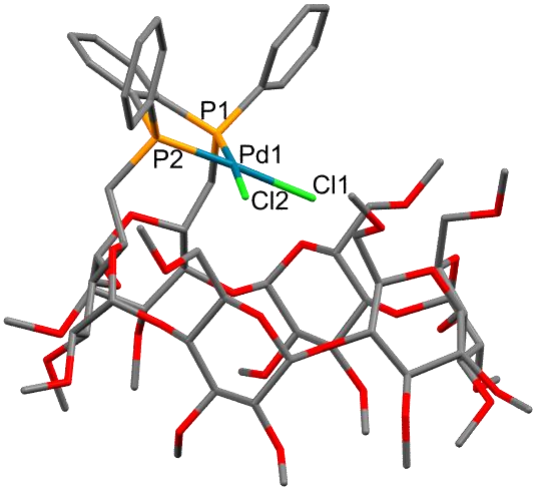

Fig 22. View of the crystal structure of complex **20**. Hydrogen atoms and solvent molecules are omitted for clarity. Important bond lengths (Å) and angles (°) for complex **4**: P1-Pd1: 2.224 (3), P2-Pd1: 2.217 (3), Pd1-Cl1: 2.342 (3), Pd1-Cl2: 2.335 (3), P1-Pd1-P2 : 86.83 (10), P1-Pd1-Cl1 : 90.42 (10), P1-Pd1-Cl2 : 175.77 (10), P2-Pd1-Cl1 : 175.79 (11), P2-Pd1-Cl2 : 88.93 (10), Cl1-Pd1-Cl2 : 93.82 (11).

The X-ray crystal structure shows that the palladium complex **20** has a typical square planar geometry in keeping with the NMR measurements (see above). Despite the fact that the two palladium complexes **17** and **20** are both *cis*-chelate complexes and a similar geometry, the way the $PdCl_2$ unit is located in the cavity is quite different both in the solid state and in solution (see above). Whereas the five-membered chelate ring is almost perpendicular to the macrocyclic moiety in **17**, the angle between the $PPPdCl_2$ and the O(4) atoms plane in **20** is only 21.45°, thus making the chelate unit only slightly tilted towards the cavity center and the metal center less protected by the CD hollow, in particular at the metal axial positions. Furthermore, it is clear that the two chlorido ligands, unlike those in **17**, no longer experience very different steric environments and are almost equivalent.

The PdMeCl analog **21** was also prepared in 61% yield by reaction of **L4** with [PdMeCl(COD)] in THF.

For references, see page 175.

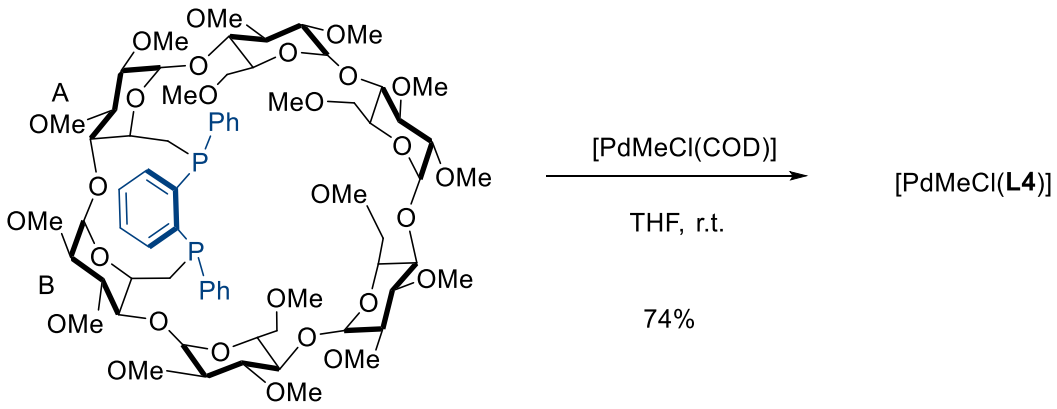

Scheme 9. Synthesis of the PdMeCl complex **21** derived from **L4**.

The reaction mixture was purified by standard column chromatography through silica and first characterized by ESI-MS. The mass spectrum shows an intense peak at *m/z* 1575.55, corresponding to the $[M–Cl]^+$ cation.

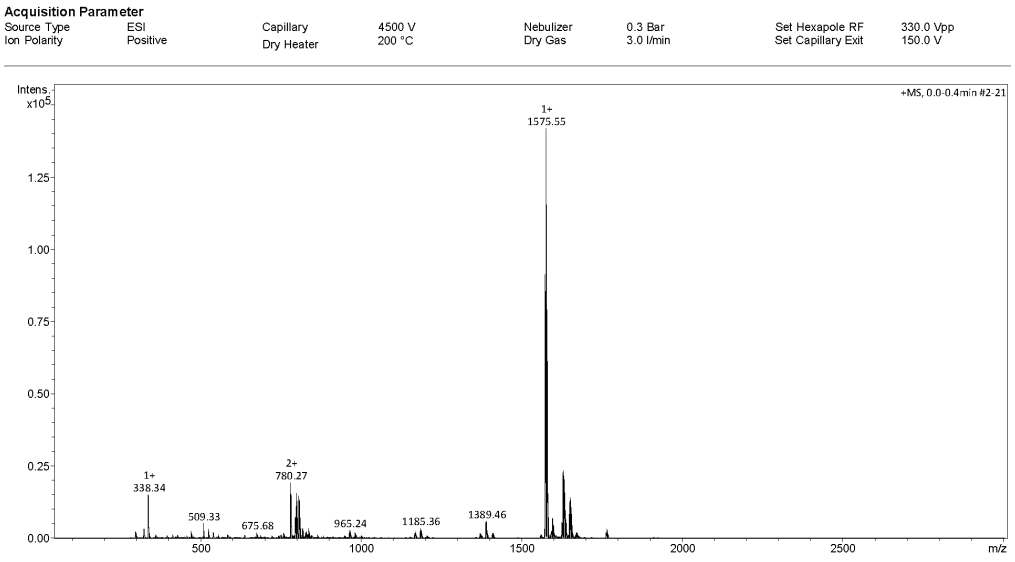

Fig 23. Full ESI-MS spectrum of **21**.

For references, see page 175.

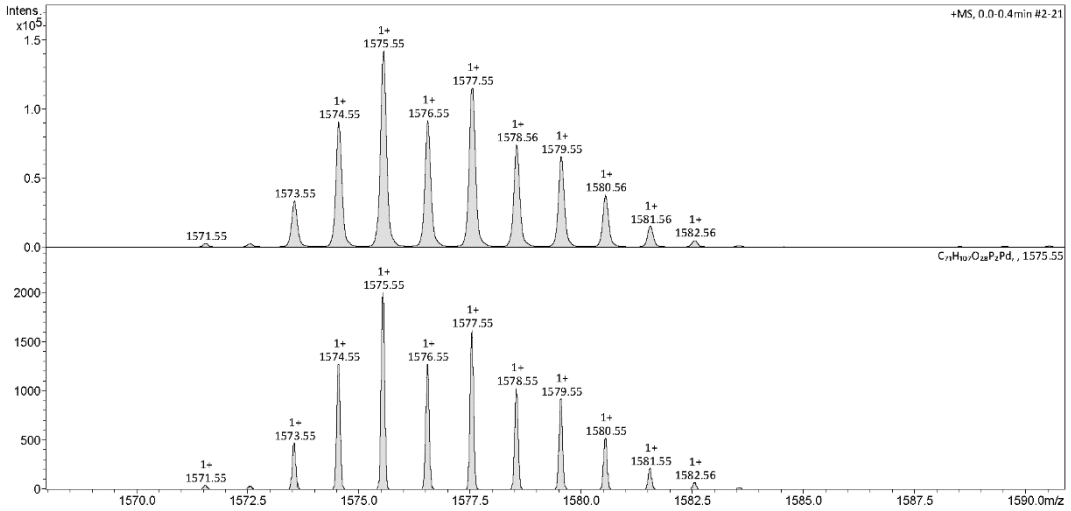

Fig 24. Partial ESI-MS spectrum of **21**.

As for the PdMeCl complexes of **L3**, the NMR spectra of **21** revealed the presence of two different geometrical isomers (**21a** and **21b**) in a 60:40 mixture. For each compound, the two phosphorus atoms resonate as a pair of doublets in the $^{31}P\{^{1}H\}$ NMR spectrum of the mixture (δ_{31P} = 41.76, 54.48 ppm with $^{3+2}J_{P,P}$ = 25.9 Hz for the major isomer and δ_{31P} = 34.63, 63.75 ppm with $^{3+2}J_{P,P}$ = 26.6 Hz for the minor one). Given the complexity of the NMR spectra of the mixture **21a**, **b**, full assignment of protons belonging to isomers **21a** and **21b** could not be achieved and the exact position of the methyl group within the cavity in both isomers could not be determined. However, the ^{1}H-^{31}P HMQC spectrum, as for **18a**, **18b**, shows clearly that the phosphorus atom belonging to one of the bridged unit in either **21a** or **21b** correlates strongly with the *trans*-disposed palladium-bound methyl protons, whereas the cross-peaks are much less intense for correlations between the same methyl group and the second P(III) atom, which is *cis* to the methyl group in both **21a** and **21b**. This methyl group resonates as a doublet of doublet at δ_{1H} = 0.39 ppm ($^{2}J_{P\mathit{trans}H}$ = 8.3 Hz and $^{2}J_{P\mathit{cis}H}$ = 3.9 Hz) for **21a** and 0.47 ppm ($^{2}J_{P\mathit{trans}H}$ = 8.5 Hz and $^{2}J_{P\mathit{cis}H}$ = 3.4 Hz) for **21b** with in both cases a much larger coupling constant for the *trans*-arranged P(III) and methyl groups compared to the *cis*-arranged ones. The localization of the methyl group within the cavity in both complexes should also have been achievable with a ROESY experiment provided all inner-cavity H-5 protons are fully assigned at least for one of the geometrical isomers. Unfortunately, again the complexity of the different NMR spectra and overlaping signals prevented an assignment of the CD H-5 protons.

For references, see page 175.

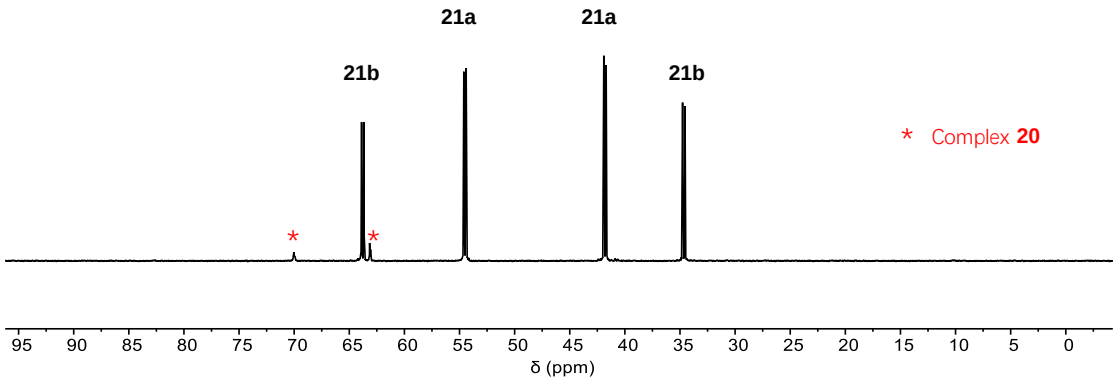

Fig 25. $^{31}P\{^{1}H\}$ NMR spectrum of palladium complexes **21a**, **b** in CD_2Cl_2.

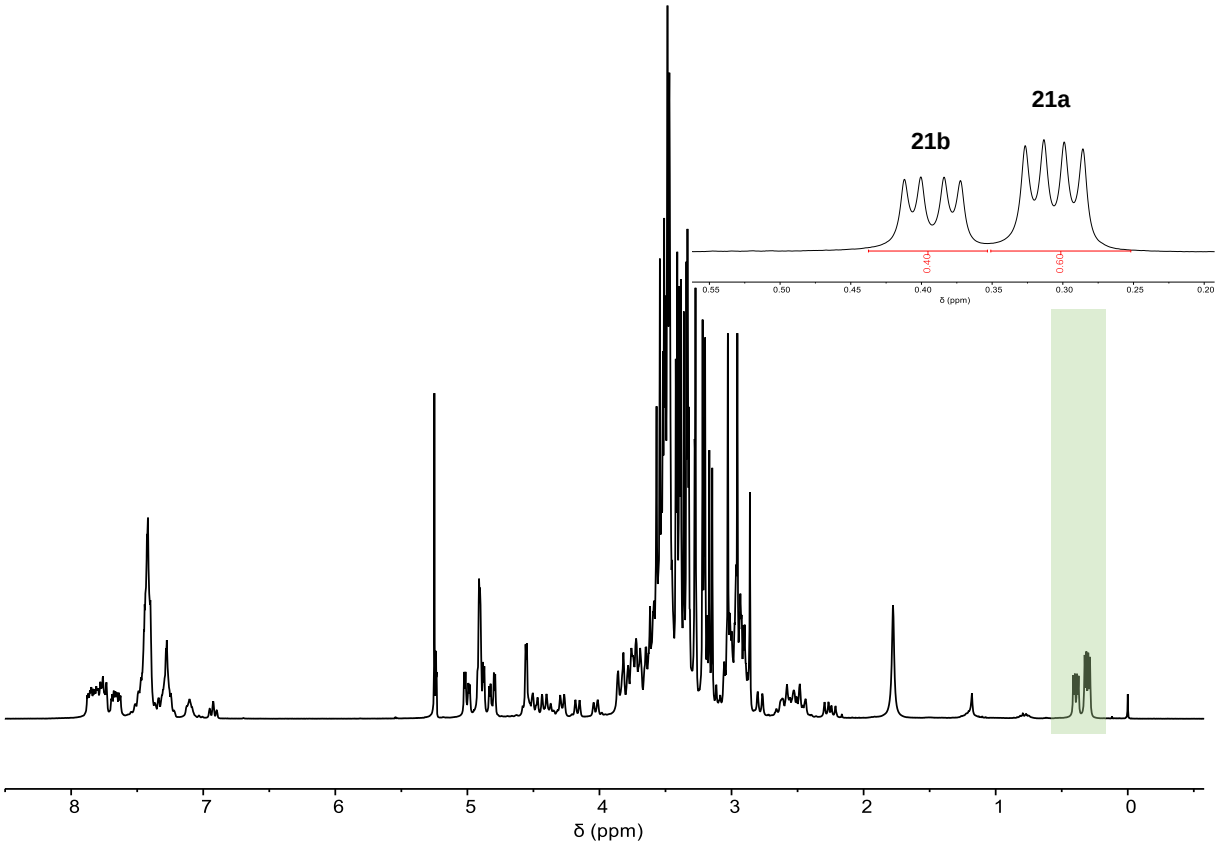

Fig 26. ^{1}H NMR spectra of complexes **21a**, **b** in CD_2Cl_2.

For references, see page 175.

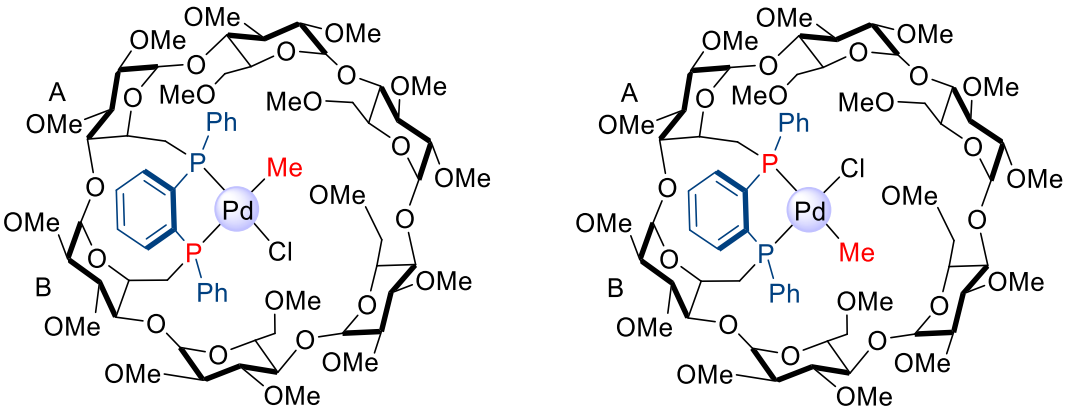

Fig 27. Structures of two geometrical isomers of **21a**, **21b**

Single crystals suitable for X-ray diffraction analysis were obtained by slow diffusion of *n*-pentane into a solution of **21a**, **b** in dichloromethane. Both geometrical isomers **21a** and **21b** are present in a 7:3 ratio respectively in the single crystal. Only the molecular structure of the major one (**21a**) is depicted below. The single crystals used for X-ray diffraction analysis were redissolved in CD_2Cl_2 and the NMR spectra quickly measured. The same **21a**/**21b** ratio (7:3) as that found previously in CD_2Cl_2 solution was measured. It is therefore possible that **21a** is also the major isomer in CD_2Cl_2 solution. However, this hypothesis should be taken with caution since isomeric ratios can vary on going from the solid state to the solution state in particular if the two isomers are in equilibrium.

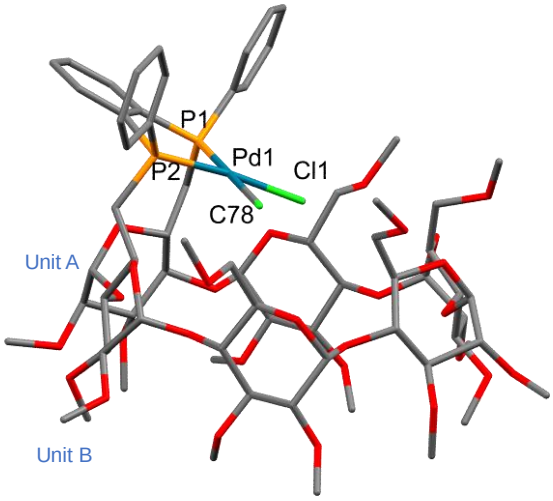

Fig 28. View of the X-ray crystal structure of complex (70:30 disorder, 70% Cl1 C78 (**21a**), 30% Cl1A C78A (**21b**). The atoms C78/Cl1A and C78A/Cl1 are positioned at the same place.

For references, see page 175.

The distances Pd-Cl1/Pd-C78 and Pd-Cl1A/Pd-C78A are therefore averages). Hydrogen atoms and solvent molecules are omitted for clarity. Important bond lengths (Å) and angles (°) for complex **4**: Pd1-P1: 2.282 (4), Pd1-P2: 2.237 (3), Pd1-Cl1: 2.294 (4), Pd1-Cl1A: 2.238 (7), P2-Pd1-P1: 86.45 (11), P1-Pd1-Cl1: 95.4 (2), P2-Pd1-Cl1: 174.34 (16), P2-Pd1-Cl1A: 93.6 (3), P1-Pd1-Cl1A: 179.8 (2), Cl1-Pd1-Cl1A: 84.5 (3).

The X-ray crystal structure of **21a**, **21b** clearly shows a square planar cis-chelate complex as in its $PdCl_2$ analog **20**. The angle between the $PPPdL_2$ plane and the CD O(4) atoms plane is 21.76°, a value almost identical to that observed in **20**. These two complexes experience therefore a very similar steric environment within the CD cavity. Unsurprisingly, the two Pd-Cl/Me and two P-Pd bonds have different bond lengths (Δd = 0.056 and 0.045 Å, respectively), unlike the $PdCl_2$ complexes **17** and **19**.

As in the case of **L3**, the metal complexation was conducted in different solvents and at different temperatures. Again, the same proportion of two isomers (60:40) was found when the reaction was carried out in THF at either room temperature or at low temperature (-78 °C), but the ratios turned out to be 47:53 and 42:58 when the reaction was conducted in CH_2Cl_2 at room temperature and at -78 °C, respectively. The three samples which had after metal complexation different isomeric ratios were analyzed by NMR spectroscopy over a prolonged period of time (1, 3 and 7 days). Unlike the geometrical isomers **18a**, **18b**, the proportion of **21a** and **21b** gradually changed (Table 1) with time before finally reaching a constant value close to 20:80. Clearly, in this case the two geometrical isomers are in equilibrium in stark contrast with **18a**, **18b**. This is hardly surprising given the fact that the two phosphorus donor atoms are electronically equivalent and the two exogeneous ligands experience very similar steric environments within the CD cavity.

Table 1. Isomeric ratios of **21a** and **21b** observed over a prolonged period of time at 25 °C.

Sample	Isomeric ratios of **21a** and **21b**			
	start	1 day	3 days	7 days
1 (THF, 25 °C)	60:40	60:40	55:45	22:78
2 (CH_2Cl_2, 25 °C)	47:53	47:53	45:55	22:78
3 (CH_2Cl_2, -78 °C)	42:58	42:58	35:65	22:78

For references, see page 175.

The nickel complex with ligand **L4** (**22**) was also synthesized and, like diphosphine analog **19** but not the P,N complex **6**, was sufficiently stable to be purified by standard column chromatography. As observed for **19**, halido exchange occurred during purification by column chromatography on silica, and as for **19** the chlorido species were converted back to the dibromido complex by stirring the mixture with LiBr in MeOH for 2 h at room temperature. The pure $NiBr_2$ complex was then characterized by NMR. The $^{31}P\{^{1}H\}$ NMR spectrum comprises two downfield-shifted doublets at 62.34 and 72.80 ppm with a $^{2}J_{P,\,P}$ coupling constant of 58.5 Hz.

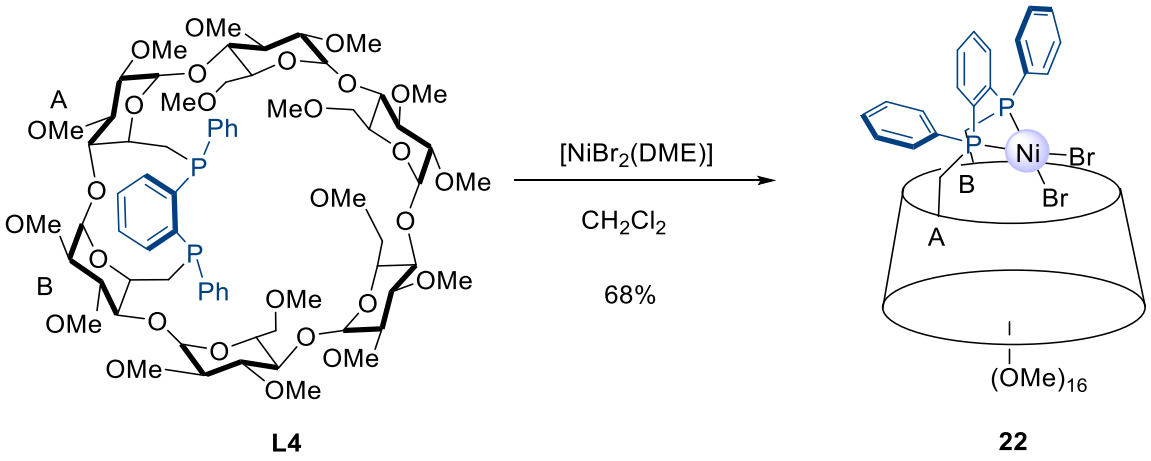

Scheme 10. Synthesis of the Ni(II) complex **22** derived from **L4**.

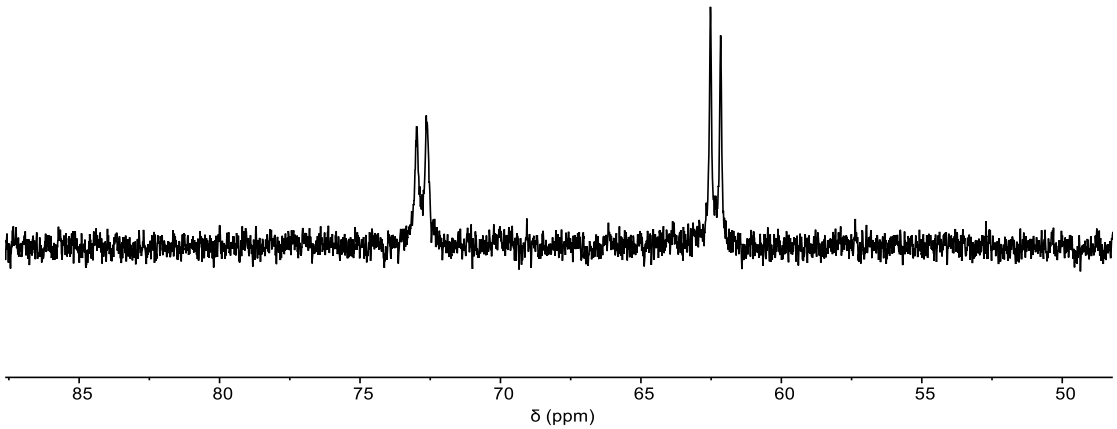

Fig 29. ^{31}P NMR spectrum of the nickel complex **22** in CD_2Cl_2.

For references, see page 175.

The fact that this compound displays sharp NMR signals is a clear indication for its diamagnetic character in keeping with a square planar geometry. This feature was confirmed by a X-ray single crystal diffraction study. Single crystals could be obtained by slow diffusion of *n*-pentane into a solution of **22** in benzene.

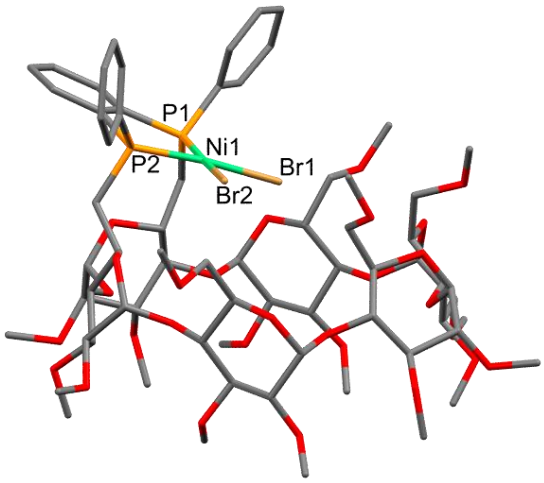

Fig 30. View of the X-ray crystal structure of complex **22**. Hydrogen atoms and solvent molecules are omitted for clarity. Important bond lengths (Å) and angles (°) for complex **22**: P1-Ni1: 2.1372 (6), P2-Ni1: 2.1348 (6), Ni1-Br1: 2.3291 (4), Ni1-Br2: 2.3098 (4), P1-Ni1-P2: 87.75 (2), P1-Ni1-Br1: 88.202 (18), P1-Ni1-Br2: 174.91 (2), P2-Ni1-Br1: 172.83 (2), P2-Ni1-Br2: 88.987 (19), Br1-Ni1-Br2: 95.438 (12).

The molecular structure of **22** is very similar to that of its palladium analog, with the $PPMX_2$ plane however even more parallel to the CD O(4) atoms plane than in the Pd complexes **20**, **21a** and **21b** (angle between the $PPNiBr_2$ and the CD O(4) atoms is 17.27°). This is to be expected because of the great repulsion between the bulkier $NiBr_2$ unit and the CD torus. As for P,N complexes, all X-ray crystal structures of the above diphosphine complexes display an undistorted, circular CD unit with all glucose units adopting the standard $^4C_1$ conformation.
For comparison purpose, cavity-free diphosphine **L5** was also prepared according to a literature procedure[16] and then used for Ni complexation. The resulting nickel complex (**23**) was fully characterized (see Experimental Part). The commercially available nickel complex $[NiBr_2(DPPE)]$ (**24**) was used for the same reason.

For references, see page 175.

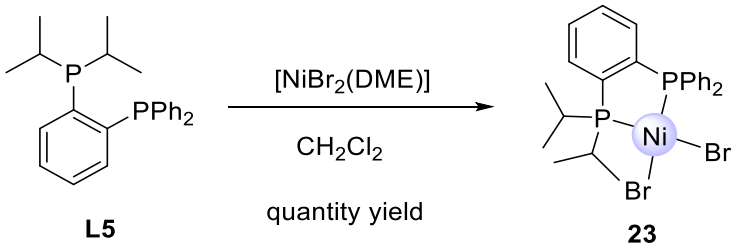

Scheme 11. The synthesis of the nickel(II) complex **23** derived from **L5**.

UV-vis spectra (Fig 32 and 33) were recorded to evaluate the impact of the cavity on the electronic properties of the different diphosphine Ni(II) and Pd(II) complexes as for the P,N complexes.

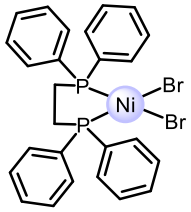

Fig 31. Structure of the nickel(II) complex **24**.

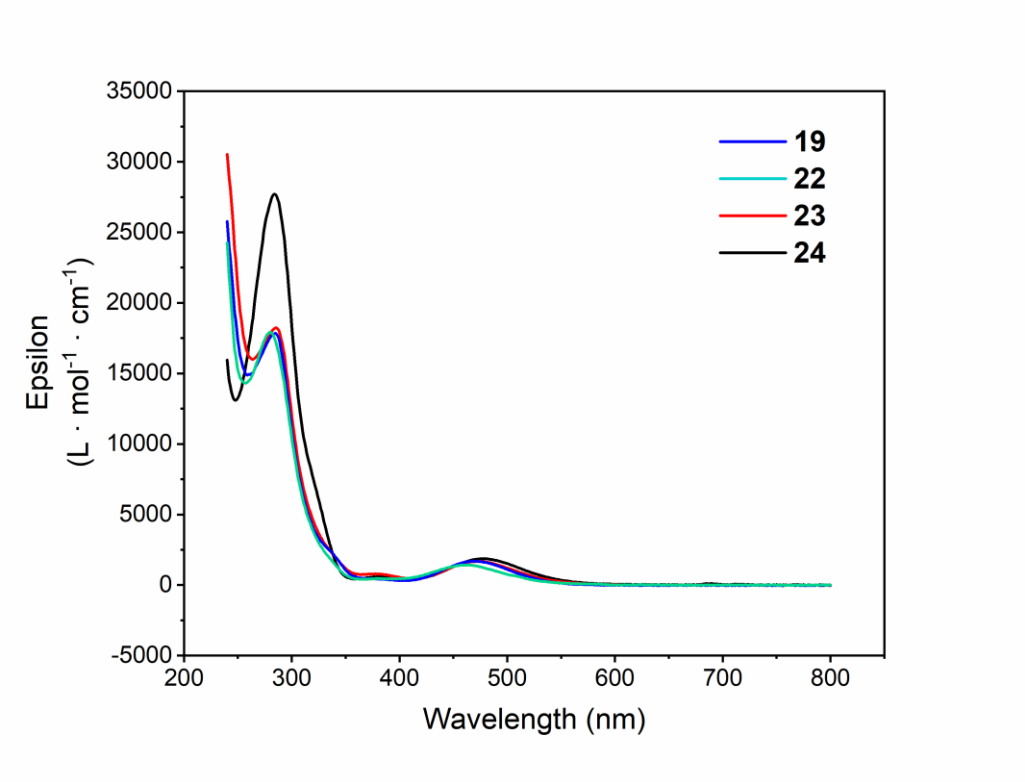

Fig 32. UV-vis spectra of nickel complexes **19** and **22-24**.

For references, see page 175.

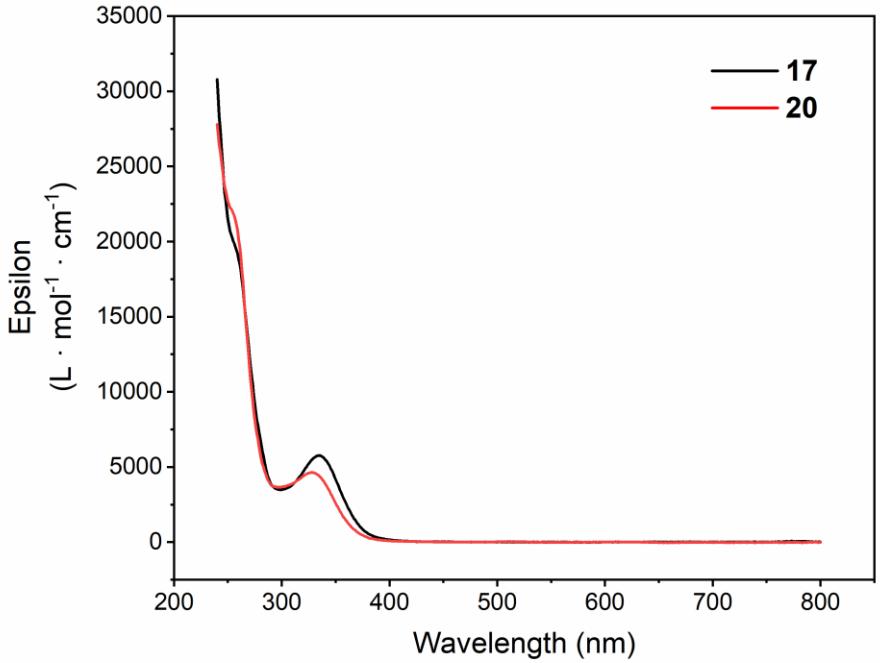

Fig 33. UV-vis spectra of palladium complexes **17** and **20**.

Table 2. UV-vis maximum absorption wavelength and band assignments for Ni(II) and Pd(II) complexes.

Peaks	**19**	**22**	**23**	**24**	**17**	**20**
MLCT transition (nm)	280	285	285	284	335	328
d-d transition (nm)	464	469	473	474	-	-

The assignments of these spectra are shown in Table 2. In this case, the presence of the CD torus has little influence on the complexes electronic properties.

III. 3. Conclusion

In conclusion, CD-based diphosphines **L3** and **L4** were prepared according to procedures developed before in our group. These two ligands were then used to synthesize Pd(II) and Ni(II) complexes. All of the complexes are 1:1 ligand/metal *cis*-chelates, but the structures of these complexes are quite different depending on the diphosphine used, as revealed by several single crystal X-ray diffraction studies. Complexes derived from **L3** have structures very similar to those with the P,N bidentate ligand **L1**. The five-membered chelate ring is nearly

For references, see page 175.

orthogonal to the macrocyclic structure, and the axial positions of the metal center are well-protected by the CD 6-OMe groups with the two exogeneous ligands sterically differentiated. Conversely, the chelate ring is nearly parallel to the macrocyclic structure in the case of complexes based on **L4**. The axial positions of the metal center, which is located slightly above the CD cavity, are no longer protected and the two exogeneous ligands are pretty much equivalent. Furthermore, the proportion of geometrical isomers in nonsymmetrical PdMeCl complexes derived from both **L3** and **L4** depends of the reaction solvent. While these geometrical isomers are in equilibrium in the case of **L4**, they are not when **L3** was employed as chelating ligand. The metal complexation of the more electronically and sterically dissymmetrical **L3** ligand is more selective than that of **L4** for this particular type of complexes. UV-vis analyses showed that the introduction of a CD macrocyclic moiety has little influence on the electronic properties of the complexes. However, the different steric environments experienced by the metal in the two types of complexes could have an impact on their catalytic properties.

III. 4. Experimental part

III. 4. 1. General procedures

All reactions and manipulations were carried out under an inert atmosphere (nitrogen or argon) using standard Schlenk techniques. All glassware was stored in the oven prior to use under an inert atmosphere of gas (Argon). All commercial reagents were used as supplied unless otherwise stated. Solvents were dried by conventional methods and distilled immediately prior to use. Deuterated solvents were passed through a 5 cm-thick alumina column and stored under nitrogen over molecular sieves (4 Å). Column chromatography was performed on silica gel 60 (particle size 40-63 µm, 230-240 mesh). Routine ^{1}H, $^{31}P\{^{1}H\}$ and $^{13}C\{^{1}H\}$ NMR spectra were recorded on Bruker FT instruments (AVANCE 300, 400, 500, 600 spectrometers) at room temperature unless otherwise stated. ^{1}H NMR spectral data were referenced to residual protiated solvents (δ = 7.26 ppm for $CDCl_3$, 7.15 ppm for C_6D_6 and 5.32 ppm for CD_2Cl_2), $^{13}C\{^{1}H\}$ chemical shifts are reported relative to deuterated solvents (δ = 77.16 ppm for $CDCl_3$, 128.02 ppm for C_6D_6 and 53.84 ppm for CD_2Cl_2) and the $^{31}P\{^{1}H\}$ NMR data are given relative to external H_3PO_4. Mass spectra were recorded on a Bruker MicroTOF spectrometer (ESI-TOF) using CH_2Cl_2, CH_3CN or CH_3OH as the solvent. Elemental analyses were performed by the Service de Microanalyse, Institut de Chimie UMR 7177, Strasbourg. Melting points were

For references, see page 175.

determined with a Buchi 535 capillary melting point apparatus. In this chapter, the cyclodextrins are depicted as seen from the secondary face, the glucose units following counterclockwise squence in the order: A, B, C, D, E, F. The numbering of the atoms within a glucose unit is as follows:

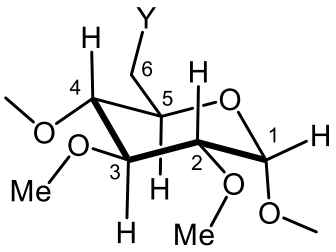

III. 4. 2. Synthesis and characterization

$6^A,6^B$-Dideoxy-$6^A,6^B$[(*R*)-2-diphenylphosphinophenylphosphinidene]-$2^A,2^B,2^C,2^D,2^E,2^F$, $3^A,3^B,3^C$, $3^D,3^E,3^F,6^C,6^D,6^E,6^F$-hexadeca-O-methyl-α-cyclodextrin (L3)[9]

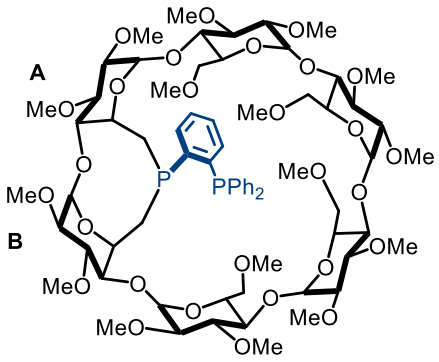

A solution of LDA in heptane (2.0 M, 1.11 mL, 2.22 mmol) was added dropwise to a stirred solution of primary phosphine **13** (0.098 g, 0.89 mmol) in THF (10 mL) at -78 °C. The red solution was stirred at -78 °C for 10 min before being allowed to reach 0 °C. The resulting red suspension maintained at 0 °C was transferred by cannula within 5 min into a stirred solution of dimesylate **1** (1.00 g, 0.74 mmol) in THF (24 mL) at 0 °C. The reaction mixture was stirred for 12 h at room temperature. The solvent was then removed *in vacuo* and excess LiHPAr was protonated with MeOH (5 mL). Removal of the solvent *in vacuo*, afforded a colourless solid, which was filtered over a short plug of silica using CH_2Cl_2/MeOH (500 mL, 90/10, *v*/*v*) as solvent. After removal of the solvent *in vacuo*, the resulting colourless residue was subjected to column chromatography (SiO_2, CH_2Cl_2/MeOH, 97/3, *v*/*v*) to afford pure **L3** (yield: 0.61 g, 57%) as a colourless solid. R_f (SiO_2, CH_2Cl_2/MeOH, 97/3, *v*/*v*) = 0.18. M.p. = 156-158 °C. ^{1}H NMR (500 MHz, $CDCl_3$, 25 °C): δ (assignment by combined COSY, ROESY, TOCSY and HSQC) = 1.76 (m, 1H, H-$6a^A$), 1.78 (m, 1H, H-$6a^B$), 2.94 (s, 3H, OMe), 2.94 (m, 1H, H-$6b^B$), 3.09 (s, 3H, OMe), 3.34 (s, 3H, OMe), 3.43 (s, 3H, OMe), 3.46 (s, 6H, OMe), 3.47 (s, 6H, OMe), 3.49 (s, 3H, OMe), 3.50 (s. 3H, OMe), 3.60 (s, 3H, OMe), 3.61 (s, 3H, OMe), 3.63 (s, 6H, OMe), 3.64

For references, see page 175.

(s, 3H, OMe), 3.66 (s, 3H, OMe), 2.95-4.01 (31H, H-2, H-3, H-4, H-5^{C,D,E,F}, H-6^{C,D,E,F}, H-6b^{A}), 4.06 (m, 1H, H-5^{B}), 4.21 (m, 1H, H-5^{A}), 4.92 (d, 1H, $^{3}J_{H\text{-}2,\,H\text{-}1}$ = 3.1 Hz, H-1), 4.95 (d, 1H, $^{3}J_{H\text{-}2,\,H\text{-}1}$ = 3.0 Hz, H-1), 5.04 (d, 1H, $^{3}J_{H\text{-}2,\,H\text{-}1}$ = 3.3 Hz, H-1), 5.07 (d, 1H, $^{3}J_{H\text{-}2,\,H\text{-}1}$ = 3.2 Hz, H-1), 5.07 (d, 1H, $^{3}J_{H\text{-}2,\,H\text{-}1}$ = 4.1 Hz, H-1), 5.08 (d, 1H, $^{3}J_{H\text{-}2,\,H\text{-}1}$ = 3.2 Hz, H-1), 6.92 (m, 1H, aromatic H), 7.10-7.23 (5H, aromatic H), 7.24-7.38 (7H, aromatic H), 7.62 (m, 1H, aromatic H) ppm; $^{13}C\{^{1}H\}$ NMR (126 MHz, $CDCl_3$, 25 °C): δ (assignment by HSQC) = 27.92 (d, $^{1}J_{P,C}$ = 10.3 Hz, C-6^{B}), 34.33 (d, $^{1}J_{P,C}$ = 16.3 Hz, C-6^{A}), 57.47, 57.89, 57.94 [x2], 58.10 [x2], 58.80, 59.20, 59.32, 61.64, 61.78 [x2], 62.08, 62.09 [x2] (OMe), 66.50, 70.31, 70.51, 71.09, 71.27, 71.32 [x2], 71.35, 71.40, 71.96 (C-5, C-6^{C,D,E,F}), 81.05, 81.30, 81.42 [x2], 81.46, 81.61, 81.70 [x2], 81.97, 82.01, 82.06, 82.32, 82.36, 82.38, 82.45, 83.27, 87.94, 89.68 (C-2, C-3, C-4), 97.37, 99.75, 99.91, 100.00 [x2], 100.84 (C-1), 128.36 (s, aromatic C), 128.55 (s, aromatic C), 128.60 (s, aromatic C), 128.66 (s, aromatic C), 129.19 (s, aromatic C), 129.85 (s, aromatic C), 131.52 (d, $^{2}J_{P,C}$ = 8.1 Hz, aromatic C), 133.29 (d, $^{2}J_{P,C}$ = 9.8 Hz, aromatic C), 133.44 (d, $^{2}J_{P,C}$ = 9.7 Hz, aromatic C), 134.54 (d, $^{2}J_{P,C}$ = 6.6 Hz, aromatic C), 137.89 (dd, $^{1}J_{P,C}$ = 13.0 Hz, $^{4}J_{P,C}$ = 2.4 Hz, aromatic C), 138.45 (dd, $^{1}J_{P,C}$ = 13.8 Hz, $^{4}J_{P,C}$ = 8.5 Hz, aromatic C), 141.91 (dd, $^{1}J_{P,C}$ = 30.9 Hz, $^{2}J_{P,C}$ = 9.7 Hz, aromatic C), 148.04 (dd, $^{1}J_{P,C}$ = 33.6 Hz, $^{2}J_{P,C}$ = 10.1 Hz, aromatic C) ppm; $^{31}P\{^{1}H\}$ NMR (162 MHz, $CDCl_3$, 25 °C): δ = -28.7 (d, $^{3}J_{P,P}$ = 167 Hz), -14.7 (d, $^{3}J_{P,P}$ = 167 Hz) ppm; elemental analysis (%) calcd for $C_{70}H_{104}O_{28}P_2 \cdot 3CH_2Cl_2$: C 51.27, H 6.48, found: C 51.38, H 6.41; MS (ESI-TOF) for $C_{70}H_{104}O_{28}P_2$: *m/z* (%): 1477.62 (100) [*M* + Na]$^{+}$.

Dichloro[{6^{A},6^{B}-Dideoxy-6^{A},6^{B}[(*R*)-2-diphenylphosphinophenylphosphinidene]-2^{A},2^{B},2^{C}, 2^{D},2^{E},2^{F},3^{A},3^{B},3^{C},3^{D},3^{E},3^{F},6^{C},6^{D},6^{E},6^{F}-hexadeca-O-methyl-α-cyclodextrin}-κ^{2}P,P] palladium(II) (17)

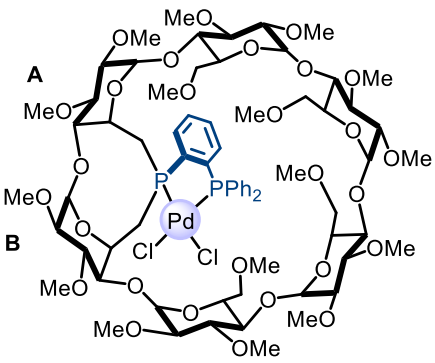

A solution of [$PdCl_2$(COD)] (0.098 g, 0.34 mmol) in CH_2Cl_2 (6 mL) was added to a solution of **L3** (0.5 g, 0.34 mmol) in CH_2Cl_2 (6 mL). The reaction mixture was stirred for 2 h at room temperature and then evaporated to dryness under reduced pressure. The resulting yellow residue was subjected to column chromatography (SiO_2, CH_2Cl_2/MeOH, 97/3, *v/v*) to afford pure **17** (0.42 g, 75%) as a yellow solid. A crystalline material was obtained by slow diffusion of *n*-pentane into a benzene solution of **17**. ^{1}H NMR (500 MHz, $CDCl_3$, 25 °C): δ (assignment by combined COSY, ROESY, TOCSY and HSQC) = 2.15 (m, 1H, H-6a^{A}), 2.34 (m, 1H, H-6a^{B}), 2.67 (s, 3H, OMe), 3.30 (s, 3H, OMe), 3.36 (s, 3H, OMe), 3.38 (s, 3H, OMe),

For references, see page 175.

3.43 (s, 3H, OMe), 3.45 (s, 3H, OMe), 3.46 (s, 9H, OMe), 3.52 (s. 3H, OMe), 3.61 (s, 3H, OMe), 3.62 (s, 3H, OMe), 3.64 (s, 9H, OMe), 3.69 (s, 3H, OMe), 3.04-4.30 (32H, H-2, H-3, H-4, H-$5^{C,D,E,F}$, H-$6^{C,D,E,F}$, H-$6b^{A,B}$), 4.80 (m, 1H, H-5^{B}), 4.95 (m, 2H, H-1), 5.05 (d, 1H, $^{3}J_{H\text{-}2,\ H\text{-}1}$ = 3.5 Hz, H-1), 5.06 (m, 2H, H-1), 5.16 (d, 1H, $^{3}J_{H\text{-}2,\ H\text{-}1}$ = 4.2 Hz, H-1), 5.30 (m, 1H, H-5^{A}), 7.41 (5H, aromatic H), 7.50 (m, 2H, aromatic H), 7.62 (m, 1H, aromatic H), 7.67-7.76 (5H, aromatic H), 7.98 (m, 1H, aromatic H) ppm; $^{13}C\{^{1}H\}$ NMR (126 MHz, $CDCl_3$, 25 °C): δ (assignment by HSQC) = 33.63 (d, $^{1}J_{P,C}$ = 30.1 Hz, C-6^{B}), 43.15 (d, $^{1}J_{P,C}$ = 26.5 Hz, C-6^{A}), 57.36, 57.46, 57.52, 57.71, 57.78, 57.86, 58.30, 58.85, 58.98, 59.22, 61.78, 61.83, 61.89, 61.92, 62.19, 62.51 (OMe), 66.07 (C-5^{B}), 67.52 (C-5^{A}), 70.06, 70.64, 70.71, 70.83, 71.19, 71.51, 71.68, 72.34, 80.21, 81.08, 81.19, 81.64, 82.08, 82.23, 82.31, 82.42, 82.59, 88.31, 88.38, 90.51 (C-2, C-3, C-4, C-$5^{C,D,E,F}$, C-$6^{C,D,E,F}$), 98.12, 99.70, 99.78, 99.89, 100.42, 101.48 (C-1), 128.88, 128.98, 129.14, 129.24, 129.53 [x2] (aromatic C), 131.85 (d, $J_{P,C}$ = 19.1 Hz, aromatic C), 132,17 (d, $J_{P,C}$ = 30.2 Hz, aromatic C), 133.21 (d, $J_{P,C}$ = 6.4 Hz, aromatic C), 133.39, 133.47, 133.52, 133.88, 133.93, 134.06, 134.15 (aromatic C), 138.92 (dd, $^{1}J_{P,C}$ = 54.3 Hz, $^{2}J_{P,C}$ = 35.8 Hz, aromatic C), 144.55 (dd, $^{1}J_{P,C}$ = 53.1 Hz, $^{2}J_{P,C}$ = 37.4 Hz, aromatic C) ppm; $^{31}P\{^{1}H\}$ NMR (162 MHz, $CDCl_3$, 25 °C): δ = 55.53 (d, $^{2}J_{P,P}$ = 13.6 Hz), 61.65 (d, $^{2}J_{P,P}$ = 13.6 Hz) ppm; elemental analysis (%) calcd for $C_{70}H_{104}O_{28}P_2PdCl_2 \bullet 0.95\ CH_2Cl_2$: C 49.73, H 6.23, found: C 49.53, H 6.33; MS (ESI-TOF) for $C_{70}H_{104}O_{28}P_2PdCl_2$: *m/z* (%): 1655.45 (100) $[M + Na]^+$.

[PdMeCl(L3)] (18a, 18b)

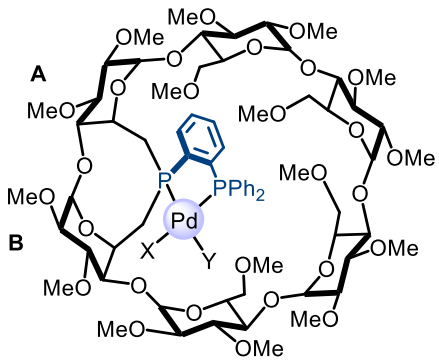

18a, X = Me, Y = Cl
18b, X = Cl, Y = Me

A solution of [PdMeCl(COD)] (0.025 g, 0.096 mmol) in THF (1 mL) was added to a solution of **L3** (0.14 g, 0.096 mmol) in THF (1 mL). The reaction mixture was stirred for 2 h at room temperature and then evaporated to dryness under reduced pressure. The resulting yellow residue was subjected to column chromatography (SiO_2, CH_2Cl_2/MeOH, 97/3, *v/v*) to afford the product as a yellow solid (0.124 g, 80%). The ^{1}H NMR spectrum shows two isomers in a ca. 25/75 ratio of **18a**/**18b** in C_6D_6 at room temperature. ^{1}H NMR (500 MHz, C_6D_6, 25 °C): δ (assignment by combined COSY, ROESY, TOCSY and HSQC) = 1.13 (dd, $^{3}J_{H,P}$ = 7.3 Hz, $^{3}J_{H,P}$ = 2.5 Hz, PdMe, **18a**), 1.23 (dd, $^{3}J_{H,P}$ = 8.7 Hz, $^{3}J_{H,P}$ = 3.2 Hz, PdMe, **18b**), 2.06 (m, H-$6a^{A\ or\ B}$, **18b**), 2.13 (m, H-$6a^{B\ or\ A}$, **18b**), 3.49 (m, H-$6b^{A\ or\ B}$, **18b**), 3.91 (m, H-$6a^{B\ or\ A}$, **18b**), 2.10 (m, H-$6a^{A\ or\ B}$, **18a**), 2.27 (m, H-$6a^{B\ or\ A}$, **18a**), 3.38 (m, H-$6b^{A\ or\ B}$, **18a**), 3.59 (m, H-$6a^{B\ or\ A}$, **18a**), 3.14 (s, OMe, **18b**), 3.25 (s, OMe,

For references, see page 175.

18b), 3.30 (s, OMe, **18b**), 3.32 (s, OMe, **18b**), 3.34 (s, OMe, **18b**), 3.34 (s, OMe, **18b**), 3.41 (s, OMe, **18b**), 3.48 (s, OMe, **18b**), 3.50 (s, OMe, **18b**), 3.51 (s, OMe, **18b**), 3.67 (s, OMe, **18b**), 3.69 (s, OMe, **18b**), 3.84 (s, OMe, **18b**), 3.84 (s, OMe, **18b**), 3.87 (s, OMe, **18b**), 3.89 (OMe, **18b**), 2.92-4.96 (H-2, H-3, H-4, H-$5^{C,D,E,F}$, H-6), 4.63 (m, H-$5^{A\ or\ B}$, **18b**), 5.31 (m, H-$5^{B\ or\ A}$, **18b**), 4.44 (m, H-$5^{A\ or\ B}$, **18a**), 4.74 (m, H-$5^{B\ or\ A}$, **18a**), 4.73, 4.78 (H-1, **18a**), 4.78, 4.83 (H-1, **18b**), 5.24-5.42 (H-1, **18a** and **18b** signals overlap), 6.86-7.99 (aromatic H) ppm; $^{13}C\{^{1}H\}$ NMR (126 MHz, C_6D_6, 25 °C): δ (assignment by HSQC) = 3.68 (PdMe, **18a**, $^{2}J_{P4,C}$ = 109.8 Hz, $^{2}J_{P3,C}$ = 2.5 Hz), 11.72 (PdMe, **18b**, $^{2}J_{P1,C}$ = 113.4 Hz, $^{2}J_{P2,C}$ = 1.9 Hz), 30.25, 41.42 (C-$6^{A,B}$, **18b**), 32.39, 43.40 (C-$6^{A,B}$, **18a**), 57.24, 57.25, 57.42, 57.45 [x2], 57.63, 58.71, 59.00, 59.12, 59.32, 61.75, 61.80, 61.85, 61.90, 62.21, 62.38 (OMe, **18b**), 66.14 (d, $^{2}J_{P,C}$ = 5.1 Hz, C-$5^{A\ or\ B}$, **18b**), 66.29 (d, $^{2}J_{P,C}$ = 6.2 Hz, C-$5^{A\ or\ B}$, **18a**), 68.51 (d, $^{2}J_{P,C}$ = 6.3 Hz, C-$5^{A\ or\ B}$, **18a**), 68.84 (d, $^{2}J_{P,C}$ = 7.8 Hz, C-$5^{A\ or\ B}$, **18b**), 71.34, 71.37, 71.64, 71.72 (C-$5^{C,D,E,F}$, **18b**), 71.68 [x2], 71.82, 72.22 (C-$5^{C,D,E,F}$, **18a**), 72.16, 72.50, 72.97, 73.13 (C-$6^{C,D,E,F}$, **18a**), 72.43, 72.63, 73.27, 73.77 (C-$6^{C,D,E,F}$, **18b**), 80.60-91.52 (C-2, C-3, C-4), 98.39, 100.01 [x2], 98.25, 100.01, 100.14, 100.85, 100.95, 101.47 (C-1, **18a**), 98.39, 100.01 [x2], 100.49, 100.72, 101.25 (C-1, **18b**), 147.36-128.44 (aromatic C) ppm; $^{31}P\{^{1}H\}$ NMR (202 MHz, C_6D_6, 25 °C): δ = 29.15 (d, $^{2}J_{P,P}$ = 25.7 Hz, **18b**), 40.98 (d, $^{2}J_{P,P}$ = 23.6 Hz, **18a**), 41.72 (d, $^{2}J_{P,P}$ = 23.6 Hz, **18a**), 51.72 (d, $^{2}J_{P,P}$ = 25.7 Hz, **18b**) ppm; elemental analysis (%) calcd for $C_{71}H_{107}O_{28}P_2PdCl \cdot 0.7\ CH_2Cl_2 \cdot 0.05\ C_5H_{12}$: C 51.58, H 6.56, found: C 51.59, H 6.57; MS (ESI-TOF) for $C_{71}H_{107}O_{28}P_2PdCl$: *m/z* (%): 1633.51 (100) $[M + Na]^+$.

Dibromo[{6^A,6^B-Dideoxy-6^A,6^B[(*R*)-2-diphenylphosphinophenylphosphinidene]-2^A,2^B,2^C,2^D,2^E,2^F,3^A,3^B,3^C,3^D,3^E,3^F,6^C,6^D,6^E,6^F-hexadeca-O-methyl-α-cyclodextrin}-κ^{2}P,P] nickel(II) (19)

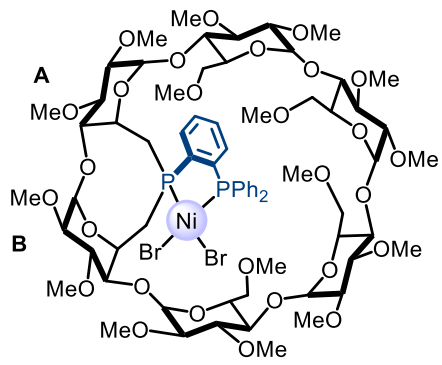

A solution of $[NiBr_2(DME)]$ (0.053 g, 0.16 mmol) in CH_2Cl_2 (5 mL) was added to a solution of **L3** (0.227 g, 0.16 mmol) in CH_2Cl_2 (5 mL). The reaction mixture was stirred for 2 h at room temperature and then evaporated to dryness under reduced pressure. The resulting orange residue was subjected to column chromatography (SiO_2, CH_2Cl_2/MeOH, 97/3, *v/v*). The solution was dried under vacuum and the resulting solid was redissolved with MeOH and reacted with LiBr for 30 min. The reaction mixture was extracted with CH_2Cl_2/H_2O and dried over $MgSO_4$. The solvent in organic layer was removed and afford pure **19** (0.226 g, 86%) as an orange solid. ^{1}H NMR

For references, see page 175.

(500 MHz, C_6D_6, 25°C): δ (assignment by combined COSY, ROESY, TOCSY and HSQC) = 2.22 (m, 1H, H-6a^{B}), 2.42 (m, 1H, H-6a^{A}), 3.00 (m, 1H, H-4^{B}), 3.02 (m, 1H, H-6b^{A}), 3.07 (m, 1H, H-4^{A}), 3.29 (s, 3H, OMe), 3.29 (s, 3H, OMe), 3.30 (s, 3H, OMe), 3.31 (s, 3H, OMe), 3.33 (s, 3H, OMe), 3.36 (s, 3H, OMe), 3.40 (s, 3H, OMe), 3.53 (s, 3H, OMe), 3.57 (s, 3H, OMe),3.59 (s, 3H, OMe), 3.74 (s, 3H, OMe), 3.78 (s, 3H, OMe), 3.84 (s, 3H, OMe), 3.84 (s, 3H, OMe), 3.84 (s, 3H, OMe), 3.84 (s, 3H, OMe), 3.21-4.73 (28H, H-2, H-3, H-4^{C,D,E,F}, H-5^{C,D,E,F}, H-6b^{B}, H-6a^{C}, H-5^{D,E,F}), 4.74 (m, 1H, H-5^{B}), 4.76 (d, 1H, $^{3}J_{H\text{-}2,\ H\text{-}1}$ = 4.3 Hz, H-1), 4.85 (d, 1H, $^{3}J_{H\text{-}2,\ H\text{-}1}$ = 3.5 Hz, H-1), 5.10 (m, 1H, H-6b^{C}), 5.31 (d, 1H, $^{3}J_{H\text{-}2,\ H\text{-}1}$ = 3.4 Hz, H-1), 5.33 (d, 1H, $^{3}J_{H\text{-}2,\ H\text{-}1}$ = 3.3 Hz, H-1), 5.35 (d, 1H, $^{3}J_{H\text{-}2,\ H\text{-}1}$ = 3.4 Hz, H-1), 5.44 (d, 1H, $^{3}J_{H\text{-}2,\ H\text{-}1}$ = 3.2 Hz, H-1), 5.60 (m, 1H, H-5^{A}), 6.88 (m, 1H, aromatic H), 6.98-7.14 (8H, aromatic H), 7.82 (m, 1H, aromatic H), 7.92 (m, 4H, aromatic H) ppm; $^{13}C\{^{1}H\}$ NMR (126 MHz, C_6D_6, 25°C): δ (assignment by HSQC) = 35.49 (d, $^{1}J_{P,C}$ = 31.8 Hz, C-6^{B}), 43.45 (d, $^{1}J_{P,C}$ = 25.5 Hz, C-6^{A}), 57.22, 57.31 [x2], 57.34, 57.61, 57.67, 58.99, 59.04, 59.14, 59.34, 61.71, 61.89, 61.91 [x2], 62.21, 62.31 (OMe), 66.83 (d, $^{2}J_{P,C}$ = 8.4 Hz, C-5^{B}), 68.64 (C-5^{A}), 71.14, 71.30, 71.64, 71.14, 71.30, 71.64, 71.72, 72.38, 72.78, 72.93, 73.74, 80.91, 81.89, 81.93, 81.96, 82.33, 82.59, 82.90, 82.97, 83.13, 83.29, 83.43, 83.56, 83.66 (C-2, C-3, C-4^{C,D,E,F}, C-5^{C,D,E,F}, C-6$^{C.D,E,F}$), 88.60 (C-4^{B}), 91.04 (C-4^{A}), 98.46, 99.92, 100.12, 100.60, 100.62, 101.69 (C-1), 128.65-134.39 (aromatic C), 141.66 (dd, $^{1}J_{P,C}$ = 48.7 Hz, $^{2}J_{P,C}$ = 37.2 Hz, aromatic C), 147.38 (dd, $^{1}J_{P,C}$ = 46.0 Hz, $^{2}J_{P,C}$ = 39.4 Hz, aromatic C) ppm; $^{31}P\{^{1}H\}$ NMR (202 MHz, C_6D_6, 25°C): δ = 54.83 (d, $^{2}J_{P,P}$ = 57.9 Hz), 65.22 (d, $^{2}J_{P,P}$ = 57.9 Hz) ppm; elemental analysis (%) calcd for $C_{70}H_{104}O_{28}P_2NiBr_2$ • 1.3 C_5H_{12}: C 51.98, H 6.82, found: C 51.92, H 6.93; MS (ESI-TOF) for $C_{70}H_{104}O_{28}P_2NiBr_2$: *m/z* (%): 1591.47 (100) $[M - Br]^{+}$.

6^{A},6^{B}-Dideoxy-6^{A},6^{B}[(1*R*,2*S*)-1,2-phenylenebis(phenylphosphino)]-2^{A},2^{B},2^{C},2^{D},2^{E},2^{F},3^{A}, 3^{B},3^{C},3^{D}, 3^{E},3^{F},6^{C},6^{D},6^{E},6^{F}-hexadeca-O-methyl-α-cyclodextrin (L4)[9]

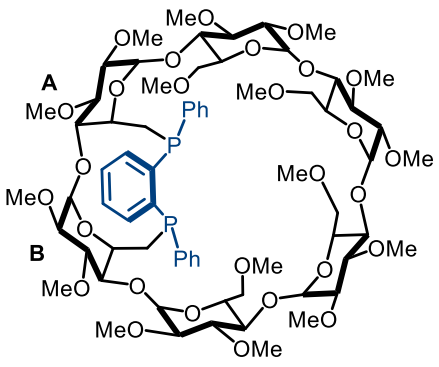

A solution of *n*-BuLi in hexane (1.6 M, 2.77 mL, 4.33 mmol) was added dropwise to a stirred solution of primary phosphine **13** (0.326 g, 1.11 mmol) in THF (16 mL) at -78 °C. After 10 min, the reaction mixture was allowed to reach room temperature and then kept at this temperature for 8 h under stirring. The resulting red suspension was transferred by cannula within 15 min into a stirred solution of dimesylate **1** (0.75 g, 0.55 mmol) in THF (45 mL). The reaction mixture was stirred for 12 h at room temperature. The solvent was then removed *in vacuo*, mesitylene

For references, see page 175.

(20 mL) was added and the resulting solution was heated at reflux for 4 h. Removal of the solvent *in vacuo*, afforded a colourless solid, which was filtered over a short plug of silica using CH_2Cl_2/MeOH (500 mL, 90/10, *v*/*v*) as solvent. The resulting coulourless residue was then subjected to column chromatography (SiO_2, CH_2Cl_2/MeOH, 97/3, *v*/*v*) to afford pure **L4** (yield: 0.38 g, 47%) as a colourless solid. R_f (SiO_2, CH_2Cl_2/MeOH, 97/3, *v*/*v*) = 0.21. M.p. = 159-161 °C. ^{1}H NMR (500 MHz, $CDCl_3$, 25 °C): δ (assignment by combined COSY, ROESY, TOCSY and HSQC) = 2.26 (m, 1H, H-6a^A), 2.50 (m, 1H, H-6a^B), 2.69 (s, 3H, OMe), 2.94 (d, 1H, $^2J_{H\text{-}6b,H\text{-}6a}$ = 10.1 Hz, H-6a^C), 2.99 (d, 1H, $^2J_{H\text{-}6b,H\text{-}6a}$ = 14.5 Hz, H-6b^B), 3.08 (m, 1H, H-6b^A), 3.10 (s, 3H, OMe), 3.34 (s, 3H, OMe), 3.41 (s, 3H, OMe), 3.43 (s, 3H, OMe), 3.46 (s, 3H, OMe), 3.47 (s, 3H, OMe), 3.48 (s, 3H, OMe), 3.51 (s, 3H, OMe), 3.52 (s, 3H, OMe), 3.61 (s, 6H, OMe), 3.63 (s, 3H, OMe), 3.65 (s, 6H, OMe), 3.67 (s, 3H, OMe), 3.10-3.97 (29H, H-2, H-3, H-4, H-5^{C,D,E,F}, H-6^{D,E,F}, H-6b^C), 4.36 (m, 1H, H-5^A), 4.45 (m, 1H, H-5^B), 4,79 (d, 1H, $^3J_{H\text{-}2,H\text{-}1}$ = 3.4 Hz, H-1^B), 4.95 (d, 1H, $^3J_{H\text{-}2,H\text{-}1}$ = 2.9 Hz, H-1^A), 5.03 (d, 1H, $^3J_{H\text{-}2,H\text{-}1}$ = 3.3 Hz, H-1), 5.04 (d, 1H, $^3J_{H\text{-}2,H\text{-}1}$ = 3.1 Hz, H-1), 5.07 (d, 1H, $^3J_{H\text{-}2,H\text{-}1}$ = 3.3 Hz, H-1), 5.16 (d, 1H, $^3J_{H\text{-}2,H\text{-}1}$ = 3.3 Hz, H-1), 6.57 (m, 1H, aromatic H), 7.01 (m, 1H, aromatic H), 7.15 (m, 1H, aromatic H), 7.25-7.43 (6H, aromatic H), 7.52 (3H, aromatic H), 7.63 (m, 2H, aromatic H) ppm; ^{13}C{^{1}H} NMR (126 MHz, $CDCl_3$, 25 °C): δ (assignment by HSQC) = 30.52 (dd, $^1J_{P,C}$ = 15.7 Hz, $^4J_{P,C}$ = 4.9 Hz, C-6^B), 33.32 (d, $^1J_{P,C}$ = 15.3 Hz, C-6^A), 57.53, 57.69, 57.90, 58.18, 58.19, 58.37, 58.12, 58.73, 59.09, 59.21, 61.68, 61.88, 61.92, 61.94, 62.04, 62.17 (OMe), 69.68, 70.81, 70.87, 71.51 (C-6^{C,D,E,F}), 70.73 and 71.29 [x3] (C-5^{C,D,E,F}), 73.08 (d, $^2J_{P,C}$ = 25.8 Hz, C-5^B), 73.30 (d, $^2J_{P,C}$ = 18.6 Hz, C-5^A), 80.43, 81.29, 81.40, 81.43, 81.57 [x2], 81.67, 81.76, 81.93 [x2], 82.05, 82.09, 82.16, 82.18 and 82.42 [x2] (C-2, C-3, C-4^{C,D,E,F}), 88.58 (d, $^3J_{P,C}$ = 11.5 Hz, C-4^B), 89.68 (d, $^3J_{P,C}$ = 9.6 Hz, C-4$_A$), 99.46, 99.62, 100.14, 100.23, 100.39 and 100.88 (C-1), 128.23, 128.36, 128.46 (aromatic C), 128.48 (d, $^3J_{P,C}$ = 6.1 Hz, aromatic C), 128.69 (d, $^3J_{P,C}$ = 6.3 Hz, aromatic C), 128.92 (aromatic C), 130.65 (d, $^2J_{P,C}$ = 8.7 Hz, aromatic C), 131.92 (d, $^2J_{P,C}$ = 18.8 Hz, aromatic C), 133.21 (d, $^2J_{P,C}$ = 19.0 Hz, aromatic C), 133.97 (dd, $^2J_{P,C}$ = 3.7 Hz, $^3J_{P,C}$ = 3.3 Hz, aromatic C), 137.44 (dd, $^1J_{P,C}$ = 17.9 Hz, $^4J_{P,C}$ = 15.3 Hz, aromatic C), 141.41 (dd, $^1J_{P,C}$ = 11.7 Hz, $^4J_{P,C}$ = 5.3 Hz, aromatic C), 143.47 (dd, $^1J_{P,C}$ = 28.1 Hz, $^2J_{P,C}$ = 13.6 Hz, aromatic C), 150.43 (dd, $^1J_{P,C}$ = 35.1 Hz, $^2J_{P,C}$ = 12.0 Hz, aromatic C) ppm; ^{31}P{^{1}H} NMR (162 MHz, $CDCl_3$, 25 °C): δ = -27.2 (d, $^3J_{P,P}$ = 176 Hz), -19.0 (d, $^3J_{P,P}$ = 176 Hz) ppm; elemental analysis (%) calcd for $C_{70}H_{104}O_{28}P_2$: C 57.76, H 7.20, found: C 57.52, H 7.21; MS (ESI-TOF) for $C_{70}H_{104}O_{28}P_2$: *m/z* (%): 1477.61 (100) $[M + Na]^+$.

For references, see page 175.

Dichloro[{6^{A},6^{B}-Dideoxy-6^{A},6^{B}[(1*R*,2*S*)-1,2-phenylenebis(phenylphosphino)]-2^{A},2^{B},2^{C},2^{D},2^{E},2^{F},3^{A},3^{B},3^{C},3^{D},3^{E},3^{F},6^{C},6^{D},6^{E},6^{F}-hexadeca-O-methyl-α-cyclodextrin}-κ^{2}P,P] palladium(II) (20)

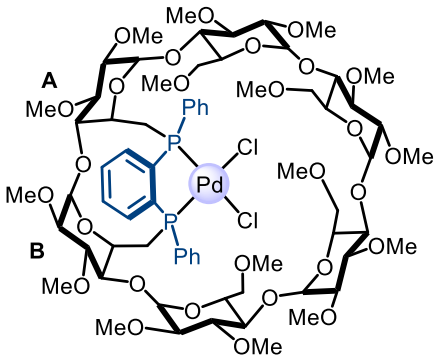

A solution of [PdCl$_2$(COD)] (0.04 g, 0.16 mmol) in CH_2Cl_2 (5 mL) was added to a solution of **L4** (0.228 g, 0.16 mmol) in CH_2Cl_2 (5 mL). The reaction mixture was stirred for 2 h at room temperature and then evaporated to dryness under reduced pressure. The resulting yellow residue was subjected to column chromatography (SiO_2, CH_2Cl_2/MeOH, 97/3, *v/v*) to afford pure **20** (0.198 g, 77%) as a yellow solid. A crystalline material was obtained by slow diffusion of *n*-pentane into a dichloromethane solution of **20**. ^{1}H NMR (500 MHz, $CDCl_3$, 25°C): δ (assignment by combined COSY, ROESY, TOCSY and HSQC) = 2.53 (m, 1H, H-6a^{A}), 2.58 (m, 1H, H-6a^{B}), 2.65 (m, 1H, H-6b^{A}), 2.99 (m, 1H, H-2^{B}), 3.01 (m, 1H, H-4^{A}), 3.15 (s, 3H, OMe), 3.29 (s, 3H, OMe), 3.31 (s, 3H, OMe), 3.34 (s, 3H, OMe), 3.40 (s, 3H, OMe), 3.43 (s, 3H, OMe), 3.45 (s, 3H, OMe), 3.49 (s, 3H, OMe), 3.51 (s, 3H, OMe), 3.54 (s, 3H, OMe), 3.60 (s, 3H, OMe), 3.60 (s, 3H, OMe), 3.63 (s, 3H, OMe), 3.63 (s, 3H, OMe), 3.68 (s, 3H, OMe), 3.69 (s, 3H, OMe), 3.08-4.03 (27H, H-2^{A,C,D,E,F}, H-3^{A,B,C,D,E,F}, H-4^{B,C,D,E,F}, H-5^{D,E}, H-6b^{B}, H-6^{C,D,E,F}), 4.30 (m, 1H, H-5^{F}), 4.40 (m, 1H, H-5^{C}), 4.58 (d, $^{3}J_{H\text{-}2,H\text{-}1}$ = 3.2 Hz, 1H, H-1), 4.75 (m, 1H, H-5^{B}), 4.84 (m, 1H, H-5^{A}), 4.97 (d, $^{3}J_{H\text{-}2,H\text{-}1}$ = 3.2 Hz, 1H, H-1), 5.08 (m, 2H, H-1), 5.10 (d, $^{3}J_{H\text{-}2,H\text{-}1}$ = 3.1 Hz, 1H, H-1), 5.14 (d, $^{3}J_{H\text{-}2,H\text{-}1}$ = 3.2 Hz, 1H, H-1), 7.08-7.92 (14H, aromatic H); ^{13}C{^{1}H} NMR (126 MHz, $CDCl_3$, 25°C): δ (assignment by HSQC) = 31.74 (d, $^{1}J_{P,C}$ = 34.2 Hz, C-6^{B}), 36.77 (d, $^{1}J_{P,C}$ = 31.7 Hz, C-6^{A}), 57.46, 57.59, 58.02, 58.09, 58.16, 58.21, 58.99, 59.08, 59.16, 59.41, 61.27, 61.90, 62.03, 62.05, 62.18 (OMe), 71.03, 71.15, 71.22, 71.26, 71.55, 71.70, 71.83, 72.10, 72.14, 72.57 (C-5^{A,B,C,D,E,F}, C-6^{C,D,E,F}), 79.50, 79.53 [x2], 79.87, 79.89 [x2], 80.69, 81.19, 81.36, 81.38, 81.61, 81.65, 81.98, 82.08, 82.22, 82.53, 82.93, 82.94 (C-2^{A,B,C,D,E,F}, C-3^{A,B,C,D,E,F}, C-4^{A,B}), 89.72 (d, $^{3}J_{P,C}$ = 13.5 Hz C-4^{B}), 91.33 (d, $^{3}J_{P,C}$ = 13.3 Hz C-4^{A}), 99.74, 100.12, 100.43, 100.52, 101.34 and 102.15 (C-1), 128.77, 128.80, 128.86, 129.08, 129.17, 131.06, 131.72 [x2], 131.95 [x2], 132.99, 133.04, 133.38, 133.48 (aromatic C); ^{31}P{^{1}H} NMR (202 MHz, $CDCl_3$, 25°C): δ = 62.4 (d, $^{2}J_{P,P}$ = 9.3 Hz, P), 69.0 (d, $^{2}J_{P,P}$ = 9.3 Hz, P) ppm; elemental analysis (%) calcd for $C_{70}H_{104}O_{28}P_2PdCl_2$: C 51.49, H 6.42, found: C 51.49, H 6.42; MS (ESI-TOF) for $C_{70}H_{104}O_{28}P_2PdCl_2$: *m/z* (%): 1655.45 (100) [*M* + Na]$^{+}$.

[PdMeCl(L4)] (21a, 21b)

For references, see page 175.

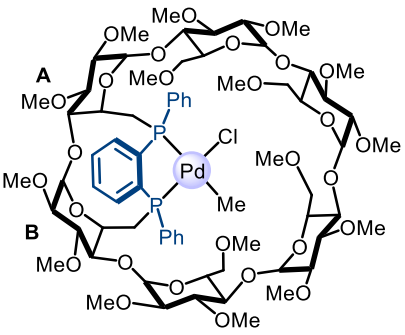
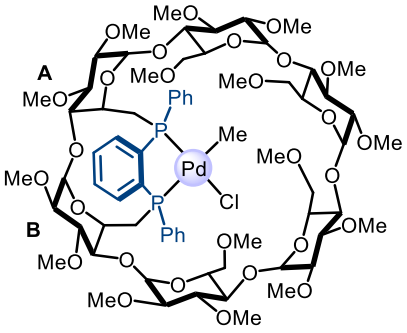

A solution of [PdMeCl(COD)] (0.013 g, 0.05 mmol) in THF (1 mL) was added to a solution of **L4** (0.073 g, 0.05 mmol) in THF (1 mL). The reaction mixture was stirred for 2 h at room temperature and then evaporated to dryness under reduced pressure. The resulting yellow residue was subjected to column chromatography (SiO_2, CH_2Cl_2/MeOH, 97/3, *v/v*) to afford the product as a yellow solid (0.06 g, 74%). The ^{1}H and $^{31}P\{^{1}H\}$ NMR spectra show two isomers in a *ca*. 60:40 ratio in CD_2Cl_2 at room temperature.

$^{31}P\{^{1}H\}$ NMR (121 MHz, CD_2Cl_2, 25°C): δ = 34.63 (d, $^{3+2}J_{P,P}$ = 26.7 Hz, $P_{\mathbf{21a}}$), 41.76 (d, $^{3+2}J_{P,P}$ = 25.9 Hz, $P_{\mathbf{21b}}$), 54.48 (d, $^{3+2}J_{P,P}$ = 25.9 Hz, $P_{\mathbf{21b}}$), 63.75 (d, $^{3+2}J_{P,P}$ = 26.7 Hz, $P_{\mathbf{21a}}$) ppm; elemental analysis (%) calcd for $C_{71}H_{107}O_{28}P_2PdCl \bullet 0.75\ CH_2Cl_2$: C 51.42, H 6.52, found: C 51.41, H 6.50; MS (ESI-TOF) for $C_{71}H_{107}O_{28}P_2PdCl$: *m/z* (%): 1575.55 (100) $[M - Cl]^+$.

Dibromo[{6^{A},6^{B}-Dideoxy-6^{A},6^{B}[(1*R*,2*S*)-1,2-phenylenebis(phenylphosphino)]-2^{A},2^{B},2^{C},2^{D},2^{E},2^{F},3^{A},3^{B},3^{C},3^{D},3^{E},3^{F},6^{C},6^{D},6^{E},6^{F}-hexadeca-O-methyl-α-cyclodextrin}-κ^{2}P,P]nickel(II) (22)

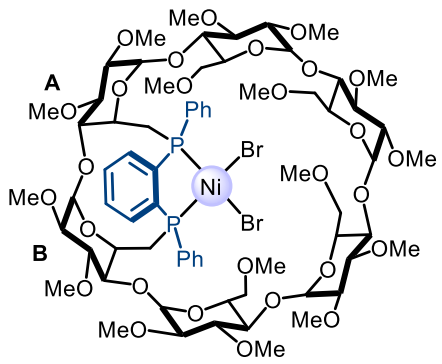

A solution of [$NiBr_2$(DME)] (0.062 g, 0.17 mmol) in CH_2Cl_2 (3 mL) was added to a solution of **L4** (0.258 g, 0.17 mmol) in CH_2Cl_2 (3 mL). The reaction mixture was stirred for 2 h at room temperature and then evaporated to dryness under reduced pressure. The resulting orange residue was subjected to column chromatography (SiO_2, CH_2Cl_2/MeOH, 97/3, *v/v*). The solution was dried under vacuum and the resulting solid was redissolved with MeOH and reacted with LiBr for half an hour. The reaction mixture was extracted with CH_2Cl_2/H_2O and dried over $MgSO_4$. The solvent in organic layer was removed and afford pure **22** (0.202 g, 68%) as an orange solid. A crystalline material was obtained by slow diffusion of *n*-pentane into a benzene solution of **22**.

^{1}H NMR (500 MHz, CD_2Cl_2, 25°C): δ(assignment by combined COSY, ROESY, TOCSY and HSQC) = 2.48 (m, 2H, H-6$^{A\ or\ B}$), 2.53 (m, 1H, H-6a$^{B\ or\ A}$), 3.83 (m, 1H, H-6b$^{B\ or\ A}$), 3.17 (s, 3H, OMe), 3.22 (s, 3H, OMe), 3.25 (s, 3H, OMe), 3.36 (s, 3H, OMe), 3.38 (s, 6H, OMe), 3.41

For references, see page 175.

(s, 3H, OMe), 3.47 (s, 3H, OMe), 3.49 (s, 3H, OMe), 3.50 (s, 3H, OMe), 3.53 (s, 3H, OMe), 3.54 (s, 3H, OMe), 3.58 (s, 3H, OMe), 3.60 (s, 3H, OMe), 3.62 (s, 3H, OMe), 3.66 (s, 3H, OMe), 2.95-3.93 (27H, H-2, H-3, H-4, H-5, H-6), 4.10 (m, 2H, H-5, H-6), 4.38 (d, $^{3}J_{\text{H-5, H-6}}$ = 9.8 Hz, H-5), 4.58 (m, 1H, H-1), 4.90 (m, 1H, H-1), 4.94 (d, 1H, $^{3}J_{\text{H-2, H-1}}$ = 3.9 Hz, H-1), 4.99 (d, 1H, $^{3}J_{\text{H-2, H-1}}$ = 3.2 Hz, H-1), 5.06 (d, 1H, $^{3}J_{\text{H-2, H-1}}$ = 2.6 Hz, H-1), 5.09 (d, 1H, $^{3}J_{\text{H-2, H-1}}$ = 3.3 Hz, H-1), 5.08 (m, 1H, H-5$^{\text{B or A}}$), 5.25 (m, 1H, H-5$^{\text{A or B}}$), 6.98 (m, 1H, aromatic H), 7.32-7.61 (9H, aromatic H), 7.86 (m, 2H, aromatic H), 7.95 (m, 2H, aromatic H) ppm; $^{13}C\{^{1}H\}$ NMR (126 MHz, CD_2Cl_2, 25°C): δ (assignment by HSQC) = 31.68 (d, $^{1}J_{P,C}$ = 35.0 Hz, C-6$^{\text{A or B}}$), 36.99 (br, C-6$^{\text{B or A}}$), 57.23, 57.69, 58.40, 58.58, 58.90 [x2], 58.92 [x2], 59.21, 59.26, 60.94, 61.76, 61.90, 61.96, 61.98, 62.11 (OMe), 71.29, 71.36, 71.60, 71.68, 71.88 (C-5), 71.76, 72.02, 72.52 [x2] (C-6$^{\text{C,D,E,F}}$), 80.07-83.45, 89.51 (br), 91.33 (br) (C-2, C-3, C-4), 99.70, 99.72, 100.13, 100.64, 101.11, 102.24 (C-1), 127.98, 128.17, 128.37, 128.62, 128.70, 129.24, 129.32, 131.48 [x3], 132.12, 132.42, 132.50, 132.65, 132.70, 133.01, 133.56, 133.64, 134.37 (aromatic C) ppm; $^{31}P\{^{1}H\}$ NMR (202 MHz, CD_2Cl_2, 25°C): δ = 62.4 (d, $^{2}J_{P,P}$ = 58.1 Hz, P), 72.9 (d, $^{2}J_{P,P}$ = 58.1 Hz, P) ppm; elemental analysis (%) calcd for $C_{70}H_{104}O_{28}P_2NiBr_2 \bullet 0.15\ C_6H_6$: C 50.52, H 6.27, found: C 50.63, H 6.15; MS (ESI-TOF) for $C_{70}H_{104}O_{28}P_2NiBr_2$: *m/z* (%): 1593.47 (100) $[M - Br]^+$.

2-(diisopropylphosphaneyl)diphenylphosphine (L5) [16]

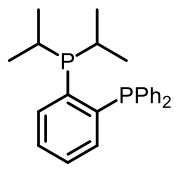

A Schlenk tube under argon atmosphere was charged with (2-bromophenyl)diphenylphosphine (0.5 g, 1.36 mmol) in THF (15 mL). The solution was cooled at -78 °C and *n*-BuLi (1.92 mmol, 1.2 equiv.) was added dropwise then the yellow-orange solution was maintained at this temperature for 2 h before slowly returning to room temperature. The reaction flask was then placed at 0 °C before chloro(diisopropyl)phosphine was added dropwise. The mixture was allowed to rise slowly to room temperature and stirred for 3 h. 15 mL of saturated NHCl was added to quench the reaction. The mixture was then extracted with AcOEt. The combined organic layers were washed with brine and dried over $MgSO_4$. Concentration under vacuum gave the crude material which was purified by flash chromatography on silica gel (SiO_2; PE/DCM, 50/50, *v/v*) to afford **6** as a white solid (0.248 g, 48%). ^{1}H NMR (400 MHz, $CDCl_3$, 25 °C) : 7.56-7.3 (m, 1H), 7.30-7.10 (m, 12H), 6.93-6.74 (m, 1H), 2.11-1.87 (m, 2H), 1.05 (dd, *J* = 14.5, 7.0 Hz, 6H), 0.74 (dd, *J* = 12.0, 7.0 Hz, 6H); $^{31}P\{^{1}H\}$ NMR (121 MHz, $CDCl_3$, 25 °C): δ = -3.43 (d, $^{3}J_{P,P}$ = 158.9 Hz), -12.7 (d, $^{3}J_{P,P}$ = 158.9 Hz) ppm. All spectral data are consistent with the literature values.

Nickel dibromo[(2-(diisopropylphosphaneyl-κP)phenyl)diphenylphosphine-κP)] (23)

For references, see page 175.

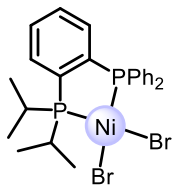

[$NiBr_2$(DME)] (0.063 g, 0.20 mmol) was added to a solution of **6** (0.075 g, 0.20 mmol) in CH_2Cl_2 (8 mL). The mixture was stirred at room temperature for 4 h and then filtered through Celite. Concentration under vacuum gave the crude filtrate which was dried under reduced pressure to afford **7** as an orange powder (0.118 g, in quantitative yield). ^{1}H NMR (500 MHz, CD_2Cl_2, 25 °C) : 7.85-7.72 (m, 5H), 7.68-7.54 (m, 2H), 7.58-7.50 (m, 2H), 7.48-7.38 (m, 5H), 2.97 (m, 2H), 1.52 (d, *J* = 7.0 Hz, 3H), 1.48 (d, *J* = 7.0 Hz, 3H), 1.37 (d, *J* = 7.1 Hz, 3H), 1.34 (d, *J* = 7.1 Hz, 3H); ^{13}C{^{1}H} NMR (126 MHz, CD_2Cl_2, 25 °C): δ = 144.38 (dd, *J* = 51.2, 32.5 Hz), 138.46 (t, *J* = 38.7 Hz), 134.47 (d, *J* = 10.1 Hz), 133.79 (dd, *J* = 14.0, 1.8 Hz), 133.28 (dd, *J* = 6.2, 1.9 Hz), 132.65 (dd, *J* = 5.2, 2.0 Hz), 132.02, 131.88, 131.75 (d, *J* = 2.9 Hz), 131.14, 130.70, 128.91 (d, *J* = 11.1 Hz), 28.95 (d, *J* = 27.4 Hz), 19.94 (d, *J* = 1.8 Hz), 18.85 (d, *J* = 2.0 Hz). ^{31}P{^{1}H} NMR (121 MHz, CD_2Cl_2, 25 °C): δ = 91.44 (d, $^3J_{P,P}$ = 59.9 Hz), 63.36 (d, $^3J_{P,P}$ = 59.9 Hz) ppm; elemental analysis (%) calcd for $C_{24}H_{28}Br_2NiP_2$: C 48.29, H 4.73, found: C 48.00, H 4.65; HRMS (ESI-TOF): *m/z* (%): 515.0198 (100) $[M-Br]^+$.

III. 4. 3. X-ray crystal structures

Complex **17**. A single crystal suitable for X-ray crystal-structure analysis was obtained as described in the Experimental Part. Data were collected at 173(2) K on a Bruker APEX-II Duo KappaCCD diffractometer (Cu-Kα radiation, λ = 1.54178 Å). The structure was solved by direct methods (SHELXS-2013) and refined against F^2 using the SHELXL-2014 software. The non-hydrogen atoms were refined anisotropically, using weighted full-matrix least-squares on F^2. The H-atoms were included in calculated positions and treated as riding atoms using SHELXL default parameters. The crystallographic data are reported in Table 3.

Complex **20**. A single crystal suitable for X-ray crystal-structure analysis was obtained as described in the Experimental Part. Data were collected at 130.15 K on a CCD Saphire 3 Xcalibur diffractometer (Mo-Kα radiation, λ = 0.71073 Å). The structure was solved by direct methods (SHELXS-2013) and refined against F^2 using the SHELXL-2014 software. The non-hydrogen atoms were refined anisotropically, using weighted full-matrix least-squares on F^2. The H-atoms were included in calculated positions and treated as riding atoms using SHELXL default parameters. The crystallographic data are reported in Table 4.

For references, see page 175.

Complex **21**. A single crystal suitable for X-ray crystal-structure analysis was obtained as described in the Experimental Part. Data were collected at 120(2) K on a Bruker PHOTON-III CPAD diffractometer (Mo-Kα radiation, λ = 0.71073 Å). The structure was solved by direct methods (SHELXS-97) and refined against F^2 using the SHELXL-2018 software. The non-hydrogen atoms were refined anisotropically, using weighted full-matrix least-squares on F^2. The H-atoms were included in calculated positions and treated as riding atoms using SHELXL default parameters. The crystallographic data are reported in Table 5.

Complex **22**. A single crystal suitable for X-ray crystal-structure analysis was obtained as described in Experimental Part. Data were collected at 120.15 K on a Bruker PHOTON-III CPAD diffractometer (Mo-Kα radiation, λ = 0.71073 Å). The structure was solved by direct methods (SHELXS-2013) and refined against F^2 using the SHELXL-2014 software. The non-hydrogen atoms were refined anisotropically, using weighted full-matrix least-squares on F^2. The H-atoms were included in calculated positions and treated as riding atoms using SHELXL default parameters. The crystallographic data are reported in Table 6.

For references, see page 175.

Table 3. Crystallographic and structure refinement data for **17**.

Crystal Data	
Crystal size/mm^3	0.35 × 0.25 × 0.15
Empirical formula	$2(C_{70}H_{104}O_{28}P_2Cl_2Pd)•6(C_6H_6)•H_2O$
Formula Weight	3752.19
Crystal system	monoclinic
Space group	$P2_1$
Temperature/K	173(2)
Unit cell parameters	
a/Å	20.7357(5)
b/Å	21.4928(6)
c/Å	21.9876(6)
α/°	90
β/°	104.586(2)
γ/°	90
V/Å^3	9483.4(4)
Z	2
$D_{(calc)}$ g/cm^3	1.314
F (000)	3956.0
μ/mm^{-1}	3.041

Data Processing and Reduction	
2θ range for data collection/°	4.404 to 138.478
Index ranges	$-24 \leq h \leq 23$, $-25 \leq k \leq 25$, $-26 \leq l \leq 26$
Reflections collected	170863
Independent reflections	33318 [R_{int} = 0.0539, R_{sigma} = 0.0476]
Data / restraints / parameters	33318/1/1998
Goodness-of-fit on F^2	1.063
Final R indices [$I > 2\sigma(I)$]	R_1 = 0.0530, wR_2 = 0.1446
R indices (all data)	R_1 = 0.0637, wR_2 = 0.1534
Largest diff. peak and hole/eÅ^{-3}	0.93/-0.68
Flack parameter	0.022(2)

For references, see page 175.

Table 4. Crystallographic and structure refinement data for **20**.

Crystal Data	
Crystal size/mm^3	0.337 × 0.76 × 0.13
Empirical formula	$C_{70}H_{104}O_{28}P_2Cl_2Pd$•0.5($C_{2.5}Cl$)•5($CH_2Cl_2$)
Formula Weight	2090.14
Crystal system	orthorhombic
Space group	$P2_12_12_1$
Temperature/K	130.15
Unit cell parameters	
a/Å	14.1571(2)
b/Å	21.8506(4)
c/Å	32.0204(8)
α/°	90
β/°	90
γ/°	90
V/Å^3	9905.2(3)
Z	4
$D_{(calc)}$ g/cm^3	1.402
F (000)	4336.0
μ/mm^{-1}	0.626

Data Processing and Reduction	
2θ range for data collection/°	6.60 to 54
Index ranges	$-18 \leq h \leq 18$, $-27 \leq k \leq 27$, $-38 \leq l \leq 40$
Reflections collected	84724
Independent reflections	21577 [R_{int} = 0.1662, R_{sigma} = 0.1918]
Data / restraints / parameters	21577/1/1083
Goodness-of-fit on F^2	1.052
Final R indices [$I > 2\sigma(I)$]	R_1 = 0.0962, wR_2 = 0.2031
R indices (all data)	R_1 = 0.1919, wR_2 = 0.2488
Largest diff. peak and hole/eÅ^{-3}	0.86/-0.49
Flack parameter	-0.01(5)

For references, see page 175.

Table 5. Crystallographic and structure refinement data for **21**.

Crystal Data	
Crystal size/mm^3	0.2 × 0.2 × 0.15
Empirical formula	$2(C_{71}H_{107}O_{28}P_2ClPd)\bullet5(CH_2Cl_2)$
Formula Weight	3649.33
Crystal system	orthorhombic
Space group	$P2_12_12_1$
Temperature/K	120(2)
Unit cell parameters	
a/Å	14.1758(7)
b/Å	21.8479(13)
c/Å	31.863(2)
α/°	90
β/°	90
γ/°	90
V/Å^3	9868.4(10)
Z	2
$D_{(calc)}$ g/cm^3	1.228
F (000)	3820.0
μ/mm^{-1}	0.449

Data Processing and Reduction	
2θ range for data collection/°	3.846 to 55.958
Index ranges	$-17 \le h \le 18$, $-28 \le k \le 28$, $-41 \le l \le 42$
Reflections collected	154369
Independent reflections	23661 [R_{int} = 0.1111, R_{sigma} = 0.0790]
Data / restraints / parameters	23661/54/1004
Goodness-of-fit on F^2	1.007
Final R indices [$I > 2\sigma(I)$]	R_1 = 0.0952, wR_2 = 0.2552
R indices (all data)	R_1 = 0.1447, wR_2 = 0.2920
Largest diff. peak and hole/eÅ^{-3}	1.04/-1.18
Flack parameter	0.005(8)

For references, see page 175.

Table 6. Crystallographic and structure refinement data for **22**.

Crystal Data	
Crystal size/mm^3	0.25 × 0.2 × 0.15
Empirical formula	$C_{71}H_{107}O_{28}P_2ClPd•7(C_6H_6)$
Formula Weight	2220.839
Crystal system	orthorhombic
Space group	$P2_12_12_1$
Temperature/K	120.15
Unit cell parameters	
a/Å	14.2347(8)
b/Å	27.9371(17)
c/Å	28.0821(15)
α/°	90
β/°	90
γ/°	90
V/Å^3	11167.6(11)
Z	4
$D_{(calc)}$ g/cm^3	1.321
F (000)	4683.1
μ/mm^{-1}	0.991

Data Processing and Reduction	
2θ range for data collection/°	4.08 to 55.86
Index ranges	$-18 \leq h \leq 18$, $-36 \leq k \leq 36$, $-36 \leq l \leq 36$
Reflections collected	189195
Independent reflections	26682 [R_{int} = 0.0649, R_{sigma} = 0.0485]
Data / restraints / parameters	26682/0/1310
Goodness-of-fit on F^2	1.033
Final R indices [$I > 2\sigma(I)$]	R_1 = 0.0321, wR_2 = 0.0634
R indices (all data)	R_1 = 0.0459, wR_2 = 0.0694
Largest diff. peak and hole/eÅ^{-3}	0.36/-0.50
Flack parameter	0.021(2)

For references, see page 175.

III. 5. References

1. Kamer, P. C.; Leeuwen, P. W. v., *Phosphorus(III) Ligands in Homogeneous Catalysis Design and Synthesis*. UK: John Wiley & Sons, **2012**.

2. (a) Fey, N.; Orpen, A. G.; Harvey, J. N., Building ligand knowledge bases for organometallic chemistry: Computational description of phosphorus(III)-donor ligands and the metal–phosphorus bond. *Coord. Chem. Rev.* **2009,** *253*, 704-722. (b) Spessard, G. O.; Miessler, G. L., *Organometallic Chemistry*. OXFORD UNIVERSITY PRESS: **2010**. (c) Crabtree, R. H., *The organometallic chemistry of the transition metals*. Canada: John Wiley & Sons, **2009**.

3. (a) Matt, D.; Harrowfield, J., Phosphines and other P(III)‐derivatives with Cavity‐shaped Subunits: Valuable Ligands for Supramolecular Metal Catalysis, Metal Confinement and Subtle Steric Control. *ChemCatChem* **2021,** *13*, 153-168. (b) Dennett, J. N. L.; Gillon, A. L.; Heslop, K.; Hyett, D. J.; Fleming, J. S.; Lloyd-Jones, C. E.; Orpen, A. G.; Pringle, P. G.; Wass, D. F.; Scutt, J. N.; Weatherhead, R. H., Diphosphine Complexes of Nickel(II) Are Efficient Catalysts for the Polymerization and Oligomerization of Ethylene: Steric Activation and Ligand Backbone Effects. *Organometallics* **2004,** *23*, 6077-6079. (c) Chen, C., Designing catalysts for olefin polymerization and copolymerization: beyond electronic and steric tuning. *Nat. Rev. Chem.* **2018,** *2*, 6-14.

4. (a) Pignolet, L. M., *homogeneous catalysis with metal phosphine complexes*. New York: Plenum Press, **1983**. (b) Van Leeuwen, P. W. N. M.; Kamer, P. C. J.; Reek, J. N. H.; Dierkes, P., Ligand Bite Angle Effects in Metal-catalyzed C−C Bond Formation. *Chem. Rev.* **2000,** *100*, 2741-2770. (c) Birkholz (Née Gensow), M.-N.; Freixa, Z.; Van Leeuwen, P. W. N. M., Bite angle effects of diphosphines in C–C and C–X bond forming cross coupling reactions. *Chem. Soc. Rev.* **2009,** *38*, 1099. (d) Freixa, Z.; Van Leeuwen, P. W. N. M., Bite angle effects in diphosphine metal catalysts: steric or electronic? *Dalton Trans.* **2003,** *2003*, 1890-1901. (e) Lejeune, M.; Sémeril, D.; Jeunesse, C.; Matt, D.; Peruch, F.; Lutz, P. J.; Ricard, L., Diphosphines with Expandable Bite Angles: Highly Active Ethylene Dimerisation Catalysts Based on Upper Rim, Distally Diphosphinated Calix[4]arenes. *Eur. J. Chem.* **2004,** *10*, 5354-5360.

5. (a) Ojima, I., *Catalytic Asymmetric Synthesis*. Canada: John Wiley & Sons, Inc., **2010**. (b) Evans, D.; Osborn, J. A.; Wilkinson, G., Hydroformylation of alkenes by use of rhodium complex catalysts. *J. Chem. Soc. A: Inorganic, Physical, Theoretical* **1968**, 3133. (c) Gual, A.; Godard, C.; Castillón, S.; Claver, C., Highlights of the Rh-catalysed asymmetric hydroformylation of alkenes using phosphorus donor ligands. *Tetrahedron: Asymmetry* **2010,**

For references, see page 175.

21, 1135-1146. (d) Ungváry, F., Application of transition metals in hydroformylation. *Coord. Chem. Rev.* **2007,** *251*, 2087-2102. (e) van Leeuwen, P. W. N. M., *Homogeneous Catalysis-Understanding the Art*. Dordrecht: Kluwer, **2004**. (f) van Leeuwen, P. W. N. M., Decomposition pathways of homogeneous catalysts. *Appl. Catal. A: Gen.* **2001,** *212*, 61-81. (g) Moteki, S. A.; Wu, D.; Chandra, K. L.; Reddy, D. S.; Takacs, J. M., TADDOL-Derived Phosphites and Phosphoramidites for Efficient Rhodium-Catalyzed Asymmetric Hydroboration. *Org. Lett.* **2006,** *8*, 3097-3100. (h) Klosin, J.; Landis, C. R., Ligands for Practical Rhodium-Catalyzed Asymmetric Hydroformylation. *Acc. Chem. Res.* **2007,** *40*, 1251-1259. (i) Saudan, L. A., Hydrogenation Processes in the Synthesis of Perfumery Ingredients. *Acc. Chem. Res.* **2007,** *40*, 1309-1319. (j) Chakrabortty, S.; Almasalma, A. A.; De Vries, J. G., Recent developments in asymmetric hydroformylation. *Catal. Sci. Technol.* **2021,** *11*, 5388-5411. (k) Jagtap, S. A.; Bhanage, B. M., Rhodium/Phosphine catalysed selective hydroformylation of biorenewable olefins. *Appl. Organomet. Chem.* **2018,** *32*, e4478. (l) Császár, Z.; Bakos, J.; Farkas, G., Sulfonated Phosphine Ligands in the Ruthenium Catalyzed Biphasic Hydrogenation of Unsaturated Hydrocarbons. *Cata. Lett.* **2020,** *150*, 2529-2536.

6. (a) Jouffroy, M.; Gramage-Doria, R.; Semeril, D.; Armspach, D.; Matt, D.; Oberhauser, W.; Toupet, L., Phosphinocyclodextrins as confining units for catalytic metal centres. Applications to carbon-carbon bond forming reactions. *Beilstein J. Org. Chem.* **2014,** *10*, 2388-405. (b) Engeldinger, E.; Poorters, L.; Armspach, D.; Matt, D.; Toupet, L., Diastereospecific synthesis of phosphinidene-capped cyclodextrins leading to "introverted" ligands. *Chem. Commun.* **2004,** *2004*, 634-635.

7. (a) Gadzikwa, T.; Bellini, R.; Dekker, H. L.; Reek, J. N. H., Self-Assembly of a Confined Rhodium Catalyst for Asymmetric Hydroformylation of Unfunctionalized Internal Alkenes. *J. Am. Chem. Soc.* **2012,** *134*, 2860-2863. (b) García-Simón, C.; Gramage-Doria, R.; Raoufmoghaddam, S.; Parella, T.; Costas, M.; Ribas, X.; Reek, J. N. H., Enantioselective Hydroformylation by a Rh-Catalyst Entrapped in a Supramolecular Metallocage. *J. Am. Chem. Soc.* **2015,** *137*, 2680-2687. (c) Tran, D. N.; Legrand, F. X.; Menuel, S.; Bricout, H.; Tilloy, S.; Monflier, E., Cyclodextrin-phosphane possessing a guest-tunable conformation for aqueous rhodium-catalyzed hydroformylation. *Chem. Commun. (Camb)* **2012,** *48*, 753-755.

8. (a) Gramage-Doria, R.; Armspach, D.; Matt, D.; Toupet, L., A Cavity-Shaped Diphosphane Displaying "Oschelating" Behavior. *Angew. Chem.* **2011,** *123*, 1592-1597. (b) Gramage-Doria, R.; Rodriguez-Lucena, D.; Armspach, D.; Egloff, C.; Jouffroy, M.; Matt, D.; Toupet, L., Regioselective Double Capping of Cyclodextrin Scaffolds. *Eur. J. Chem.* **2011,** *17*, 3911-3921. (c) Gramage-Doria, R.; Armspach, D.; Matt, D.; Toupet, L., Non-conventional coordination of

For references, see page 175.

cavity-confined metal centres. *Dalton Trans.* **2012,** *41*, 8786-8796. (d) Poorters, L.; Armspach, D.; Matt, D.; Toupet, L.; Choua, S.; Turek, P., Synthesis and properties of TRANSDIP, a rigid chelator built upon a cyclodextrin cavity: is TRANSDIP an authentic trans-spanning ligand? *Chemistry* **2007,** *13*, 9448-9461.

9. Phan, T.-A., PhD Thesis. *Université de Strasbourg* **2019**.

10. (a) Basra, S.; De Vries, J. G.; Hyett, D. J.; Harrison, G.; Heslop, K. M.; Orpen, A. G.; Pringle, P. G.; Von Der Luehe, K., Efficient asymmetric hydrogenation with rhodium complexes of C(1)-symmetric 2,5-dimethylphospholane-diphenylphosphines. *Dalton Trans.* **2004,** *2004*, 1901-1905. (b) Bonnaventure, I.; Charette, A. B., Probing the Importance of the Hemilabile Site of Bis(phosphine) Monoxide Ligands in the Copper-Catalyzed Addition of Diethylzinc to N-Phosphinoylimines: Discovery of New Effective Chiral Ligands. *J. Org. Chem.* **2008,** *73*, 6330-6340.

11. Machnitzki, P.; Nickel, T.; Stelzer, O.; Landgrafe, C., Novel Syntheses of Mono- and Bisphosphonated Aromatic Phosphanes by Consecutive Pd-Catalyzed P–C Coupling Reactions and Nucleophilic Phosphanylation – X-ray Structure of $Ph_2P–C_6H_4–m\text{-}PO_3Na_2·5.5\ H_2O·iPrOH$. *Eur. J. Inorg. Chem.* **1998,** *1998*, 1029-1034.

12. (a) Snape, T. J., A truce on the Smiles rearrangement: revisiting an old reaction—the Truce–Smiles rearrangement. *Chem. Soc. Rev.* **2008,** *37*, 2452. (b) Henderson, A. R. P.; Kosowan, J. R.; Wood, T. E., The Truce–Smiles rearrangement and related reactions: a review. *Can. J. Chem.* **2017,** *95*, 483-504. (c) Holden, C. M.; Greaney, M. F., Modern Aspects of the Smiles Rearrangement. *Eur. J. Chem.* **2017,** *23*, 8992-9008.

13. Kyba, E. P.; John, A. M.; Brown, S. B.; Hudson, C. W.; Mcphaul, M. J.; Harding, A.; Larsen, K.; Niedzwiecki, S.; Davis, R. E., Triligating 11-membered rings containing tert-phosphino sites. Synthesis and structure. *J. Am. Chem. Soc.* **1980,** *102*, 139-147.

14. (a) Agostinho, M.; Braunstein, P., Structurally characterized intermediates in the stepwise insertion of CO–ethylene or CO–methyl acrylate into the metal–carbon bond of Pd(II) complexes stabilized by (phosphinomethyl)oxazoline ligands. *Chem. Commun.* **2007,** *2007*, 58-60. (b) Verstuyft, A. W.; Redfield, D. A.; Cary, L. W.; Nelson, J. H., Palladium(II) complexes of benzylphosphorus ligands. *Inorg. Chem.* **1977,** *16*, 2776-2786. (c) Verstuyft, A. W.; Redfield, D. A.; Cary, L. W.; Nelson, J. H., "Mixed-ligand" bis-monodentate phosphorus donor ligand complexes of palladium(II), $LL'PdCl_2$. A comprehensive investigation. *Inorg. Chem.* **1976,** *15*, 1128-1133. (d) Morise, X.; Braunstein, P.; Welter, R., Enolphosphato−Phosphines: A New Class of P,O Ligands. *Inorg. Chem.* **2003,** *42*, 7752-7765.

15. Ai, P.; Danopoulos, A. A.; Braunstein, P., Non-symmetric diphosphines based on the

For references, see page 175.

imidazole scaffold: an unusual group interchange involving Pd–CH_3 and (imidazole)P–Ph cleavage. *Dalton Trans.* **2014,** *43*, 1957-1960.

16. Li, Y.; Chakrabarty, S.; Mück-Lichtenfeld, C.; Studer, A., Ortho-Trialkylstannyl Arylphosphanes by C-P and C-Sn Bond Formation in Arynes. *Angew. Chem. Int. Ed.* **2016,** *55*, 802-806.

For references, see page 175.

Chapter IV

Ethylene oligomerization catalyzed by nickel and palladium complexes derived from cavity-shaped *cis*-chelating ligands

IV. 1. Introduction

As the most produced polymeric material on the market, polyolefins have played a pivotal role in the development of macromolecular chemistry and have had an enormous impact on society since the 1950s.[1] The shorter analogs of polyolefins that are the linear α-olefins (LAO), which are alkenes with a double bond positioned at the chain end, have seen a parallel development since both types of compounds, polyethylene and LAOs, are usually produced by means of metal catalysts that bear strong resemblance. These unsaturated short chains have their own economic importance as they are used as co-monomers for the production of branched polyolefins. They also constitute starting materials for the production of detergents, lubricants, oilfield chemicals and many chemical intermediates.[2] There are several processes that can be used to produce LAOs, the main ones being the cracking of waxes, Fischer-Tropsch synthesis and the oligomerization of ethylene. Since ethylene is a cheap and readily available feedstock, the metal-catalyzed oligomerization of ethylene is now the most common way of producing LAOs in industry.[3] The remarkable development of the polyolefin and LAO industry is largely attributable to the use of efficient and versatile olefin polymerization/oligomerization catalysts based on transition metals. The development of such metal catalysts has gone through three main phases that were first initiated by the serendipitous discovery of the "nickel effect" which occurs when small amounts of nickel salts are mixed with triethylaluminium ($AlEt_3$) in the presence of ethylene and leads to the dimerization of ethylene.[4] Shortly after the Ziegler-Natta catalyst which combines a group 4 metal salt, usually titanium, with a trialkylaluminium co-catalyst (eg. [$TiCl_4 \cdot AlEt_3$]) was developed as the first generation of transition metal catalysts for ethylene polymerization and opened a new chapter in the development of the polyolefin industry.[5] In these systems, the trialkylaluminum compound acts as Lewis acid that abstracts the halide from the transition metal and at the same time serves as an alkylating agent so that the propagation reaction can be triggered in the presence of ethylene. The seminal work in the field of metal-catalyzed olefin polymerization carried out by Ziegler and Natta was rewarded with the Nobel Prize in Chemistry in 1963.[6] Despite the fact that Ziegler-Natta catalysts are of great importance for academic and industrial research in the field of polyolefins, the heterogeneous nature of this system has prevented further detailed investigation of the catalytic mechanism, as well as the design of new catalysts.[7] To overcome these problems, the next breakthrough was the development of homogeneous single-site metallocene catalysts together with the discovery of methylaluminoxane (MAO) as co-catalyst by Kaminsky and his co-

For references, see page 191.

workers in 1980s.[8] These metallocene catalysts which possess well-defined active sites, were found to allow more precise control of the polymer structure in terms of molecular weight, molecular-weight dispersity, as well as polymer stereochemistry, resulting in their widespread use in industrial polyolefin production. However, most of these systems require alkylaluminium compounds or MAO in large excess (> 500 equivalents) as cocatalyst to generate the active alkyl-M (M = Ti, Zr, etc.), adding to the cost of the process and making it not as attractive to industry as initially predicted. Furthermore, metallocene catalysts are unable to catalyze the copolymerization of olefins with polar functional groups because their metal centers are sensitive to deactivation by the polar functional groups during copolymerization.[1, 9]

In 1995, Brookhart and co-workers[10] reported catalysts based on nickel(II) and palladium(II) complexes of bulky bidentate diimine ligands. These systems were the first examples of late transition metal catalysts capable of producing high molecular weight polyolefins instead of butene. This was another important step in ethylene polymerization and remains a very active research area. Modification of the catalysts used for polymerization can lead to a shortening of the chains, in particular with less bulky ligands, resulting in oligomerization catalysts aimed at producing LAOs.[11] However, specific catalysts have been developed over the years aiming at this type of molecule. In particular, Keim and co-workers introduced nickel catalysts based on chelating P,O-ligands, which are currently used industrially in the "SHOP" (Shell Higher Olefin Process) ethylene oligomerization process (Fig 1).[12] Since then, numerous other bidentate ligands coordinated to late transition metals such as Ni(II) and Pd(II), including some in our laboratory, have since been designed for the same purposes but with the objective of improving chain-length selectivity among them mainly [N,N] of the diimine type, but also [N,O], [P,O], [NHC,O][7,9b,9c,11a,13]. Alternatively, access to linear α-olefins with very narrow distributions is also possible with chromium-type catalysts such as the Phillips Trimerization System.[14] Unlike SHOP-type systems, these catalysts rely on the formation of metallocyclic intermediates and do not operate via a 1,2 insertion (Cossee-Arlman[15]) mechanism.

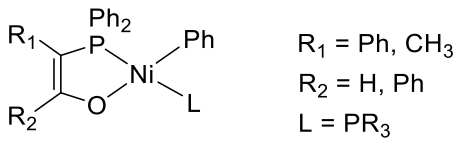

Fig 1. Molecular active Ni catalyst (SHOP process).

For references, see page 191.

The general mechanism of late transition metal catalyst for ethylene oligomerization via 1,2 insertion (Cossee-Arlman) is represented in Scheme 1.[13f]

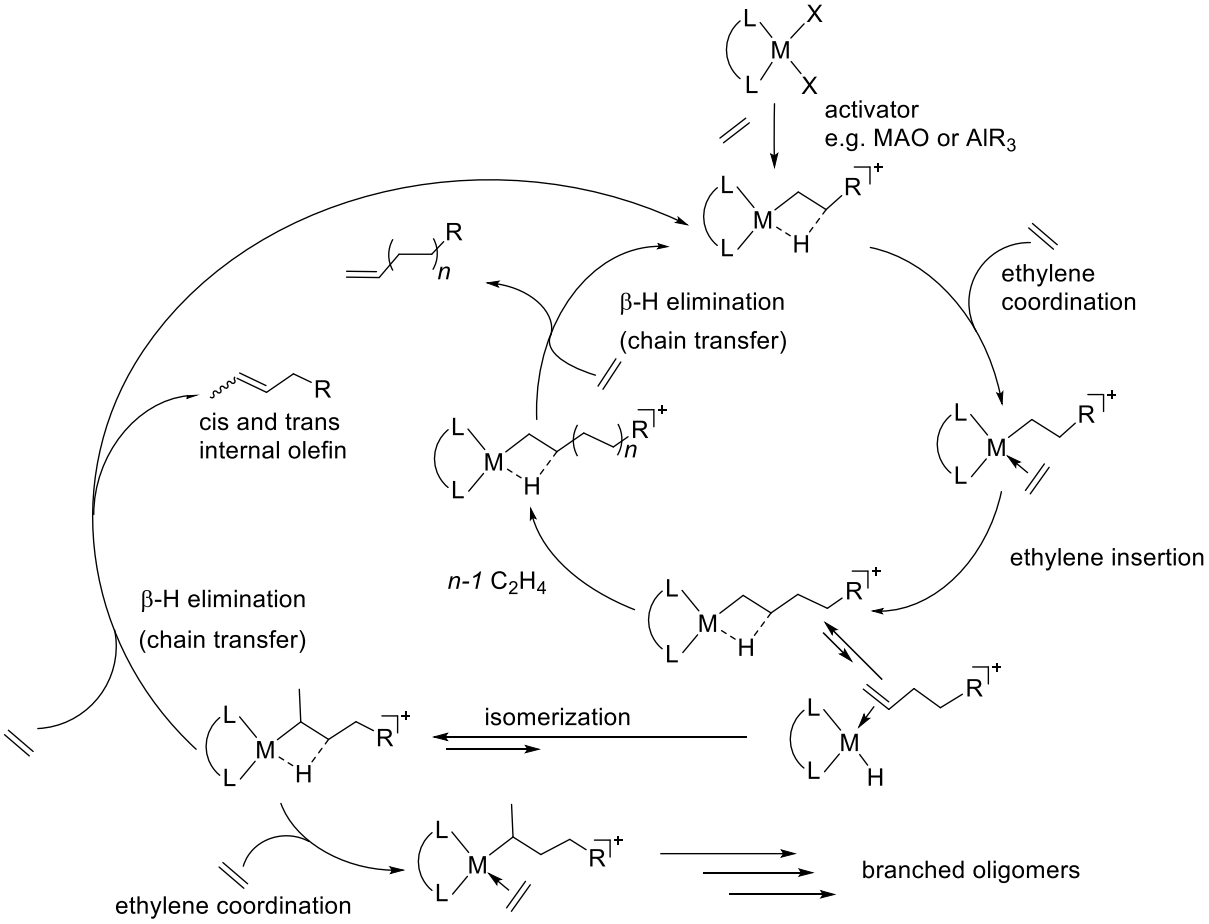

Scheme 1. The mechanism of catalytic ethylene oligomereization/polymerization.[13f]

There are basically two steps that control chain growth in ethylene oligomerization/polymerization. These are the propagation step (ethylene insertion) and termination step (including β-hydride elimination and chain transfer). If the kinetics of these two processes can be controlled, it should be possible to adjust the catalytic performance in terms of chain-length selectivity. Moreover, if the isomerization of the growing chain, which is the reaction in the catalytical cycle that leads eventually to chain walking and the formation of branched species, can be suppressed, linear chains with a double bond positioned at the chain-end will be produced. Classically, late transition metal catalysts most often dimerize or oligomerize ethylene due to favorable β-hydride elimination. However, the nature of the ligand, that of the co-catalyst and more generally the reaction conditions used (ethylene pressure, excess co-catalyst, temperature, reaction time, etc.) will also have a deep impact on the

For references, see page 191.

catalytic properties. A key element in designing nickel(II) and palladium(II) systems that polymerize olefins is to introduce axial bulk in square planar systems, for example through the use aryl diimine ligands ortho-disubstituted with bulky substituents including in macrocyclic systems[16]. This feature was shown to retard the rate of chain transfer relative to chain propagation and a number of nickel(II) and palladium(II) polymerization catalysts containing different bulky bidentate ligands have been designed according to these principles.[17] With this in mind, a series of Ni(II) and Pd(II) catalysts incorporating an α-CD framework was prepared. The presence of a molecular cavity encapsulating the metal center should provide axial bulk as in previous nonmacrocyclic systems and therefore promote chain growth. However, metal encapsulation is also prone to slow down propagation and therefore favor termination reactions in particular if the growing chain attached to the metal is too long. It is expected that these two opposite effects will lead to chains of a given length with a narrow chain distribution. The aim of this chapter is to study the behavior of the precatalysts that were constructed according to these principles in chapters 2 and 3 in ethylene oligomerization.

IV. 2. Results and discussion

The capability of the cavity-shaped nickel(II) complexes **6**, **19** and **22** to catalyze ethylene oligomerization in toluene were studied in the presence of excess modified-methylaluminoxane (MMAO-12) as co-catalyst. Their performances were compared to cavity-free complexes **12**, **23**, and **24** in order to evaluate the impact of the cavity on the catalytic properties.

Table 1. Ethylene oligomerization with nickel complexes **6**, **12**, **19** and **22-24** [a].

					Products weight distribution[d] (%)		
Entry	Precatalyst	Time	Activity[b]	TOF[c]	C_4 (α)[e]	C_6 (α)[f]	C_8
1	**6**	35 min	2760	5780	92 (95)	6 (70)	2
2	**6**	3 h	2190	4580	96 (95)	3 (75)	<1
3	**6**	24 h	1910	4000	85 (92)	12 (65)	3
4 [g]	**6**	35 min	2720	5700	95 (88)	4 (46)	<1
5 [h]	**6**	35 min	6440	13350	91 (89)	8 (41)	<1
6	**12**	35 min	41570	86970	77 (71)	22 (8)	1
7	**12**	3 h	17920	37490	79 (81)	19 (8)	2
8	**12**	24 h	5740	12000	75 (67)	24 (6)	1

For references, see page 191.

9	**19**	35 min	1000	2070	98 (88)	2 (100)	0
10	**19**	24 h	500	1050	91 (82)	8 (75)	<1
11 [g]	**19**	35 min	1290	2060	98 (87)	1 (100)	<1
12	**22**	35 min	10400	21800	87 (71)	11 (60)	<2
13	**22**	24 h	1220	2560	82 (74)	14 (64)	<4
14 [g]	**22**	35 min	10900	22800	87 (67)	12 (52)	<1
15	**23**	35 min	5880	12330	93 (61)	6 (50)	<1
16	**24**	35 min	8530	17870	92 (20)	7 (8)	<1
17	**24**	24 h	4180	8760	89 (6)	9 (1)	<2

[a] Conditions: amount of catalyst: 1×10^{-5} mol, amount of co-catalyst (MMAO-12): 4×10^{-3} mol (400 equiv.), T = 30-35 °C, solvent: toluene, total volume: 20 mL, 10 bar C_2H_4, every test was repeated at least twice. [b] expressed in g C_2H_4/(g Ni h). [c] expressed in mol C_2H_4/(mol Ni h). [d] % calculated by GC analysis. [e] 1-Butene *vs.* total butenes formed. [f] 1-Hexene *vs.* total hexenes formed. [g] amount of co-catalyst (MMAO-12): 8×10^{-3} mol (800 equiv.). [h] T = 60 °C.

As shown in Table 1, after activation with MMAO-12, the nickel complex **6** catalyzes the dimerization of ethylene with high C_4 (92%) and 1-butene (95%) selectivities (Table 1, entry 1), even after 24 h reaction time (Table 1, entry 3), indicating that chain-walking and post-oligomerization reactions do not readily take place. Moreover, the proportion of 1-hexene in the small C_6 fraction is also much higher with the cavity-shaped ligand (70% on average for **6**). Even if such level of selectivity is not uncommon for early transition metals, it is quite high for a nickel-catalyzed reaction. For comparison, the related nickel complex **12** (Table 1, entry 4), which has similar electronic properties, but lacks the CD cavity is about 15 times more active for short reaction times, but its activity rapidly drops with time as it is only 3 fold higher than that of **6** after 24 h (Table 1, entry 6). It is much less selective for C_4 (77%) and 1-butene (71%) as well as 1-hexene (8%), whether for short (Table 1, entry 4) or longer reaction times (Table 1, entries 5 and 6). These poor selectivities were also observed for many other P,N nickel complexes except for ligands displaying sterically hindered nitrogen or phosphorus atoms. Although moderately active (TOF = 5780 mol(C_2H_4) mol $(Ni)^{-1}$ h^{-1}) (Table 1, entry 1), the catalyst derived from **6** proved to be very robust, since loss of activity is marginal over a prolonged period of time in stark contrast with cavity-free **12**. Despite the steric protection of axial positions, which is known to retard the rate of chain transfer relative to chain propagation and improve thermal stability, including in macrocyclic complexes, hardly any C_6-olefins and

For references, see page 191.

higher oligomers were formed. The high selectivity for 1-butene strongly suggests that metal encapsulation in the rather small α-CD cavity does not allow further chain growth and largely prevents isomerization although the ligand electronic properties as revealed by slight changes in the UV spectra (see chapter 2) on going from cavity-free to cavity-shaped systems may also have an impact on the catalytic outcome.

Moreover, the influence of the quantity of co-catalyst and the starting reaction temperature for **6** were also investigated. The results show that increasing the quantity of the co-catalyst (800 equiv.) does not bring any significant changes to activity or selectivity (Table 1, entry 4). When the starting temperature was increased to 60 °C, the activity is about 3 times higher (6440 $g(C_2H_4)\ g(Ni)^{-1}\ h^{-1}$) and, as expected, the 1-butene (89%) and 1-hexene (41%) selectivities are somewhat lower although the C_4 selectivity (91%) remains almost unchanged. These observations suggest that higher temperatures may favor chain walking and isomerization to a certain extent. Complex **19**, which shares strong resemblance with P,N complex **6** in the way the metal is located in the CD cavity, shows similar tendencies to **6** in terms of selectivity, although with a somewhat lower activity (1000 $g(C_2H_4)\ g(Ni)^{-1}\ h^{-1}$). Again, as for **6,** the C4 selectivity is extremely high (98%). Although slightly lower than for **6**, 1-butene selectivity (88%) (Table 1, entry 9) remains high, even after 24 h reaction (Table 1, entry 10) (C4: 91%, 1-butene: 82%). Again, increasing the quantity of the co-catalyst (800 equiv.) does not bring any significant changes to activity or selectivity (Table 1, entry 11). Although less active than their cavity-free counterparts **23** and **24**, cavity-shaped **19** systematically outperformed all cavity-free complexes in terms of selectivity. The drop of activity on going from P,N complex **6** to the more sterically hindered P,P complex **19** is most likely a combination of steric and electronic factors since Ni complexes based on P,N complexes are known to be more active.[11, 13k, 17j, 18] Surprisingly, complex **22** is much more active (10400 $g(C_2H_4)\ g(Ni)^{-1}\ h^{-1}$) than all other cavity-shaped complexes (10 times that of **19**) and even cavity-free P,P complexes **23** and **24** over a short period of time, but, unlike **6** and **19**, its activity rapidly drops with time as it is only two-fold higher than that of **19** after 24 h (Table 1, entry 13). The surprisingly high activity of **22** is likely due to the close contact promoted by encapsulation between the metal-alkyl moiety and the coordinated ethylene. Such a feature should facilitate the ethylene insertion step in the catalytic cycle and therefore the activity if this step is rate-limiting. Moreover, the poor robustness of **22** compared to catalysts **6** and **19** is possibly due to the lack of steric protection of the axial sites. Finally, the higher activity of **22** comes at the expense of selectivity since selectivity for C_4 and α-olefins (1-butene and 1 hexene) are much lower than those produced by **6** and **19**, whether for short or long reaction times. The radically different

For references, see page 191.

behavior between these two α-CD-containing complexes might come from the very different steric environment the metal center experiences in **19** since in this complex the axial sites are well-protected and, upon methylation and halide abstraction by MMAO, the two reactive sites are strongly differentiated, which is not the case for **22**. For comparison, complex **23**, which has very similar electronic features to **19** but lacks the CD cavity, showed an activity 5 times (Table 1, entry 15) higher than that of **19** but as stated before without any good selectivities. Since the macrocyclic structure has little influence on the electronic properties of the ligands, at least in the case of the diphosphines, the differences of catalytic properties between the cavity-free and the cavity-shaped catalysts is solely due the unique steric experiment experienced by the metal center within the α-CD cavity.

The PdMeCl complexes **5** and **21a**,**b** were also tested for ethylene oligomerization using $NaBArF_{24}$ to activate the pre-catalyst, even if palladium complexes are known to be much less active catalysts than nickel ones.[19] Upon addition of one equiv. of $NaBArF_{24}$ in the presence of small amounts of the coordinating solvent MeCN (20 equiv.), the abstraction of chloride was complete after 1 h in the case of diphosphine complex **21**, but took surprisingly a longer time (2 h) for P,N complex **5**. Whereas the ^{31}P atom of P,N complex **5** underwent a 7.1 ppm downfield shift (δ_{31P} = 25.21 ppm upon addition of $NaBArF_{24}$), the mixture **21a**,**b** became a single species resonating as two downfield shifted doublets at δ_{31P} = 66.60 and 67.22 ppm with $^{3+2}J_{P,P}$ = 11.4 Hz. Unfortunately, all attempts to oligomerize ethylene with these two activated complexes failed whether in toluene or in the more polar solvent CH_2Cl_2 since the formation of only traces of butenes was observed.

For references, see page 191.

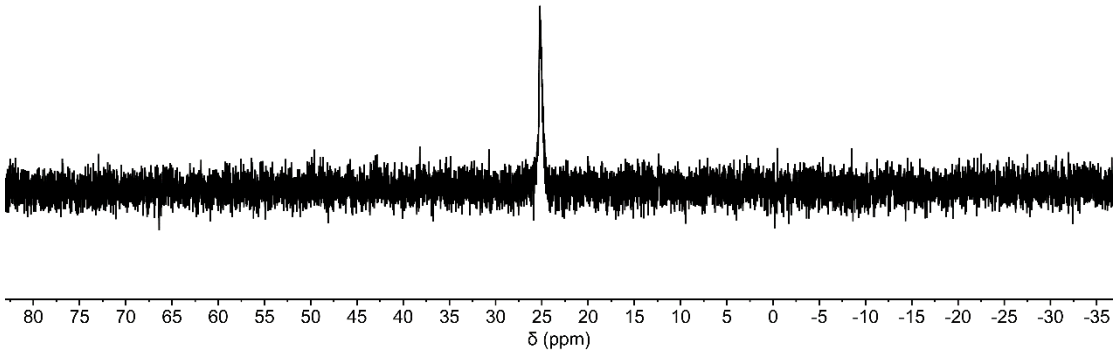

Fig 2. $^{31}P\{^{1}H\}$ NMR spectrum of **5** after activation by $NaBArF_{24}$.

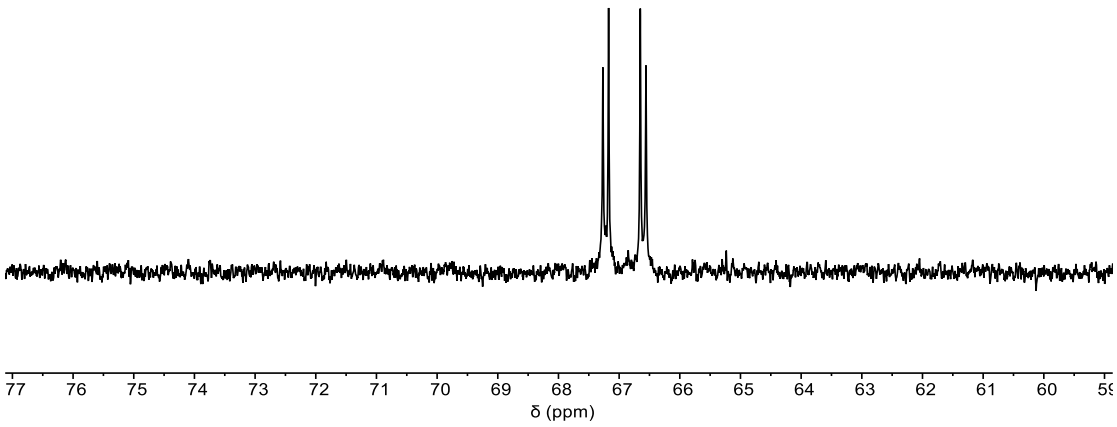

Fig 3. $^{31}P\{^{1}H\}$ NMR spectrum of **21a**, **b** after activation by $NaBArF_{24}$.

For references, see page 191.

IV. 3. Conclusion

Ni(II) and Pd(II) complexes based on cavity-shaped P,N or diphosphine bidentate ligands were tested for their ability to oligomerize ethylene and their catalytic properties were compared to the corresponding cavity-free analogs. In stark contrast with the latters, nickel(II) complexes equipped with a permethylated α-CD platform give rise to a high selectivity for C_4 (up to 96%) and 1-butene (up to 95% of the C_4 fraction) when the axial sites are protected by the cavity wall as in **6** and **19**. Complex **22**, in which the axial sites of the metal center are less protected and which halido ligands are lying in the more or less same, albeit heavily constrained, steric environment, has a much higher activity compared to all other cavity-shaped complexes **6** and **19**, but much lower selectivities and robustness. Their corresponding palladium complexes **5** and **21a,b** were also tested as precatalysts for ethylene oligomerization, but showed hardly any activity. Theoretical investigations will be carried out in the near future to thoroughly rationalize the difference of catalytic properties between the two types of Ni complexes. The synthesis of larger analogs of complexes **4**-**6**, **17**-**22** based on the wider β-CD cavity is also currently underway. It is hoped that chain growth will be more favored in these less constrained catalysts so as to obtain longer oligomers than butenes with a narrow chain distribution.

IV. 4. Experimental part

IV. 4. 1. Procedure for ethylene oligomerization reactions

IV. 4. 1. 1. Ethylene oligomerization reactions catalyzed by nickel complexes

The catalytic reactions were performed in a magnetically stirred (1200 rmp) 145 mL stainless steel autoclave. A 125 mL glass container was used to avoid corrosion of the autoclave walls. The precatalyst solution was prepared by dissolving 1×10^{-5} mol of the complex in toluene. This solution was injected into the reactor under an ethylene flux, followed by the co-catalyst solution (400 equiv. for MMAO-12 in toluene). After injection of the catalyst and co-catalyst solutions under a constant low flow of ethylene, which is considered as the t_0 time, the reactor was immediately pressurized to 10 bar of ethylene. The 10 bar working pressure was maintained through a continuous feed of ethylene from a bottle placed on a balance to allow monitoring of the ethylene uptake. The reaction mixture was stirred for the given reaction time. At the end of each test, a dry ice bath was used to rapidly cool the reactor. When the inner

For references, see page 191.

temperature reached 0 °C, the ice bath was removed, allowing the temperature to slowly rise to 18 °C. The gaseous phase was then transferred into a 10 L polyethylene tank filled with water. An aliquot of this gaseous phase was transferred into a Schlenk flask, previously evacuated, for GC analysis. The amount of ethylene consumed was thus determined by differential weighting of the bottle (accuracy of the scale: 0.01g). To this amount of ethylene, the remaining ethylene (calculated using the GC analysis) in the gaseous phase was subtracted. Although this method is of limited accuracy, it was used throughout and it gave satisfactory reproducibility. The reaction mixture in the reactor was quenched *in situ* by the addition of ethanol (5 mL), transferred into a Schlenk flask, and separated from the metal complexes by trap-to-trap evaporation into a second Schlenk flask previously immersed in liquid nitrogen in order to avoid loss of product for GC analysis. Each catalytic test was performed at least twice to ensure the reproducibility of the results.

IV. 4. 1. 2. Ethylene oligomerization reactions catalyzed by palladium complexes

The catalytic reactions were performed in a magnetically stirred (1200 rmp) 145 mL stainless steel autoclave. A 125 mL glass container was used to avoid corrosion of the autoclave walls. A Schlenk tube was charged with PdMeCl complex (1 equiv.) and CH_2Cl_2 under an argon atmosphere. After the addition of MeCN (20 equiv.) followed by $NaBArF_{24}$ (1 equiv.), the solution was stirred at room temperature for 2 h. After evaporation of volatile compounds, the oily residue was washed with *n*-pentane. The product was then obtained after drying under high vacuum. A solution containing this product (1×10^{-5} mol) and toluene or dichloromethane was quickly injected into the autoclave under a constant low flow of ethylene, which is considered as the t_0 time, the reactor was immediately pressurized to 10 bar of ethylene. The 10 bar working pressure was maintained through a continuous feed of ethylene from a bottle placed on a balance to allow monitoring of the ethylene uptake. The reaction mixture was stirred for the given reaction time. At the end of each test, a dry ice bath was used to rapidly cool the reactor. When the inner temperature reached 0 °C, the ice bath was removed, allowing the temperature to slowly rise to 18 °C. The gaseous phase was then transferred into a 10 L polyethylene tank filled with water. An aliquot of this gaseous phase was transferred into a Schlenk flask, previously evacuated, for GC analysis. The amount of ethylene consumed was thus determined by differential weighting of the bottle (accuracy of the scale: 0.01g). To this amount of ethylene, the remaining ethylene (calculated using the GC analysis) in the gaseous phase was subtracted. Although this method is of limited accuracy, it was used throughout and it gave satisfactory reproducibility. The reaction mixture in the reactor was quenched *in situ* by

For references, see page 191.

the addition of ethanol (5 mL), transferred into a Schlenk flask, and separated from the metal complexes by trap-to-trap evaporation into a second Schlenk flask previously immersed in liquid nitrogen in order to avoid loss of product for GC analysis. Each catalytic test was performed at least twice to ensure the reproducibility of the results.

IV.5. References

1. Sauter, D. W.; Taoufik, M.; Boisson, C., Polyolefins, a Success Story. *Polymers* **2017,** *9*, 185.

2. (a) Breuil, P.-A. R.; Magna, L.; Olivier-Bourbigou, H., Role of Homogeneous Catalysis in Oligomerization of Olefins : Focus on Selected Examples Based on Group 4 to Group 10 Transition Metal Complexes. *Cata. Lett.* **2015,** *145*, 173-192. (b) Forestière, A.; Olivier-Bourbigou, H.; Saussine, L., Oligomerization of Monoolefins by Homogeneous Catalysts. *Oil Gas Sci. Technol. - Revue de l'IFP* **2009,** *64*, 649-667. (c) Belov, G. P.; Matkovsky, P. E., Processes for the production of higher linear α-olefins. *Pet. Chem.* **2010,** *50*, 283-289. (d) Skupinska, J., Oligomerization of .alpha.-olefins to higher oligomers. *Chem. Rev.* **1991,** *91*, 613-648.

3. (a) Al-Jarallah, A. M.; Anabtawi, J. A.; Siddiqui, M. A. B.; Aitani, A. M.; Al-Sa'doun, A. W., Ethylene dimerization and oligomerization to butene-1 and linear α-olefins. *Cata. Today* **1992,** *14*, 1-121. (b) Vogt, D., Oligomerization of Ethylene to Higher Linear α-Olefins. In *Applied Homogeneous Catalysis with Organometallic Complexes*, Cornils, B.; Herrmann, W. A., Eds. Weinheim, Ger: VCH, **1996**; pp 245-257.

4. Fischer, K.; Jonas, K.; Misbach, P.; Stabba, R.; Wilke, G. N., The Nickel Effect. *Angew. Chem. Int. Ed. Engl.* **1973,** *12*, 943-953.

5. Galli, P., Forty years of industrial developments in the field of isotactic polyolefins. *Macromolecular Symposia* **1995,** *89*, 13-26.

6. Galli, P.; Vecellio, G., Technology: driving force behind innovation and growth of polyolefins. *Prog. Polym. Sci.* **2001,** *26*, 1287-1336.

7. Kaiser, J. M.; Long, B. K., Recent developments in redox-active olefin polymerization catalysts. *Coord. Chem. Rev.* **2018,** *372*, 141-152.

8. Sinn, H.; Kaminsky, W.; Vollmer, H.-J.; Woldt, R., "Living Polymers" on Polymerization with Extremely Productive Ziegler Catalysts. *Angew. Chem. Int. Ed. Engl.* **1980,** *19*, 390-392.

9. (a) Makio, H.; Terao, H.; Iwashita, A.; Fujita, T., FI Catalysts for Olefin Polymerization—A Comprehensive Treatment. *Chem. Rev.* **2011,** *111*, 2363-2449. (b) Luk, Y.-Y. G.; Foucher,

For references, see page 191.

D. A.; Gossage, R. A., Recent advances in the homogeneous polymerisation of olefins mediated by nickel complexes. *C. R. Chim.* **2013,** *16*, 573-579. (c) Mu, H.; Pan, L.; Song, D.; Li, Y., Neutral Nickel Catalysts for Olefin Homo- and Copolymerization: Relationships between Catalyst Structures and Catalytic Properties. *Chem. Rev.* **2015,** *115*, 12091-12137.

10. Johnson, L. K.; Killian, C. M.; Brookhart, M., New Pd(II)- and Ni(II)-Based Catalysts for Polymerization of Ethylene and alpha-Olefins. *J. Am. Chem. Soc.* **1995,** *117*, 6414-6415.

11. (a) Wang, Z.; Liu, Q.; Solan, G. A.; Sun, W.-H., Recent advances in Ni-mediated ethylene chain growth: Nimine-donor ligand effects on catalytic activity, thermal stability and oligo-/polymer structure. *Coord. Chem. Rev.* **2017,** *350*, 68-83. (b) Guan, Z., *Metal Catalysts in Olefin Polymerization*. Berlin Heidelberg: Springer, **2009**. (c) Guan, Z., Recent Progress of Catalytic Polymerization for Controlling Polymer Topology. *Chem.: Asian J.* **2010,** *5*, 1058-1070. (d) Chen, C., Designing catalysts for olefin polymerization and copolymerization: beyond electronic and steric tuning. *Nat. Rev. Chem.* **2018,** *2*, 6-14.

12. Keim, W., Oligomerization of Ethylene to α-Olefins: Discovery and Development of the Shell Higher Olefin Process (SHOP). *Angew. Chem. Int. Ed.* **2013,** *52*, 12492-12496.

13. (a) Ye, Z.; Xu, L.; Dong, Z.; Xiang, P., Designing polyethylenes of complex chain architectures via Pd–diimine-catalyzed "living" ethylene polymerization. *Chem. Commun.* **2013,** *49*, 6235. (b) Chen, Z.; Brookhart, M., Exploring Ethylene/Polar Vinyl Monomer Copolymerizations Using Ni and Pd α-Diimine Catalysts. *Acc. Chem. Res.* **2018,** *51*, 1831-1839. (c) Ravasio, A.; Boggioni, L.; Tritto, I., Late-Transition Metal Complexes with Mixed NO, NS, NP Chelating Ligands for Olefin Polymerization Catalysis. In *Olefin Upgrading Catalysis by Nitrogen-based Metal Complexes I*, Dordrecht: Springer, **2011**; pp 27-118. (d) Olivier-Bourbigou, H.; Breuil, P. A. R.; Magna, L.; Michel, T.; Espada Pastor, M. F.; Delcroix, D., Nickel Catalyzed Olefin Oligomerization and Dimerization. *Chem. Rev.* **2020,** *120*, 7919-7983. (e) Ittel, S. D.; Johnson, L. K.; Brookhart, M., Late-Metal Catalysts for Ethylene Homo- and Copolymerization. *Chem. Rev.* **2000,** *100*, 1169-1204. (f) F. Speiser, P. B., L. Saussine, Catalytic Ethylene Dimerization and Oligomerization: Recent Developments with Nickel Complexes Containing P, N- Chelating Ligands. *Acc. Chem. Res.* **2005,** *2005*, 784-793. (g) Guan, Z.; Popeney, C. S., Recent Progress in Late Transition Metal α-Diimine Catalysts for Olefin Polymerization. In *Metal Catalysts in Olefin Polymerization*, Berlin Heidelberg: Springer, **2009**; pp 179-220. (h) Kuhn, P.; Semeril, D.; Matt, D.; Chetcuti, M. J.; Lutz, P., Structure-reactivity relationships in SHOP-type complexes: tunable catalysts for the oligomerisation and polymerisation of ethylene. *Dalton Trans.* **2007,** *2007*, 515-528. (i) Ren, X.; Wesolek, M.; Braunstein, P., Cu(i), Ag(i), Ni(ii), Cr(iii) and Ir(i) complexes with tritopic

For references, see page 191.

N(imine)C(NHC)N(amine) pincer ligands and catalytic ethylene oligomerization. *Dalton Trans.* **2019,** *48*, 12895-12909. (j) Hameury, S.; de Frémont, P.; Breuil, P.-A. R.; Olivier-Bourbigou, H.; Braunstein, P., Bis(ether-functionalized NHC) Nickel(II) Complexes, *Trans* to *Cis* Isomerization Triggered by Water Coordination, and Catalytic Ethylene Oligomerization. *Organometallics* **2014,** *34*, 2183-2201. (k) Gottfried, A. C.; Brookhart, M., Living Polymerization of Ethylene Using Pd(II) α-Diimine Catalysts. *Macromolecules* **2001,** *34*, 1140-1142.

14. Salian, S. M.; Bagui, M.; Jasra, R. V., Industrially relevant ethylene trimerization catalysts and processes. *Appl. Petrochem. Res.* **2021,** *11*, 267-279.

15. (a) Arlman, E., Ziegler-Natta catalysis III. Stereospecific polymerization of propene with the catalyst system $TiCl_3$-$AlEt_3$. *J. Catal.* **1964,** *3*, 99-104. (b) Arlman, E., Ziegler-Natta catalysis II. Surface structure of layer-lattice transition metal chlorides. *J. Catal.* **1964,** *3*, 89-98. (c) Cossee, P., Ziegler-Natta catalysis I. Mechanism of polymerization of $alpha;-olefins with Ziegler-Natta catalysts*1. *J. Catal.* **1964,** *3*, 80-88.

16. (a) Bézier, D.; Daugulis, O.; Brookhart, M., Oligomerization of Ethylene Using a Diphosphine Palladium Catalyst. *Organometallics* **2017,** *36*, 443-447. (b) Zhang, D.; Nadres, E. T.; Brookhart, M.; Daugulis, O., Synthesis of Highly Branched Polyethylene Using "Sandwich" (8-p-Tolyl naphthyl α-diimine)nickel(II) Catalysts. *Organometallics* **2013,** *32*, 5136-5143. (c) Camacho, D. H.; Salo, E. V.; Ziller, J. W.; Guan, Z., Cyclophane-Based Highly Active Late-Transition-Metal Catalysts for Ethylene Polymerization. *Angew. Chem.* **2004,** *116*, 1857-1861.

17. (a) Lu, Z.; Chang, G.; Wang, H.; Jing, K.; Dai, S., A Dual Steric Enhancement Strategy in α-Diimine Nickel and Palladium Catalysts for Ethylene Polymerization and Copolymerization. *Organometallics* **2021,** *41*, 124-132. (b) Liu, Y. S.; Harth, E., Distorted Sandwich α-Diimine Pd^{II} Catalyst: Linear Polyethylene and Synthesis of Ethylene/Acrylate Elastomers. *Angew. Chem. Int. Ed.* **2021,** *60*, 24107-24115. (c) Ge, Y.; Li, S.; Wang, H.; Dai, S., Synthesis of Branched Polyethylene and Ethylene-MA Copolymers Using Unsymmetrical Iminopyridyl Nickel and Palladium Complexes. *Organometallics* **2021,** *40*, 3033-3041. (d) Burns, C. T.; Jordan, R. F., Ethylene Polymerization by Sterically Crowded Palladium(II) Complexes that Contain Bis(heterocycle)methane Ligands. *Organometallics* **2007,** *26*, 6737-6749. (e) Gottfried, A. C.; Brookhart, M., Living and Block Copolymerization of Ethylene and α-Olefins Using Palladium(II)−α-Diimine Catalysts. *Macromolecules* **2003,** *36*, 3085-3100. (f) Shultz, L. H.; Tempel, D. J.; Brookhart, M., Palladium(II) β-Agostic Alkyl Cations and Alkyl

For references, see page 191.

Ethylene Complexes: Investigation of Polymer Chain Isomerization Mechanisms. *J. Am. Chem. Soc.* **2001,** *123*, 11539-11555. (g) Mecking, S.; Johnson, L. K.; Wang, L.; Brookhart, M., Mechanistic Studies of the Palladium-Catalyzed Copolymerization of Ethylene and α-Olefins with Methyl Acrylate. *J. Am. Chem. Soc.* **1998,** *120*, 888-899. (h) Takeuchi, D.; Tojo, Y.-A.; Osakada, K., Synthesis of a Ni Complex Chelated by a [2.2]Paracyclophane-Functionalized Diimine Ligand and Its Catalytic Activity for Olefin Oligomerization. *Molecules* **2021,** *26*, 2719. (i) Cooley, N. A.; Green, S. M.; Wass, D. F.; Heslop, K.; Orpen, A. G.; Pringle, P. G., Nickel Ethylene Polymerization Catalysts Based on Phosphorus Ligands. *Organometallics* **2001,** *20*, 4769-4771. (j) Si, G.; Na, Y.; Chen, C., Ethylene (co)Oligomerization by Phosphine-Pyridine Based Palladium and Nickel Catalysts. *ChemCatChem* **2018,** *10*, 5135-5140.

18. (a) Shi, P.-Y.; Liu, Y.-H.; Peng, S.-M.; Liu, S.-T., Palladium(II) Complexes Containing P∼N∼O Donors. Ligand Effect of Tridentate versus Bidentate Coordination on the Oligomerization of Ethylene. *Organometallics* **2002,** *21*, 3203-3207. (b) Sirbu, D.; Consiglio, G.; Gischig, S., Palladium and nickel complexes of (P,N)-ligands based on quinolines: Catalytic activity for polymerization and oligomerization. *J. Organomet. Chem.* **2006,** *691*, 1143-1150. (c) Bézier, D.; Daugulis, O.; Brookhart, M., Polymerization of Ethylene Catalyzed by Phosphine-Iminophosphorane Palladium Complexes. *Organometallics* **2017,** *36* (15), 2947-2951.

19. Ananikov, V. P., Nickel: The "Spirited Horse" of Transition Metal Catalysis. *ACS Cata.* **2015,** *5*, 1964-1971.

For references, see page 191.

Conclusion générale et perspectives

Dans ce mémoire de thèse qui relève de la chimie des métallo-cavitands, nous avons décrit la synthèse de ligands bidentes *cis*-chélatants de type P,N et diphosphine équipés d'une α-cyclodextrine (α-CD) perméthylée. La caractéristique principale des ligands étudiés est d'avoir l'un des deux ou les deux centres coordinateurs orientés vers l'intérieur de la cavité moléculaire. Cette disposition particulière des atomes donneurs a permis de *cis*-chélater un centre métallique au sein de cette dernière comme l'a montré une étude des propriétés coordinantes des ligands d'intérêt vis-à-vis de cations d^8. La possibilité de confiner un métal *cis*-chélaté nous a conduit à étudier le comportement de ces ligands en oligomérisation de l'éthylène catalysée par le nickel.

La mise au point que constitue le **premier chapitre** donne une vision globale de la conception et de la préparation de ligands cavitaires chélatants dans lesquels les deux sites de coordination sont différenciés (à l'exclusion des systèmes assemblés par voie supramoléculaire) ainsi que de leur utilisation en reconnaissance moléculaire et catalyse, notamment en catalyse asymétrique. Chaque fois que cela a été possible, une comparaison des propriétés des systèmes cavitaires avec celles de leurs analogues dépourvus de cavité a été faite afin d'évaluer l'influence de la cavité sur les propriétés des systèmes étudiés, notamment catalytiques.

Dans le **chapitre II**, nous avons décrit une synthèse efficace d'un nouveau ligand P,N bâti sur une plateforme α-CD reposant sur le pontage stéréoselectif de deux unités glucose adjacentes (pontage AB). La présence d'une anse coordinante rigide comportant un atome donneur P(III) a permis de confiner un centre métallique d^8 ou d^{10} dans la cavité moléculaire et de ce fait contrôler parfaitement la première sphère de coordination du métal. Nous avons ainsi mis en évidence le caractère *cis*-chélatant du ligand P,N en présence de cations d^8 qui conduit après coordination à des complexes de géométrie plan-carré dans lesquels les deux ligands exogènes, à savoir des halogénures ou méthyle, sont stériquement différenciés. En effet, des études par spectroscopie RMN et radiocristallographiques ont permis de montrer que l'un d'entre eux est encapsulé dans la cavité tandis que le second pointe clairement vers l'extérieur du macrocycle. Par ailleurs, la structure moléculaire d'un complexe d'or(I) linéaire obtenue par diffraction des rayons X indique que seul l'atome de phosphore coordine dans ce cas le centre métallique et est donc responsable du confinement du métal. Un ligand P,N non cavitaire de structure analogue a également synthétisé et ses propriétés de coordination vis-à-vis des cations d^8 Ni(II) et Pd(II) étudiées à des fins de comparaison. Nous avons ainsi montré que l'encapsulation du métal dans la cavité empêche la formation de complexes bis(phosphine) et ce en présence d'une unité plus faiblement coordinante de type amine tertiaire, ce qui conduit à la formation exclusive de complexes chélate de stœchiométrie métal/ligand 1:1. Une étude UV-vis des

différents complexes, cavitaires et non cavitaires, a permis de montrer que la présence de l'unité macrocyclique impactait légèrement les propriétés électroniques des complexes, notamment la bande MLCT.

Le **chapitre III** est consacré à la chimie de coordination de deux ligands cavitaires diphosphine préalablement préparés au laboratoire vis-à-vis de cations d^8 de type palladium(II) et nickel(II). A nouveau, comme dans le cas du ligand P,N cavitaire, seuls des complexes plan-carré de stœchiométrie métal/ligand 1:1 comportant un centre métallique cis-chélaté ont été mis en évidence. Cependant, bien que présentant un métal confiné dans une cavité α-CD, la seconde sphère de coordination du métal est très différente selon le type de diphosphine utilisée comme l'a montré des études par spectroscopie RMN et radiocristallographiques. Dans les complexes issus de la première diphosphine (**L3**) qui s'apparente au ligand P,N d'un point de vue géométrique et stérique, les deux sites de coordination exogènes sont très différenciés et la paroi interne de l' α-CD protège les positions axiales du métal. Au contraire, dans la deuxième diphosphine, les deux sites axiaux ne sont plus protégés et l'environnement stérique des deux sites de coordination exogènes est très similaire. La complexation des deux phosphines par le précurseur métallique [PdMeCl(COD)] conduit à la formation de deux isomères géométriques dont les proportions varient en fonction du solvant dans lequel ils ont été synthétisés. Cependant, tandis que pour la première diphosphine (**L3**), ces proportions ne varient pas au cours du temps lorsque le mélange de complexes est laissé en solution, un état d'équilibre entre les deux isomères est atteint au bout de quelques jours dans le cas de la diphosphine **L4** avec une proportion identique quelle que soit la proportion des deux isomères au départ. Il est probable que cette différence de comportement soit due au fait que les propriétés électroniques des deux atomes donneurs dans **L3** sont différentes comme dans le ligand P,N tandis qu'elles sont identiques dans **L4**. Contrairement au cas des complexes P,N, une étude UV-vis a montré que la présence de la cavité CD dans les complexes avaient une influence négligeable sur les propriétés électroniques des complexes.

Le **dernier chapitre** du manuscrit a trait à l'étude des propriétés catalytiques des complexes de nickel et de palladium précités, qu'ils soient cavitaires ou non, après activation par un co-catalyseur adéquat (MMAO-12 ou $NaBArF_{24}$). La réaction d'oligomérisation de l'éthylène a été spécifiquement ciblée en raison de son importance économique, du rôle des facteurs stériques sur le devenir de la réaction et d'une taille de substrat (éthylène) compatible avec la petite taille de la cavité α-CD. Comparés aux complexes de nickel non cavitaires, les complexes dotés d'une cavité CD présentent une très haute sélectivité, tant pour la fraction C4 (jusqu'à 96%) qu'en α-oléfines (jusqu'à 95% de but-1-ène dans la fraction C4) et une robustesse

remarquable malgré une activité moindre. La sélectivité remarquable de certains complexes de nickel cavitaires a été attribuée à l'encapsulation du métal et plus précisément à la protection des sites axiaux par la paroi interne de la cavité. Les complexes PdMeCl ont également été testés en oligomérisation de l'éthylène après activation par le sel $NaBArF_{24.}$ Malheureusement seules des traces de butènes ont été détectées dans le milieu réactionnel.

Les différentes études réalisées dans le cadre de cette thèse ont montré que le confinement d'un métal *cis*-chélaté à l'intérieur d'une cavité α-CD permettait d'améliorer sensiblement les propriétés d'un catalyseur métallique, notamment en termes de robustesse et de sélectivité. On peut anticiper que l'augmentation de la taille de la cavité ainsi que le remplacement de la fonction amine tertiaire ou triarylphosphine par une autre unité coordinante soient de nature à améliorer les propriétés catalytiques des complexes cavitaires en oligomérisation de l'éthylène. C'est ce que des travaux futurs examineront. Parmi les modifications spécifiques pouvant avoir un impact positif sur les performances des catalyseurs, on peut citer :

- Le remplacement de la cavité α-CD par une cavité β-CD plus grande afin de favoriser la réaction de propagation tout en limitant les réactions de terminaison.
- Le remplacement du groupement coordinant non pontant par un groupement donneur plus faible comportant par exemple un atome d'oxygène comme dans les catalyseurs SHOP.

Afin d'expliquer les différences de réactivité entre les complexes issus des ligands **L1** et **L3** d'une part et **L4** d'autre part, des études théoriques reposant sur la méthode semi-empirique GFN-xTB développée par Grimme[1] seront également mises en œuvre prochainement. Nécessitant des durées de calcul limitées, cette méthode est adaptée aux molécules de grande taille comprenant des métaux de transition.[2]

References

1. (a) Grimme, S.; Bannwarth, C.; Shushkov, P., A Robust and Accurate Tight-Binding Quantum Chemical Method for Structures, Vibrational Frequencies, and Noncovalent Interactions of Large Molecular Systems Parametrized for All spd-Block Elements (Z = 1–86). *J. Chem. Theory Comput.* **2017,** *13*, 1989-2009. (b) Bannwarth, C.; Ehlert, S.; Grimme, S., GFN2-xTB-An Accurate and Broadly Parametrized Self-Consistent Tight-Binding Quantum Chemical Method with Multipole Electrostatics and Density-Dependent Dispersion Contributions. *J. Chem. Theory Comput.* **2019,** *15*, 1652-1671.

2. Kaya, Z.; Andna, L.; Matt, D.; Bentouhami, E.; Djukic, J.-P.; Armspach, D., A Comparative Study of Confining Ligands Derived from Methylated Cyclodextrins in Gold-Catalyzed Cycloisomerization of 1,6-Enynes. *Eur. J. Org. Chem.* **2019,** *2019*, 4528-4537.

Dalton Transactions

ROYAL SOCIETY OF CHEMISTRY

COMMUNICATION

View Article Online
View Journal

Cite this: DOI: 10.1039/d2dt01553f

Received 18th May 2022,
Accepted 28th June 2022

DOI: 10.1039/d2dt01553f

rsc.li/dalton

A cavity-shaped *cis*-chelating P,N ligand for highly selective nickel-catalysed ethylene dimerisation†

Yang Li, [a] Katrin Pelzer, [a] Damien Sechet,[b] Geordie Creste, [a] Dominique Matt, [b] Pierre Braunstein *[a] and Dominique Armspach *[a]

The presence of a permethylated α-cyclodextrin (α-CD) cavity in a chelating P,N ligand promotes exclusive formation of 1 : 1 ligand/metal complexes. In MX_2 complexes, one of the two halido ligands is forced to reside inside the CD hollow while the second one is pointing outside. Unlike its cavity-free analogue, a Ni(II) complex of the CD ligand is a highly selective precatalyst for ethylene dimerisation (96% C_4 selectivity with up to 95% of 1-butene within the C_4 fraction).

Inwardly directed donor atoms rigidly grafted on a macrocyclic host molecule are capable of facilitating a metal centred reaction to take place inside the cavity-shaped ligand.[1–5] This feature is prone to produce high substrate recognition,[6–14] catalytic chemo-[15] and regioselectivity[16–20] as well as enantioselectivity if the receptor is optically active.[21] By connecting two C-6 carbon atoms of two glucose units of an α-, β- or γ-CD with a single donor atom such as nitrogen[22] or phosphorus,[23–25] (Fig. 1i) or a short NHC unit[26–28] (Fig. 1ii), it was previously shown that the resulting bridge is sufficiently rigid to force the donor atom lone pair to point towards the CD interior. Doubly bridged ligands with a similar metal confining feature have also been prepared (Fig. 1iii).[23,24] Almost all ligands of that type are monodentate or *trans*-chelating bidentate. However, most metal-catalysed reactions involve *cis*-chelate complexes. Increasing the structural diversity of *cis*-chelating ligands displaying a metal confining unit[22,29–31] would considerably widen the scope of metal binding host molecules, in particular if catalytically relevant P(III) atoms could be incorporated into the macrocyclic structure. Self-assembled, *cis*-chelating P,N ligands consisting of a water-soluble phosphine ligand included in a mono-*N*,*N*-dialkylamino-β-CD were already prepared in water, but in these complexes, the metal centre is not located in the CD cavity.[32,33]

Herein, we describe a rare example of P(III)-containing CD (**1**) capable of forcing the exclusive formation of a 1 : 1 ligand/metal complex, showing *cis*-chelation inside the receptor hollow when associated with a N donor atom. A Ni(II) complex of this new P,N ligand was investigated for its potential as pre-catalyst in ethylene oligomerisation, a reaction of continuing considerable interest[34,35] and its properties were compared to those of a cavity-free analogue.

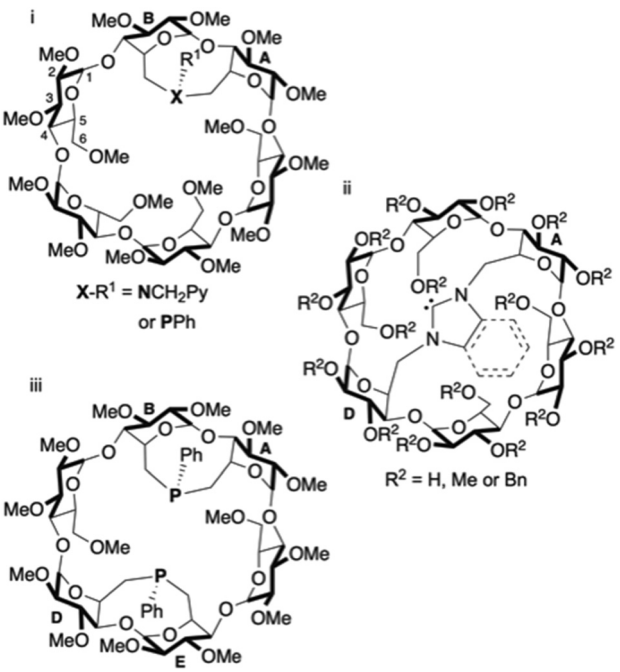

Fig. 1 Examples of α-CD-based metal confining ligands with one (i and ii) or two (iii) bridging coordinating units. Bn stands for benzyl.

[a]*Equipe Confinement Moléculaire et Catalyse, Institut de Chimie de Strasbourg, UMR 7177 CNRS, Université de Strasbourg, 4, rue Blaise Pascal, CS 90032, 67081 Strasbourg Cedex, France. E-mail: d.armspach@unistra.fr*

[b]*Laboratoire de Chimie Inorganique Moléculaire et Catalyse, Institut de Chimie de Strasbourg, UMR 7177 CNRS, Université de Strasbourg, 4, rue Blaise Pascal, CS 90032, 67081 Strasbourg Cedex, France*

†Electronic supplementary information (ESI) available: Synthesis and characterization data. CCDC 2163655 (**8**), 2163663 (**9**), 2163657 (**10**), 2163751 (**11**), 2163658 (**12**) and 2163666 (**13**). For ESI and crystallographic data in CIF or other electronic format see DOI: **https://doi.org/10.1039/d2dt01553f**

An improved procedure (Scheme 1) was devised to synthesise diethyl [2-(*N*,*N*-dimethylamino)phenyl]phosphonate (**3**) from 2-bromoaniline (**2**).[36] Its reduction afforded the key functional primary phosphine **4**, which upon deprotonation reacted with dimesylate **5** to afford P,N ligand **1** in 63% yield. Although **1** is seemingly a very basic phosphine (δ_{31P} = −28.4 ppm), this ligand is considerably more stable towards air than its PhP-bridged analogue (δ_{31P} = −16.2 ppm)[23] and can be purified by standard column chromatography without noticeable formation of phosphine oxide. For comparison, the related cavity-free ligand **7**[37] was also synthesised in 40% yield from 2-bromo-*N*,*N*-dimethylaniline by *ortho*-lithiation followed by nucleophilic substitution of chlorodiethylphosphine.[38] Resistance to oxidation was also observed for **7** (δ_{31P} = −25.1 ppm) as in analogous P,N ligands of the Me-DalPhos family (Fig. 2).[39]

When reacted with [$PdCl_2$(cod)] (cod = 1,5-cyclooctadiene) in CH_2Cl_2, confining ligand **1** produced only chelate complex **8**, even in the presence of excess ligand (Fig. S80†). Chelating behaviour was also observed when **1** or the cavity-free **7** were reacted with [$NiBr_2$(dme)] (dme = 1,2-dimethoxymethane) to produce complexes **9** and **10**, respectively.[40] In stark contrast, the reaction of **7** with one equiv. of [$PdCl_2$(cod)] in CH_2Cl_2 gave a 9 : 1 mixture of the chelate complex **11** and the cationic bis(phosphine) complex **12**, respectively. As expected, raising the ligand/metal ratio to 2 : 1 caused the proportion of complex **12** to increase significantly (**11**/**12** ratio of 3 : 7) (Fig. S80†). The structures of both **11** and **12** were established by X-ray diffraction analyses (Fig. 3). The single crystal X-ray structure of cationic **12** clearly shows that two phosphines but only one tertiary amine are coordinated to palladium (Fig. 3). Furthermore, line broadening upon heating **12** in $CDCl_3$ (Fig. S66 and S67†) suggests fluxional behaviour possibly involving the slow coordination/decoordination of the NMe_2 units on the NMR time scale (Fig. S1†). Confirmation of the metal confining character of ligand **1** in solution came from a

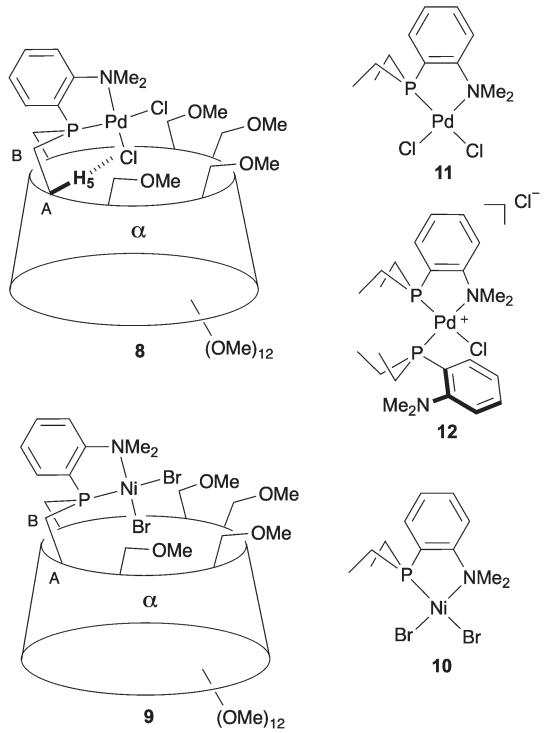

Fig. 2 Cavity-shaped Pd and Ni chelate complexes **8** and **9**, their cavity-free counterparts **11** and **10**, and cationic Pd complex **12**.

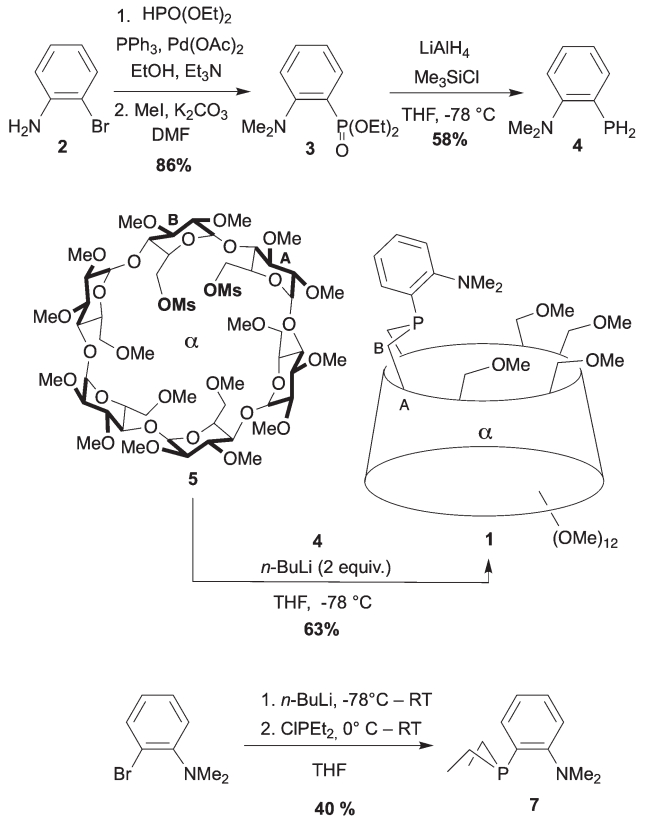

Scheme 1 Synthesis of the confining ligand **1** and its cavity-free analogue **7**. Ms stands for methylsulfonyl.

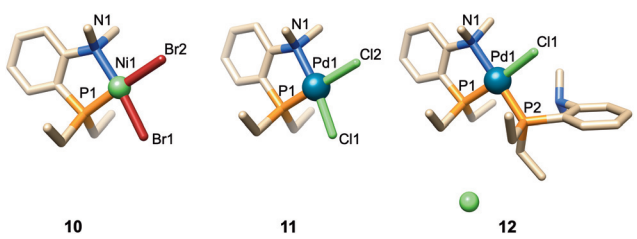

Fig. 3 Single crystal X-ray structures of cavity-free Pd complexes **11** and **12** as well as Ni complex **10**. Solvent molecules have been omitted for clarity. Selected bond lengths (Å) and angles (°): **10**, Ni1–P1 2.1248 (10), Ni1–N1 2.010(3), NI1–Br1 2.3122(6), Ni1–Br2 2.3626(5); P1–Ni1–N1 88.63(9), P1–Ni1–Br1 85.25(3), N1–Ni1–Br2 94.48(8), Br1–Ni1–Br2 91.64 (2); **11**, Pd1–P1 2.1857(9), Pd1–N1 2.111(3), Pd1–Cl1 2.2982(9), Pd1–Cl2 2.4087(9); P1–Pd1–N1 86.68(8), P1–Pd1–Cl1 87.20(3), N1–Pd1–Cl2 94.33(8), Cl1–Pd1–Cl2 91.81(3); **12**, Pd1–P1 2.2326(15), Pd1–P2 2.2724 (14), Pd1–N1 2.185(5), Pd1–Cl1 2.3728(14); P1–Pd1–N1 84.71(17), P1–Pd1–P2 95.45(5), N1–Pd1–Cl1 91.36(17), P2–Pd1–Cl1 88.28(5).

detailed analysis of the ^{1}H NMR spectrum of the square planar Pd(II) complex **8**, the ^{31}P NMR chemical shift of which is in the expected range (δ_{31P} = 32.5 ppm). As previously reported for a CD-encapsulated M–X unit, the inner-cavity H-5 proton of bridging unit A in **8** is unusually downfield shifted (δ_{1H} = 5.19 *vs.* 4.30 ppm for ligand **1**) as a result of weak CH···Cl H-bonding within the CD hollow. The deshielding of this proton proves that **1** is indeed metal confining in solution. Such a feature was confirmed in the solid state by the single crystal X-ray structure of **8** (Fig. 4), which revealed a square planar $PdCl_2$ unit seating just above the cavity and nearly orthogonal to the macrocyclic structure (86.05°).‡ As expected from the solution studies, one of the two chlorido ligands points toward the interior of the cavity and displays short contact with the H-5 proton of bridging unit A (2.840 Å). The other is clearly pointing outside and is at a much longer distance to palladium (2.368 Å) than the encapsulated one (2.295 Å). This is to be expected because of the larger *trans* influence of the P(III) donor atom. Both complexes **9** and **10** are diamagnetic in keeping with their square planar structures (Fig. 4 and 3 respectively) and low temperature NMR studies in CD_2Cl_2 revealed at −60 °C a well-defined ^{31}P singlet at 10.4 and 41.4 ppm, respectively.§ It is noteworthy that the single crystal X-ray structures of **8** and **9**, which are very similar, clearly establish that each halido ligand experiences a very different steric environment, an unprecedented feature in metal confining ligands that could have a great impact on catalytic properties. In the Pd complex **8**, the $PNMX_2$ unit is slightly more included in the cavity than in its Ni counterpart **9** (angle between CD O-4 atoms and the C6–P1–C16 planes = 50.27° *vs.* 54.82° respectively). Moreover, both cavity-free and cavity-shaped complexes of d^8 metals have a very similar first coordination sphere, the only significant difference between the two types of complexes being an elongation of the external Ni–Br bond by *ca.* 0.02 Å on going from **10** to **9** and a shortening of the corresponding M–X bond by *ca.* 0.04 Å on going from Pd complexes **11** to **8** (Fig. 3 and 4). The gold(I) complex **13** was also synthesised quantitatively by reacting **1** with [AuCl(tht)] (tht = tetrahydrothiophene). Unlike its d^8 counterparts, the d^{10} metal cation is not chelated by the ligand but only bound to the P(III) atom, leaving the NMe_2 unit uncoordinated above the encapsulated metal centre, as revealed by its single crystal X-ray structure (Fig. 4). As in monophosphine analogues,[23,24] the phosphorus donor atom imposes the overall orientation of the metal with respect to the cavity. The steric protection provided by the CD cavity is responsible for a remarkable control of the metal coordination sphere and prevents the formation of bis(phosphine) complexes analogous to **12**. Such a feature is also expected to be retained under catalytic reaction conditions.

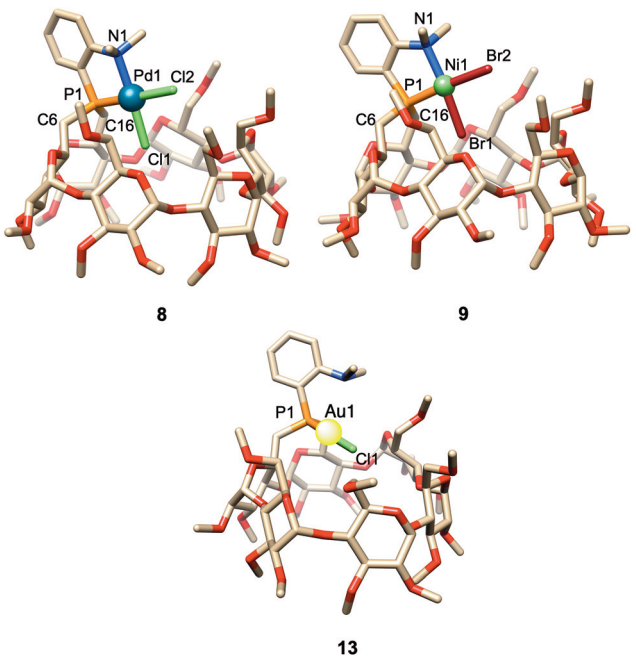

Fig. 4 Single crystal X–ray structures of chelate Pd complex **8** and Ni complex **9**, and monophosphine Au complex **13** displaying metal encapsulation. Solvent molecules have been omitted for clarity. Selected bond lengths (Å) and angles (°): **8**, Pd1–P1 2.1947(14), Pd1–N1 2.125(4), Pd1–Cl1 2.2949(14), Pd1–Cl2 2.3676(15); P1–Pd1–N1 86.83(12), P1–Pd1–Cl1 88.49(5), N1–Pd1–Cl2 92.05(12), Cl1–Pd1–Cl2 92.63(6); **9**, Ni1–P1 2.1263(15), Ni1–N1 2.007(6), Ni1–Br1 2.3063(10), Ni1–Br2 2.3807(9); P1–Ni1–N1 88.53(15), P1–Ni1–Br1 84.06(5), N1–Ni1–Br2 95.01(15), Br1–Ni1–Br2 92.40(3); **13**, Au1–P1 2.2329(18), Au1–Cl1 2.2755(19); P1–Au1–Cl1 178.16(7).

Numerous Ni complexes derived from P,N ligands, most of them of the pyridine–phosphine type,[41–43] have been evaluated in the catalytic oligomerisation of ethylene.[44,45] Many studies have focused on varying the electronic properties of both P- and N-donor atoms, but steric factors have also been found to play a crucial role in the metal-catalysed oligomerisation of ethylene to α-olefins.[46,54] In particular, the presence of steric bulk at the metal axial sites tends to inhibit termination reactions, thus favouring chain growth.[47] The cavity-shaped complex **9** exhibits a unique steric environment, in which the phosphorus atom is heavily congested and forces the chelated metal to be encapsulated in the CD with both axial sites protected by CD 6-methoxy groups. Moreover, unlike their cavity-free analogues, the two active coordination sites involved in the oligomerisation process, generated by bromide abstraction and methylation of **9**, will experience very different steric environments. While one of the active sites is deeply buried in the CD cavity, the other is much less protected. The unusual steric environment around the metal in Ni complex **9** prompted us to evaluate it as a precatalyst in ethylene oligomerisation. For comparison, the cavity-free analogue **10** was also tested under similar reaction conditions.

After activation with MMAO, the Ni complex **9** catalysed the dimerisation of ethylene with high C_4 (96%) and 1-butene (95%) selectivities (Table 1, entry 2), even after 24 h reaction time (Table 1, entry 3), indicating that chain-walking and post-isomerisation reactions do not readily take place. Moreover, the proportion of 1-hexene in the small C_6 fraction is also much higher with the cavity-shaped ligand (70% on average for **9**). Even if such level of selectivity is not uncommon for early transition metals,[48] it is very high for a nickel-catalysed

Table 1 Ethylene oligomerisation with nickel complexes **9** and **10** as precatalysts in the presence of MMAO[a]

Entry	Precatalyst	Time	Activity [$g(C_2H_4)\ g(Ni)^{-1}\ h^{-1}$]	TOF [$mol(C_2H_4)\ mol(Ni)^{-1}\ h^{-1}$]	Products weight distribution[b] [%]		
					C_4 (α)[c]	C_6 (α)[d]	C_8
1	**9**	35 min	2760	5780	92 (95)	6 (70)	2
2	**9**	3 h	2190	4580	96 (95)	3 (75)	<1
3	**9**	24 h	1910	4000	85 (92)	12 (65)	3
4	**10**	35 min	41 570	86 970	77 (71)	22 (8)	1
5	**10**	3 h	17 920	37 490	79 (81)	19 (8)	2
6	**10**	24 h	5740	12 000	75 (67)	24 (6)	1

[a] Conditions: amount of catalyst: 1×10^{-5} mol, amount of cocatalyst (MMAO-12): 4×10^{-3} mol (400 equiv.), T = 30–35 °C, solvent: toluene, total volume: 20 mL, 10 bar C_2H_4, every test was repeated at least twice. [b] % calculated by GC analysis. [c] 1-Butene *vs.* total butenes formed. [d] 1-Hexene *vs.* total hexenes formed.

reaction.[44,45] For comparison, the related nickel complex **10** (Table 1, entry 4), which has similar electronic properties, but lacks the CD cavity is about 15 times more active for short reaction times, but its activity rapidly drops with time as it is only 3 fold higher than that of **9** after 24 h (Table 1, entry 6). It is much less selective for C_4 (77%) and 1-butene (71%) as well as 1-hexene (8%), whether for short (Table 1, entry 4) or longer reaction times (Table 1, entries 5 and 6). These poor selectivities are also observed for many other P,N Ni complexes except for ligands displaying sterically hindered nitrogen or phosphorus atoms[49,50] Although moderately active (TOF = 5780 mol (C_2H_4) $mol(Ni)^{-1}$ h^{-1}) (Table 1, entry 1), the catalyst derived from **9** proved to be very robust, since loss of activity is marginal over a prolonged period of time in stark contrast with cavity-free **10**. Despite the steric protection of axial positions, which is known to retard the rate of chain transfer relative to chain propagation and improve thermal stability,[47] including in macrocyclic complexes,[51] hardly any C_6-olefins and higher oligomers were formed. The high selectivity for 1-butene strongly suggests that metal encapsulation in the rather small α-CD cavity does not allow further chain growth and largely prevents isomerisation although the ligand electronic properties as revealed by slight changes in the UV spectra of complexes **8–11** (Fig. S87 and S88†) on going from cavity-free to cavity-shaped systems may also have an impact on the catalytic outcome.[52,53] Further *cis*-chelating and confining ligands with different donor atoms and larger cavities will be tested next in our group to see whether access to longer oligomers with a narrow mass distribution can be achieved. The present study also revealed that encapsulation exclusively leads to complexes with a 1 : 1 ligand/metal ratio, allowing the possibility to introduce in the potentially chelating unit a much weaker donor group susceptible to display catalytically relevant hemilability in solution. This unusual behaviour constitutes a promising development in the design of hybrid functional ligands.

Conflicts of interest

There are no conflicts to declare.

Acknowledgements

We thank the China Scholarship Council for a PhD studentship awarded to Y. L. (CSC201808420261).

Notes and references

‡ Angle between the CD O-4 atoms plane and the 5-membered chelate ring.
§ Line broadening at room temperature is common with this type of complexes.

1 R. Gramage-Doria, D. Armspach and D. Matt, *Coord. Chem. Rev.*, 2013, **257**, 776–816.
2 S. H. A. M. Leenders, R. Gramage-Doria, B. de Bruin and J. N. H. Reek, *Chem. Soc. Rev.*, 2015, **44**, 433–448.
3 V. Mouarrawis, R. Plessius, J. I. van der Vlugt and J. N. H. Reek, *Front. Chem.*, 2018, **6**, 623.
4 D. Matt and J. Harrowfield, *ChemCatChem*, 2021, **13**, 153–168.
5 G. R. F. Orton, B. S. Pilgrim and N. R. Champness, *Chem. Soc. Rev.*, 2021, **50**, 4411–4431.
6 B.-Y. Wang, T. Žujović, D. A. Turner, C. M. Hadad and J. D. Badjić, *J. Org. Chem.*, 2012, **77**, 2675–2688.
7 A. Cavarzan, J. N. H. Reek, F. Trentin, A. Scarso and G. Strukul, *Catal. Sci. Technol.*, 2013, **3**, 2898–2901.
8 M. Otte, P. F. Kuijpers, O. Troeppner, I. Ivanović-Burmazović, J. N. H. Reek and B. de Bruin, *Chem. – Eur. J.*, 2014, **20**, 4880–4884.
9 P. F. Kuijpers, M. Otte, M. Dürr, I. Ivanović-Burmazović, J. N. H. Reek and B. de Bruin, *ACS Catal.*, 2016, **6**, 3106–3112.
10 M. Otte, *ACS Catal.*, 2016, **6**, 6491–6510.
11 D. Zhang, J.-P. Dutasta, V. Dufaud, L. Guy and A. Martinez, *ACS Catal.*, 2017, **7**, 7340–7345.
12 T. Chavagnan, C. Bauder, D. Sémeril, D. Matt and L. Toupet, *Eur. J. Org. Chem.*, 2017, 70–76.
13 C. Tugny, N. del Rio, M. Koohgard, N. Vanthuyne, D. Lesage, K. Bijouard, P. Zhang, J. Meijide Suárez, S. Roland and E. Derat, *ACS Catal.*, 2020, **10**, 5964–5972.
14 J. Meijide Suárez, O. Bistri-Aslanoff, S. Roland and M. Sollogoub, *ChemCatChem*, 2022, **14**, e202101411.

15 G. Xu, S. Leloux, P. Zhang, J. Meijide Suárez, Y. Zhang, E. Derat, M. Ménand, O. Bistri-Aslanoff, S. Roland, T. Leyssens, O. Riant and M. Sollogoub, *Angew. Chem., Int. Ed.*, 2020, **59**, 7591–7597.
16 T. Gadzikwa, R. Bellini, H. L. Dekker and J. N. H. Reek, *J. Am. Chem. Soc.*, 2012, **134**, 2860–2863.
17 M. Jouffroy, R. Gramage-Doria, D. Armspach, D. Sémeril, W. Oberhauser, D. Matt and L. Toupet, *Angew. Chem.*, 2014, **126**, 4018–4021.
18 C. García-Simón, R. Gramage-Doria, S. Raoufmoghaddam, T. Parella, M. Costas, X. Ribas and J. N. Reek, *J. Am. Chem. Soc.*, 2015, **137**, 2680–2687.
19 P. Zhang, J. Meijide Suárez, T. Driant, E. Derat, Y. Zhang, M. Ménand, S. Roland and M. Sollogoub, *Angew. Chem., Int. Ed.*, 2017, **56**, 10821–10825.
20 N. Endo, M. Inoue and T. Iwasawa, *Eur. J. Org. Chem.*, 2018, 1136–1140.
21 Z. Kaya, E. Bentouhami, K. Pelzer and D. Armspach, *Coord. Chem. Rev.*, 2021, **445**, 214066.
22 D. Sechet, Z. Kaya, T. A. Phan, M. Jouffroy, E. Bentouhami, D. Armspach, D. Matt and L. Toupet, *Chem. Commun.*, 2017, **53**, 11717–11720.
23 E. Engeldinger, L. Poorters, D. Armspach, D. Matt and L. Toupet, *Chem. Commun.*, 2004, 634–635.
24 R. Gramage-Doria, D. Rodriguez-Lucena, D. Armspach, C. Egloff, M. Jouffroy, D. Matt and L. Toupet, *Chem. – Eur. J.*, 2011, **17**, 3911–3921.
25 M. Jouffroy, D. Armspach and D. Matt, *Dalton Trans.*, 2015, **44**, 12942–12969.
26 M. Guitet, P. Zhang, F. Marcelo, C. Tugny, J. Jiménez-Barbero, O. Buriez, C. Amatore, V. Mouriès-Mansuy, J. P. Goddard and L. Fensterbank, *Angew. Chem., Int. Ed.*, 2013, **52**, 7213–7218.
27 P. Zhang, C. Tugny, J. Meijide Suárez, M. Guitet, E. Derat, N. Vanthuyne, Y. Zhang, O. Bistri, V. Mouriès-Mansuy, M. Ménand, S. Roland, L. Fensterbank and M. Sollogoub, *Chem*, 2017, **3**, 174–191.
28 Z. Kaya, L. Andna, D. Matt, E. Bentouhami, J. P. Djukic and D. Armspach, *Chem. – Eur. J.*, 2018, **24**, 17921–17926.
29 I. Tabushi and Y. Kuroda, *J. Am. Chem. Soc.*, 1984, **106**, 4580–4584.
30 O. Sénèque, M. Campion, B. Douziech, M. Giorgi, Y. Le Mast and O. Reinaud, *Dalton Trans.*, 2003, 4216–4218.
31 M. Jouffroy, D. Sémeril, D. Armspach and D. Matt, *Eur. J. Org. Chem.*, 2013, 6069–6077.
32 C. Machut, J. Patrigeon, S. Tilloy, H. Bricout, F. Hapiot and E. Monflier, *Angew. Chem., Int. Ed.*, 2007, **46**, 3040–3042.
33 J. Patrigeon, F. Hapiot, M. Canipelle, S. Menuel and E. Monflier, *Organometallics*, 2010, **29**, 6668–6674.
34 O. L. Sydora, *Organometallics*, 2019, **38**, 997–1010.
35 Z. Wang, Q. Liu, G. A. Solan and W.-H. Sun, *Coord. Chem. Rev.*, 2017, **350**, 68–83.
36 F. Y. Xu, O. M. Duke, D. Rojas, H. M. Eichelberger, R. S. Kim, T. B. Clark and D. A. Watson, *J. Am. Chem. Soc.*, 2020, **142**, 11988–11992.
37 F. G. Mann and H. R. Watson, *J. Chem. Soc.*, 1957, 3945–3949.
38 F. Benvenuti, C. Carlini, M. Marchionna, R. Patrini, A. M. Raspolli Galletti and G. Sbrana, *J. Mol. Catal. A: Chem.*, 1999, **140**, 139–155.
39 R. J. Lundgren, B. D. Peters, P. G. Alsabeh and M. Stradiotto, *Angew. Chem., Int. Ed.*, 2010, **49**, 4071–4074.
40 W. Levason and K. G. Smith, *Inorg. Chim. Acta*, 1980, **41**, 133–141.
41 P. Espinet and K. Soulantica, *Coord. Chem. Rev.*, 1999, **193–195**, 499–556.
42 F. Speiser, P. Braunstein and L. Saussine, *Acc. Chem. Res.*, 2005, **38**, 784–793.
43 A. Kermagoret and P. Braunstein, *Organometallics*, 2008, **27**, 88–99.
44 H. Olivier-Bourbigou, P. A. R. Breuil, L. Magna, T. Michel, M. F. Espada Pastor and D. Delcroix, *Chem. Rev.*, 2020, **120**, 7919–7983.
45 G. E. Bekmukhamedov, A. V. Sukhov, A. M. Kuchkaev and D. G. Yakhvarov, *Catalysts*, 2020, **10**, 498.
46 F. Wang and C. Chen, *Polym. Chem.*, 2019, **10**, 2354–2369.
47 D. Zhang, E. T. Nadres, M. Brookhart and O. Daugulis, *Organometallics*, 2013, **32**, 5136–5143.
48 F. L. Grasset, R. Welter, P. Braunstein, H. Olivier-Bourbigou and L. Magna, *ChemCatChem*, 2021, **13**, 2167–2178.
49 J. Flapper, H. Kooijman, M. Lutz, A. L. Spek, P. W. N. M. van Leeuwen, C. J. Elsevier and P. C. J. Kamer, *Organometallics*, 2009, **28**, 3272–3281.
50 J. Flapper, P. W. N. M. van Leeuwen, C. J. Elsevier and P. C. J. Kamer, *Organometallics*, 2009, **28**, 3264–3271.
51 D. H. Camacho, E. V. Salo, J. W. Ziller and Z. Guan, *Angew. Chem., Int. Ed.*, 2004, **43**, 1821–1825.
52 P. W. N. M. van Leeuwen, P. C. J. Kamer, J. N. H. Reek and P. Dierkes, *Chem. Rev.*, 2000, **100**, 2741–2769.
53 K. Yamamoto, K. Higuchi, M. Ogawa, H. Sogawa, S. Kuwata, Y. Hayashi, S. Kawauchi and T. Takata, *Chem. – Asian J.*, 2020, **15**, 356–359.
54 L. Cao, Z. Cai and M. Li, *Macromolecules*, 2022, **55**, 3513–3521.

Yang LI

Ligands cavitaires *cis*-chélatants pour l'oligomérisation métallo-catalysée sélective de l'éthylène

Résumé

Cette thèse de doctorat est consacrée à la synthèse de ligands cis-chélatants bidentes de type P,N et diphosphine équipés d'une cavité cyclodextrine (CD) perméthylée, à l'étude de leurs propriétés coordinantes vis-à-vis de cations d^8 and d^{10} et à leur utilisation pour l'oligomérisation de l'éthylène catalysée par des complexes du nickel. Nous montrons que le confinement du métal dans la cavité CD conduit à la formation de complexes chélates de stœchiométrie métal/ligand 1 :1. La présence du métal à l'intérieur de la cavité CD a été établie à l'aide d'études radiocristallographiques et de RMN 2D. Tous les complexes de nickel ont été testés en catalyse d'oligomérisation de l'éthylène. Cette étude a permis de montrer que la sélectivité de la réaction en termes de longueur de chaîne (C4) et de régiosélectivité (formation d'α-oléfines), ainsi que la robustesse du catalyseur sont améliorées lorsque les positions axiales du métal sont protégées par la paroi interne de la CD.

Mots-clés : ligand P,N ; phosphine ; *cis*-chelate ; cyclodextrine ; nickel(II) ; palladium(II) ; oligomérisation de l'éthylène

Résumé en anglais

This PhD thesis deals with the synthesis of cavity-shaped, cis-chelating bidentate ligands, the study of their coordination behavior towards d^8 and d^{10} metal cations and their use in nickel-catalyzed ethylene oligomerization. The ligands of interest are of the P,N or diphosphine type built on a permethylated α-cyclodextrin unit. Metal encapsulation in the cyclodextrin cavity was shown to promote exclusive formation of 1 :1 ligand/metal chelate complexes at the expense of bis(phosphine) complexes. The presence of the metal inside the cyclodextrin cavity was revealed by 2D NMR characterization and radiocrystallographic studies. All nickel complexes were tested for the catalytic oligomerization of ethylene. It was found that the selectivity of the reaction, both in terms of chain length (C4) and regioselectivity (α-olefin formation), and the robustness of the catalysts are significantly improved when the axial positions of the metal center are protected by the cavity wall.

Key words: P,N ligand ; phosphine ; *cis*-chelate ; cyclodextrin ; nickel(II) ; palladium(II) ; ethylene oligomerization